LASER MACHINING OF CARBON FIBRE REINFORCED POLYMER COMPOSITE

A thesis submitted to The University of Manchester for the degree of

Doctor of Philosophy (PhD)

in the Faculty of Engineering and Physical Sciences

2016

Adel Salama

School of Mechanical, Aerospace and Civil Engineering

TABLE OF CONTENTS

LIST OF FIGURES

LIST OF TABLES

NOMENCLATURE

Notation	Description
λ	Light wavelength
d	Ablation depth
F	Fluence
F_{th}	threshold fluence
l	Machined length
M^2	Beam quality factor
θ	Beam divergence angle
p	The number of radial zero fields
f	Focal length of the lens
n	Number of experiments
z	number of responses
p	Number of model parameters
s	Number of passes
k	Thermal conductivity
ρ	Density
v	Scanning speed
a	Cross section area
P_c	Composite property
P_m	Matrix property
P_f	Fibre property
V_f	Matrix volume fraction
Vm	Fibre volume fraction
d_{min}	Beam spot diameter
ξ	Overall desirability
α	Absorption coefficient
γ	Thermal loading
R^2	correlation coefficient
y	Response variable
$\acute{R}^2$	Regression coefficient

LIST OF ABBREVIATIONS

FRC	Fibre reinforced composite material
MMCs	Metal-matrix composite
CMCs	Ceramic-matrix composite
PMC	Polymer-matrix composite material
FRP	Fibre-reinforced polymer composite material
CFRP	Carbon fibre-reinforced polymer composite material
GFRP	glass fibre reinforced polymer
AFRP	Aramid fibre reinforced polymer
CAMCs	Carbon matrix composites
PAN	Polyacrylonitrile
HAZ	Heat affected zone
AWJ	Abrasive waterjet
TEA	Transversely Excited Atmospheric pressure
CW	Continuous wave mode
df	Degree of Freedom
WJ	Waterjet
DPSS	diode pumped solid state
ps	Picosecond
DoE	Design of Experiment
CCD	Central composite design
RSM	Response surface modelling
Vap	Vaporization
tem	Temperature
SEM	Scanning Electron Microscope
Sp	Specific
ANOVA	Analysis of Variance
YAG	Yttrium-aluminium garnet
MRR	Material removal rate
DOF	Depth of focus
TEM	Transverse electromagnetic mode
PCD	Polycrystalline diamond

LIST OF PUBLICATIONS

A. Salama, L. Li, P. Mativenga, A. Sabli, High-power picosecond laser drilling/machining of carbon fibre-reinforced polymer (CFRP) composites. Applied Physics A: Materials Science and Processing 122, 1 (2016). DOI: 10.1007/s00339-016-9607-8.

A. Salama, P. Mativenga L. Li, , TEA CO_2 laser machining of carbon fibre-reinforced Polymer composites, in ICALEO 2012 - 31st International Congress on Applications of Lasers and Electro-Optics. (2012), pp. 302-308.

A. Salama, L. Li, P. Mativenga, S. Cheetham, S. Dilworth, C. Grafton-Reed, Picosecond laser machining of carbon fibre reinforced plastic composites. In 3rd International Laser Applications Symposium (ILAS), Association of Laser Users, March 2013 Nottingham.UK.

A.Salama, L. Li, P. Mativenga, D. Whitehead, TEA CO_2 laser machining of CFRP composite. Applied Physics A: Materials Science and Processing 122, (2016).

A. Salama, L. Li, P. Mativenga, D. Whitehead, A. Sabli, Understanding the self-limiting effect in picosecond laser single and multiple parallel pass drilling/machining of CFRP composite and mild steel. Materials & Design 107 (2016): 461-469.

A. Salama, L. Li, P. Mativenga, C. Soutis, Statistical modelling of pulsed fibre laser drilling and machining of CFRP composite. Under preparation.

A. Salama, L. Li, P. Mativenga, C. Soutis, Pulsed fibre laser re-manufacturing and bonded repair of CFRP composite plates. Under preparation.

A. Salama, L. Li, P. Mativenga, Sequential laser and mechanical drilling of CFRP composite. Under preparation.

ABSTRACT

Name of the University: The University of Manchester
Submitted by: Adel Salama
Degree Title: Doctor of Philosophy (PhD)
Thesis Title: Laser machining of carbon fibre reinforced polymer composite
Date: 25/02/2016

Carbon fibre reinforced polymer (CFRP) composites have found a wide range of applications in the aerospace, marine, sports and automotive industries owing to their lightweight and acceptable mechanical properties compared to the commonly used metallic materials. The currently dominating method of machining CFRP is by mechanical means that has found many problems including extensive tool wear, fibre pull-out and delamination. Lasers as non-contact tools have been widely applied for cutting and drilling materials. However, machining of CFRP composites using lasers can be challenging due to inhomogeneity in the material properties and structures, which can lead to thermal damage such as charring, heat affected zones (HAZs), resin recession and delamination. In previous studies, Nd:YAG, diode pumped solid state (DPSS), CO_2 (continuous wave), disk and fibre lasers were used in machining CFRP composites and the control of damage such as the size of heat affected zones (HAZ) and achieving comparable material removal rate with the mechanical processes remain a challenge. Most reported work showed a typical heat affected zone of 0.2-1.2 mm. The availability of short pulsed transversely excited atmospheric (TEA) CO_2 lasers and ultra-short laser pulse sources such as picosecond lasers make it possible to improve the laser machining quality of CFRP materials.

In this research, the machining of CFRP composites using a microsecond pulsed TEA CO_2 laser, a state of the art high power picosecond laser and a 1 kW single mode fibre laser system was investigated. The yielded heat affected zone was less than < 25 µm for the TEA CO_2 and the picosecond laser machining, although the material removal rate was low. Additionally, it has been shown that the pulsed fibre laser improved the machining quality compared to that with the continuous mode. A potential application of the fibre laser for composite repair and remanufacturing was investigated. The interactions between picosecond laser beam and CFRP composite were studied in more detail including understanding the self-limiting effect in single and multiple parallel tracks drilling/machining through both experimental and theoretical studies. Furthermore, a sequential laser and mechanical drilling of CFRP was investigated to improve the machining rate.

The work performed in this PhD was driven by aerospace industry needs, with the collaboration of Rolls-Royce plc and BAE Systems as industrial partners.

DECLARATION

I hereby declare that no portion of the work referred to in the thesis has been submitted in support of an application for another degree or qualification of this or any other university or other institute of learning.

COPY RIGHT STATEMENT

ACKNOWLEDGMENTS

I would like to sincerely thank my supervisors Professor Lin Li and Professor Paul Matevinga for their continuous support and guidance. They have been always ready and happy to help. I would also like to extend my gratitude to Professor Constantinos Soutis for his support and helpful advice. Also, I would like to thank Dr. David Whitehead, Dr Wei Guo, Dr Yinzhou Yan and Mr Daniel Wilson for their cooperation and useful suggestions during my work.

Special thanks to Miss Beverley Knight and Miss Rachel Wood-Harper for their help and support.

I am extremely grateful to my entire family, especially my parents and my wife for their love and understanding throughout the study.

Finally, I would like to thank all my friends and all members of Laser Processing Research Centre for their cooperation and wonderful time.

DEDICATION

To

My parents

My wife

My entire family

For their endless love, support and encouragement

CHAPTER 1 INTRODUCTION

1.1 Research motivation

CFRPs are gaining widespread uses in many applications where light weight, high strength and corrosion resistance are essential, such as in the aerospace, automotive and marine industries [1]. Although the structures made by composites are often constructed and cured to the required shape, machining, such as trimming of the edges and drilling of assembly/fastening holes, remains unavoidable [2]. A carbon fibre reinforced polymer consists of higher strength abrasive carbon fibres bonded within a weak polymer. This structure is heterogeneous and anisotropic depending on the constituent's physical properties, fibre orientation and laminar arrangement.

The inhomogeneity in the material properties and structures of CFRP composites makes their machining difficult by using mechanical, electrical discharge, and abrasive water jet machining [3]. CFRP composites are more difficult to machine than conventional materials generally because they are heat sensitive and the carbon fibres are very abrasive [4]. Furthermore, the machining process can significantly affect these materials, leading to various forms of damage, such as delamination, fibrepull-out and resin recession. This can result in components being rejected at the last stage of their production sequence [5]. The main machining techniques used for CFRPs are mechanical cutting such as sawing, milling, drilling or grinding. Also, abrasive water jet (AWJ) cutting is used, due to its low tool wear and avoidance of heat-affected zones. Mechanical machining of CFRP composites often leads to excessive tool wear and delamination (e.g. Figure 1.1) on fibres. These result in an under-utilisation of tools, as they have to be changed at low tool wear levels to control the process quality. These conditions increase machining time and cost. Abrasive water jet machining as an alternative processing technique yields good cut quality (no heat affected zones) with lower tool wear than mechanical processing. However, such techniques need to cope with the water treatment, acoustic noise hazards and abrasive slurry disposal. In addition, they introduce moisture absorption and abrasive penetration of the cut surfaces [6]. Delamination and abrasive embedment between plies are also of major concern during AWJ machining of composites [7].

Figure 1.1 Fibre delamination of CFRP at the hole-exit in a mechanically drilled hole

A laser as a focused, coherent beam of light has been widely used in various industrial applications for cutting and drilling due to its high speed, flexibility, ease of automation and being a non-contact process [8]. It offers several advantages, such as being free of tool wear and contact force-induced problems [9]. However, as laser machining of CFRP composite is based on the interaction of a laser beam with at least two different materials with large material property differences, defects that are thermal in origin, such as HAZ, charring, matrix recession and delamination are generated which are major obstacles in advancing laser machining of CFRP composites [3]. Among these defects HAZs may damage the structural properties of the composite materials [6, 10]. Consequently, it is considered as a critical quality parameter in assessing the quality of the laser cutting of CFRP composites in this work. The large difference in thermal properties between the two constituent materials of CFRP composites results in excessive heat affected zones [11]. This is considered as the major obstacle for wide industry applications of laser machining of CFRP composites. Minimising or eliminating HAZ in the polymer matrix is a major challenge of laser processing of CFRP [7]. Since the HAZ is correlated to the laser-material interaction time, an approach to decrease it could involve the use of faster scanning speeds or shorter laser pulses. The release of high peak power in short time in pulsed laser mode results in quick evaporation of the material. This would reduce the heat absorbed by the matrix and hence limiting HAZ extension. Furthermore, the use of lasers in the pulsed mode allows for some cooling of the processed materials during the pulse-off time [12].

1.2 Aim and Objectives

The aim of this research is to investigate the basic characteristics of machining CFRP composites using three different types of laser system(pulsed TEA CO_2 laser, picosecond laser and fibre laser) targeting a heat affected zone < 10 µm, zero taper and drilling time < 15 sec / hole. Whereas, in sequential laser and mechanical drilling the requirement was heat affected zone <250 µm which could be then removed by mechanical reaming. These requirements were set according to the aerospace industry needs with the collaboration of Rolls-Royce plc and BAE Systems as industrial partners.

To address this aim the following objectives were set:

1. To review literature on laser cutting of composite materials and identify the state of the art and knowledge gaps.
2. To understand the laser process parameter interactions and their effects on the cut quality characteristics using design of experiments and statistical modelling.
3. To investigate and understand the self-limiting effect in picosecond laser single and multiple parallel track machining of CFRP composite.
4. To investigate a potential application of the lasers for composite repair and remanufacturing
5. To investigate the feasibility of high production rate machining of CFRP by a sequential laser and mechanical drilling technique.

1.3 Thesis Structure

This thesis consists of eleven chapters. The introduction was presented in current chapter.

Chapter 2 presents an overview of composite materials including CFRP composite properties and their applications.

Chapter 3 discusses the non-laser machining methods for CFRP composite processing and their characteristics. These include mechanical, water jet and electrical discharge machining.

Chapter 4 reviews the fundamentals of lasers, laser optics and a review of laser machining of CFRP composite and identifies the knowledge gaps.

Chapter 5 presents an investigation of pulsed TEA CO_2 laser machining of CFRP composite using design of experiment and statistical modelling to understand the interactions between the process parameters and their effects on the cut quality characteristics.

Chapter 6 reports an investigation on the drilling and machining of CFRP composites using a state-of-the art high power picosecond laser system. The effect of laser processing parameters, such as laser power, scanning speed and repetition rate on HAZ sizes and ablation depth is investigated in this chapter.

Chapter 7 presents an understanding of the self-limiting effect in high power picosecond laser single and multiple parallel track drilling/machining of carbon fibre reinforced composite and mild steel both experimentally and theoretically.

Chapter 8 presents the statistical modelling of pulsed fibre laser drilling and machining of CFRP composite. The interaction of the machining process parameters such as laser power, scanning speed, laser off time and gas pressure and their effects on HAZ, hole circularity, hole taper and drilling time were investigated.

Chapter 9 introduces pulsed fibre laser re-manufacturing (repair) and bonded repair of CFRP composite plates. In this chapter the feasibility of using a pulsed fibre laser, delivered through an optical fibre cable, for the repair of CFRP composite plates is investigated. The effects of laser drilling parameters on geometry accuracy, taper angle, and heat affected zone are discussed in addition to bonded repair of such plates is presented.

Chapter 10 presents the sequential fibre laser and mechanical drilling of carbon fibre reinforced polymer composite. This chapter investigates the capability of eliminating the HAZ and improve the geometrical quality using sequential fibre laser and mechanical drilling of CFRP composite

Chapter 11 provides conclusions of the research and future work**.**

CHAPTER 2 A REVIEW OF COMPOSITE MATERIALS AND THEIR PROPERTIES

Composite materials have gained wide acceptance for applications in many industries such as aerospace, automotive, wind power and sport industries due to their superior properties (e.g. light weight and acceptable strengths) compared to metals [13]. Due to their unique properties and being anisotropic, inhomogeneous and very abrasive, it makes laser machining of composites difficult [14]. Therefore, an overview of composite materials is introduced in the following sections to understand the composite machinability and material responses to machining.

2.1 Definition of composite

Different materials can be considered as composite materials such as bricks, concrete, wood, metal ceramic matrices and fibre-reinforced plastics (FRP) [15]. A composite material can be defined as a mixture of two or more materials to produce properties that are different from those of separate materials. In contrast to metallic alloys, the constituents of composite material retain their own properties. Their geometry and distribution affect the properties of composite material [16-17]. Commonly, two constituents of composite materials are reinforcement and a matrix. The reinforcement is usually stiffer, and stronger; its role is to improve the mechanical properties of the matrix, whereas the matrix is weaker [18], and its role is to surround and join the reinforcements and distribute the load over them [19].

2.2 Constituent Materials

2.2.1 Reinforcements

There are different forms of reinforcements such as fibres, particulates or whiskers and are characterized as high strengths, high stiffness, and low density. Their roles are to improve the mechanical properties (e.g. strength and stiffness) of composite materials. Various types of carbon fibres, nanotubes, graphite nanoplatelets, and silica

nanoparticle are used as reinforcements for composite materials [20]. Fibres with diameters ranging from 5 μm to 20 μm are the most used reinforcements for advanced composites owing to their high strength and stiffness; they may be continuous or discontinuous, long or short, and organic or inorganic fibres depending on the application [21]. Glass, carbon, aramid and boron fibres are generally used as reinforcements in composite materials. The properties of these reinforcements are summarised in Table 2.1. Among these fibres, carbon fibres are one of the most widely used enforcements for advanced composites and are present in many forms with different stiffness and strengths. Their melting point is high compared to other fibres.

Table 2.1 Properties of reinforcing fibres [22].

Material	Diameter (μm)	Density (ρ) (g/cm^3)	Tensile Moduli es (E) (GPa)	Tensile Strength (σ) (GPa)	Specific Modulus (E/ρ)	Specific Strength (σ /ρ)	Melting Point (°C)	% Elongation at Break	Realtive Cost
Fibres									
E-glass	7	2.54	70	3.45	27	1.35	1540+	4.8	Low
S-glass	15	2.50	86	4.50	34.5	1.8	1540+	5.7	Moderate
Graphite,high modulus	75	1.9	400	1.8	200	0.9	>3500	1.5	High
Graphite,high Strength	75	1.7	240	2.6	140	1.5	>3500	0.8	High
Boron	130	2.6	400	3.5	155	1.3	2300	-	High
Kevlar 29	12	1.45	80	2.8	55.5	1.9	500(D)	3.5	Moderate
Kevlar 49	12	1.45	130	2.8	89.5	1.9	500(D)	2.5	Moderate
Bulk materials									
Steel		7.8	208	0.34-2.1	27	0.04-0.27	1480	5-25	<Low
Aluminium alloys		2.7	69	0.14-0.62	26	0.05-0.23	600	8-16	Low

2.2.2 Matrices

The matrices can be polymeric, metallic, ceramic or carbon. With the exception of ceramics, most matrix composites are weak and are not as strong as fibres [23-25]. The matrix keeps the fibres in the appropriate direction, separate and protects them from the surrounding environments. The commonly used matrices are polymeric, which can be thermosets or thermoplastics, whereas metallic, ceramic, and carbon matrices are used for high temperature applications. Thermoset polymers are the most dominant types of

matrix systems. They usually decompose thermally at high temperature. The most commonly used thermosets are polyesters, epoxies and vinylesters. The low decomposition temperature of the polymeric matrix limits the overall service temperature of the composites [19].

2.3 Types and classification of composites

Composites can be categorized based on the type, geometry and orientation of the reinforcement as shown in Figure 2.1. According to the types of reinforcements used in composite materials (Particulate filler, whiskers and continuous/discontinuous fibres) the composites can be considered as isotropic, quasi-isotropic and non-isotropic, depending on the reinforcements, whether all oriented along one direction or randomly distributed.

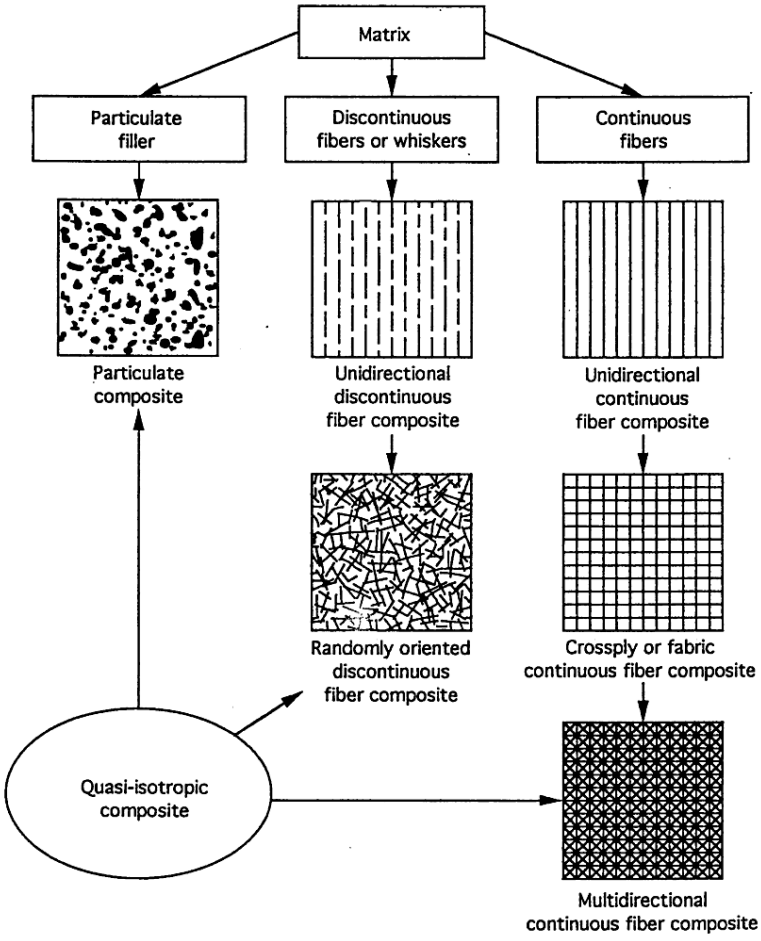

Figure 2.1 Classification of composite material systems [19].

Continuous fibre composites are usually orientated in definite directions, such as unidirectional or woven fibre laminas. These type of composites are made into laminates by stacking many lamina (Figure 2.2) of continuous fibres at chosen orientations to construct a multidirectional laminate in order to achieve the desired strength and stiffness [23]. Furthermore, the composite materials can be classified according to the materials used for the matrix. The main classes of composite materials based on the matrix material include; polymer matrix composite (PMC), metal matrix composites (MMCs), ceramic matrix composites (CMCs) and carbon matrix composites (CAMCs) [17, 26]. Among these classifications, PMCs contain thermosetting matrices (epoxy or polyester) reinforced with long fibres (e.g. glass, carbon and aramid) that are referred to as fibre reinforced plastic (FRP) and are increasingly used in many industrial applications [27]. An example of fibre-reinforced polymer is a carbon fibre reinforced polymer (CFRP) composite, the composite of interest in this study.

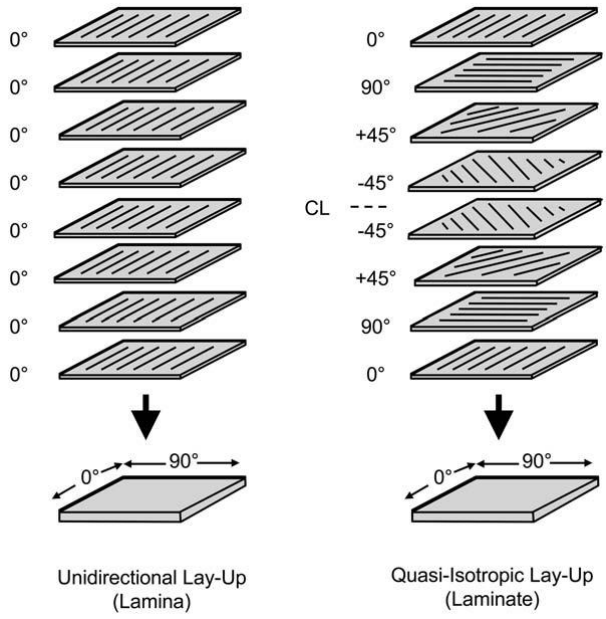

Figure 2.2 Lamina and laminate lay-ups of composites [23].

2.4 Carbon fibre reinforced polymer composite

A CFRP composite is considered as an advanced composite material that has high strengths, lightweight, and high stiffness. Owing to these properties it is being widely used in many industrial applications. It is a polymer matrix (epoxy) composite material

consisting of a plastic matrix reinforced with high strength continuous fibre to give the best reinforcing [20, 28]. Carbon fibres are commonly produced from three organic fibres, such as rayon, polyacrylonitrile (PAN), and pitch. PAN is the most popular that is drawn into fibres and then stretched and thermally treated for sizing to increase their mechanical properties [29-30]

The use of CFRP in laminated structure form with different fibre directions among the layers provides mechanical and thermal anisotropic properties to the final properties of the composite material. Anisotropic properties of CFRP composite challenge the machining of this material. The stiffness in radial direction is much lower and the coefficient of thermal expansion is much higher than in the axial direction [18].

2.4.1 Properties of CFRP composites

Properties of CFRP are different from metals or polymers that are considered as homogeneous, isotropic and their properties are independent of direction [31]. In contrast, CFRP material properties are directional which means that they are non-homogeneous and anisotropic. Nevertheless, CFRP composites are lightweight, high strength and stiffness with improved resistance to fatigue corrosion compared to conventional materials [32].

The mechanical, physical, and thermal properties of CFRP depend significantly on the properties of the constituents such as quantity, type, fibre directions and void content [33]. For example, in unidirectional structures the mechanical properties parallel to the fibres are maximum, while in transverse direction to the fibres are mostly equal to that of the matrix [34-35]. Additionally, the fibre orientation and thermal properties of the constituents also affect the thermal behaviour of CFRP composite. For instance, the thermal conductivity along the fibres is much higher than that in the perpendicular direction; also, heat is conducted faster along the fibres than through the polymer matrix. These differences in thermal properties make CFRP composites respond very differently to the heat load. Consequently, during laser processing of these materials, the carbon fibre vaporises at an extremely different temperature than that of a matrix as shown in Table 2.2. These conditions challenge laser machining of CFRP and necessitate the need for special machining technologies to obtain uniform and high quality machining [36].

The properties of composites are dependent on the properties of the constituents. Therefore, the 'rule of mixtures' can be used to predict some of the final properties of the composite materials (density, *D*, tensile strength,σ, Young's modulus, E, and thermal conductivity, *k*) [20, 34]:

$$P_c = P_f V_f + P_m V_m \quad (2\text{-}1)$$

Where *P* is a property and *V* is volume fraction. Subscripts *c*, *f* and *m* stand for composite, fibre and matrix respectively.

Table 2.2 Properties of selected fibres and matrixes [37].

Material	Density ρ (g/cm^3)	Conductivity *k* $(W/cm/°C)/10^{-2}$	Sp. heat C (J/g/°C)	Diffusivity λ (cm^2/sec)	Vap.tem. T_v (°C)	Vap. heat H_v (J/g)
Resin	1.25	0.2	1.2	1.3	500	1000
Aramid fibre	1.44	0.05	1.42	0.24	950	4000
Graphite fibre	1.85	50	0.71	380	3300	43 000
Glass fibre	2.55	1	0.85	4.6	2300	31 000

2.5 Applications of Composites

Due to its high strength-to-weight ratios, corrosion resistance and low thermal expansion, CFRP composites have become attractive for use in many applications such as aerospace, automobile, marine, medical and sports equipment components [2, 11-12]. In the aerospace field, CFRP used in aeroengine fan blades, fuselage and wing construction [6]. For example, more than 30% and 50%, of CFRP laminate were used in Airbus A350 and Boeing B787 respectively [36]. Also, about 25% of the F-22 fighter weight is CFRP [38]. Figure 2.3 shows the use of composite materials in the Boeing 787.

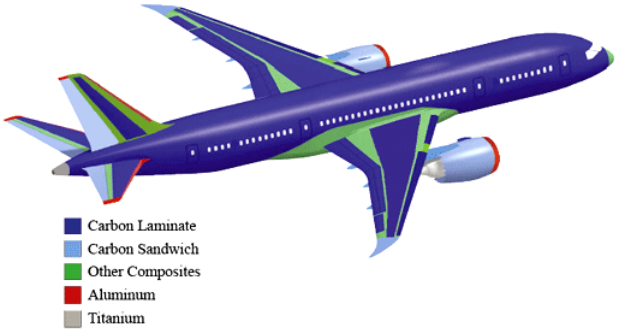

Figure 2.3 The use of composite materials in Boeing 787 [23].

The use of CFRP in space vehicles and automobiles ensures that weight reduction, and hence fuel consumption and efficiency are improved [38]. An example of such applications can be found in the space telescope and BMW M6 roof panel [38]. Furthermore, BMW used CFRP to construct the passenger compartment (Figure 2.4) for its first mass production BMW i3 electrical car [39]. However, the corrosion resistance and high strength-to-weight ratios of CFRP enables longer car's lifespan and lightweight car body than metal [40]. In medical field, CFRP used for hip-joint end-prosthesis, whereas in sport fields, CFRP used in tennis racquet, sailboats, bicycle frames and golf sticks [6].

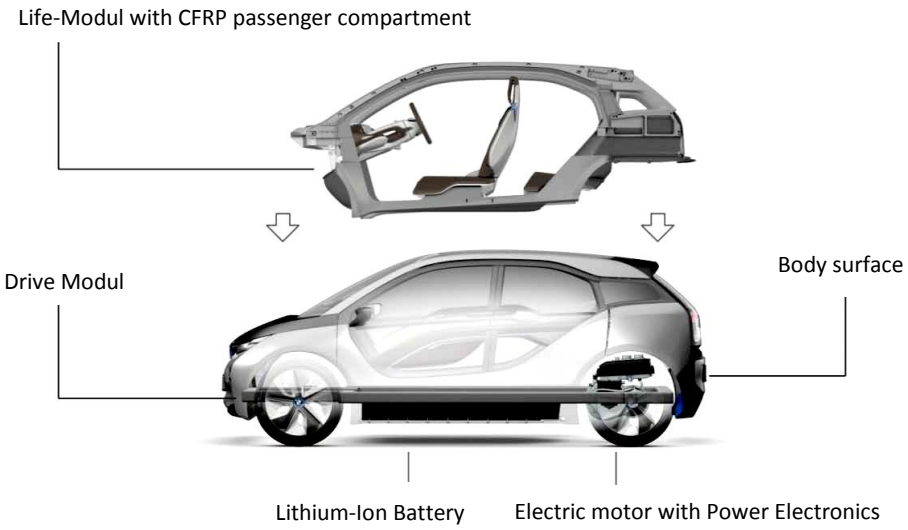

Figure 2.4 The use of CFRP in BMW i3 passenger compartment [39].

The increase in use of CFRP necessitates the need for the successful development of machining technologies for this material in order to obtained better quality.

2.6 Summary

Carbon fibre reinforced polymer composite materials are the most used composites they gained wide acceptance in different fields of applications such as aerospace, automotive and marine industries due to their superior properties. Being anisotropic, inhomogeneous and very abrasive, there machining is difficult. Therefore, efficient machining method to obtain better quality is essential.

CHAPTER 3 MACHINING OF CFRP COMPOSITES – NON-LASER BASED TECHNIQUES

Non-laser machining processes, such as mechanical, abrasive water jet (AWJ) and electrical discharge (EDM) machining can be used to machine CFRP composites. Their characteristics are discussed in the following sections.

3.1 Mechanical machining

Although composite materials are pre-formed in a near net shape, additional operations, such as drilling holes and trimming edges, are still essential for the assembly requirements [41-42]. Machining of CFRP composites is difficult and different from machining of metals due to their specific physical and mechanical properties (anisotropic, non-homogeneous, heat sensitive and very abrasive). Composites are often subjected to damage during mechanical machining [17]. The type of damage includes delamination, fibre pull-out, tool wear and thermal damage, which may lead to the rejection of the composite components at the last stages of their production [5, 43].

Due to the availability of well-established equipment and experience in conventional mechanical machining, different mechanical machining processes such as drilling, turning, milling, sawing and grinding can be applied to composite materials [15]. Mechanical drilling is commonly used to produce holes in CFRP composites for the purpose of component assembly. About 60 % of finished composite products are rejected due to poor hole quality [44]. This demonstrates the challenges in the hole drilling process. Amongst all the damage , delamination due to mechanical drilling of CFRP must be avoided because it produces laminar cracks and weakens the structure by reducing its load carrying capacity [45]. Delamination-free drilling techniques of composite materials were studied by Hocheng and Tsao [46]. They found that delamination occurred on the entrance (peel-up) and exit sides (push-out) of the drilled parts as shown in Figure 3.1 [47]. Therefore, additional drilling techniques such as step drilling, pilot hole and back-up plate and speciality drill bits are required to prevent

delamination. Besides delamination, tool wear due to the high abrasiveness of carbon fibres is another serious problem of mechanical drilling of CFRP composites [48].

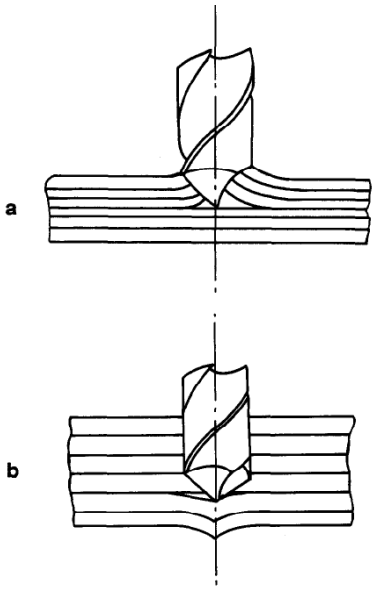

Figure 3.1 Schematic of delamination mechanisms; (a) Peel-up (b) push-out [15].

This adds extra cost due to the requirement of special and abrasive resistance tools to machine CFRP materials (Figure 3.2) [45]. However, recommended carbide drills or polycrystalline diamond (PCD) drills for an acceptable drill life are very expensive [6, 49].

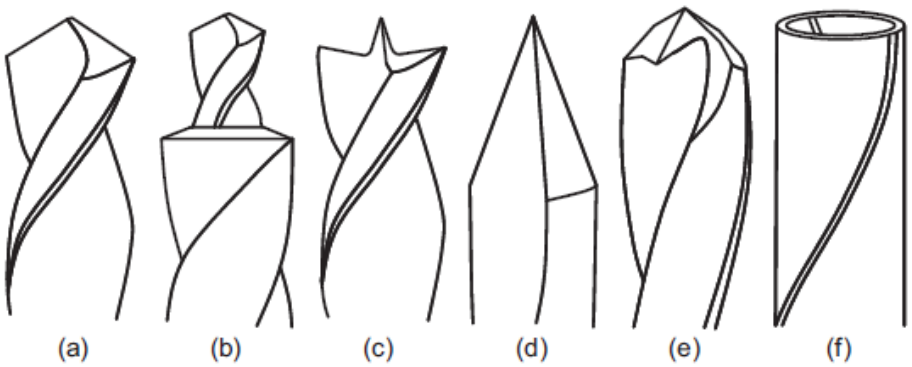

Figure 3.2 Schematic of special drill bit geometries used for drilling of fibre reinforced composites: (a) standard twist drill; (b) step drill; (c) candle stick drill; (d) dagger drill; (e) core drill; (f) multi-faceted drill [45].

Furthermore, another serious problem of CFRP machining is the generation of airborne dusts that may cause health hazards for both humans and machines, which necessitate careful filtration and extraction [50-51].

3.2 Abrasive water jet machining

Abrasive water jet machining is a commonly used method for processing CFRP composite materials, because it is flexible, has a low cutting force, no tool wear (except the cutting nozzle) and no thermal damages [52-53]. Therefore, it only requires simple fixtures during machining and the matrix degradation is reduced compared with mechanical machining [49]. Up to 10 mm thick CFRP laminates can be cut using AWJ [54]. Abrasive water jet machining with garnet, aluminium oxide and silicon carbide abrasives are typically used to cut CFRP materials [55-57]. A schematic illustration of the AWJ system is shown in Figure 3.3.

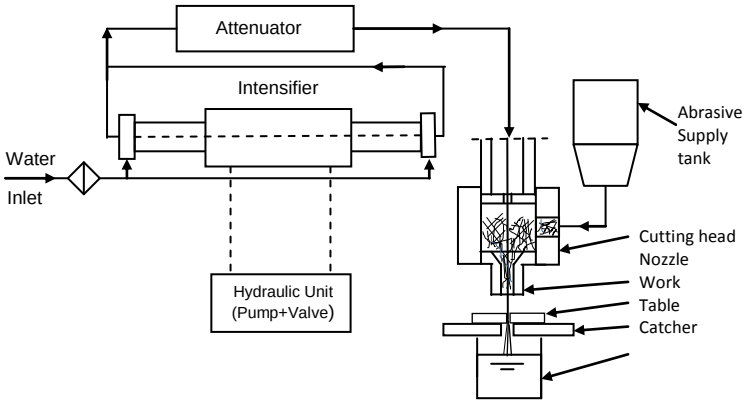

Figure 3.3 Schematic illustration of abrasive water jet system [56].

The tool wear and thermal damage encountered during mechanical machining of CFRP are avoided in AWJ machining. Nevertheless, machining of CFRP laminates using this technique is subject to delamination and abrasives trapping as shown in Figure 3.4 [58-59]. Moreover, starting at the edge of the material or in a pre-drilled hole is needed when cutting CFRP laminates. Also, AWJ machining is noisy and generates abrasive slurry [12].

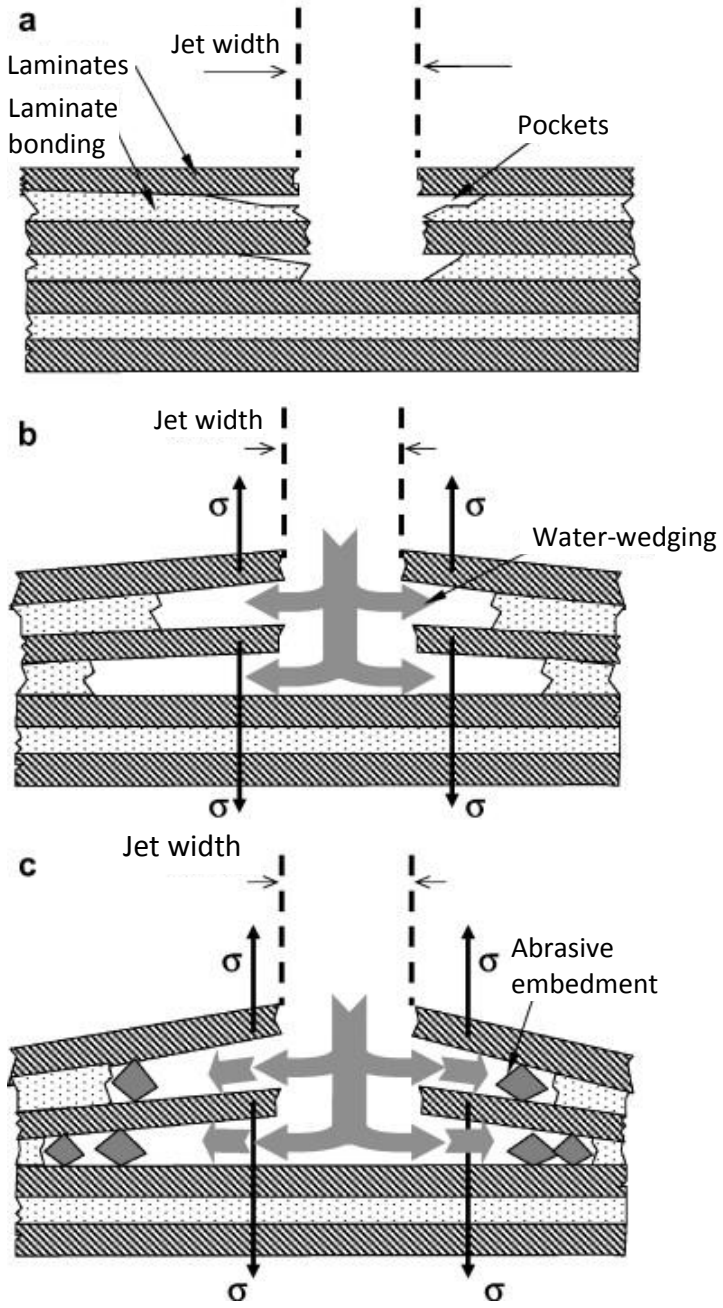

Figure 3.4 Delamination initiation in AWJ machining: (a) fracture initiation,(b) water-wedging and (c) abrasive embedment [59].

3.3 Electrical discharge machining

Electrical discharge machining is an electro-thermal process that uses thermal energy to erode electrically conductive parts [60-61]. Due to its contact free tool advantage (no mechanical stresses and vibration), it has gained wide acceptances in the manufacture of moulds, automotive, aerospace and medical components [62-63]. Die sinker (Figure

3.5) and wire EDMs are the two types of EDM systems. Different types of materials such as copper, brass and graphite are used as electrodes in EDM [64]. CFRP can be machined using EDM because it is electrically conductive. As EDM is a thermal process, the high temperature at high current damages the CFRP samples [46]. Therefore, it needs to be operated at high frequencies and low current in order to obtain high machining quality. The low machining rate and frequent replacement of electrodes limits the use of EDM process with CFRP [65].

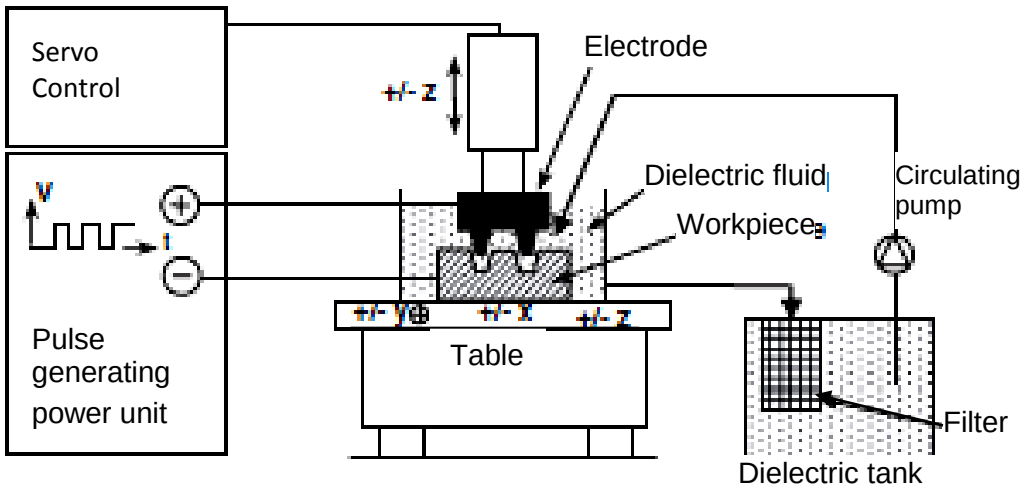

Figure 3.5 Schematic of a die sinker EDM system [33].

3.4 Ultrasonic machining

Ultrasonic machining (USM) is a mechanical material removal method, its use not affected by the electrical or chemical properties of the machined workpiece [66]. It is used to machine both conductive and nonconductive materials. However, it is appropriate for machining metals, ceramics and composites [67]. This method involves the use of a vibrated tool by converting the high frequency energy into mechanical vibrations using a transducer [66]. Moreover, abrasive slurry such as aluminium oxide or silicon carbide mixed with water or oil is pumped into the cutting region between the tool and the workpiece. Figure 3.6 shows the material removal mechanism. Due to tool vibration along its longitudinal axis, the abrasive particles impact the workpiece surface and remove material by microchipping [68]. The slurry cools the tool and the

workpiece, also it is offers a better tool, abrasive and workpiece acoustic bonding and drives away the chips and debris removed during the process. USM is a non-thermal and stress free process; it does not generate thermal damage and significant residual stress [66]. Therefore, damage such as HAZ, delamination, fibre pull-out are reduced during USM of composite materials [69]. However, despite the good quality that can be obtained in USM of composite materials, the process is associated with low material removal rates and higher tool wear [70-71].

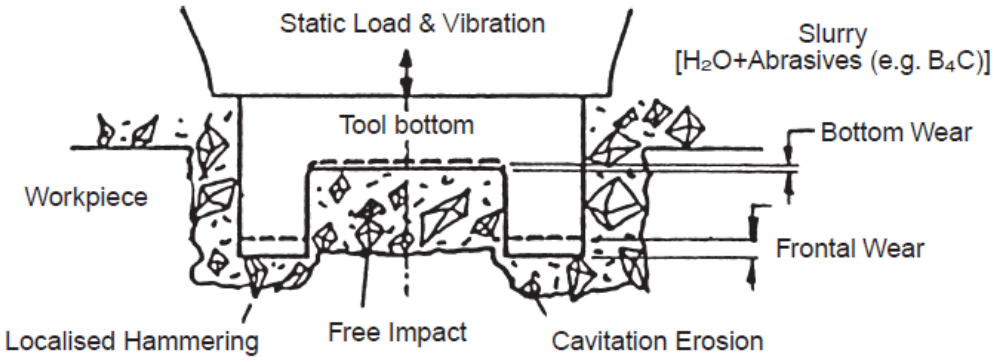

Figure 3.6 USM material removal mechanism [66].

3.5 Summary

The main machining techniques used for CFRPs are mechanical, abrasive water jet and EDM Methods. Machining of CFRP composites using mechanical methods often leads to excessive tool wear and delamination. The tools need to be changed frequently at low tool wear levels to control the process quality, which adds extra cost and time to the machining process. For lower tool wear than mechanical methods and better quality (no heat affected zone), abrasive water jet machining as an alternative processing technique is used to machine CFRP composites. However, the main drawbacks of such techniques are the noise hazards, abrasive slurry disposal, material delamination due to abrasive embedment and the moisture introduced to the cut surfaces. The low machining rate, tool wear and the frequent replacement of electrodes limit the use of EDM and USM of CFRP.

CHAPTER 4 A REVIEW OF STATE OF THE ART IN LASER MACHINING OF CFRP COMPOSITES

4.1 Laser fundamentals

A laser is an acronym for *light amplification by the stimulated emission of radiation*. It differs from normal light because it is coherent, i.e. it has photons of the same frequency, wavelength and phase in the visible, infrared or ultraviolet regions of the electromagnetic spectrum. Thus, unlike normal light laser beams are directional, have high power density and better focusing characteristics. These characteristics mean a laser beam can potentially be a useful tool in processing materials as an alternative tool for machining composites [36, 72].

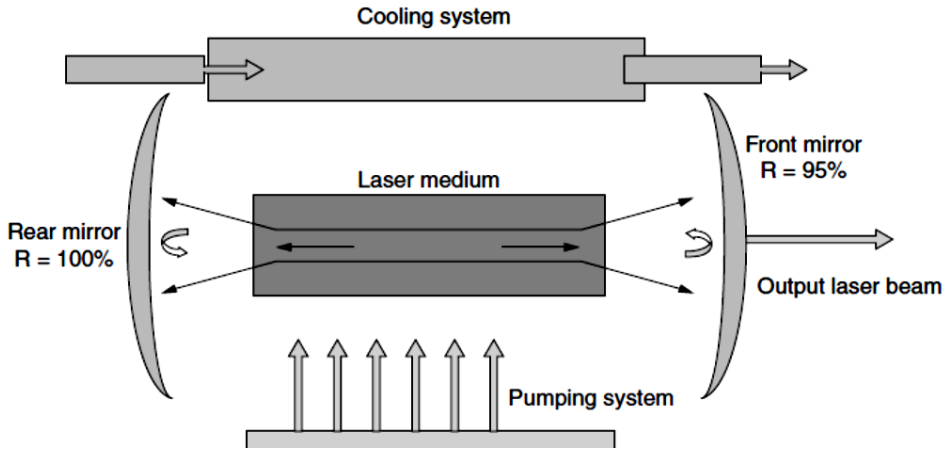

Figure 4.1 The essential elements of a laser device [73].

A typical laser device consists of three main components as shown in Figure 4.1. They are the lasing medium, a pumping system and an optical resonator [72]. The pumping system provides the energy in a suitable form to excite the atoms of the laser medium. The transition of excited atoms from high to low energy levels emits photons, which in turn stimulates further emission, with the same phase, and at the same wavelength, a

process called stimulated emission. The emitted radiation is quickly amplified, directed and controlled by the optical resonator allowing a portion of the radiation to pass as a near-parallel beam whereas the remaining part is circulated inside the cavity to sustain the laser action. The output radiation is usually monochromatic with high spatial and temporal coherences [74].

4.1.1 Laser beam properties

Compared to normal light, a laser beam has special properties that makes it useful for a wide range of applications including material processing and measurements. These properties include monochromaticity, coherence, high brightness and directionality, which are discussed briefly in the following sections.

4.1.1.1 Monochromaticity

The light emitted by normal light sources consists of a wide range of wavelengths (Colours), whereas a laser emits only a very narrow range of wavelengths. The monochromaticity is a very important property of a laser beam that enables it to be focused to a very small region. The focusing property of a laser beam is useful in laser processing of materials which helps to concentrate a large amount of laser energy on the materials surfaces [75].

4.1.1.2 Coherence

Coherence of a laser beam is defined in terms of spatial coherence and temporal coherence. It determines the degree to which light waves are in phase in both time and space. The beam is spatially coherent if the phase relationships at two points of the beam does not change over time as shown in Figure 4.2, while temporal coherence relates the phases at a single point in space for long time. The intensity of coherent laser light is much higher than that of incoherent light of same power [76].

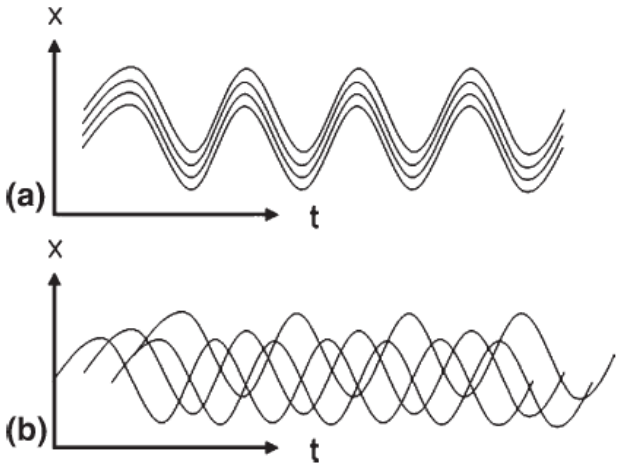

Figure 4.2 Schematic diagram of : (a) coherent light and (b) incoherent light [77].

4.1.1.3 Directionality

Laser sources emits radiation in one direction depending on the axis of the laser cavity. Therefore, laser beams are considered as directional. They can be transmitted for long distances without major divergence unlike normal light, which emits radiation in different directions. The directionality gives a laser beam low divergence which means that it keeps almost the same diameter for several metres [78]. Consequentially, it can be directed and focused by a lens to produce very small spot. The directionality of the laser beam usually is defined in terms of beam divergence [79],[75].

4.1.1.4 Brightness

Brightness or radiance of a laser is defined as the amount of laser power per unit area per solid angle. The very small divergence of the laser beam allows focusing the laser into a very small area for high brightness. In materials processing, the brightness of the laser beam is a very important factor and controls the intensity or fluence of the laser beam [77].

4.1.2 Laser beam parameters

4.1.2.1 Wavelength

Wavelength (λ) is the distance between two points of a propagating wave separated by 2π phase difference. The absorption of a material depends on the laser wavelength and material type**.** A shorter wavelength is highly absorbed by metallic materials due to the higher photon energy of such wavelengths. Furthermore, using shorter-wavelength lasers allows smaller spot sizes to be achieved [80]. Lasers can be classified into infrared, visible and ultraviolet lasers according to their light wavelength. Table 4.1 shows the wavelengths of different lasers.

Table 4.1 Wavelengths of some industrial lasers [80].

Type of Lasers	Wavelength [μm]
Carbon dioxide	10.6
Carbon monoxide	5.4
Nd:YAG	1.06
Nd:glass	1.06
Diode GaAs	0.75-0.87
Diode GaP	054
Excimer KrF	0.248

4.1.2.2 Laser Modes

A laser beam is usually described using longitudinal and transverse spatial modes. The transverse electromagnetic mode (TEM) has more influence on the beam characteristics than the longitudinal mode. Therefore it is often used to characterize the laser beam [80]. Different beam mode forms are shown in Figure 4.3. TEM_{00} is referred to as the Gaussian beam distribution. TEM indicates the variation in beam intensity in a plane perpendicular to the direction of beam propagation (Figure 4.4). The mode order controls the beam focal spot size in which a smaller spot size can be formed for lower order modes. Many factors such as optical cavity geometry, the alignment and spacing of internal cavity optics and the apertures in the optical cavity effect the form of the TEM [76].

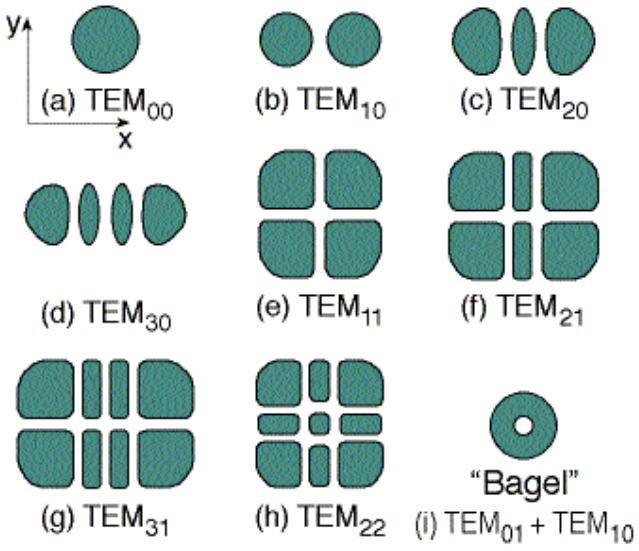

Figure 4.3 Various mode patterns [81].

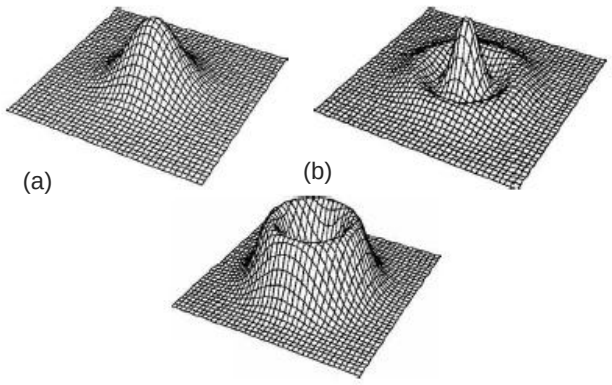

Figure 4.4 Intensity distributions in (a) TEM_{00}, (b) TEM_{10} and (c) TEM_{01}^{*} modes [76].

4.1.2.3 Laser Power and intensity

The laser power is defined as the energy per second whereas the intensity of the laser beam is the power per focused area (W/m^2). For laser processing of materials, a high beam intensity is essential, which can be obtained by focusing the laser beam to a small

spot size. For a pulsed laser, the peak power plays a very important role while for a continuous wave laser the average power is of most significance for macro-processing applications. Both types of laser can achieve high power beams, but focusability of the laser beam remains vital for high intensity beams [76].

4.1.2.4 Spot size and depth of focus

To increase the power density of the laser beam sufficiently for materials processing such as cutting and welding, it must be focused to a small spot size, typically 0.1-0.5 mm diameter [82]. However, the size of the focused beam depends on the focal length of the lens used and several other parameters. A small spot can be obtained by using smaller focal length lenses, but more care is required to prevent lens damage by spatter [61]. The focusing diameter is measured between the points where the intensity has fallen to $1/e^2$ of the central peak irradiance value. For a circular beam, the smallest focal diameter is given by [80]:

$$d_{\min} = 2.44\, f\lambda / \mathrm{D} \tag{4.1}$$

While for a multi-mode beam TEM_{plq}, the minimum focal spot size is obtained by [80]:

$$d_{\min} = 2.44\,(f\lambda / D)(2p + l + 1) \tag{4.2}$$

Where

f = the focal length of the lens,

D = beam diameter,

λ = wavelength of the laser light,

p = the number of radial zero fields and

l = the number of angular zero fields.

The beam is converged down to a minimum waist as shown in Figure 4.5. The depth of focus (DOF) is the distance where the focused beam almost has the same intensity; it is defined as the distance over which the focal spot size changes by 5%. DOF for a Gaussian beam is given by [80]:

$$DOF \cong 2.56\,\lambda\,(f/D)^2 \tag{4.3}$$

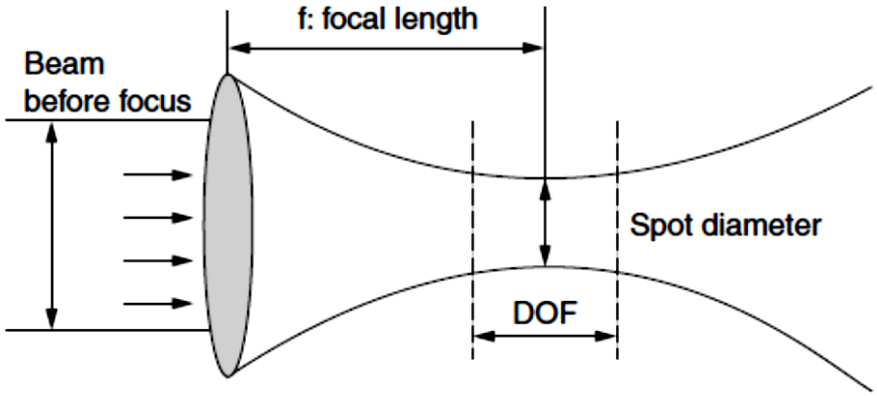

Figure 4.5 Depth of focus of laser beam [73].

The depth of focus and the spot size are both related to lens focal length and beam diameter (equation 4.2 and 4.3) [82].

4.1.2.5 Beam quality

Laser beam quality is measured by a M^2 factor, which shows how close a laser is to a Gaussian beam (M^2=1.0), also shows how small a laser can be focused. The closer M^2 is to 1.0 the better the beam can be focused. Moreover, the lower the M^2 value the higher the beam quality. M^2 factor can be calculated by [76]:

$$M^2 = \frac{\pi D \theta}{4\lambda} \tag{4.4}$$

Where θ is the full beam divergence angle and D is the diameter of the incident beam.

4.1.3 Types of industrial lasers

The most commonly used lasers in material processing are CO_2, Nd:YAG, diode, disk, excimer and fibre lasers. A brief description of these lasers is given below.

4.1.3.1 Carbon Dioxide laser

The CO_2 laser was first used in 1971 to cut plywood dye boards for the packaging industry. Since then the technology has developed and CO_2 lasers are now used with great success to cut almost any material [78]. A CO_2 laser is based on a gas mixture as the gain medium that contains carbon dioxide, helium and nitrogen. It emits an infrared laser beam with a wavelength of 10.6 μm. However, a CO_2 laser requires high gas purity (99.99%) of the three gases [76]. The nitrogen and helium are added to the mixture to improve the efficiency of the laser by increasing the absorption and helping to transfer heat to the walls [76, 83].

A CO_2 laser mostly operates in a continuous mode, but by pulsing the electrical power supply can be operated in a pulsed mode [83]. CO_2 lasers with a wall-plug efficiency (i.e. electrical to optical energy conversion rate) of about 15%, with near Gaussian beam quality, high depth of focus and smaller beam diameter become available nowadays for processing different material thickness [84]. Carbon dioxide laser types include sealed gas, slow axial flow, fast axial flow, transverse flow and transversely excited atmospheric pressure (TEA) [82].

A TEA CO_2 laser is a pulsed laser operating at 1 atm gas pressure or higher. This allows extraction of large amounts of energy per pulse. A TEA laser is excited by a pulsed electrical discharge applied transverse to the optical axis. Large voltages are required for excitation due to the high gas pressure used [76]. The main advantage of the TEA laser is its ability to produce short high energy pulses. The short pulse duration (within the range of microseconds) and high peak power (several hundred kWs) of TEA CO_2 lasers enable them to find wide applications in industrial materials processing [83].

4.1.3.2 Nd: YAG laser

A Nd: YAG laser is a solid state laser in which the active medium is a solid host material of yttrium aluminium garnet (YAG) doped with neodymium Ions (Nd^{3+}) [75]. Both types of laser modes, continuous and pulsed mode, can be produced with YAG lasers with multi kilowatt power in the continuous operation. The limited output power,

poorer beam quality and low wall plug efficiency i.e. 4% or less are the main drawbacks of the Nd: YAG lasers compared with CO_2 lasers. However, these can be enhanced with diode pumped Nd:YAG lasers [76, 80, 82].

4.1.3.3 Diode laser

A diode laser is also called a semiconductor laser and uses a small chip of an alloy aluminium gallium arsenide or indium gallium arsenide phosphide of semiconducting material as the active medium [83]. The first diode laser was demonstrated in 1962 [85]. Diode lasers directly convert electrical current into laser light. Therefore, their efficiency is in the range of 30-50% [75, 80]. The optical cavity in a diode laser is formed by cleaving two opposite ends of the semiconductor wafer [85-86]. Diode lasers can operate in continuous wave, quasi-continuous wave mode with 100 µsec pulse duration or pulsed mode by pulsing the input current generating nanosecond pulse durations. The higher peak power of the quasi-continuous mode made it suitable for pumping solid state laser materials [83]. The attractive advantages of diode lasers are their high efficiency, compact size, longer service life, lightweight, low power consumption, and operation with a low voltage power supply [83, 85]. Imbedding diode lasers with other lasers such as in the case of diode-pumped solid-state lasers can overcome the diode lasers weaknesses such as high beam divergence, workpiece colours absorption dependent and direct generation of high peak power short pulsed beam using Q-switching and enabling them to compete with other lasers on materials processing [85].

4.1.3.4 Disk lasers

The disk lasers are solid-state lasers in which a thin (thickness 100-200 µm) is used as an active medium pumped with a semiconductor laser. One end of the disk is coated by a reflective surface to acts as rear mirror inside the resonator, whereas the other end is mounted to a water-cooled heat sink (Figure 4.6). The cooling arrangement results in uniform and efficient heat dissipation from the disk into the heat sink. Therefore, thermal lensing is reduced as compared to a rod type lasers. The large diameter and high cooling rate of a disk shape medium laser compared to a rod shape medium lasers, guarantee high beam quality of the disk lasers. For a single disk, a power of 1 kW may be generated. However, many disks can be combined to generate multiple kilowatts. A thin-disk laser up to 16 kW power is commercially available these days for material processing. A Nd:YVO_4 picoseconds disk laser pumped by 808 nm wavelength

semiconductor laser can emit radiation at 1064 nm and generate 10 ps pulses duration at a high repetition rate (up to 30 MHz) [87-88].

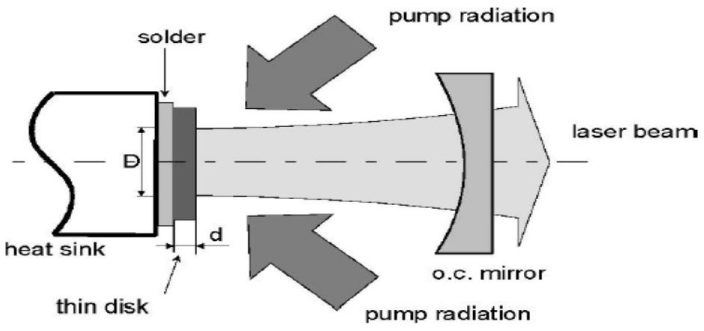

Figure 4.6 Thin-disk laser design[89].

4.1.3.5 Excimer laser

Excimer lasers operate in the ultraviolet wavelength range by a fast electrical discharge in a high-pressure mixture of rare gas (krypton, argon or xenon) and a halogen gas (fluorine or hydrogen chloride). The combination of rare gas and halogen determines the output wavelength. [83]. The most used excimer laser gases are ArF with a wavelength at 193 nm, KrF at 248 nm, XeCl at 308 nm and XeF at 351 nm [58]. The excimer laser pulse energy is in the range of mill joules to joules, an average power up to several hundred watts, repetition rates between 20 to 1000 Hz, peak powers up to 50 MW and a pulse duration from few to a hundred nanoseconds. Operating in the UV wavelength region ensures small spot size and good laser material coupling which makes excimer lasers suitable for processing a wide range of materials, including metals, ceramics, semiconductors and polymers [76].

4.1.3.6 Fibre laser

Due to its high power with low beam divergence, high efficiency, low maintenance cost, small beam focus diameter and flexible beam delivery, fibre lasers have gained wide uses for processing of materials [90-91]. The active medium of a single mode fibre laser is a core of the fibre doped with a rare earth (erbium, ytterbium, neodymium) and is excited by a diode laser source. The laser cavity is made directly with an active fibre. The pump beam is launched longitudinally along the fibre length and guided by the core

as shown in Figure 4.7. Two Bragg gratings reflect a certain incident wavelength light while passing the other wavelength light with high beam quality [90]. A coil of ytterbium-doped multi-clad fibre with an emission wavelength of 1.07-1.08 µm make up the high power fibre lasers that are used widely for cutting and welding applications. The wall plug efficiency of a ytterbium fibre laser is typically 20-30 %, and it needs less maintenance compared to other lasers because there is no need to replace flash lamps or diodes. A 1 kW fibre laser can be focused to a 50 um spot size [90].

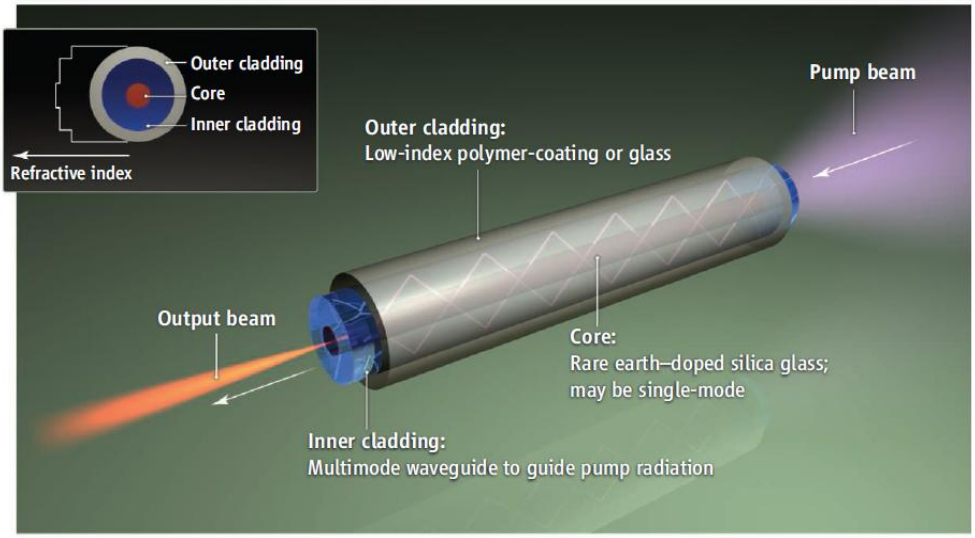

Figure 4.7 Schematic of fibre laser construction [92].

4.1.3.7 Ultra-short lasers

The use of ultrashort pulsed lasers (femtosecond; 10^{-15} s and picosecond; 10^{-12} s) improves the material processing quality as compared to long pulsed lasers because of its high precision machining and minimum thermal/ mechanical damage[93-94]. The reduction in beam/material interaction time using ultrashort lasers leads to higher quality machining by reducing the HAZ [95]. High energy femtosecond pulsed lasers can be generated via the chirped-pulse amplification (CPA) technique as shown in Figure 4.8. In this technique the pulse generated by the oscillator is stretched prior to amplification to reduce the pulse peak power and prevent optics damage inside the amplifier. The stretched pulse is then amplified by the amplifier. At the last stage of high energy ultrashort pulse generation, the amplified long pulse is recompressed in the

compressor to its original duration [96]. Owing to its excellent performance, the self-mode-locked Ti:sapphire laser has become the dominant source for generating femtosecond pulses [97]. However, despite the high processing quality of these lasers, they are expensive, complex and their processing rate is low. Overcoming these limitations necessitates the presence of ultrashort pulse lasers with higher average power and repetition rate. Picosecond laser systems with compact size, high average power and high repetition rate have showed important advantages over femtosecond lasers [98].

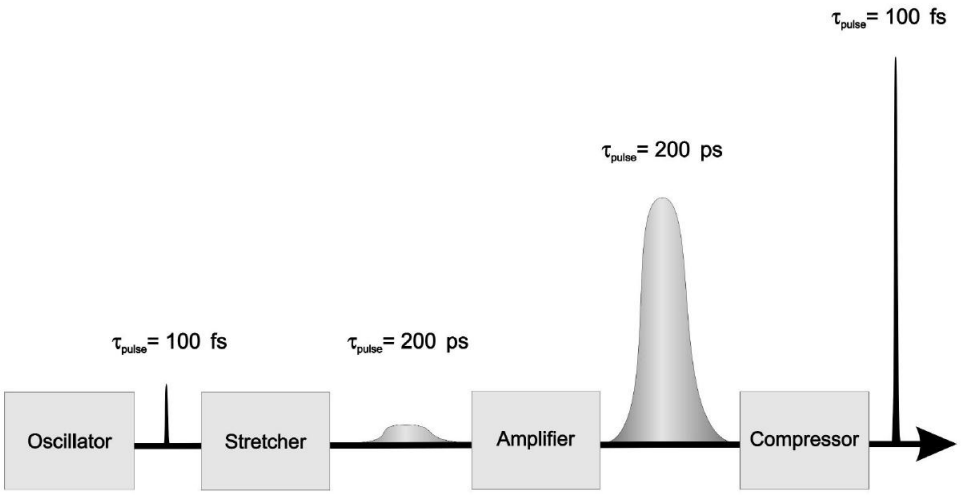

Figure 4.8 Schematic of the Chirped Pulse Amplification (CPA) technique [96].

Picosecond lasers are similar to continuous-wave operation lasers, some mode-locker is installed, which can be either an acousto-optic modulator (AOM) for active mode-locking or semiconductor storable absorber mirror (SESAM) for passive mode-locking [99]. The standard sources of picosecond pulses depend on diode-pumped cw Nd:YAG or Nd:YLF lasers, mode-locked with an acousto-optic modulator [97]. A 10 ps pulse duration at 30 GHz repetition rate can be generated using Nd:YVO_4 laser, which is pumped by semiconductor laser (808 nm) to emit radiation at 1064 nm [88].

4.1.4 Laser beam operating modes

Lasers can be operated in both continuous wave (CW), and pulsed beam modes [100], with average powers ranging from microwatts to over a million watts. In the continuous beam operation, constant power is released for a long time whereas for pulsed mode operation the energy is rapidly released into short duration pulses of high peak power. A pulsed output can be generated by different methods such as normal pulsing, Q-switching, and mode locking [77]. However, the type of the mode used during laser processing of materials strongly affects the obtained quality. Large amount of laser heat generated by high CW power deteriorates the cut quality, while in the pulsing mode, the laser power can be used to reduce these problems allowing better quality cuts, although the production rate reduces. The high peak power removes the material and the laser off time between the pulses allows for some cooling period. The pulse repetition rate is an important parameter in pulsed laser operation mode that can affect the cutting quality [77].

4.1.5 Laser materials interactions

When the laser strikes the surface of a material may be reflected, scattered or absorbed. The interaction of laser with the material leads to heat generation/conduction and material removal with different mechanisms depending on the wavelength, power density, interaction time as well as material properties. The absorption of laser radiation is the most important phenomena in laser processing of materials, which produces different effects such as heating, melting, vaporization, plasma formation and ablation as shown in Figure 4.9.

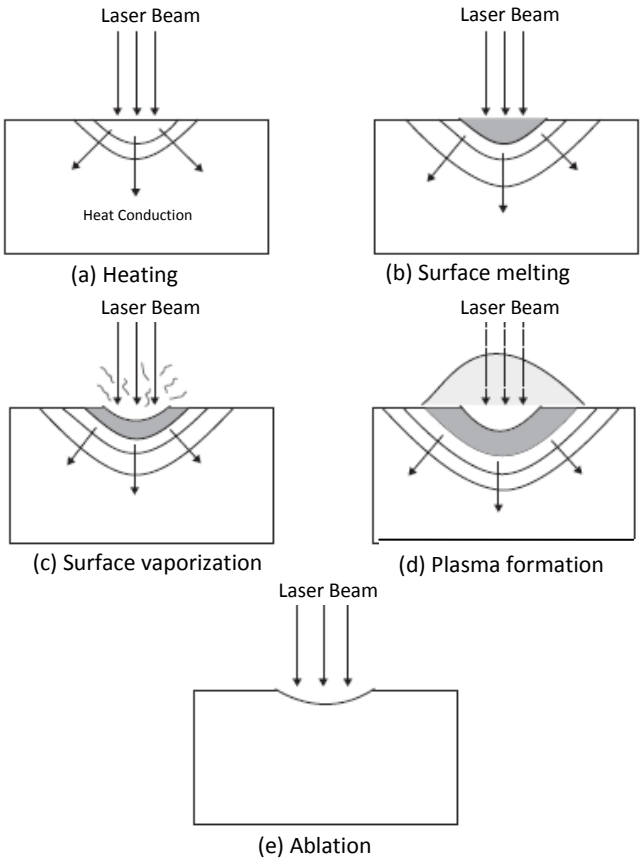

Figure 4.9 Effect of laser materials interactions [101].

The laser energy hits the material propagates to the ambient material through the electron subsystem within a certain relaxation time (T_e) [102] as shown in Figure 4.10. The T_e is less than the lattice heating time T_i, because the electron heating capacity is lower than the lattice heat capacity. For laser pulse durations (T_l) in millisecond and nanosecond *($T_e < T_i < T_l$)* the laser energy absorbed by electrons has enough time to transfer to the lattice. After thermal equilibrium between electron and lattice is reached, heat is conducted into the solid target. When the heat conducted into the target material is high enough it leads to melting and evaporation of the target surface. When the laser intensity become sufficiently high ($> 10^5$-10^8 W/cm^2) the surface vaporization starts and the vapour particles escape from the surface. The interaction of generated vapour and the incident laser beam results in highly ionized vapour (plasma). The generation of plasma shields the laser beam from reaching the material.

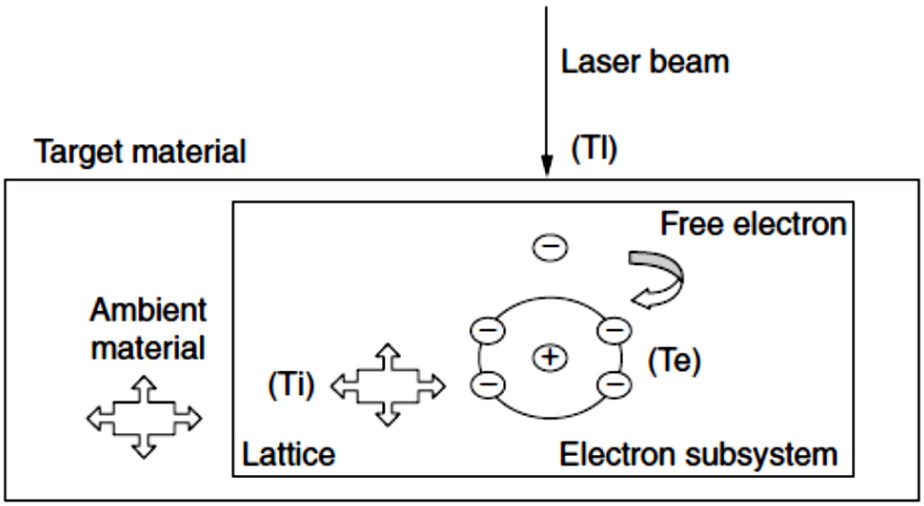

Figure 4.10 The absorption of laser energy by target material [73].

For ultrashort-pulsed lasers such as femtosecond lasers, the pulse duration (T_l) is less than the electron relaxation time *($T_l < T_e < T_i$).* The electrons are heated rapidly and for high laser energy intensity, the energy transferred from the electrons to lattice which is sufficient to break the bonding structure with neglected heat conducted into the target material. In this case direct solid- vapour transition occurs, resulting in significant reduction of heat affected zone. For picoseconds laser pulses *($T_l < T_e < T_i$)* are in the transitional state; a melting zone occurs and some heat transfer conducted to the substrate. However, the removal mechanism in picoseconds regime is still a solid-vapour transition [103].

The absorption of the laser beam by the material depends on the wavelength and the mechanism of material removal depends on the photon energy of the laser beam. If the photon energy is low as in CO_2 lasers (0.12 eV) it is only sufficient to excite molecular vibrations on the surface and produce thermal effects and the process is known as "photo-thermal". A photo-thermal ablation occurs when the temperature at the surface exceeds the boiling point (at large laser energy) and causes rapid vaporization. With high photon energy (UV lasers), the process is electronic excitation and it is known as "photo-chemical" ablation. However, when the laser photon results in direct bond breaking of the molecular chains of the organic materials, the material is removed with negligible thermal damage [104]. The photon energy of the laser wavelength in this process needs to be more than the molecular bond energy (6.4–3.5 eV) [77].

Carbon fibres and epoxy present a high absorption for CO_2 laser (10.6 μm wavelength). The absorption by epoxy chains is converted into heat energy by vibration excitation (heating). The photon energy of CO_2 laser is too low and has insufficient energy to break a chemical bond of a three- dimensional lattice of epoxy. Therefore, localized heating of the targeted material is required in order for a chemical bond to absorb a sufficient number of photons and results in evaporation of the epoxy. However, the CO_2 laser-epoxy interaction produces thermal effects and the epoxy is subjected to melting [105].

4.2 Laser Cutting

Laser cutting is one of the non-conventional cutting processes, widely used to produce complex geometries in nearly all engineering materials including metals, non-metals and advanced materials such as ceramics and composites [106-107]. It can be used to machine small or thin components without mechanical forces [108]. Laser cutting is a thermal process in which the efficiency of machining depends on thermal and physical properties of the material rather than the mechanical properties [109-110]. In laser cutting, when a focused laser beam is incident upon the workpiece, part of the heat generated is absorbed by the material surface and then conducted to the workpiece. Depending on the power density, the absorbed energy heats and converts a portion of the processing zone into a molten, vaporize or chemically degrade the material (in the case of resin matrix material) creating a narrow kerf width with a certain depth through the thickness of the workpiece. With the help of a coaxial gas jet or recoil pressure, the volume of evaporated or melted material is removed from the cutting zone (Figure 4.11) [111-112].

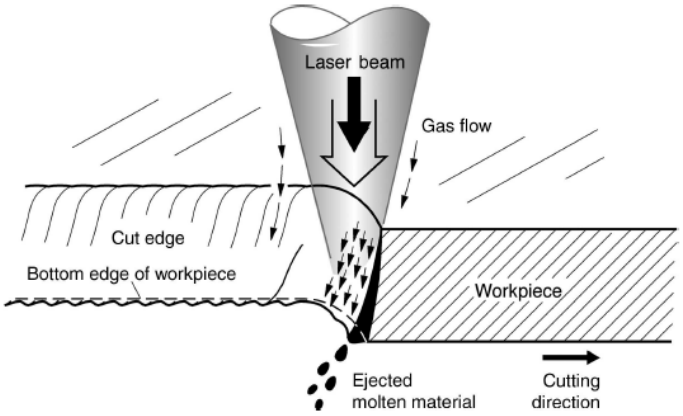

Figure 4.11 Schematic of laser cutting process [84].

4.2.1 Laser cutting techniques

Based on the interaction of the laser beam with the workpiece and the assist gas roles during the material removal process, different laser techniques can be used to cut the material such as fusion cutting, reactive gas fusion cutting, vaporization cutting and chemical degradation cutting. The selection of optimum cutting technique depends on the thermo-physical properties of the material, workpiece thickness and type of laser used [77].

4.2.1.1 Laser fusion cutting

This process involves melting of the base material using laser heat energy. The molten material is then driven out of the machined kerf using high pressure inert gas (mainly nitrogen, helium or argon). During laser fusion cutting, the laser beam only heats up the material above the molten temperature and the melt ejection is done by the gas jet. The gas also shields the cut zone and protects the laser optics. This process is applicable to all metals, thermoplastic polymers and some ceramics. However, the formation of striations on the cut surface and dross at the lower cut edge are the major drawbacks of fusion cutting. Hence, striations and dross free cutting is the main challenge in this technique [75-76, 78]. Less energy is required in fusion cutting compared to evaporative cutting due to the primary phase transformation being melting [77, 113].

4.2.1.2 Laser reactive gas fusion cutting

Laser reactive gas fusion cutting is also known as laser oxygen cutting. In this process the inert gases are replaced with a reactive gas such as oxygen or a mixture containing oxygen. Besides ejecting the melted material, the oxygen gas also reacts with the melted material, through an exothermic reaction, which enhances the cutting process by providing additional heat inputs to the cutting zone allowing for higher cutting speeds than laser fusion cutting with inert gases only [33, 76, 80]. A mixture of oxygen with nitrogen gas was found to improve the machining quality in laser cutting of CFRPs [3].

4.2.1.3 Laser vaporization cutting

Laser vaporization cutting involves heating the material to the vaporization temperature by a high intensity (over 10^6 W/mm^2) focused laser beam. The material is vaporized and ejected with molten material by the help of the assist gas jet. Generally a pulsed laser combined with a coaxial jet of inert gas is used with this process [80]. In short pulse lasers, most of the material is vaporized due to the high peak power. Less melting during the process helps to achieve high edge equality. Some polymers, wood and polymer composites are cut through vaporization cutting [76].

4.2.1.4 Laser chemical degradation cutting

This process is known as a cold cutting process due to little heat being generated. Material removal in cold cutting depends on material degradation by breaking the chemical bonds by the laser beam energy. This technique was observed with the introduction of high-powered excimer lasers working in the ultraviolet radiation with a photon energy of 4.9 eV, which is similar to or higher than the bond energy for many organic materials. This mechanism is most common for machining aramid composites, thermoset polymers and wood[33]. However, despite the higher cut quality, the cutting rate of this process is lower than the abovementioned processes.

4.2.2 Laser cutting process parameters

Laser cutting is governed by various parameters, which should be considered when performing the cutting process. Some of these parameters can be optimised in order to improve the cut quality and achieve the required cutting results. Moreover, the relationship between these parameters has a significant role for high cutting quality. These parameters are grouped into four categories as shown in Figure 4.12 [33, 80].

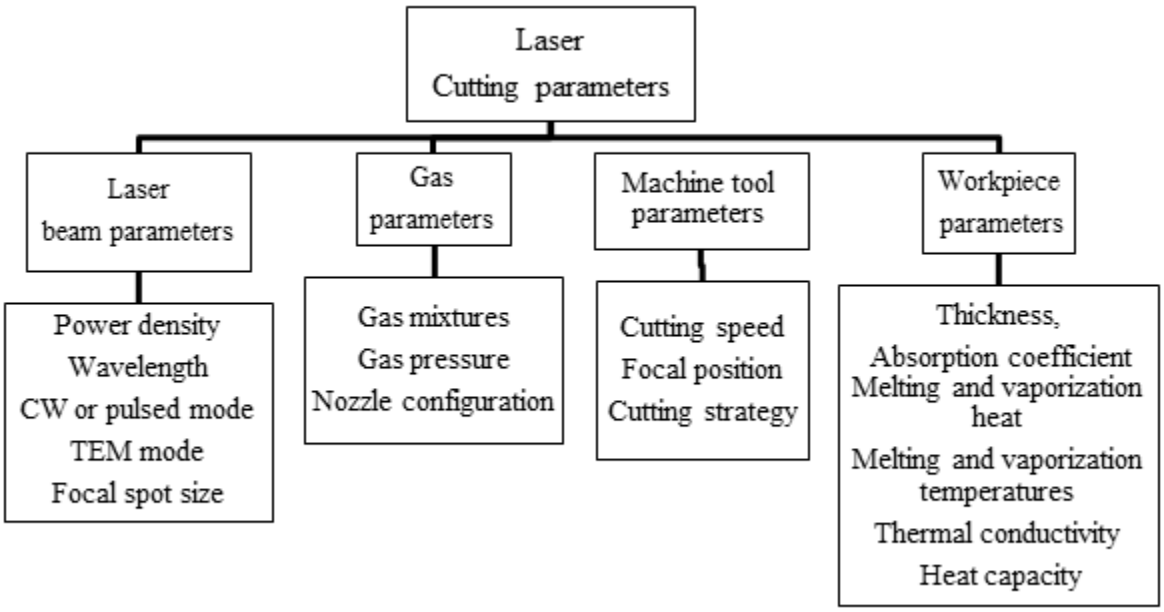

Figure 4.12 Laser cutting process parameters categories.

4.3 A review of laser machining of CFRP composites

Machining of CFRP composites differs considerably from machining conventional metals due to their inhomogeneous properties, heat sensitivity and the fact that carbon fibre are very abrasive [4]. Although non-laser machining of CFRP composites such as mechanical and AWJ are common in industry, they are associated with delamination, noise, dust, short tool life and long term damage to the composites due to the use of coolant and water in the mechanical and water jet machining [13, 114]. Alternative processing methods such as laser machining can be very useful in overcoming the above obstacles in the machining of CFRP composite material [22, 36].

Laser machining as a non-contact process offers several advantages, such as tool wear free, no contact force induced problems and nonabrasive or the requirement of a liquid media [8, 36]. Furthermore, laser cutting can be can be performed at high cutting speeds [115]. However, as laser machining is a thermal process and depends on the interaction of a laser beam with the composites. Suitable care concerning the selection of the cutting parameter ranges is required in order to minimize or eliminate machining defects

that are thermal in origin such as HAZ, charring, resin recession and delamination [116-117]. Yilbas [118] studied and examined the laser cutting of composite materials. He indicated that the cutting quality could be improved by the proper selection of laser parameters.

4.3.1 Quality of CFRP composites in laser machining

Cutting quality is of great importance in order to exploit the industrial advantages of laser technologies over rival manufacturing processes. Laser machining quality of CFRP composite is defined according to the final use of the produced component, by considering several characteristics, such as kerf width, extension of heat affected zone near the kerf surface and below the surface, cut edge perpendicularity (or taper) and surface roughness [119]. These qualities depend on the setting of various process parameters such as laser power, scanning speed, assist gas type and pressure, material thickness, mode of operation (continuous wave or pulsed mode) and machining strategy [33, 120]. Figure 4.13 shows schematically the characteristics of laser cutting of CFRP composites.

The morphology of the CFRP cut edge is affected by the constituent's thermal properties and the fibre's arrangement and directions. More heat is propagated in the carbon fibre's direction than that perpendicular to the fibres. It is also dependent on the laser beam power and the scanning speed. Matrix recessions, fibres protruding out of the matrix and delamination inside the laminae are typically seen at low cutting speeds and high laser powers. These damage can be reduced by either lowering the laser power or increasing the scanning speed [33, 37]. Width of the kerf formed during laser cutting is commonly wider at the top surface of the workpiece than at the bottom surface. It mainly depends on the beam spot size and is affected by the laser beam material interaction time [76]. At long interaction time, more energy is transferred to the workpiece and leads to a wider kerf [33]. Owing to the difference between the kerf width at the beam entry and at the beam exit, a taper is produced during laser processing. The decrease in the beam energy absorbed by the material with the increase of the kerf depth is a reason of the taper formation. It has been found that the taper is decreased by increasing the pulse repetition rate in pulsed laser cutting of CFRP. Higher cutting speed, higher pulse duration and higher pulse energy reduce kerf taper [33, 121].

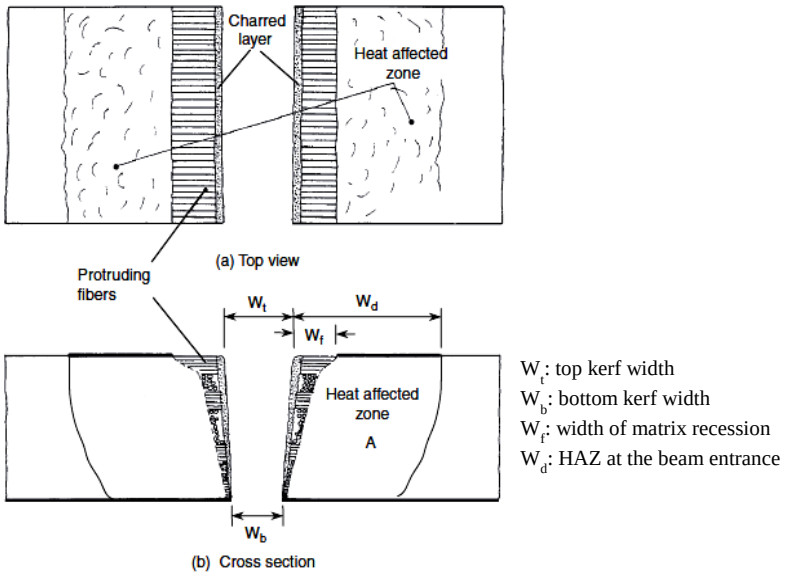

Figure 4.13 Schematic of FRP composites laser cutting characteristics [33].

The HAZ generated is typically produced by the laser heating, which is described by the length of fibre extruding out of the matrix and defined as the zone where the ability of the matrix to transfer loads to the fibres is reduced or lost[12, 115]. HAZ extension is generally decreased by reducing laser heat conduction to the surrounding materials. This can be achieved by reducing laser beam power and interaction time depending on repetition rate, pulse duration, laser delivery mode and cutting speed. For example, the HAZ can be reduced or eliminated using a short pulse duration, low repetition rates and a fast cutting speed. Consequently, short pulsed lasers and fast scanning speed reduces the HAZ under the same laser power [115, 122].

The HAZ during laser processing of materials can be estimated from the heat penetration depth (δ) [123]:

$$\delta = \sqrt{\alpha\tau} \tag{4.5}$$

Where α is the thermal diffusivity (cm^2 /s) and τ is the laser pulse duration (sec). The thermal diffusivity is defined as:

$$\alpha = \frac{k}{\rho C_p} \tag{4.6}$$

Where k is the material thermal conductivity in W/ m.K, ρ is the material density in kg/m^3 and Cp is the material specific heat capacity in J/ $kg.K$. Among all the different

machining quality parameters discussed above, HAZ is unavoidable and is a critical factor in evaluating the laser machining quality of CFRP composites. Thus, the possibility of reducing/ eliminating HAZ is an important challenge [37]. Table 4.2 summarises the cutting quality (HAZ) obtained with some laser types in processing of CFRP composites.

Table 4.2 Cutting quality (HAZ) of CFRP obtained with various laser types.

Laser type	Wavelength	Machining condition	HAZ Size	Ref.
Nd:YAG laser	1064 nm	Pulse energy: 1.4 - 2.2 J Pulse length: 0.2–1 ms Repetition rate: 30 – 50 Hz Material thickness: 2 mm	0.5–2.4 mm	[2]
Nd:YAG laser	1064 nm	Average power: 300 W Peak power: 18 kW Repetition rate: 0.01– 0.1 kHz Material thickness: 1.5 mm	0.63–0.64 mm	[124]
Disk laser	1030 nm	Average power: 3000 W Continuous wave Material thickness: 1.5 mm	1.20–1.23 mm	
CO_2 laser	10.6 µm	Average power: 500 W Repetition rate: 0.1–20 kHz Quasi- continuous wave Material thickness: 1.5 mm	1.34–1.50 mm	
Nd:YVO_4 laser	355 nm	Average power: 10 W Pulse length: 25 ns Repetition rate: 40 kHz Material thickness: 0.3, 1, 3.1 and 7 mm	0.05 mm	[36]
CO_2 laser	10.6 µm	Average power: 300 –3000 W Repetition rate: 0.01– 4 kHz Duty cycle 20–100 % Material thickness: 3 mm	0.540–1.2 mm	[121]
Yb:YAG fibre laser	1064 nm	Average power: 30 W Repetition rate 30–80 kHz Pulse length: 50 ns Peak power 10–20 kW Material thickness: 0.5 mm	0.1–0.25 mm	[125]
Nd–YAG	1064 nm	Average power: 80 W Pulse length: 10 ps Repetition rate: 0.2 –10 MHz Material thickness: 2 mm	< 5 µm	[126]
Nd:YVO_4	1030 nm	Average power: 1.1 kW Pulse length: 8 ps Repetition rate: 300 kHz Material thickness: 2 mm	< 20 µm	[127]

4.3.2 Challenges in laser machining of CFRP composites

Laser machining of CFRP composite materials is very challenging due to the large differences in physical and thermal properties of the CFRP constituents [36]. The best quality of FRP laser machining can be achieved when the thermal properties of the reinforcing fibres and polymer matrices are close to each other and reacts to the heat in a similar manner as in case of aramid fibre reinforced polyester composites [128]. Tagliaferri et al. [128] examined the morphology of the laser cut surfaces of aramid, graphite and glass cloth-reinforced polyester composites during CO_2 laser cutting and showed that quality of the cut, for both the extension of the heat-affected zone and the uniformity of the surface morphology is better for those composites which exhibit low variations between the thermal properties of the constituent materials such as CFRP composites, whereas glass fibre and graphite fibre composites showed poorer results.

In CFRP composites, the thermal conductivity, thermal diffusivity and heat of vaporization of the polymer are lower compared to the carbon fibres (Table 2.2). Hence, during laser machining of CFRP, the matrix is affected by the laser heat before the carbon fibre which needs higher temperature to vaporize [33]. Furthermore, the large amount of energy presented in the laser cutting zone is conducted away due to the high thermal conductivity of carbon fibre. Also the difference in thermal conductivities between the fibres and polymer matrix makes it difficult to obtain uniform and high quality machining of CFRP using a laser [115]. Consequently, laser processing of these materials often leads to an extended HAZ. Minimising or eliminating HAZ in the polymer matrix in laser processing of CFRP is considered as the major obstacle for its wide industrial applications [7] [18] [36]. The above mentioned factors make machining of carbon fibre reinforced composites very difficult.

4.3.3 Influence of laser parameters on CFRP cut quality

The influence of different process parameters including laser wavelength , beam transverse mode, pulse duration, repetition rate, laser power, fluence (energy density), beam spot size, scanning speed and machining strategy on laser processing quality of CFRP composite were investigated using several types of laser sources [2-3, 7, 11, 36, 114, 121, 124, 126, 129-134]. Figure 4.14 Cause-Effect-Diagram of laser beam processing of CFRP composites.

Mathew et al. [2] used a Nd: YAG pulsed laser in ms pulse range to identify and optimise the important parameters for machining of CFRP using a response surface methodology. These parameters include pulse energy, pulse duration, cutting speed, pulse repetition rate and gas pressure. The HAZ size achieved was between 0.5 mm – 2.4 mm. Herzog et al. [124] compared the effect of cutting on static strength of a CFRP laminate using a pulsed Nd: YAG laser, a disk laser and a continuous wave CO_2 laser. They found that samples processed by the Nd: YAG laser had less HAZ and higher static and bending strengths. The HAZ sizes were in the range of 0.63 mm – 1.5 mm for all three lasers. Li et al. [36] investigated the machining quality of CFRP using a diode pumped solid state UV laser. They showed that minimum HAZ (around 30-50 μm)

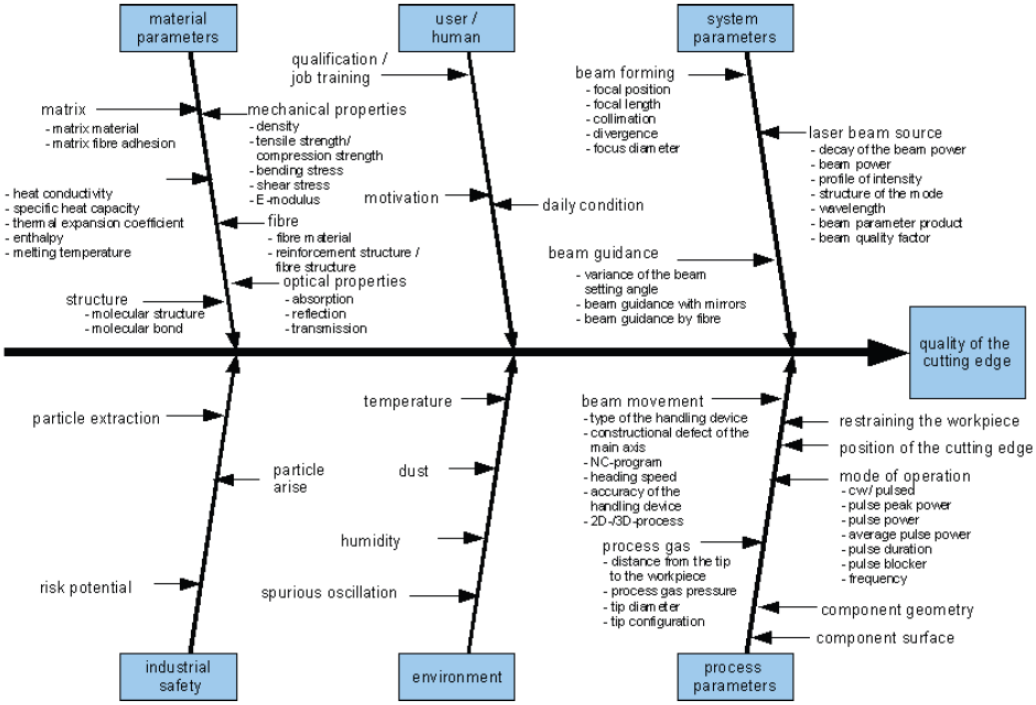

Figure 4.14 Cause-Effect-Diagram of laser beam processing of FRP composite [81].

was achieved using a nano-second pulsed UV diode pumped solid state (DPSS) laser cutting at a very high scanning speed (800 mm/s). They introduced a new drilling/machining strategy by using multiple rings in order to widen the cut kerf for more effective material removal. They also suggested that short laser-material interaction time such as short pulse and high scanning speed are needed to reduce HAZ.

Negarestani et al. [11] developed a three-dimensional model to simulate the transient temperature fields and subsequent material removal on a heterogeneous fibre- matrix mesh in laser machining of CFRP composite. They predicted the dimensions of the HAZ during laser machining of CFRP. The effect of laser parameters such as laser wavelength, power density, scanning speed and process gas on CFRP behaviour was studied by Negarestani and Li [135]. They also compared the laser machining process with other machining techniques such as mechanical and water jet techniques.

The influence of processing parameters, for both continuous and pulsed mode (millisecond) CO_2 lasers, on the cut quality of CFRP was studied by Riverio et al. [121] They found that the minimum heat affected zone (0.54 mm) was obtained using a CO_2 laser working in pulsed mode. Leone et al. [125] investigated the use of multi-pass laser scanning technique in cutting of CFRP thin sheets using a 30 W MOPA Q-switched pulsed Yb: YAG fibre laser. They found that the kerf geometry was mainly affected by the scanning speed. Furthermore, the HAZ extent was influenced by the scanning speed as well as pulse power. It was also found that the laser wavelength influences the HAZ extension in laser machining of CFRP composites. A long wavelength (IR)has low photon energy that is not enough to decompose the CFRP with negligible thermal effect [54], whereas, the photon energy of a short wavelength (UV) is high enough to decomposes the CFRP with little thermal effect [54]. Dell'Erba et al. [136] investigated the effect of wavelengths on the HAZ of aramid, glass and carbon fibre composites during CO_2 and Excimer laser cutting and drilling. They noticed that the HAZ was reduced for all three materials when processed with a 248 nm Excimer laser. Wolynski et al. [114] studied experimentally the influence of different laser parameters on machining quality and processing time during laser ablation of CFRP using a picosecond laser system operating at different wavelengths (355 nm, 532 nm and 1064 nm). They showed that a larger HAZ was obtained at the 1064 nm wavelength compared to that at 532 nm (Figure 4.15).

In addition to the effect of laser parameters, it has been found that the material properties have also an influence on the HAZ extension on CFRP cut quality due to the difference of thermal properties of composite constituents and the fibre orientation and distribution. Pan and Hocheng [122] showed during laser grooving of unidirectional fibre reinforced plastics that the size of the heat affected zone was influenced by the

orientation of fibres. A small HAZ was generated when cutting parallel to the fibre, and a large HAZ was generated when cutting perpendicular to the fibre orientation.

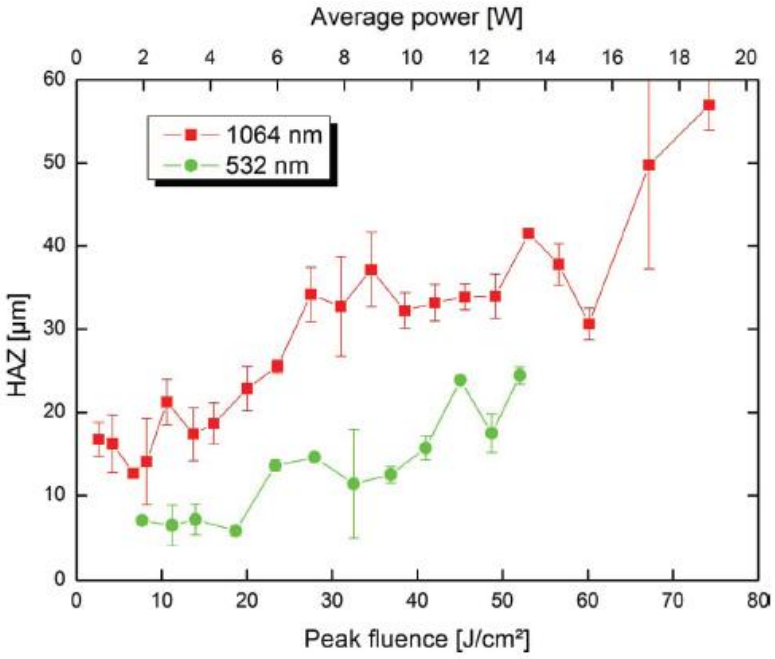

Figure 4.15 Heat affected zone for picosecond ablation of CFRP for 532 nm and 1064 nm [114].

Since the HAZ is influenced by the laser material interaction time, a short-pulsed laser is an option to reduce the laser-material interaction time and offers improvements in cutting quality due to the cooling between pulses. Therefore, the use of ultra-short laser pulsed sources such as femtosecond lasers and picosecond lasers allow the release of high pulse energy in a very short time. The laser beam directly evaporates the materials and leaves little time for the heat to propagate to the adjacent substrate and hence limiting the HAZ extension and improving the laser machining quality for processing CFRP [126]. It was found [114, 133-134] that ultrashort pulse lasers using picosecond systems could produce smaller thermal damage . Emmelmann et al. [133] analysed the extension of HAZ at the cavity edge during laser ablation of CFRP laminate by machining quadratic cavities into a CFRP laminate using two different lasers; a 1 ns fibre laser with a wavelength of 532 nm and a 2 ps solid state laser with a wavelength of 1064 nm. They concluded that pulse duration has a significant effect on the material

processing quality with shorter pulses giving much reduced HAZ. Finger et al. [126] investigated the processing of a 2 mm thick CFRP composite sample using a picosecond pulsed laser with an average power of up to 80 W. They also evaluated the influence of the average power, scanning speed and repetition rates on the ablation rates and the width of HAZ. They showed that picosecond laser processing of CFRP with a HAZ less than 5 µm and an ablation rate of 100 mm^3/min could be obtained. The use of a high average powered picosecond laser often involves high repetition rates, which can damage the processed material by excessive heat accumulation. Weber et al.[137] used a ps laser at a wavelength of 515 nm with a pulse duration of 8 ps, a maximum average power of 23 W and a repetition rate of 800 kHz to investigate the effect of heat accumulation on cut quality of CFRP. They concluded that at high repletion rates, short pulse lasers with very high scanning speed are required. Freitag et al.[127] used an ultrafast laser system with an average power of 1.1 kW, 8 ps pulse duration and 300 kHz repetition rate to investigate the effect of heat accumulation during picosecond laser processing of CFRP. They showed that the heat accumulation effect could be reduced by decreasing pulse overlaps using higher feed rates.

The large number of process parameters involved in laser processing of materials need to be optimized in order to achieve good machining quality and process efficiency. The one-factor-variation-at-a-time approach commonly used requires a large number of runs and does not allow for the investigation of process variable interactions [138]. Therefore, the use of Design of Experiment (DoE) can be very helpful in such situations where the effect of various parameters and their interactions on the machining quality can be investigated and optimized [106]. DoE is an experimentally based modelling method involving the use of analytical techniques such as analysis of variance (ANOVA) to process the data and decide on individual and interaction factors that affect the process and their significances on process performance.

Response surface modelling (RSM) with central composite design (CCD), Taguchi's method and factorial design are the most used DOE techniques in laser processing experiments. Ghosal and Manna [139] used RSM to develop comprehensive statistical models to optimize the machining parameters during laser machining of Al/Al_2O_3-MMC. Elmesalamy et al. [140] also employed the RSM based on CCD during ultra-narrow-gap laser welding of thick-section stainless steel to develop statistical models to understand the process parameters interactions and to optimize the welding parameters.

El-Taweel et al. [116] used a Taguchi method to understand the effect of laser parameters on the cut quality during CO_2 laser cutting of Kevlar-49 composite and to determine the significant parameters and optimize the cutting parameters for better quality. Among these techniques, RSM is a combination of mathematical and statistical techniques to correlate experimental responses with the input variables in mathematical models to optimize these responses. Moreover, the effect of variable interactions on responses can be graphically presented in a three dimensional surface. Mathew et al. [2] used RSM with CCD for experimental design and process parameters optimization using pulsed Nd: YAG laser to cut 2 mm thickness CFRP sheet . The input factors were pulse energy, cutting speed, pulse duration, pulse repetition rate and gas pressure while the output responses were HAZ and wall taper angle. Negarestani et al. [3] similarly performed a statistical analysis based on RSM and CCD to optimize the process parameters (pulse frequency, pulse energy and cutting speed) to improve the cut quality (fibre pull out, taper angle and material remover rate) in nano-second pulsed DPSS Nd:YAG laser cutting of CFRP composites with mixed reactive and inert gases. Negarestani et al. [132] also implemented statistical analysis based on RSM to optimise the process parameters during fibre laser cutting of carbon fibre reinforced polymeric composites.

In addition to using lasers to cut and drill CFRP, lasers have also been recently used in the repair of CFRP due their contactless machining capability and tool wear free compared to conventional milling and grinding processes. Fischer et al. [141] used a UV laser source for scarf repair of CFRP materials. They showed that it is possible to remove the damaged materials layer-by layer and generate a cavity of repair plies with a high scanning speed (up to 2 m/s). Völkermeyer et al. [142] described the use of a UV laser for the bonded repair of CFRP parts. They discussed the effect of hatch distance and number of cycles on the ablation depth and throughput. Moreover, they conducted shear strength tests and demonstrated high strengths of repaired parts with a significant drop in process time compared with mechanical processes.

4.3.4 Laser drilling techniques

The commonly used laser drilling techniques include single pulse drilling, percussion drilling, trepanning and helical drilling as shown in Figure 4.16. In single pulse drilling the hole is drilled by applying a high energy single pulse on a stationary workpiece. The

hole size is controlled by the input energy and by adjusting the spot position. Whereas, multiple laser pulses are used in percussion drilling which can improve the hole geometry compared to single pulse drilling [74]. The trepanning technique involves first piercing a hole through percussion drilling followed by moving the part or moving the laser receptively along the outer periphery of the hole geometry. In the trepanning method, piercing is necessary to reduce the thermal damage at the hole edge. The helical drilling technique involves moving the workpiece or the laser by tracking a helical path in which the materials are removed slowly with many spiral passes without the initial piercing. The use of single trepanning technique with CFRP composite was found to be only applicable with thin samples (up to 0.3 mm). For machining 1 mm thickness or above, the narrow kerf produced prevents the ablated material to escape from the machined zone. Also it produces heat accumulation and large thermal damage [143].

Li et al. [36] introduced a multi parallel ring technique (Figure 4.17) to overcome the drawbacks of single trepanning. This technique enlarges the kerf width and allows for the plume, plasma and fragmented fibres to escape from the machined area allowing the laser beam to reach the internal region and enhance the processing rate. Takahashi et al. [144] investigated the use of multi traces in disk laser cutting CFRP composites. They concluded that the distance between the traces and the scanning speed have a significant effect on the cutting quality and the processing rate. Herzog et al. recently investigated experimentally the use of parallel passes to avoid shadowing effect during cutting high thickness of carbon fibre reinforced plastics using a high-power Yb:YAG continuous wave disc laser [145]. So far, little is known on the specific self-limiting behaviour of picosecond laser machining and the role of single and multiple parallel passes on machining efficiency.

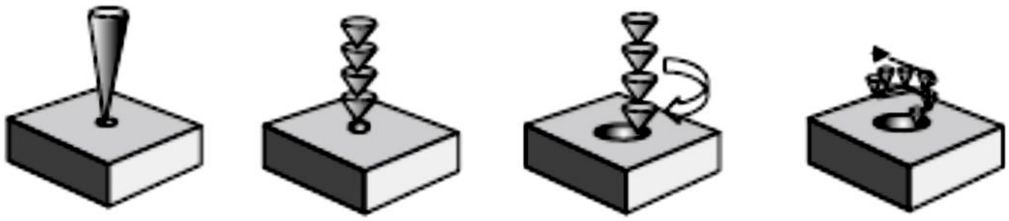

Single pulse percussion trepanning Helical trepanning

Figure 4.16 Laser drilling techniques [74]

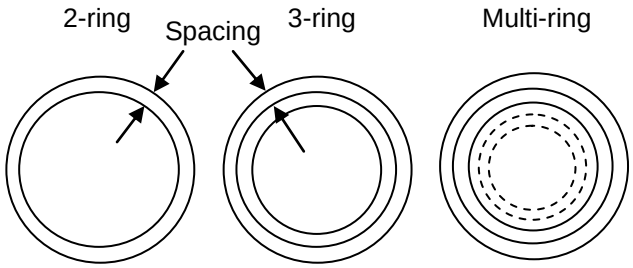

Figure 4.17 Sketch of laser beam scanning trace [36, 146]

4.4 Summary

The large differences in physical and thermal properties of the carbon fibre reinforced polymer composite constituents make laser machining of this material challenging. An extended heat affected zone (HAZ) often occurs. Eliminating the HAZ is a major challenge in laser processing of CFRP. Various studies have been conducted using different types of lasers such as CO2, Nd:YAG, excimer and fibre lasers in order to investigate the effect of different process parameters in laser processing of CFRP composites. Among these parameters; laser power, light wavelength, laser material interaction time and material properties and structure are the most significant parameters that affect the cutting quality. Shortening laser material interaction time using short pulse duration lasers, such as picosecond lasers, can improve cut quality and minimise HAZ. Due to their contactless machining capability and being free of tool wear the laser was introduced recently as new tool for CFRP composites repair. Multi ring machining introduced for laser machining of CFRP enabled improving the machining quality and enhancing the processing rate (HAZ <10 μm). Self-limiting behaviour of picosecond laser machining and the role of single and multiple parallel passes on machining efficiency need to be investigated.

CHAPTER 5 TEA CO_2 LASER MACHINING OF CFRP COMPOSITE

5.1 Introduction

In previous studies, Nd:YAG, diode pumped solid state (DPSS), CO_2 (continuous wave), disk and fibre lasers were used in cutting CFRP composites but the control of damage such as the size of heat affected zones (HAZ) remains a challenge. In this chapter, a short pulsed (8 μs) transversely excited atmospheric pressure (TEA) CO_2 laser was used, for the first time, to machine CFRP composites. Except machining of CFRP, the TEA CO_2 laser has been used in different fields of applications such as medical surgery [147], laser material processing such as paint stripping [148-150] and in non- destructive testing of composite materials in aerospace industry [151]. In contrast, considerable research work using other laser sources has been performed to investigate the laser processing of CFRP composite. A TEA CO_2 laser is a short pulsed gas laser operating with a CO_2, N_2 and He gas mixture at high pressures (1 atm or above) [75, 152] and produces higher peak powers (> 100 kW) in short pulses. The combination of high peak powers, short interaction time and good absorption of CO_2 wavelength by both matrix and fibres allows better coupling of the laser energy into the material, thus the heat damage could be reduced [7]. Design of experiment (DOE) and statistical modelling, based on response surface methodology (RSM), was also used in this chapter to understand the interactions between the process parameters such as laser fluence, repetition rate and cutting speed and their effects on the cut quality characteristics including size of HAZ, machining depth and material removal rate (MRR). Based on this study, process parameter optimisation was carried out to minimise the HAZ and maximise the material removal rate. A discussion is given on the potential applications and comparisons to other lasers in machining CFRP.

5.2 Experimental Methods

5.2.1 Design of experiments

Design Expert® software package version 7.0.0 created for Windows by Stat-Ease, Inc. was used in this work for the experimental design using response surface methodology based on central composite design to show the effect of combinations of factors on behaviour of process responses and to develop mathematical models which relate the input laser variables (laser fluence, repetition rate and scanning speed) with the output responses (cross sectional heat affected zone, machining depth and material removal rate). Table 5.1 shows the input laser variables used and their levels. Six replications of centre runs were used for accurate estimation of the overall process errors .The selection of these operating parameter ranges was based on initial screening experiment to enable CFRP machining to take place.

Table 5.1 Process variables and their levels.

Symbol	Variable	Level 1	Level 2	Level 3	Level 4	Level 5
A	Fluence [J/cm²]	60	69	83	96	105
B	Repetition rate [Hz]	37	60	94	127	150
C	Speed [mm/s]	20	35	58	80	95

5.2.2 Experimental procedure and materials

The laser cutting experiments was performed using Lumonics Impact 3150 HP TEA CO_2 laser system. The laser system specifications are listed in Table 5.2. The laser beam was delivered to the work piece by means of mirrors and focusing optics. An Aerotech

Table 5.2 TEA CO_2 laser system specifications.

Parameters	**Specifications**
Operating mode	Pulsed
Wavelength	10.6 µm
Maximum average power	300 W
Maximum pulse energy	2 J
Pulse Repetition Rate	up to 150 Hz
Pulse length	8 µs, FWHM
Focal length	200 mm

computer-controlled X-Y CNC stage was used to traverse the workpieces. A multiple pass strategy was used during the machining. The schematic diagram of experimental setup is shown in Figure 5.1. The TEA CO_2 laser beam profile shown in figure 5.2 was produced by pointing the laser beam toward a Perspex block. A 3D imaging function of Keyence digital microscope then used to visualize the profile. A square objective mask was used to select a uniform part of the laser beam and obtain beam spot with sharp edges (Figure. 5.2b). A rectangular beam spot size of 0.9 mm by 0.9 mm obtained by passing the laser through a focussing lens (focal length 200 mm) was used. The workpiece materials used for the studies were woven CFRP composite (Figure. 5.3a) of 80 mm long, 20 mm wide and 1.5 mm thick. The carbon fibre volume fraction was 55% and the matrix was epoxy resin. Experiments were performed to study the effect of laser process parameters, i.e. laser fluence, repetition rate and scanning speed on cross section HAZ, machining depth and material removal rate. Each data point for all experimental responses was obtained by averaging the measured results for three measuring places along the length of laser machining.

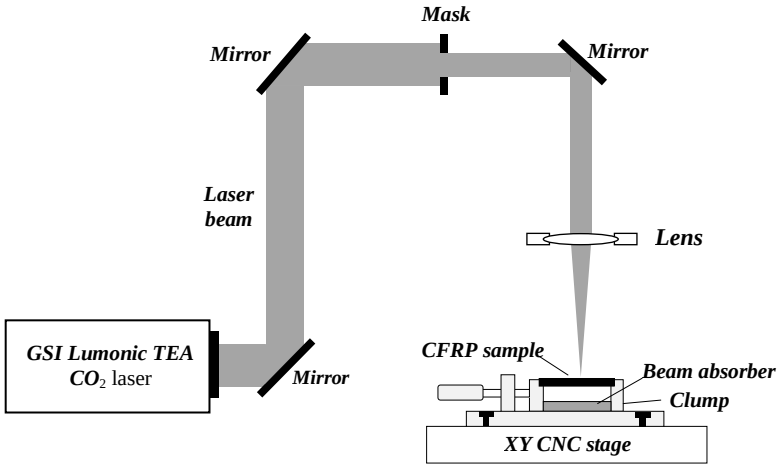

Figure 5.1 Schematic diagram of experimental setup.

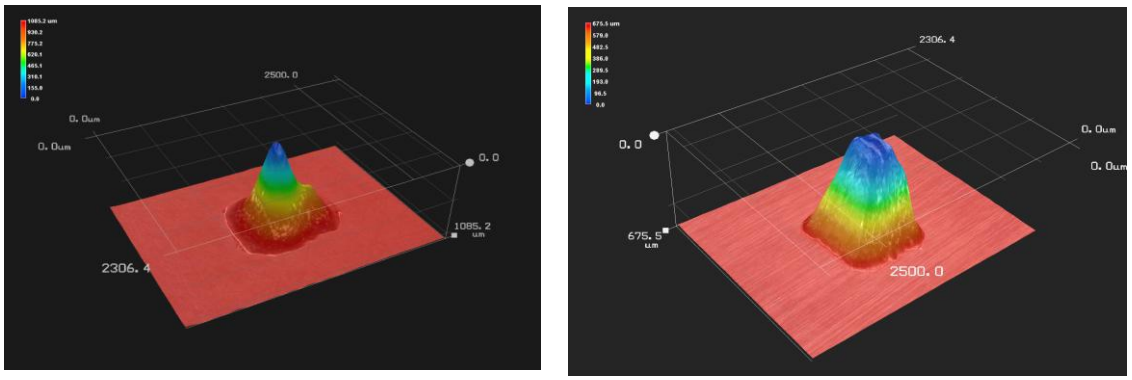

(a) (b)

Figure 5.2 TEA CO2 laser beam profile burned in a Perspex block; (a) without projective mask, (b) with projective mask.

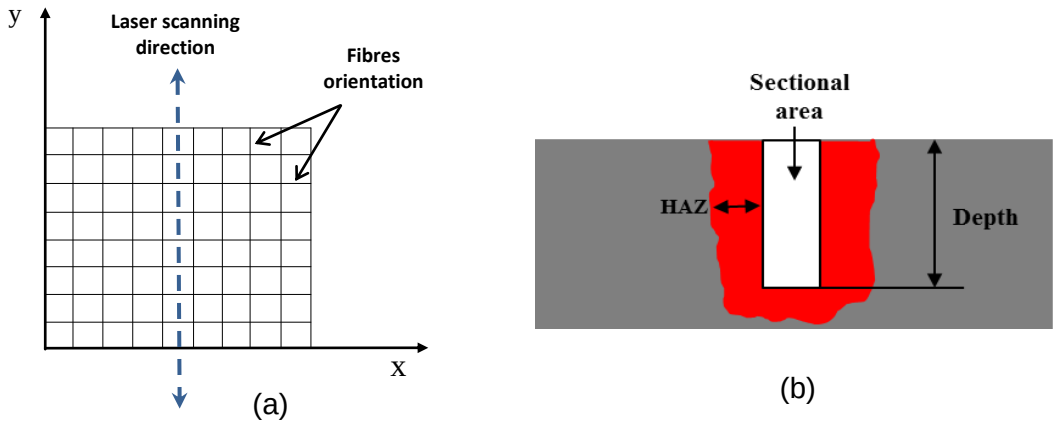

(a) (b)

Figure 5.3 Schematic view of (a) laser beam scanning direction and fibres orientation, (b) quality features of laser machined sample.

The size of the cross section HAZ (Figure. 5.3b), the ablation depth and laser machining quality were studied using digital optical microscopy. The ablation depth was measured from the cross sectional views. The material removal rate was calculated using:

$$\text{MRR} = \frac{\text{Removed volume (mm}^3\text{)}}{\text{Process time (min)}} \tag{5-1}$$

$$= \frac{al}{\frac{nl}{v}} = \frac{av}{n}$$

Where, a is measured cross section area in mm², l is machined length in mm, v is scanning speed in mm/min and n is number of machining passes.

5.3 Results

The effect of the number of laser pulses impinging on the CFRP sample surface for three different laser fluences within low, intermediate and high range is shown in Figure 5.4. A linear response of the ablation depth for an increasing of number of pulses can be clearly seen. The average ablation depth increased with the increase in the laser fluence, as expected. The ablation depth varied from 1.4 µm/pulse at low fluence (around 10 J/cm^2) to 8.3 µm/pulse at a high fluence (around 100 J/cm^2). The dependence of ablation rate on the laser fluence is shown in Figure 5.5. The R^2 and y in Figure 5.4 and Figure 5.5 are correlation coefficient and response variable (depth or ablation rate) respectively. A threshold fluence of 3.2 J/cm^2 , an effective absorption coefficient of 0.46 µm^{-1} and thermal loading of 14703 kJ/cm^3 were determined using curve fitting and Eqs. (5.2) and (5.3) [153].

$$d = \frac{1}{\alpha} \ln\left(\frac{F}{F_{th}}\right) \tag{5-2}$$

Where d the ablation depth α the effective absorption coefficient (cm^{-1}), F the laser fluence (energy density) and F_{th} the threshold fluence. Using curve fitting α and the threshold fluence can be calculated. Moreover, the thermal loading γ (J/cm^3) of the CFRP can be calculated by:

$$\gamma = F_{th} . \alpha \tag{5-3}$$

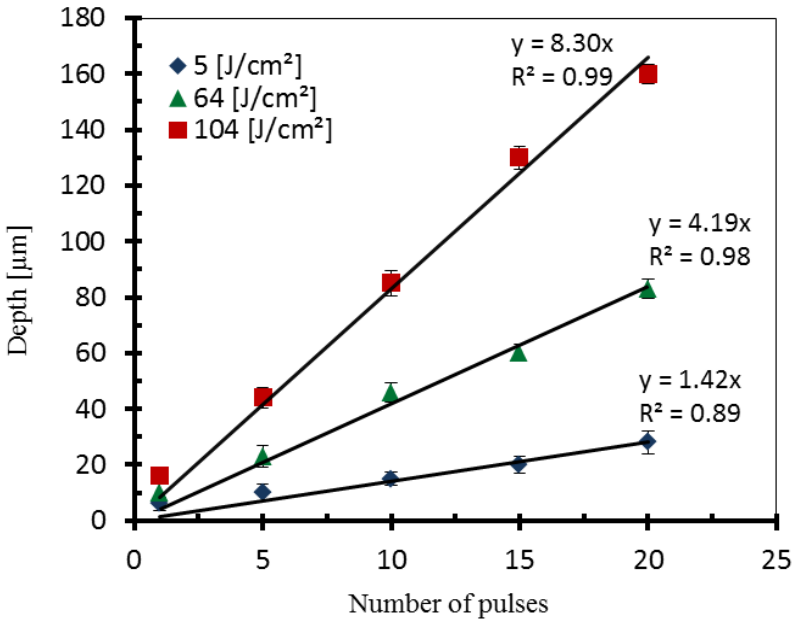

Figure 5.4 Effect of number laser pulses on the CFRP ablation depth for three different laser fluencies.

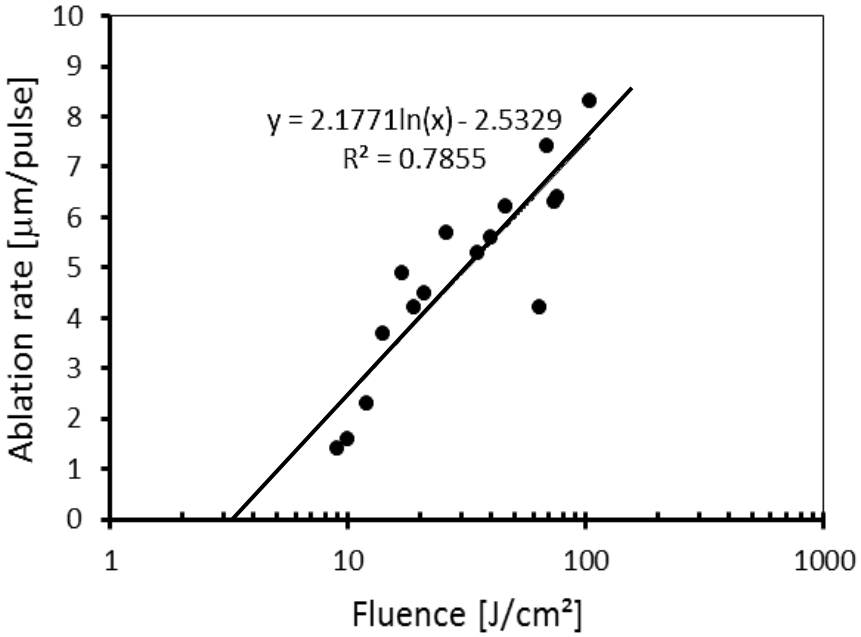

Figure 5.5 Ablation rate dependence on laser fluence.

5.3.1 Statistical models

The design matrix of process variables and the results obtained in this work are shown in Table 5.3. Statistical empirical models with the best fit for the measured responses (cross sectional HAZ, machining depth, and MRR) were developed. To obtain the best fit models, the suitability of proposed models were tested according to f-value, lack of fit and ANOVA (Tables 5.4- 5.6). The f-value for a model is a comparative test between the term variance and the residual variance. It is the Mean Square for the term divided by the Mean Square for the Residual. The Prob>f value of less than 0.05 for the model shows that the model terms are statistically significant and values greater than 0.1 indicate that the model terms are not significant. Also the fitness of the developed models was examined by the regression coefficient $\acute{R}^2$ and adjusted $\acute{R}^2$ [140]. These values indicate the suitability of the RSM models. The models are more accurate if these values are closer to one. The $\acute{R}^2$ is the ratio of squares of the model to the sum of squares of the total. The adjusted $\acute{R}^2$ was calculated according to Eq. (5-4) [140].

$$\acute{R}^2{}_{\text{adj}} = \left(\frac{\acute{n}-1}{\acute{n}-p}\right)\left(1-\acute{R}^2\right) \tag{5-4}$$

Where, $\acute{n}$ is the number of experiments and p is the number of model parameters. In addition, the models of the responses were analysed by the normal plot of residuals and the residuals as a function of predicted chart (Figure 5.6) to ensure the model suitability [154]. It can be seen in Figure 5.6 that the points follow a normal distribution and the points are scattered about the reference line. In order to optimize the response (η_r) and to analyse relationship between the response and the input variables (x_i and x_j) the general second-order polynomial Eq. (5-5) is usually used in RSM [155].

$$\eta_r = b_0 + \sum_{j=1}^{\acute{n}} b_j x_j + \sum_{j=1}^{\acute{n}} b_{jj} x_j^2 + \sum\sum_{i<j} b_{ij}\, x_i x_j \tag{5-5}$$

Where, b_0 is the responses at the centre point and b_i, b_{jj}, b_{ij} are the coefficients of linear, quadratic and interaction factors respectively.

The ANOVA Tables 5.4-5.6 for cross sectional HAZ, machining depth and MRR summarize the significant variables and the adequacy measures $\acute{R}^2$, adjusted $\acute{R}^2$ and predicted $\acute{R}^2$. The ANOVA analysis tables show that the response models are significance and the lack of fit is insignificant. In addition, the "Adeq Precision" value which measures the signal to noise ratio indicates an adequate signal and the model can navigate the design space. A ratio greater than 4 is desirable. Therefore, the developed empirical models of cross sectional HAZ, machining depth and MRR in terms of actual factors are shown in Eqs. (5-6) – (5-8) below.

$$\text{Cross sectional HAZ} = 16.27 + 0.09 \times A + 0.31 \times B - 0.40 \times C - 1.69\times10^{-3} \times B^2 + 2.90\times10^{-3}\times C^2 \quad (5\text{-}6)$$

$$\text{Machining depth} = -0.04 + 0.09 \times A + 0.08 \times B - 0.12 \times C - 9.97\times10^{-4} \times A \times C - 6.63\times10^{-4} \times B \times C + 1.55 \times10^{-3} \times C^2 \quad (5\text{-}7)$$

$$\text{Material removal rate} = -7.03 + 0.10 \times A + 0.1 \times B + 4.44 \times10^{-3} \times C \quad (5\text{-}8)$$

Where *A*, *B* and *C* are fluence, repetition rate and scanning speed respectively (dimensions shown in Table 5.1).

Table 5.3 Design matrix of process variable and measured responses

Run	Variables			Responses		
	Fluence [J/cm²]	Repetition rate [Hz]	Speed [mm/s]	HAZ [µm]	Machining depth [µm]	MRR [mm³/min]
1	83	150	58	20	6.7	15
2	60	94	58	21	3.7	8
3	69	60	35	24	4.6	6
4	83	94	58	23	4.8	10
5	83	94	58	24	4.3	12
6	96	127	80	22	4.4	14
7	83	94	20	33	10.0	9
8	83	37	58	19	2.0	4
9	83	94	58	27	4.9	12
10	96	60	35	29	5.1	8
11	83	94	58	25	4.7	13
12	83	94	58	29	3.9	12
13	69	127	80	23	3.8	13
14	83	94	58	27	4.4	12
15	96	127	35	28	9.6	17
16	96	60	80	26	2.7	8
17	105	94	58	24	5.2	14
18	69	127	35	25	9.0	13
19	83	94	95	25	3.3	11
20	69	60	80	24	2.5	7

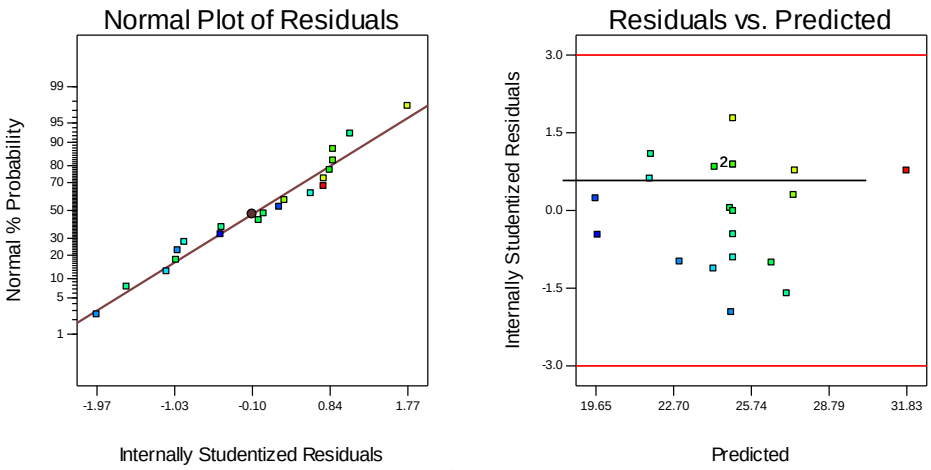

(a)

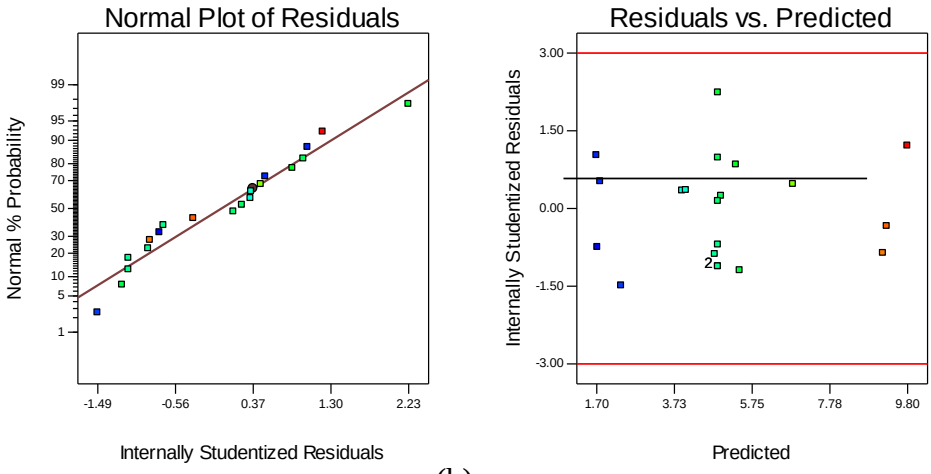

(b)

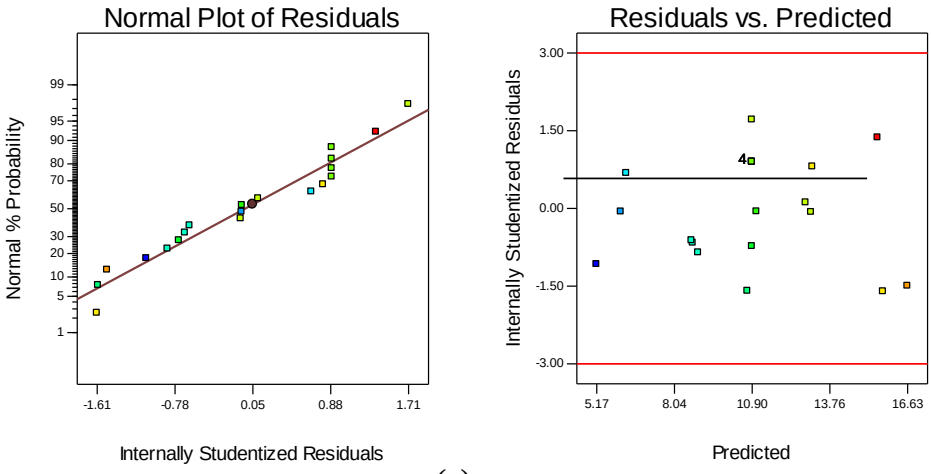

(c)

Figure 5.6 Diagnostic plots of normal plot of residuals and residual vs. predicted values for:(a) cross sectional HAZ, (b) machining depth and (c) MRR.

Table 5.4 ANOVA analysis for the cross sectional HAZ (df- degrees of freedom)

Source	Sum of squares	df	Mean squares	f-value	Prob>f	
Model	146.43	5	29.29	5.17	0.0068	Significant
A-Fluence	21.27	1	21.27	3.76	0.0731	
B-Repetition rate	7.4E-003	1	7.4E-003	1.3E-003	0.9717	
C-Speed	33.70	1	33.70	5.95	0.0286	
B^2	52.06	1	52.06	9.19	0.0090	
C^2	31.34	1	31.34	5.53	0.0338	
Residual	79.32	14	5.67			
Lack of Fit	54.48	9	6.05	1.22	0.4353	Not significant
Pure error	24.83	5	4.97			
Cor total	225.75	19				
Standard deviation = 2.38				$\acute{R}^2$ = 0.65		
Mean= 24.75				Adjusted $\acute{R}^2$ = 0.52		
Coefficient of variation = 9.62				Predicted $\acute{R}^2$ = 0.31		
Predicted residual error of sum of squares (PRESS) = 156.77				Adequate precision = 9.34		

Table 5.5 ANOVA analysis for the machining depth

Source	Sum of squares	df	Mean squares	f-value	Prob>f	
Model	89.44	6	14.91	205.78	< 0.0001	Significant
A-Fluence	2.62	1	2.62	36.22	< 0.0001	
B-Repetition rate	22.95	1	22.95	316.82	< 0.0001	
C-Speed	52.08	1	52.08	718.83	< 0.0001	
AC	0.72	1	0.72	9.94	0.0076	
BC	2.00	1	2.00	27.61	0.0002	
C^2	9.07	1	9.07	125.24	< 0.0001	
Residual	0.94	13	0.07			
Lack of Fit	0.24	8	0.03	0.22	0.9722	Not significant
Pure error	0.70	5	0.14			
Cor total	90.39	19				
Standard deviation = 0.27				$\acute{R}^2$ = 0.99		
Mean= 4.99				Adjusted $\acute{R}^2$ = 0.98		
Coefficient of variation = 5.40				Predicted $\acute{R}^2$ = 0.98		
Predicted residual error of sum of squares (PRESS) = 1.59				Adequate precision= 48.28		

Table 5.6 ANOVA analysis for the material removal rate

Source	Sum of squares	df	Mean squares	f-value	Prob>f	
Model	182.29	2	91.14	60.74	< 0.0001	Significant
A-Fluence	23.96	1	23.96	15.97	0.0009	
B-Repetition rate	158.33	1	158.33	105.51	< 0.0001	
Residual	25.51	17	1.50			
Lack of Fit	20.68	12	1.72	1.78	0.2157	Not significant
Pure error	4.83	5	0.97			
Cor total	207.80	19				
Standard deviation = 1.22					$\acute{R}^2$ = 0.88	
Mean= 10.90					Adjusted $\acute{R}^2$ = 0.86	
Coefficient of variation = 11.24					Predicted $\acute{R}^2$ = 0.83	
Prted residual error of sum of squares (PRESS) = 34.86					Adeq precision = 24.14	

5.3.2 Effect of process parameters on the machining responses

The effect of laser machining parameters and their interactions on the machining responses are presented in this section by considering perturbation graphs and 3D response surfaces for all responses.

5.3.2.1 Cross sectional HAZ

Figure 5.7 is the perturbation plot that shows the effect of process parameters on the cross sectional HAZ. It is apparent from this plot that the scanning speed is the most significant factor for HAZ. An increase in scanning speed can lead to a reduction of HAZ. It can also be observed from this Figure that an increase of laser fluence increases the HAZ. The plot also shows minimum HAZ at low and high repetition rates. The relationships between all these process parameters are provided in Figure 5.8. The values of cross sectional HAZ range from 19–29 μm. It is clearly seen in Figure 5.8a, 5.8b, and 5.8d that, reducing the laser fluence and increasing the scanning speed reduce the HAZ. The HAZ was minimum at lowest and highest repetition rate whereas at middle value it was maximum. Figure 5.9 and Figure 5.10 show the microscopic observations of the effect of lowest and highest values of process variables on cross

sectional and top surface HAZ respectively. They show tapered cross section, irregular walls shape and top surface burn.

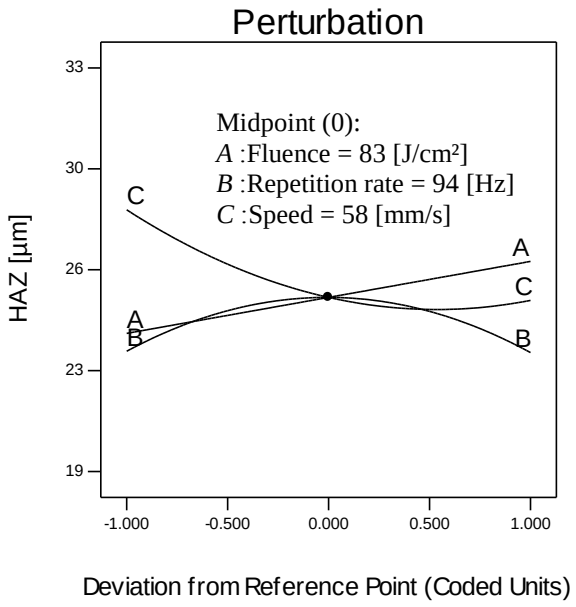

Figure 5.7 Perturbation plot of effect of parameters on the cross sectional HAZ.

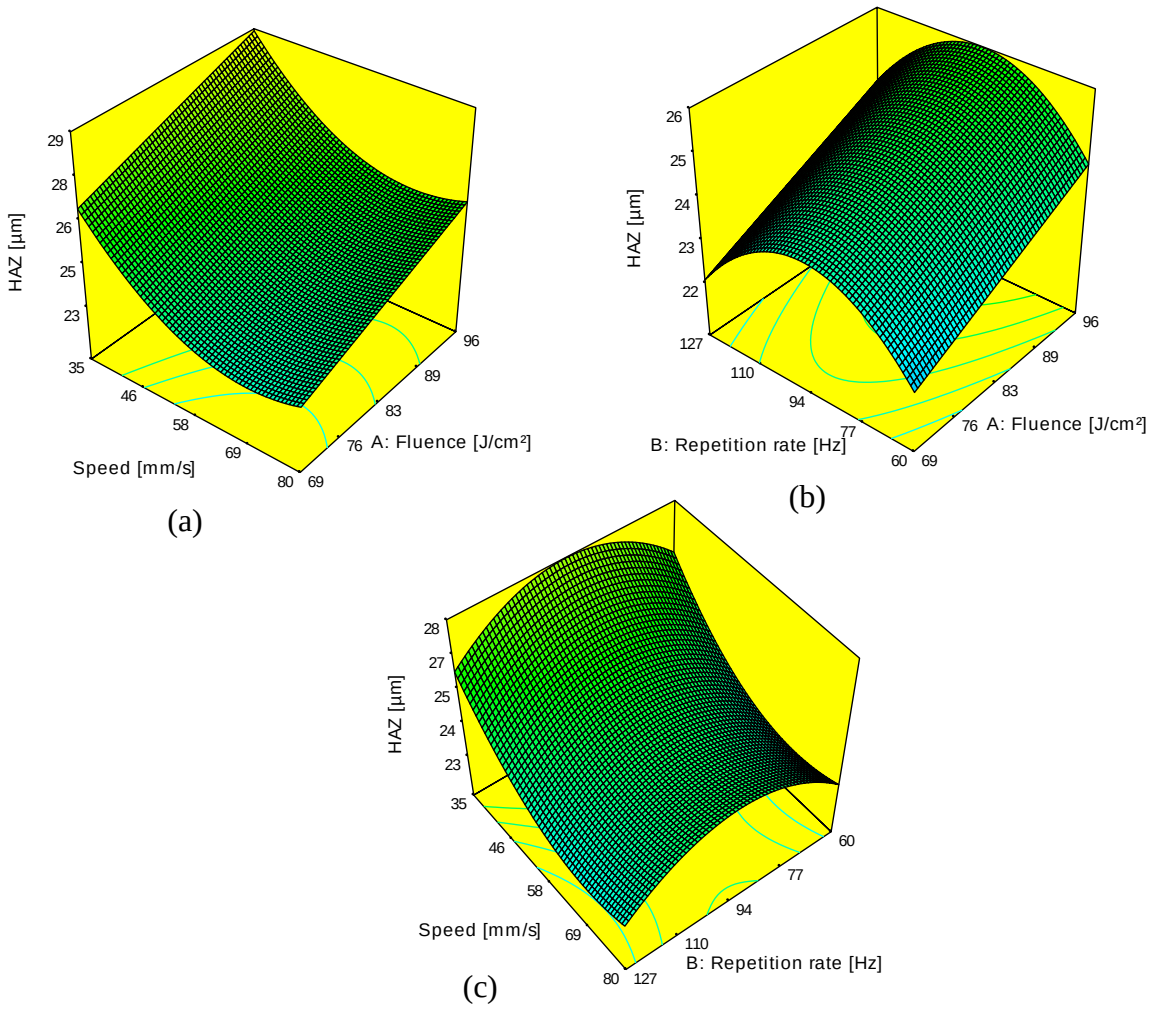

Figure 5.8 Surfaces response graphs of cross sectional HAZ model; (a) speed – fluence, (b) repetition rate – fluence, (c) speed – repetition rate.

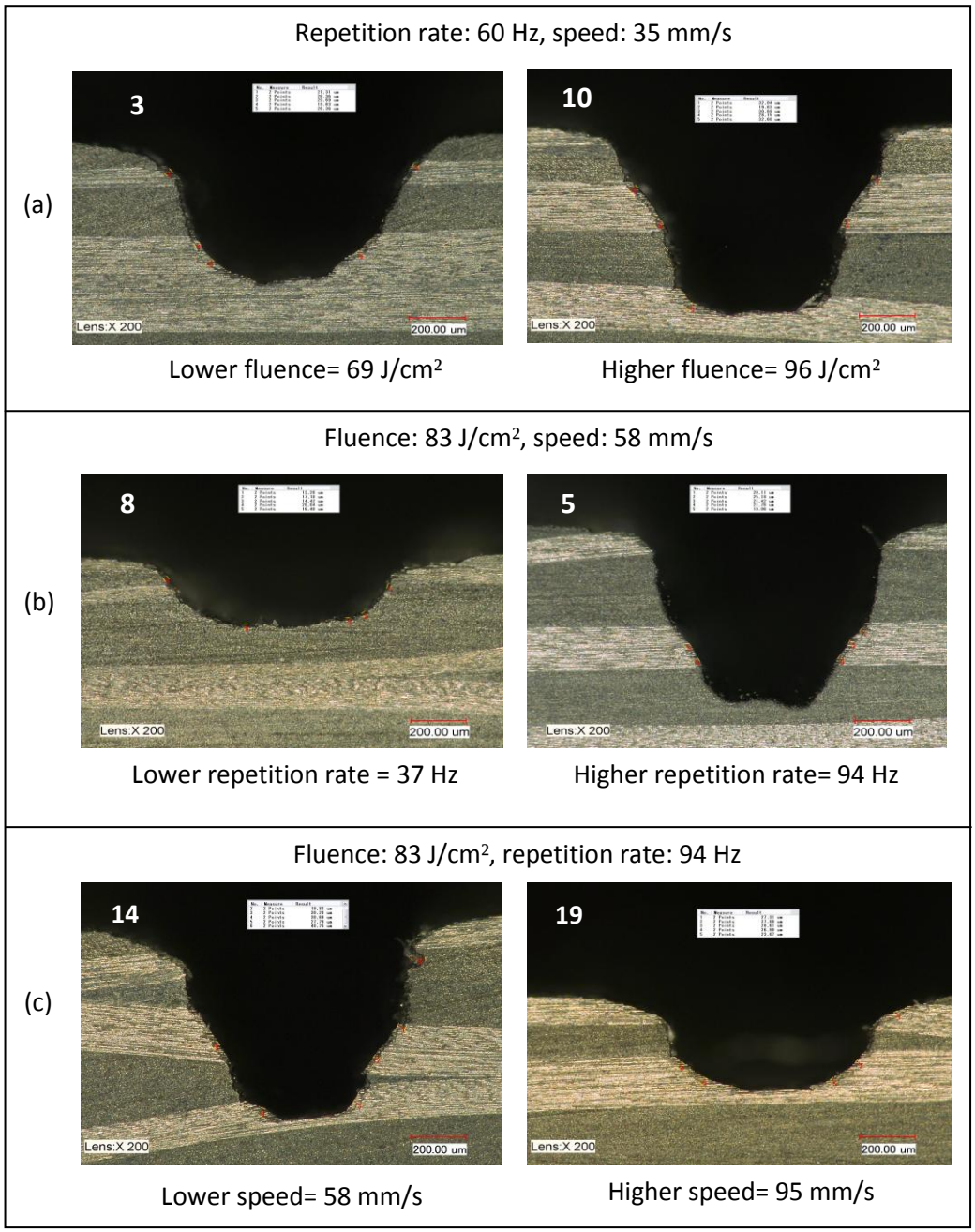

Figure 5.9 Microscopic observations of cross sectional view showing the effect of process parameters on cross sectional HAZ; (a) fluence effect, (b) repetition rate effect, (c) speed effect. The number on each Figure indicates the run number.

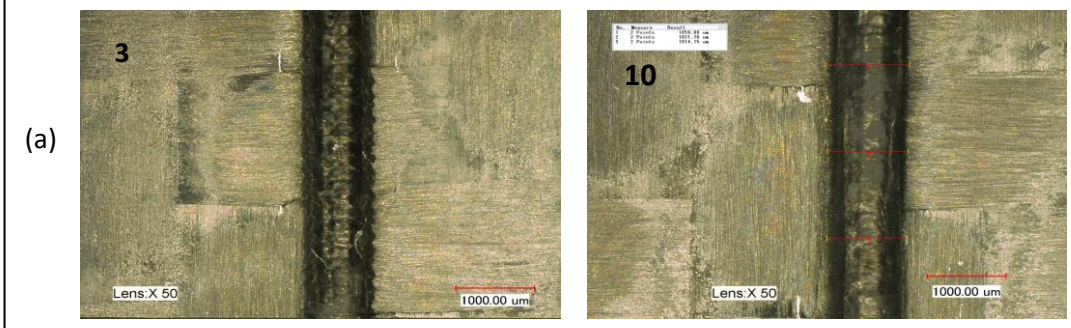

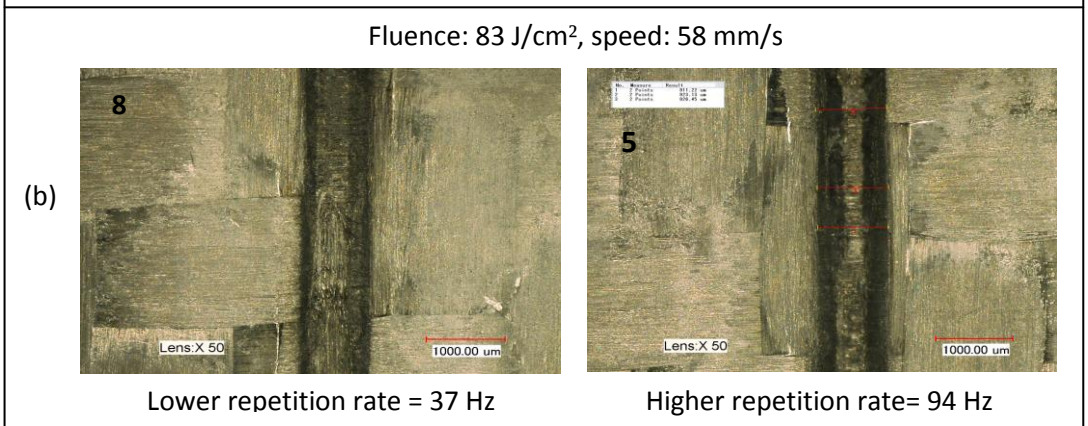

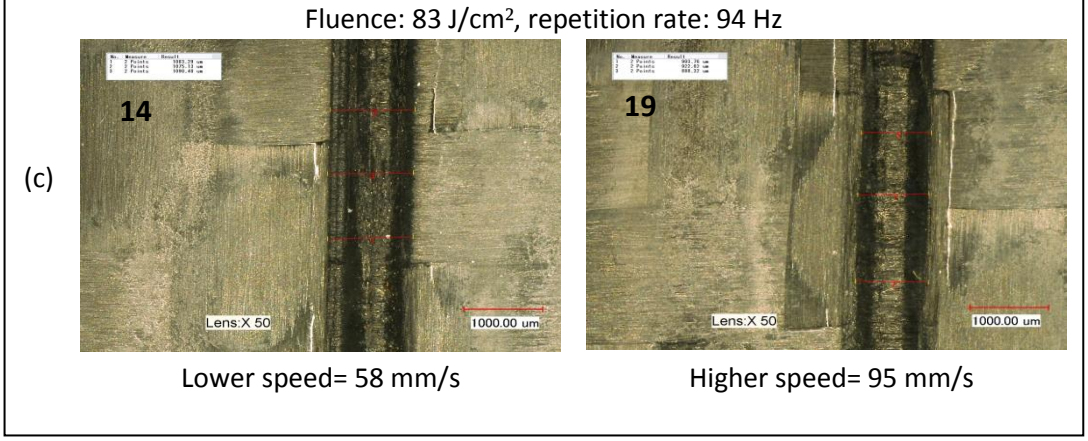

Figure 5.10 Microscopic observations of top surface view showing the effect of process parameters on top surface HAZ; (a) fluence effect, (b) repetition rate effect,(c) speed effect. The number on each Figure indicates the run number.

5.3.2.2 Machining depth

The perturbation plot in Figure 5.11 shows the effect of laser parameters on machining depth. It shows that the scanning speed has the most significant effect on the machining depth. It is also observed that the machining depth increases by increasing the fluence and repetition rate, while decreasing with increases in the scanning speed. The response surface graphs presented in Figure 5.12 show the effect of parameter interactions on the machining depth. It can be seen that the repetition rate and scanning speed interactions have a significant effect in which the highest machining depth can be obtained at a high repetition rate and a low scanning speed (Figure 5.12c), also it is seen in Figure 5.12a and 5.12b that the increase of laser fluence increases the machining depth. The effect of extreme values (low/high) of the process parameters on machining depth response is shown in Figure 5.13.

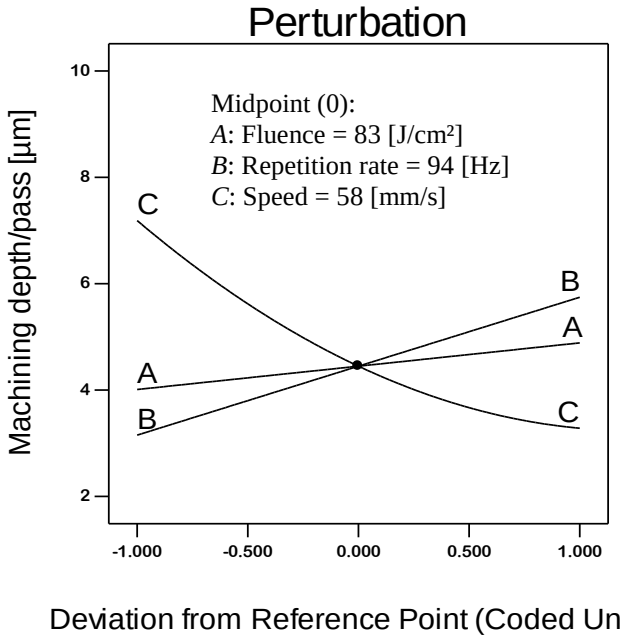

Figure 5.11 Perturbation plot of effect of parameters on the machining depth.

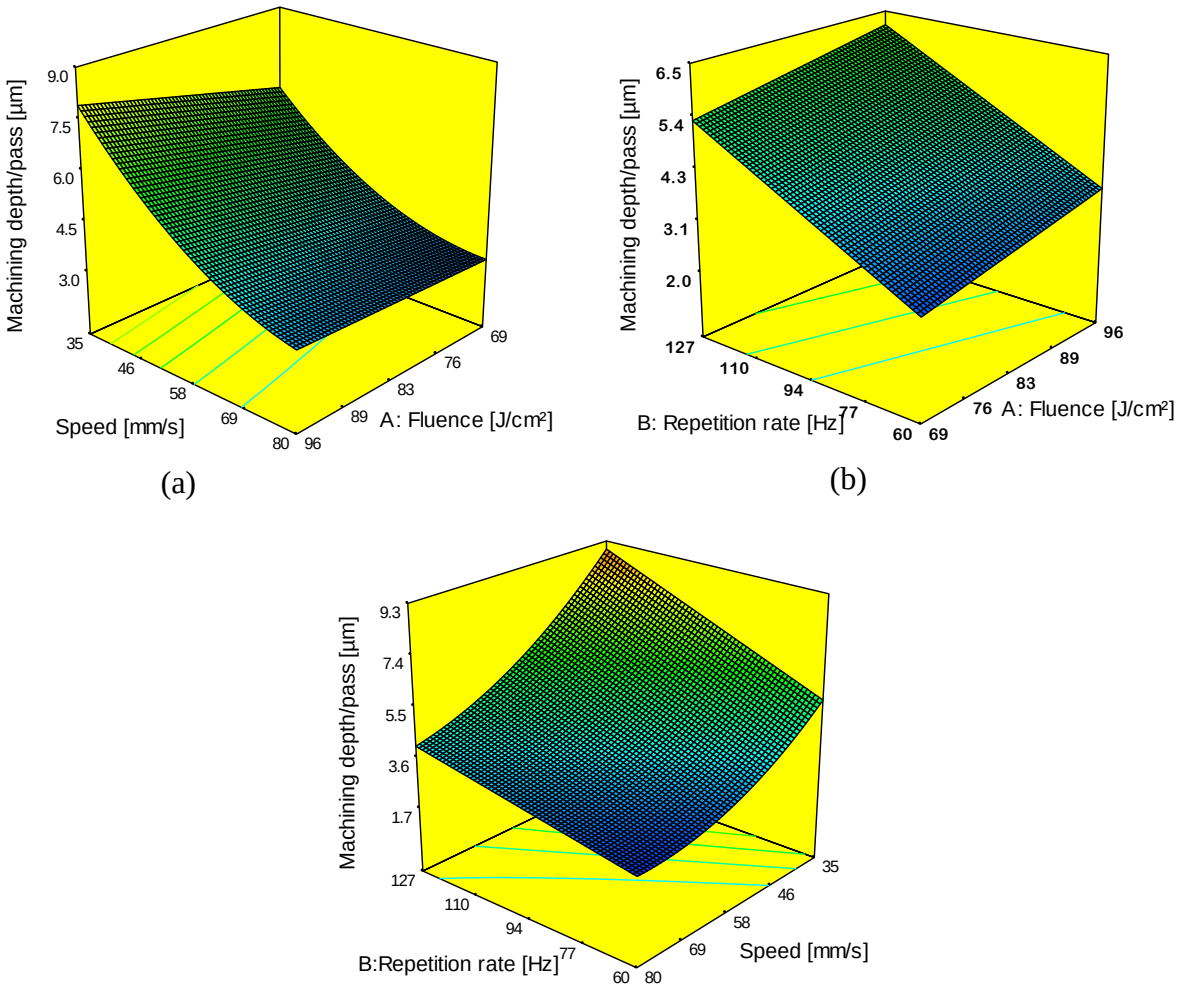

Figure 5.12 Surfaces responses graph of the machining depth model; (a) speed – fluence, (b) repetition rate – fluence, (c) repetition rate – speed.

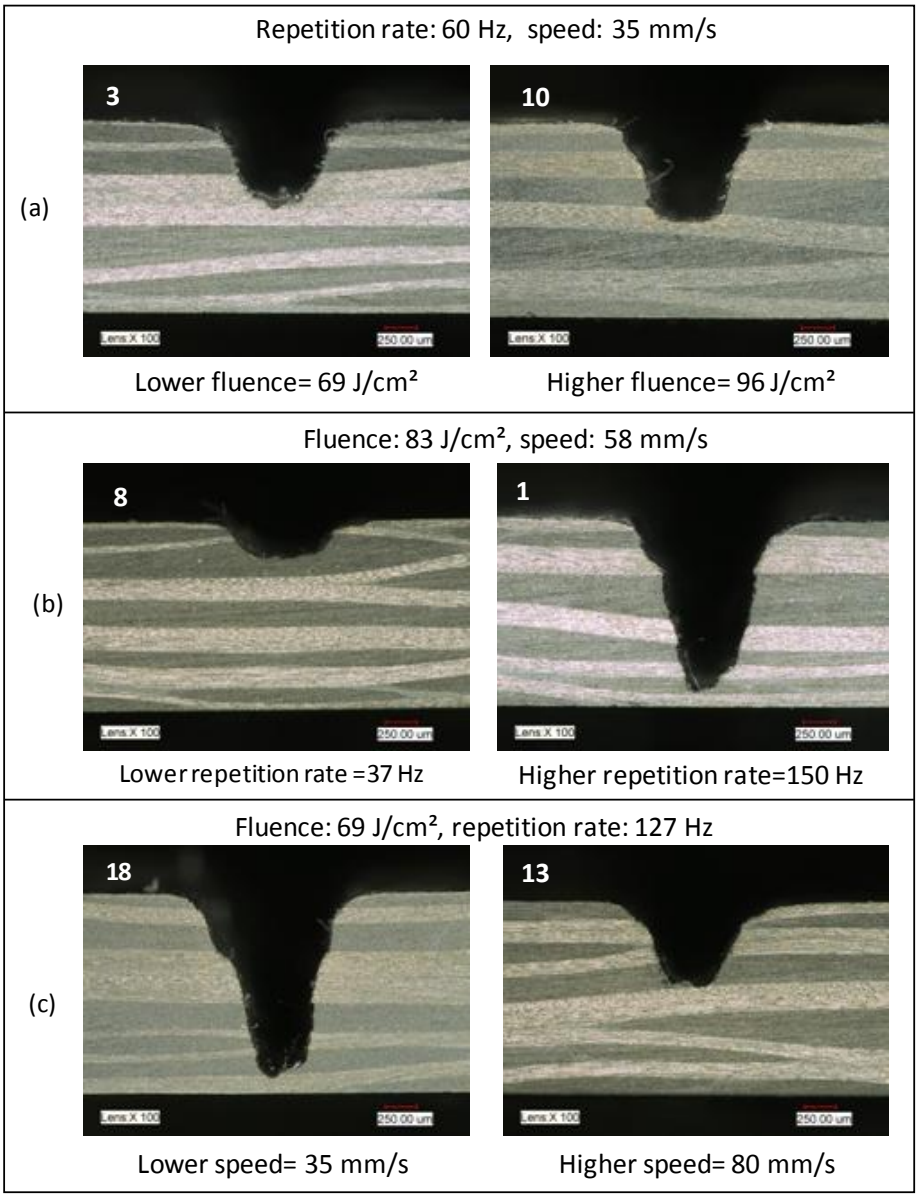

Figure 5.13 Microscopic observation of cross sectional view showing the effect of process parameters on machining depth; (a) fluence effect, (b) repetition rate effect, (c) speed effect. The number on each Figure indicates the run number.

5.3.2.3 Material removal rate

Figure 5.14 is a perturbation plot that shows the effect of laser fluence, repetition rate and scanning speed on MRR. It is observed that the repetition rate is the most effective parameter on MRR due to the high energy deposited per unit length at high repetition rate. The plot shows that the scanning speed has less effect on MRR compared with the other two parameters. The 3D surface response diagram in Figure 5.15 shows the effect of parameter interactions on material removal rate. The MRR can be improved by increasing the repetition rate and laser fluence in Figure 5.15a. Also observed in Figure 5.15b and 5.15c is that the scanning speed has less effect on the MRR.

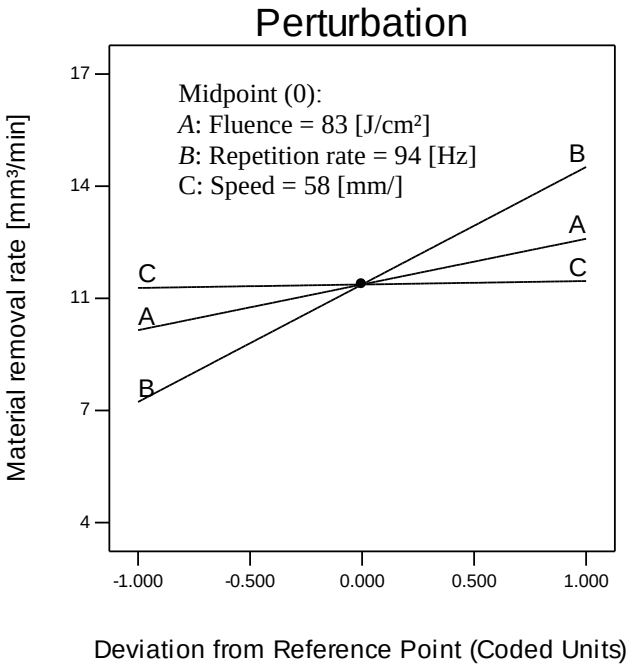

Figure 5.14 Perturbation plot of effect of parameters on the material removal rate.

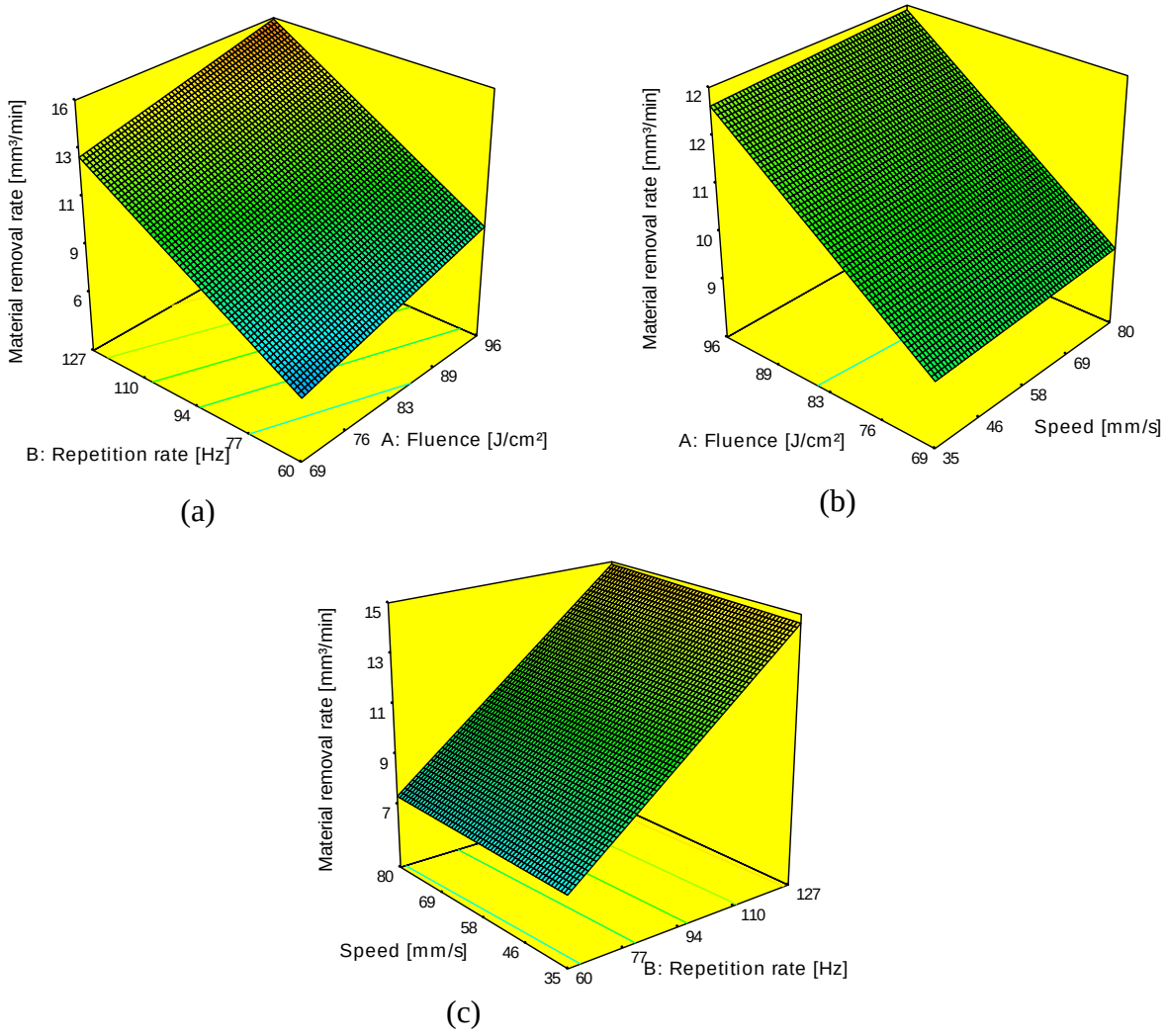

Figure 5.15 Surfaces response graphs of material removal rate model (a) repetition rate fluence, (b) fluence – speed, (c) speed – repetition rate.

5.3.3 Optimisation

The optimization of the responses was performed using numerical and graphical optimisation by choosing the preferred goals for each variable and response. The statistical optimisation was performed based on the desirability function. The desirability function (Eq. 5-9) is the geometric mean of individual desirability ranging from zero for undesirable value to one for highest desirable value [154] .

$$\xi = \left(\prod_{i=1}^{ń} d_i \right)^{\frac{1}{ń}} \tag{5-9}$$

Where ξ is the overall desirability, ń is the number of responses and d_i is the i_{th} response desirability value. The proposed solutions have the highest desirability depending on the responses obtained from the experiments. The desirability value d_i of individual responses is calculated as [156]:

$$d_i = \begin{cases} \left[\frac{ý - A}{B - A}\right]^s & , A \leq ý \leq B \\ \left[\frac{ý - C}{B - C}\right]^t & , B \leq ý \leq C \end{cases} \tag{5-10}$$

Where *ý* is the predicted response value; *A*, *B*, and *C* are minimum, target, and maximum response values respectively; *s* and *t* are exponents that qualify the proximity of responses to the target value. The desirability varies from 0 to 1 according to the goal options (i.e. none, minimum, maximum, in range or target) and the response value *ý*, d_i=1 if the response value equals the target *B*, d_i=0 if the response value less than minimum value *A* and $0<d_i>1$ if the response value varies from minimum value *A* to maximum value *C*. The first part of Eq. (5-10) is used if the maximised response is needed whereas second part is used for minimization. The numerical optimisation condition for all variables and responses are shown in Table 5.7 and the optimum numerical solution is shown in Table 5.8. The requirements in this work are to minimise cross sectional HAZ, maximise machining depth and maximise the material removal rate. The highest importance was given to minimising the cross sectional HAZ. The optimised operating window is shown in Figure 5.16. The shaded region in the overlay plots is the region of the optimal working conditions that allow for selection of the optimum machining parameters. The overlay plot of graphical optimization is practically helpful for rapid determination of a process window among the numerous laser parameters values to achieve the required responses.

Table 5.7 Numerical optimization condition

Variable and response	Goal	Lower limit	Upper limit	Importance
Fluence [J/cm²]	In range	69	105	3
Repetition rate [Hz]	In range	60	127	3
Speed [mm/s]	In range	35	95	3
HAZ [µm]	Minimize	19	33	5
Machining depth [µm]	Maximize	1.6	10	3
Material removal rate [mm³/min]	Maximize	4	17	3

Table 5.8 Optimum Numerical solution

NO	Fluence [J/cm²]	Repetition rate [Hz]	Speed [mm/s]	HAZ [µm]	Machining depth [µm]	Material removal rate [mm³/min]	Desirability
1	69	127	46	23	6.5	13	0.70

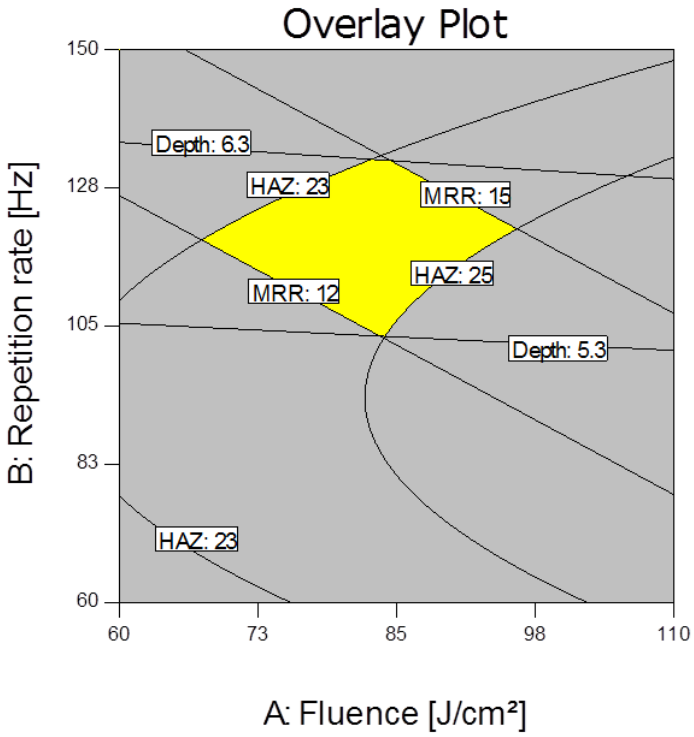

Figure 5.16 Overlay plot shows the optimal working region where the yellow zone is the optimized process window. The HAZ plotted is the cross sectional HAZ.

5.3.3.1 Optimum parameter validation

The predicted optimum numerical solution was validated experimentally. The average of three measured results were calculated and compared with predicted results. The standard deviations were considered as a measure of uncertainty. The statistical empirical models were compared with experimental results and the deviations were 1 µm for cross sectional HAZ, 0.2 µm for the machining depth and 1 mm^3/min for the material removal rate as shown in Table 5.9. The validation results show that the models developed are accurate and the deviation were in acceptable range. The microscopic observation of the quality of the machined sample using the optimum numerical solutions is shown in Figure 5.17.

Table 5.9 Predicted values, experimental values and the deviation

Responses	HAZ [µm]	Machining depth [µm]	Material removal rate [mm^3/min]
Predicted results	23	6.5	13
Experimental results	21±4	5.8±0.3	11±0.4
Deviation	1	0.2	1

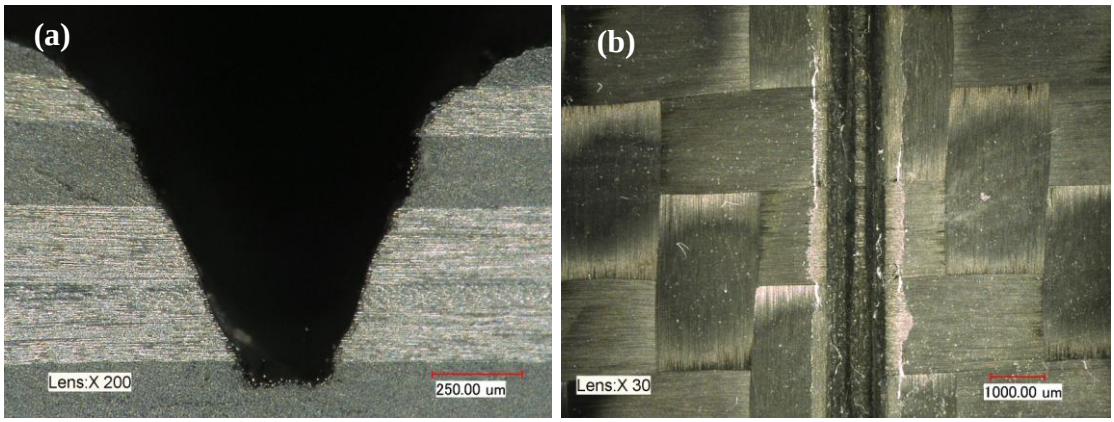

Figure 5.17 Microscopic observation of the machined sample for optimum solution; (a) cross sectional view, (b) Top surface view, plastic sacrificial mask used.

5.4 Discussion

The ANOVA results for cross sectional HAZ indicates that the fluence, *A*, the scanning speed, *C*, and the quadratic terms B^2 and C^2 are significant terms as shown in

Table 5.4. The increase of the heat input to the machining zone at high fluence results in a large HAZ. Moreover, reducing the scanning speed leads to long laser material interaction time and high pulse spot overlaps which create large HAZs. The higher the scanning speed, the less the energy input per unit length to the materials and hence lower is the HAZ. At low pulse repetition rates the pulse peak power is high enough to increase the machining ability, while giving time for the material to cool and therefore the material is removed with less heat spreading to the bulk materials. The reason for HAZ being reduced above a certain value of repetition rate can be attributed to the reduction in pulse energy as the repetition rate was increased [157]. Furthermore, the drop of peak power at higher repetition rate weakens the pulse and reduces the temperature on the machining zone [158].

Table 5.5 reveals that the fluence, repetition rate, scanning speed, the interaction between fluence and speed, the interaction between repetition rate and scanning speed, and the quadratic terms of scanning speed are the most significant terms affecting the machining depth. The effects of fluence, repetition rate and scanning speed in Figure 5.12 indicate that high machining depth can be obtained at low scanning speed and high fluence and repetition rate. This is believed to be due to long laser material interaction time at low a scanning speed and high energy deposited to the machine-ng zone due to large number of laser pulses.

The ANOVA of MRR (Table 5.6) indicates that repetition rates and laser fluences are significant terms, whereas the scanning speed has less effect compared to the repetition rate and fluence. The higher the repetition rate the higher the number of pluses deposited into the machining zone and hence enhances the removal rate of materials. The increase of laser fluence widens the machining cross section area and then improves the machining rate [2].

The microscopic observations of the cross sections in Figure 5.9 and Figure 5.13 show irregular shapes of the cross section. The difference in thermal properties between the carbon fibre and the epoxy matrix and the nature of the material composition (parallel and perpendicular fibre direction to laser motion) make the cross section not smooth. This could be attributed to the difference in thermal conductivity of the carbon fibre in axial and radial directions (higher in axial direction than radial) also to the low thermal conductivity of the matrix, i.e. 50 W/m.K for carbon fibre and 0.1 W/m.K for epoxy

[135]. In the areas where the fibres were parallel to the laser motion the kerf was wider. In these areas the heat conducted away along the fibres and acts to preheat the material ahead of the laser beam. This can enhance the energy existing in these areas, due to less heat conduction in the radial direction, and leads to more material removal, whereas, when the fibres were perpendicular to the laser motion the efficiency of the process reduced due to the loss of the generated heat from the machining zone by conducting away through fibres leading to reduction in the cross section [37].

In addition to the irregular cut section, the cross section views show taper walls of the cut in which the kerf width reduced as the machining depth increases. The reduction of the kerf width at the bottom could be due to the side wall absorption of the laser beam resulting in less laser energy at the kerf bottom thereby reducing the kerf width [159]. Moreover, the reduction of the laser energy absorbed by the material as the depth increases due to plasma/plume scattering of the laser beam and the reduction of energy density due to the laser beam divergence after the focal point is another reason for the tapering [2].

The top surface charring shown in Figure 5.10 is related to the nature of the surface (glossy surface) and beam shape (Figure 5.2) in which higher power density is at the beam centre and reduced away from the centre, also due to the plasma and ejected vapour generated which reheat the top surface and causes high thermal damage. On the contrary, little HAZ is shown at the middle of cross section along the fibre perpendicular to the cut path. This could be due to less heat localization. In Figure 5.17, some de-bonded fibres are shown at the bottom surface where the fibres direction is parallel to the cutting path. Referring to what was mentioned before, less laser energy reaching the kerf bottom and the localized heat at this region is enough to remove some of the carbon fibres but high enough to vaporize the epoxy matrix leaving some debonded fibres.

The improved quality obtained using the TEA CO_2 laser is attributable to the high absorptivity of the carbon fibres and the matrix to the CO_2 wavelength of 10.6 μm, where the laser radiations are absorbed simultaneously by both the carbon fibre and polymer making effective disintegration of polymer much more readily achieved. The advantage of that is that polymer can disintegrate more quickly. This makes the TEA CO_2 laser different from other lasers such as YAG (1064 nm) where the laser is only

absorbed by carbon fibre and is transparent to polymer, therefore it heats the carbon fibre and the heat is conducted from the carbon fibre to the polymer thus it is less effective and generates more heat-affected zone [7, 160]. Furthermore, the high peak power of the TEA CO_2 laser (250 kW) released on a short time results in rapid ablation of the CFRP composite leaving little time for the heat to propagate to the surrounding materials, and the cooling time between the pulses further improves the machining equality. Figure 5.18 compares and summarises the heat affected zone generation using laser cutting machining methods. It is clear from the Figure that, shorter pulses would enable better quality cutting for CFRPs. The current state of the art shows the capability of laser machining to achieve HAZ within tens of micrometres.

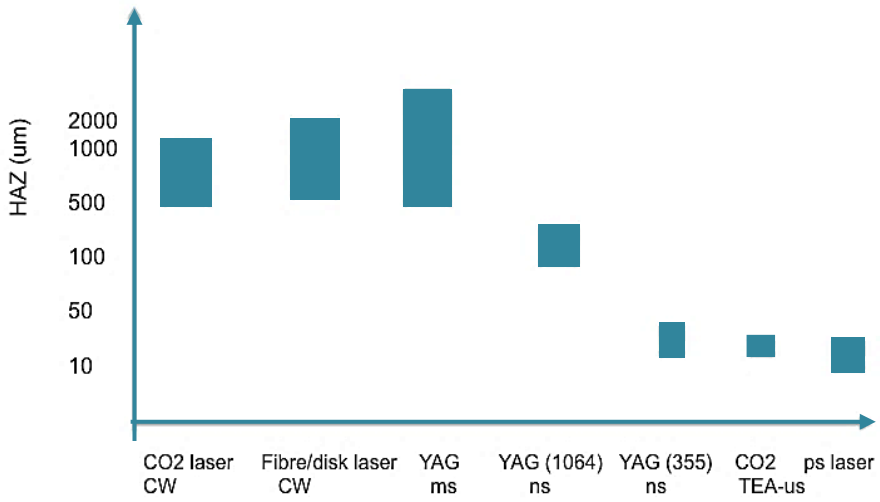

Figure 5.18 Comparison of the effect of different lasers and machining methods on HAZ (CW means continuous wave).

The TEA CO_2 laser machining of CFRP shows better quality and low machining rate than those obtained using continuous CO_2, fibre and Nd:YAG lasers [3, 161], whereas it is showing inferior quality than those obtained using femtosecond and picosecond lasers, but its machining rate is higher than fs and ps lasers [126]. Due to the highly efficient and low operating cost [162-163], better quality compared with CW CO_2, fibre and YAG lasers and higher machining rate than picosecond laser makes the TEA CO_2 laser potentially a practical tool for scarf repair of CFRP composite, acoustic hole drilling, and edge trimming applications. Furthermore, since TEA CO_2 lasers with an

average power of more than 1 kW have become available [150], practical use of TEA CO_2 lasers for machining CFRP composite may become economically and practically viable.

5.5 A method for reducing the top surface HAZ

Due to the top surface burn shown in Figure 5.10 and Figure 5.19 (1.6 – 2.6 mm) which is high compared to the optimized cross sectional HAZ (< 30 µm), a surface protection technique was used to reduce the surface damage by protecting the top surface during the TEA CO_2 laser machining of CFRP. This technique was investigated using different

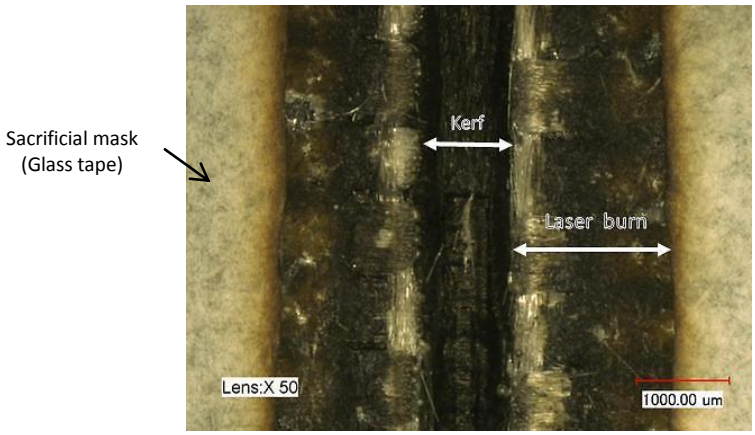

Figure 5.19 The size of the top surface burn created by laser.

sacrificial masks (plastic tape, ceramic powder mixed with silicon and glass fibre tape) over the machining surface during laser processing. Figure 5.20 shows the result of optical microscope observation of the TEA CO_2 laser machining of the CFRP sample without a sacrificial mask and using the masks. Using the sacrificial mask has improved the laser cut quality in which the top surface burn was reduced from 2.6 mm without protection mask to 78 µm using glass fibre tape mask. The optimum process parameters achieved in section 3.3 were used to investigate the effect of the different masks. The surface protection technique was further investigated using metal masks (2 mm thick mild steel) over the machining surface as shown Figure 5.21a. The metal mask reflects over 85 % of the CO2 laser beam [77] therefore it enhances the protection quality of the top surface as well as around the milling edges of the laser milled shapes. Therefore, metal protection masks make it possible to be implemented in laser based repair of

CFRP by laser milling of different profiles using pre-machined masks with various shapes as a templates. Figure 5.21b shows the typical milled CFRP sample in which elliptical and circular shapes were machined using cross milling paths. The quality was improved (Figure 5.22) compared with the quality obtained by the masks used in Figure 5.20. The top surface burn (Figure 5.19) was reduced to the range of 57-75 µm using metal sacrificial mask. The comparison of top HAZ result obtained using different masks type is shown in Figure 5.23.

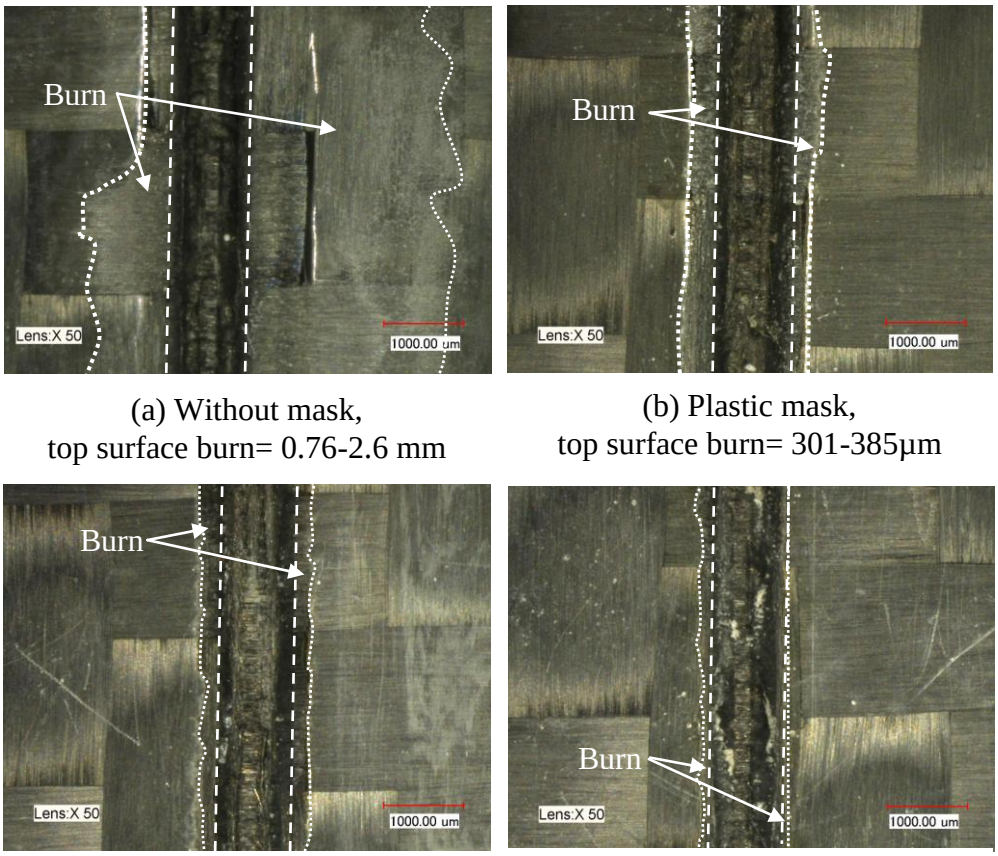

(a) Without mask,
top surface burn= 0.76-2.6 mm

(b) Plastic mask,
top surface burn= 301-385µm

(c) Ceramic /silicon powder mixture
top surface burn = 175-282 µm

(d) Glass fibre tape mask,
top surface burn= 78-93 µm

Figure 5.20 Top surface quality comparison of machining with/without sacrificial mask.

(a) (b)

Figure 5.21 Metal mask technique implementation; (a) metal mask use, (b) the machined sample using the mask.

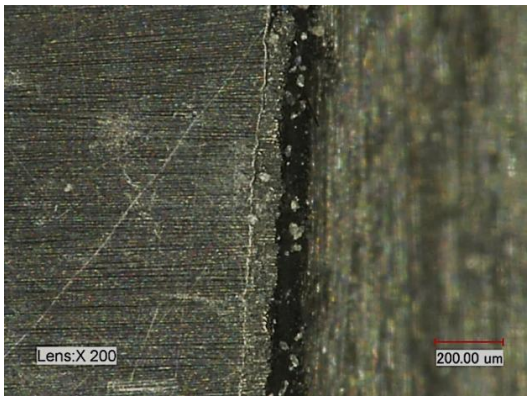

Figure 5.22 Close view of the ellipse shape's edge machined using metal mask.

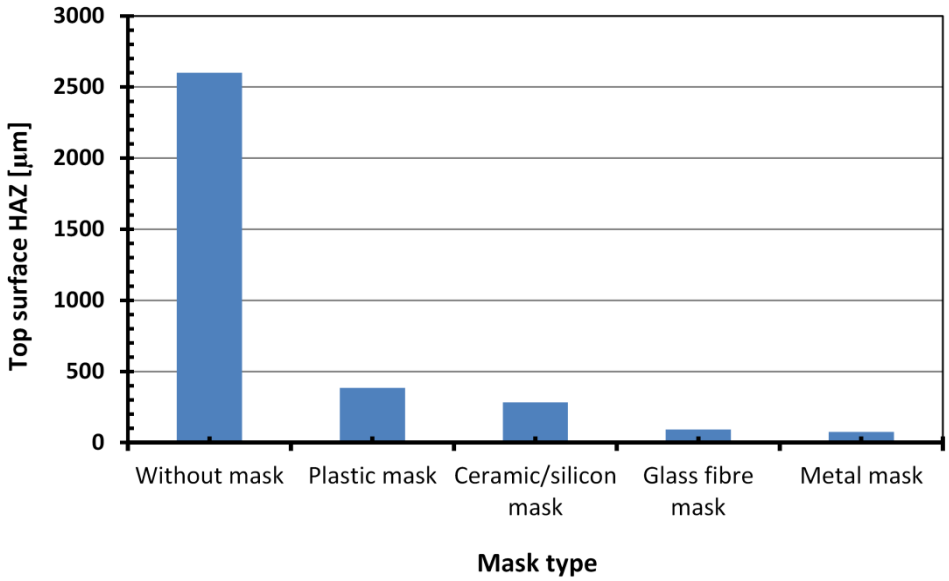

Figure 5.23 Mask technique comparison for different mask types on the top surface heat affected zone size.

5.6 Summary

This chapter presented pulsed TEA CO_2 laser machining of carbon fibre reinforced polymer composites for the first time. The influence of laser fluence, repetition rate and scanning speed on cross sectional heat affected zone extension, machining depth and material removal rate was investigated using design of experiment. Statistical empirical models of the responses and the significant process parameters among selected parameters were developed in this work. Additionally, a surface protection technique using sacrificial and metal masks used to protect the machined substrate was also demonstrated. From this work the following conclusions can be drawn:

1. The TEA CO_2 laser shows good machining quality (cross sectional HAZ) of CFRP composite. The optimum machining results achieved for average cross sectional HAZ, machining depth and material removal rate were 21±4 µm, 5.8±0.3 µm/pass and 11±0.4 mm^3/min respectively.
2. The HAZ is significantly affected by the laser fluence, scanning speed, square of repetition rate and square of scanning speed.
3. Thermal damage on the top surface can be significantly reduced (up to 57-75 µm) by using suitable sacrificial mask such as metal mask. Furthermore, the metal mask technique could be helpful during laser based repair of CFRP composite.

CHAPTER 6 HIGH-POWER PICOSECOND LASER DRILLING/MACHINING OF CARBON FIBRE-REINFORCED POLYMER (CFRP) COMPOSITES

6.1 Introduction

The availability of ultra-short laser pulse sources such as picosecond lasers makes it possible to improve the laser machining quality of these materials. This chapter reports an investigation on the drilling and machining of CFRP composites using a state-of-the art 400 W picosecond laser system. Multiple ring material removal strategy was used. Furthermore, the effect of laser processing parameters, such as laser power, scanning speed and repetition rate on HAZ sizes and ablation depth was investigated.

6.2 Experimental details

6.2.1 Experimental set-up and materials

The laser milling and drilling experiments were performed using an Edgewave picosecond Nd:YVO_4 laser system. The machine specifications are listed in Table 6.1. CFRP composites plates of 1 mm, 2 mm and 6 mm thicknesses were used as the workpiece materials. The laser beam was a delivered to the workpiece by means

Table 6.1 Picosecond laser system specifications

Parameters	Specifications
Operating mode	Pulsed
Wavelength	1064 nm
Maximum average power	400 W
Repetition rate	0.5-20 MHz
Pulse length	10 ps
Focal length	330 mm
Max. galvo scanning speed	10 m/s
Spot size at focus	125 μm ($1/e^2$)

of a 3-axis galvanometric scanner head with an f-theta focusing lens, which allowed the scanning of the laser beam with the same beam size and orientation across the scanning plane. An Aerotech computer-controlled x-y stage was used to mount the sample and for initial positioning of the experimental sample within the galvo scanning zone. The galvo-head can be moved upward and downward in the Z axis which permits the adjustment of the focal plane position initially on the upper surface of the workpiece. Figure 6.1 shows the basic experimental setup. All the experiments were carried out at a pulse frequency of 0.5 MHz, and the average powers were varied from 6 to 30 W.

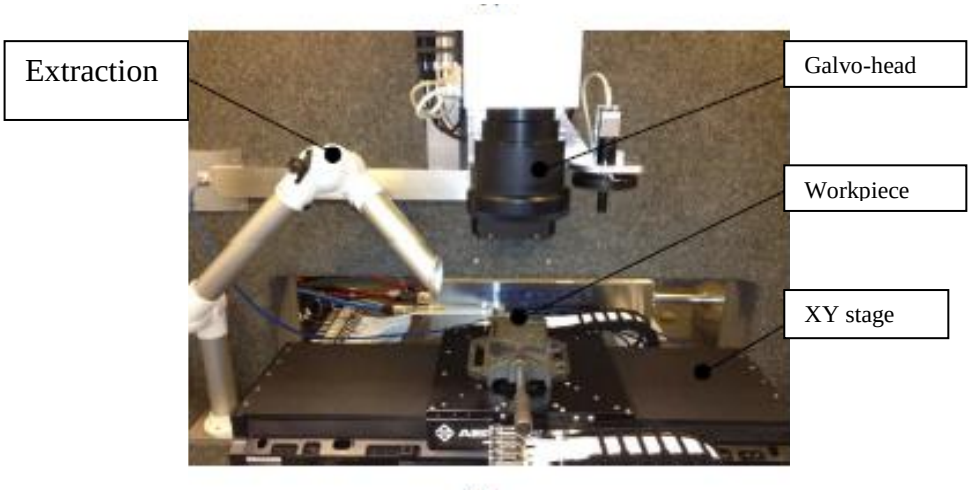

` (a)

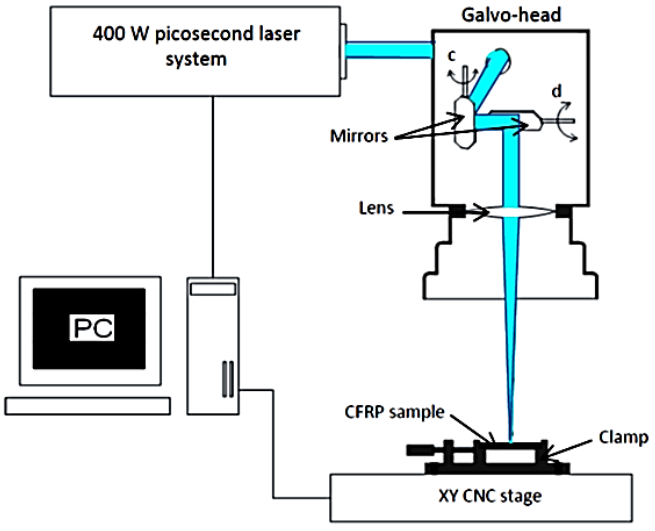

(b)

Figure 6.1 Experimental setup; (a) machine's stage/galvo-head, (b) Schematic diagram of experimental setup.

6.2.2 Experimental procedure

As the initial experimental investigations showed that using a single ring trepanning strategy for drilling 6 mm thick samples could deteriorate the machining quality considerably due to high heat accumulations. The experiments were performed using a multi-ring strategy (Figure 6.2). By removing the material layer by layer with a wide kerf (ring width) was facilitated better material ejection from the beam/material interaction zone and reduced the shielding of incident laser beam by the plume generated. The focal plane was first set at the sample's upper surface at the beginning of the drilling then it moved down by 0.25 mm for each set of 100 passes. Multi-ring drilling starts from the hole's outer diameter to create a trench to block the additional energy input generated by the internal rings from transferring along the fibres to the surrounding bulk material. Furthermore, the effect of laser process parameters, i.e. laser power, scanning speed, repetition rate and ring spacing on ablation depth and HAZ were investigated in this work. The size of the HAZ and cutting quality were studied using optical microscopy and scanning electron microscopy (SEM). The HAZ was characterised by measuring the length of fibres extruding out of the matrix and recession of the matrix.

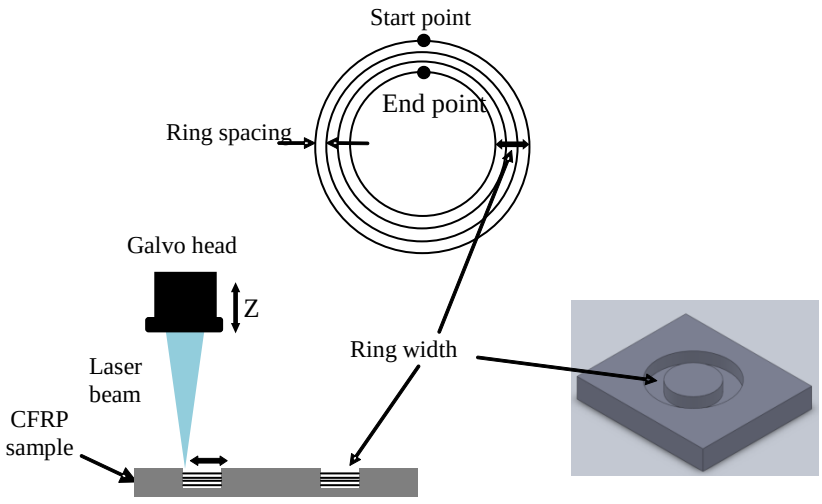

Figure 6.2 Schematic of multi-ring strategy used for laser drilling of CFRP.

6.3 Results

The ablation rate (d) dependence on the laser fluence F (J/cm²) based on the Beer-Lambert law, Equation (6-1), is shown in Figure 6.3, where a linear relationship between the ablation depth per pulse and the ln of laser fluences is shown experimentally. The ablation depth is typically between 2-15 nm/pulse. This is much smaller compared with those by ns and ms laser pulses.

$$d = \frac{1}{\alpha} \ln\left(\frac{F}{F_{th}}\right) \tag{6-1}$$

Where α the absorption coefficient (cm^{-1}) , F the laser fluence (energy density) and F_{th} the threshold fluence. Using curve fitting α and the threshold fluence can be calculated. Moreover, the thermal loading γ (J/cm^3) of the CFRP can be calculated by [164]:

$$\gamma = F_{th}.\alpha \tag{6-2}$$

A threshold fluence of 0.3 J/cm^2 , absorption coefficient of 0.25 nm^{-1} , optical penetration depth of 4 nm and thermal loading of 741 kJ/cm^3 were obtained using Figure 6.3 and equations (6-1) and (6-2).

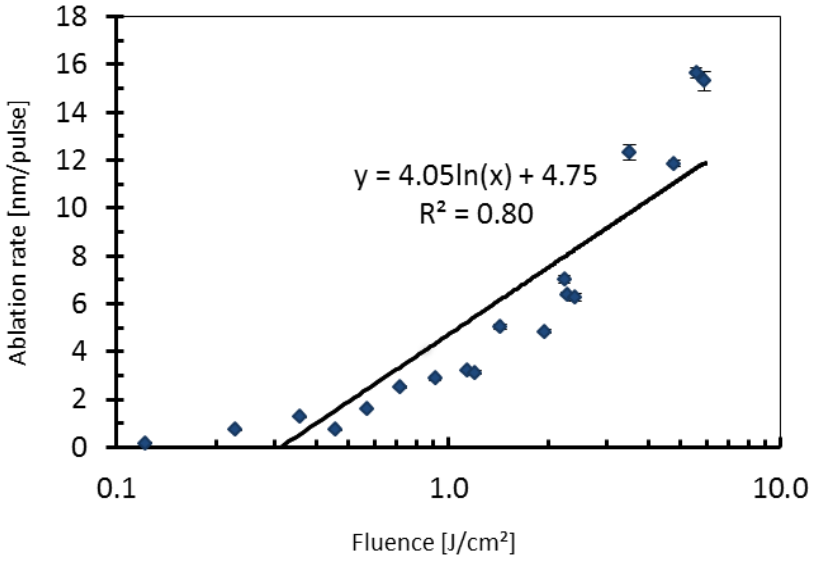

Figure 6.3 Ablation rate as a function of laser fluence.

6.3.1 Effect of laser power and scanning speed on HAZ and ablation depth

It can be seen in Figure 6.4 that the material removal depth per pass is reduced as the scanning speed increases, whereas the ablation depth increases for higher laser powers. More energy is delivered to the machining zone at high power and low cutting speed due to longer interaction time and high number of pulses per spot. Whereas high scanning speed reduces the energy input. Figure 6.5 shows the microscopic observations of the effects of scanning speed and laser power on HAZ and ablation depths.

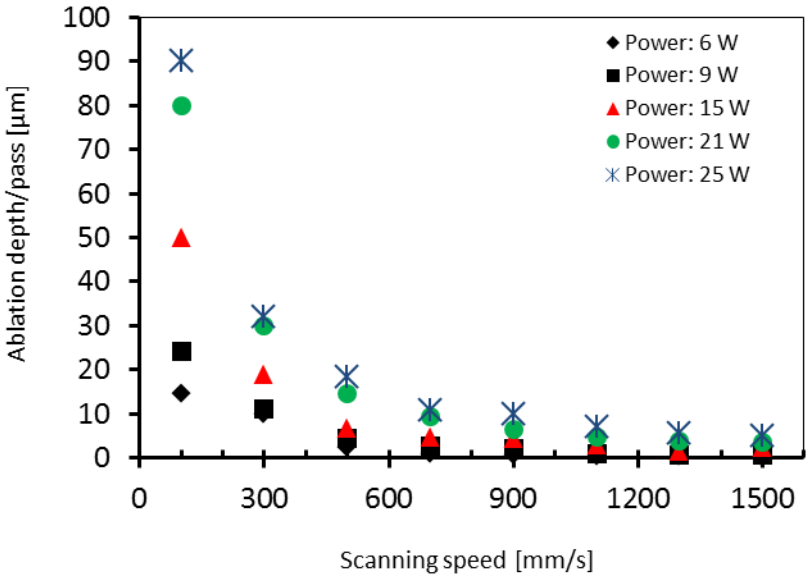

Figure 6.4 Ablation depth as a function of scanning speed.

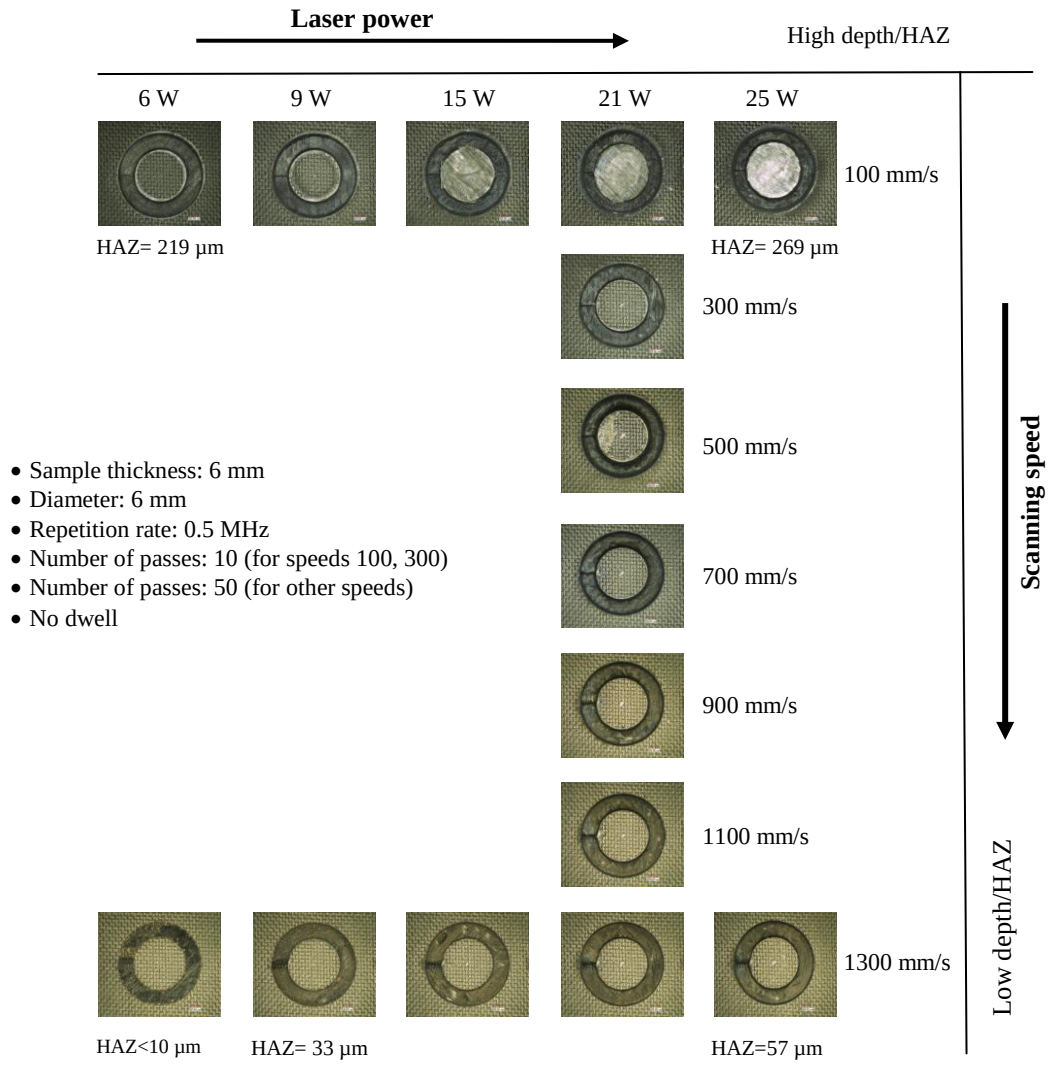

Figure 6.5 HAZ and ablation depth as a function of laser power and speed.

Figure 6.6 shows the effect of laser power on the HAZ. It is seen that the HAZ is influenced by laser power and increases with the increase of laser power. Also at low scanning speeds, the HAZ is large compared to that at the higher scanning speed. It is clear that scanning speed plays a more dominating role in controlling the HAZ size.

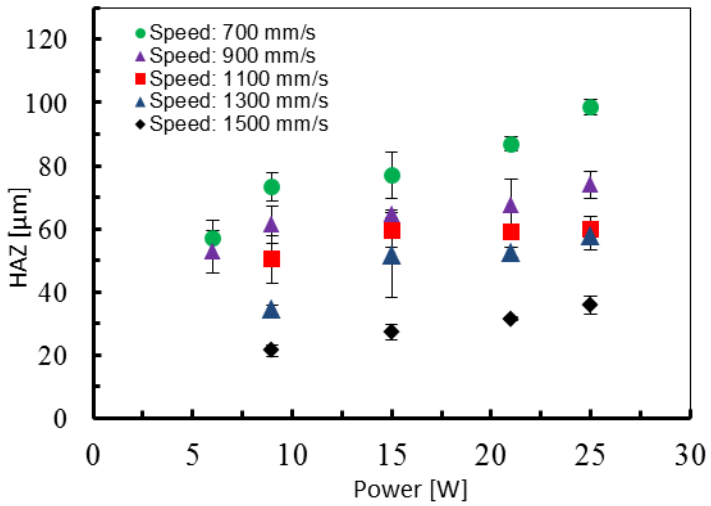

Figure 6.6 HAZ as a function of laser powers at different scanning speed

The surface quality observations for different laser powers are shown in Figure 6.7. The minimum HAZ (< 10 µm) obtained on the top surface at a low laser power (6 W) whereas, for the 25 W lasers power the HAZ was 56 µm. All the experiments to investigate the effect of laser power on milling quality were done using 50 passes continuously without allowing for short dwell time between the passes. The HAZ could be reduced by permitting a short cooling time (0.5-1 ms) between the passes.

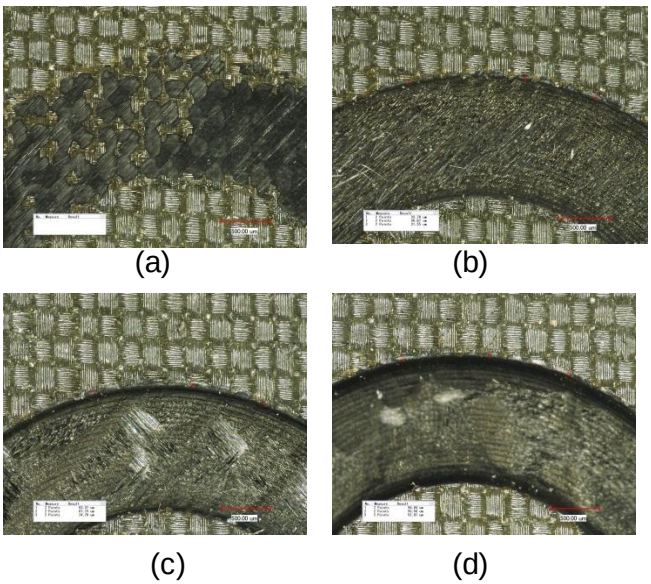

Figure 6.7 Thermal damage on the top surfaces at different powers; (a) 6 W, (b) 9 W, (c) 15 W and (d) 25 W. Repetition rate: 0.5 MHz, speed: 1300 mm/s, number of passes: 50, No dwell time.

6.3.2 Effect of repetition rate on HAZ

The HAZ increases with the increase of repetition rate as shown in Figure 6.8. A high repetition rate produces large thermal damage due to the increase of number of pulse and high pulse overlap per laser spot.

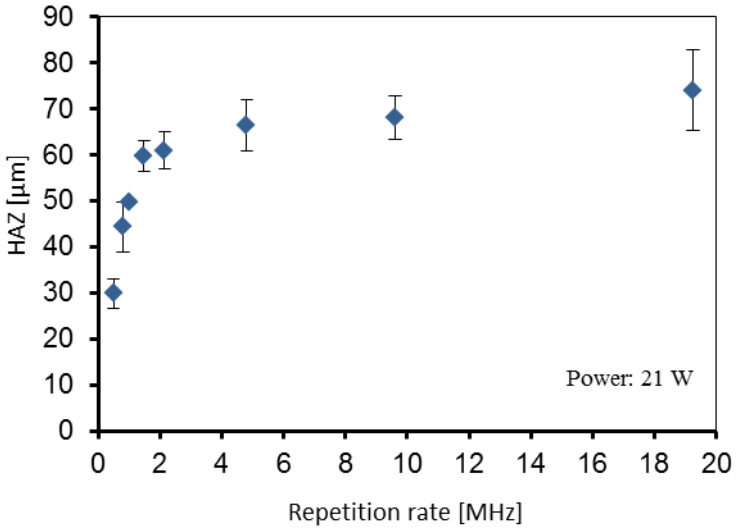

Figure 6.8 HAZ as a function of repetition rate.

The high repetition rate delivers high number of pulses to the processing zone in a short time and restricts cooling time between the pulses. The high number of pulses delivers high energy to the processing region. The microscopic observations of the milling quality (HAZ) at different repetition rates are shown in Figure 6.9. The better quality was obtained at a low repetition rate.

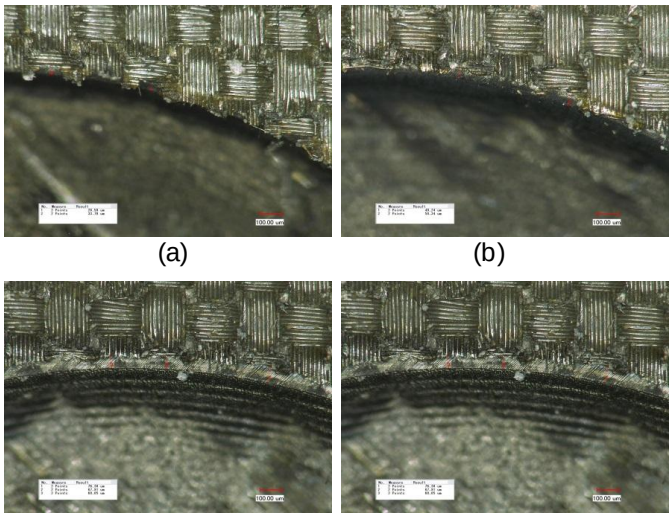

Figure 6.9 Microscopic observations of effect of repetition rate on HAZ. (a) 0.5 MHz, (b) 1 MHz, (c) 4.8 MHz, (d) 19.25 MHz. Power: 21 W, speed: 1500 mm/s, passes: 50.

6.3.3 Effect of ring spacing on thermal damages (HAZ) and ablation depth

Figures 6.10 and 6.11 show the effect of ring spacing on the machined quality and ablation depth. It is clearly seen that the HAZ is improved by increasing the spacing between the rings. However, this reduces the ablation depth. The high quality is obtained by wider ring spacing due to less energy being deposited in a unit area of the processing zone. Figures 6.12 and 6.13 show the microscopic observations of the effect of ring spacing. The larger spacing between rings produced good quality but low ablation depth and slower processing time. A ring spacing of 75 µm produced the best consistency in terms of width of HAZ.

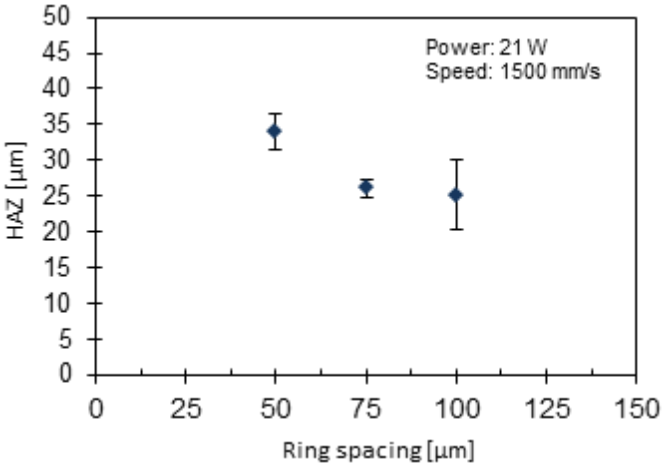

Figure 6.10 HAZ as a function of ring spacing.

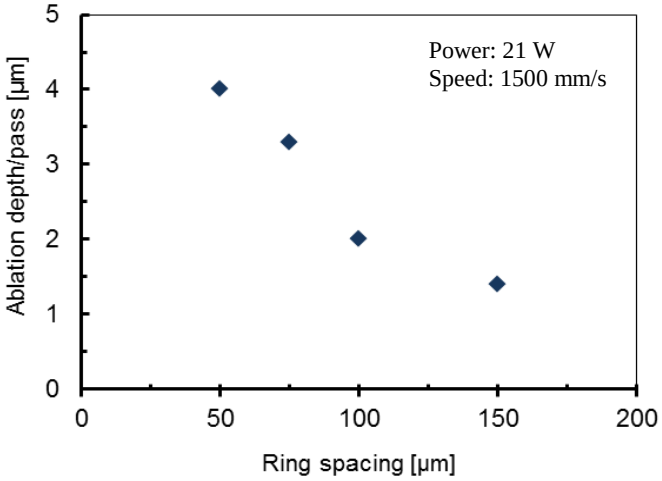

Figure 6.11 Ablation depth as a function of ring spacing.

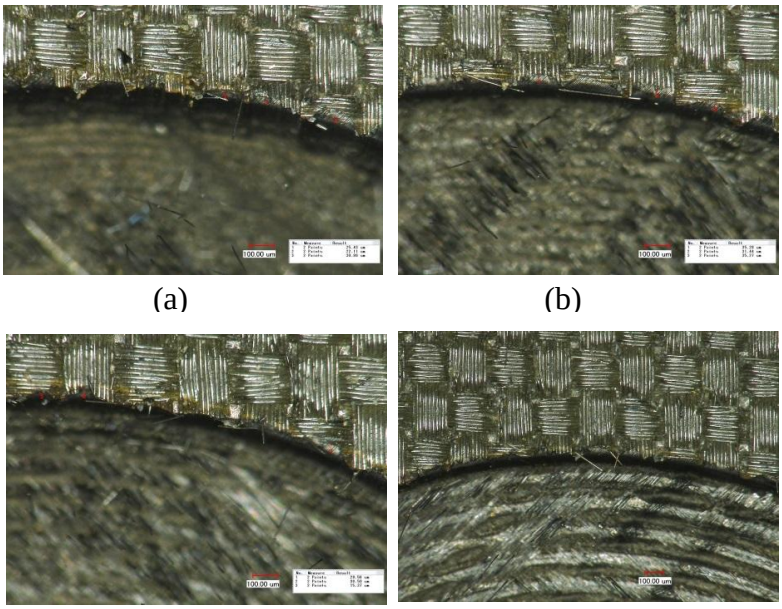

(a) (b)

(c) (d)

Figure 6.12 Effect of ring spacing on thermal damages; (a) 50 µm, (b) 75 µm, (c) 100 µm and (d) 150 µm. Power: 21 W, repetition rate: 0.5 MHz, speed: 1500 mm/s, passes: 50.

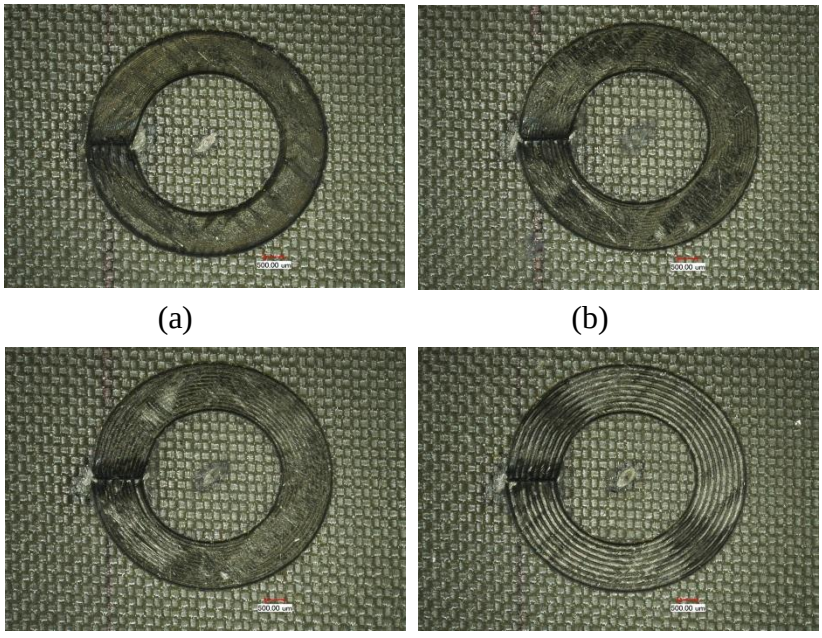

(a) (b)

(c) (d)

Figure 6.13 Effect of ring spacing on ablation depth; (a) 50 µm (b) 75 µm (c) 100 µm (d) 150 µm. Power: 21 W, repetition rate: 0.5 MHz, speed: 1500 mm/s, passes: 50.

6.3.4 Drilling of 0.3, 1 and 2 mm thick CRFP

Figures 6.14-6.17 show results of trials to drill 0.3, 1 and 2 mm thick CFRP samples.The results show the drilling quality for the holes on both the entry and the exit sides. There was less thermal damage at the cutting edges where the matrix still covers most of the fibres near the drilled edge.

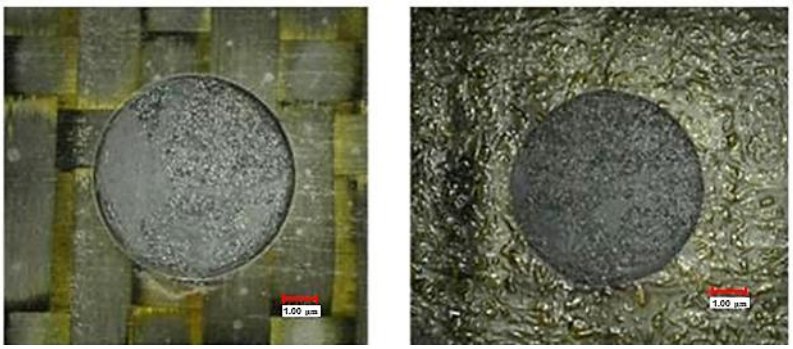

(a) (b)

Figure 6.14 Laser drilling of 0.3 mm thick CFRP; (a) entry side, (b) exit side. Power: 21 W, repetition rate: 0.5 MHz, speed: 1500 mm/s, number of passes: 100, dwell time: 5 sec.

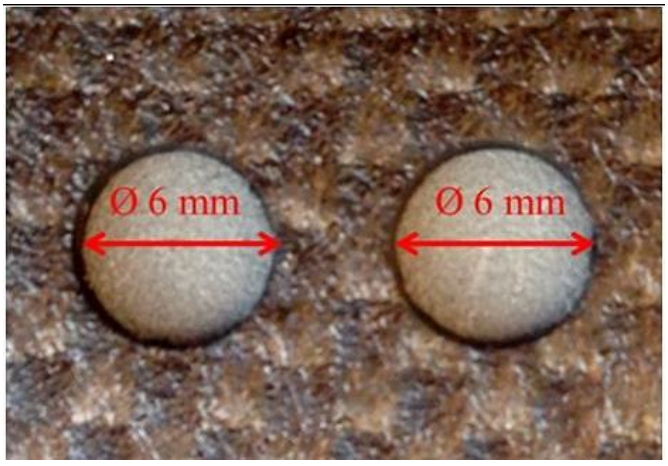

Figure 6.15 Drilling of 1 mm thick CFRP. Power: 40 W, repetition rate: 0.5 MHz, speed: 1000 mm/s, number of passes: 200, dwell time: 2 sec.

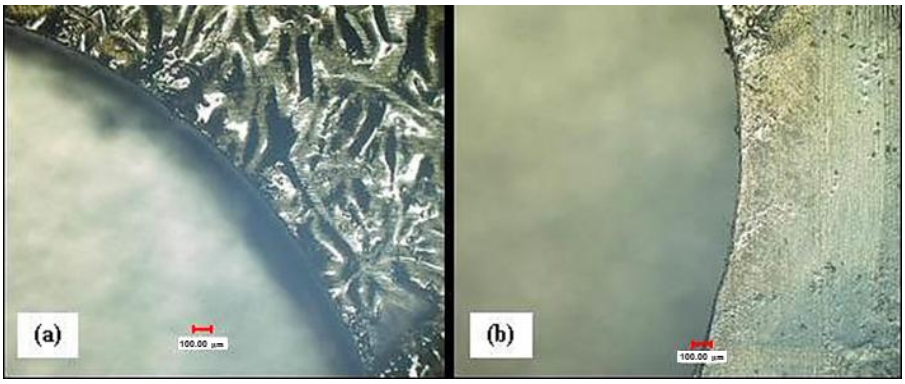

Figure 6.16 Microscopic observation of 1 mm thick CFRP: (a) entry side, (b) exit side.

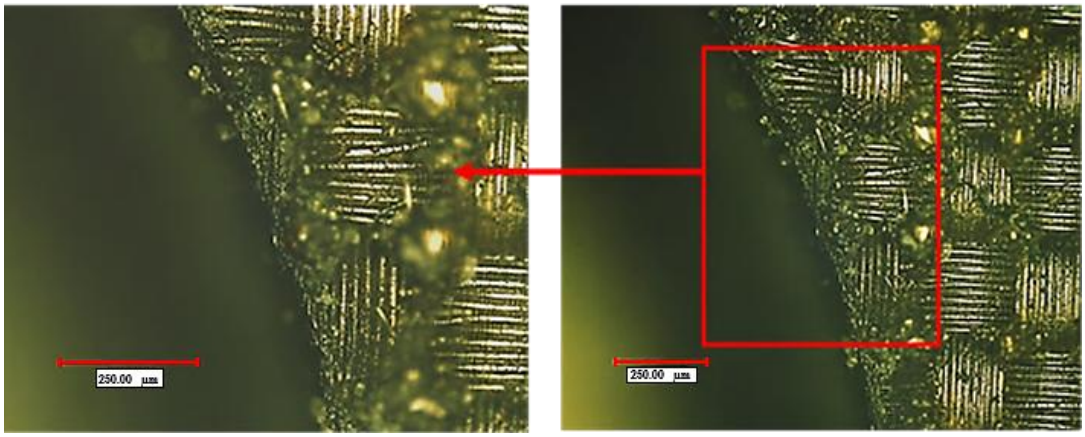

Figure 6.17 Optical microscopic observation of drilled CFRP at different magnifications. Power: 21 W, fluence: 0.3 J/cm^2, repetition rate: 0.5 MHz, speed: 2000 mm/s, number of passes: 500, dwell time: 1 sec.

6.3.5 Drilling 6 mm thick CFRP composites

The results in Figures 6.18–6.21 show a 6 mm diameter hole drilled in CFRP composites using the multi-ring strategy with a clear reduction of the HAZ on the entry side. The edge in Figure 6.19b is sharp and no obvious fibres are extruding out of the matrix. Also the polymer near the edge is not vaporized and is still holding and fills the gaps between the carbon fibres. The average measured HAZ at the top surface of sample was less than 25 µm whereas under the surface there was no noticeable thermal damage observed as shown in Figures 6.20 -6.21. Figure 6.20 shows a taper cross section in the shape for the hole drilled. The angle is about 15.39º.

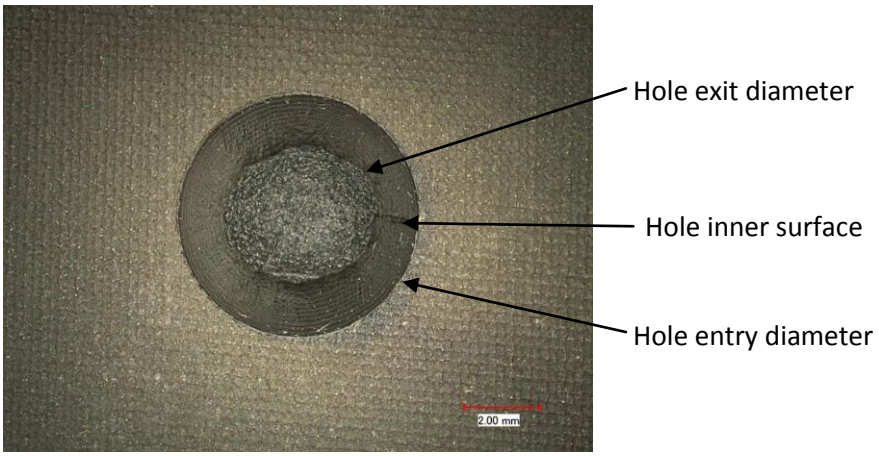

Figure 6.18 Hole of 6 mm diameter drilled in 6 mm thick CFRP composites.

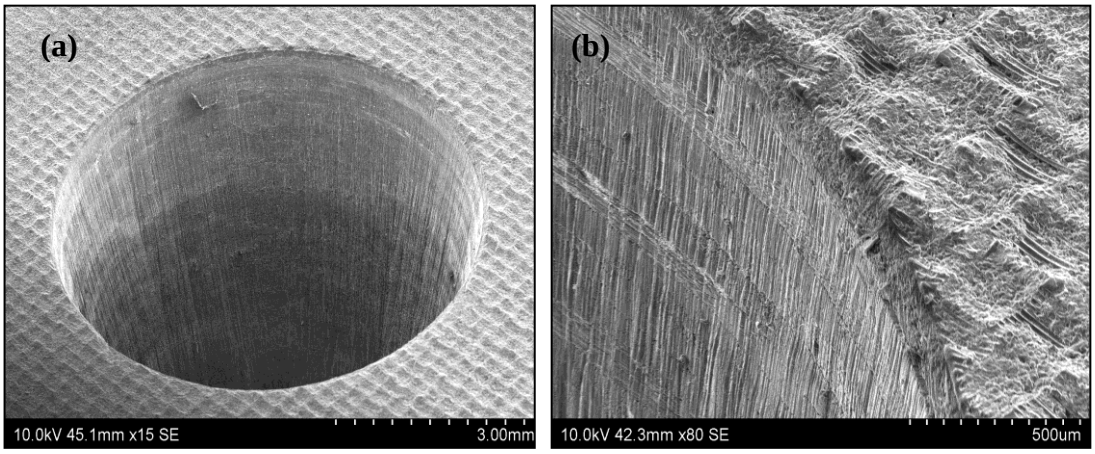

Figure 6.19 SEM observations of CFRP drilled hole; (a) top surface (b) drilling edge.

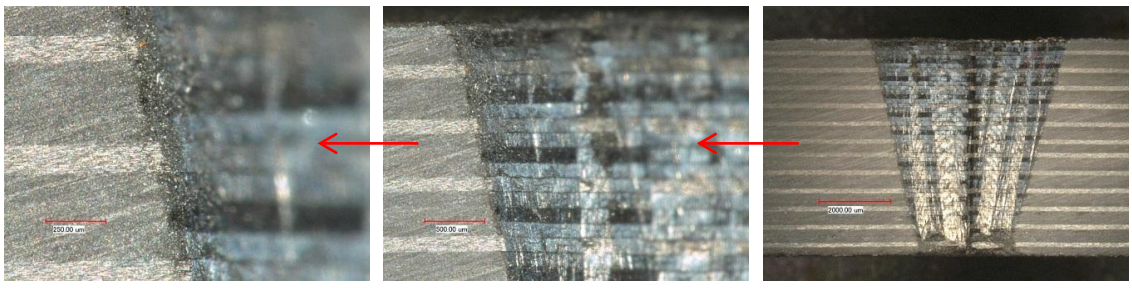

Figure 6.20 Microscopic sectional view of drilled hole at different magnifications.

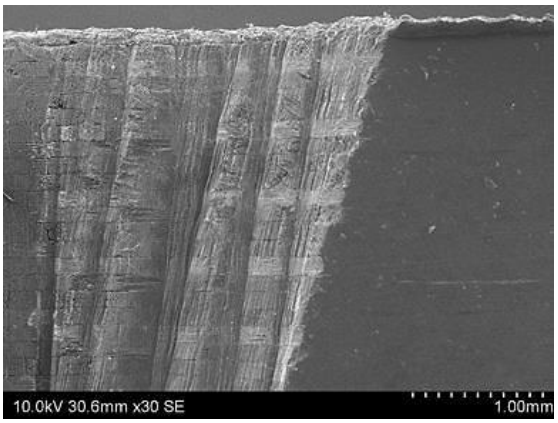

Figure 6.21 SEM sectional view of 6 mm drilled hole.

6.4 Discussion

The key challenge during laser processing of materials is reduction or elimination of HAZ. Using picosecond laser pulses reduces and eliminates the HAZ by shortening the laser material interaction time and reducing the heat diffusion into the surrounding materials [165]. The high peak power optioned due to the short pulse duration in picosecond laser machining can rapidly heat the target material and leads to faster vaporisation of the material leaving no time for heat to conduct into the bulk. In short laser pulses the laser energy is absorbed and stored by the free electrons for about 1 ps then the energy is converted into heat and transferred to the materials lattice leading to a material ablation [166]. During short picosecond laser processing (wavelength 1064 nm) of CFRP composite the laser energy is mainly absorbed by carbon fibres due to the higher absorbance of carbon fibre to the near-infrared wavelength compared to the epoxy which is approximately transparent [160]. Despite the low photon energy of the laser used, the high peak intensity results in direct ablation of the materials whereas some of the heat is conducted along the fibres due to the high thermal conductivity of the fibre (50 W/m.k) compared to the epoxy resin (0.1 W/m.k) and leads to evaporation of surrounding matrix. Furthermore, the multi-pass technique used in this work helps to slice the fibre into small pieces when machining perpendicular to the fibre direction. In this case the heat accumulation raises the temperature between the laser traces. When this temperature is high enough to evaporate the matrix material, the epoxy around the fibres evaporate leaving the chopped carbon fibres unattached which are then blown out by vapour force. Moreover, the multi-pass widens the kerf and allows for the plume,

plasma and fragmented fibres to escape from the machined area allowing for the laser beam to reach the internal material and enhance the processing rate. This technique helps to reduce the thermal damage by blocking the heat conduction to the surrounding materials when cutting the outer ring first [36] .

The cross section views in Figure 6.20 show taper walls of the drilled hole in which the hole diameters reduce as the machining depth increases. The reduction of the hole size at the bottom could be accredited to the lower contribution of the energy reflected from the machined sides where the laser beam is absorbed by carbon fibre instead of reflected like metals resulting in less laser energy at the hole bottom thereby reducing the hole size [159]. The reduction of the laser energy absorbed by the material as the depth increases due to plasma blocking is another reason for the taper shape [2]. Moreover, due to the higher thermal conductivity of CFRP the heat generated in the machined area conducted to the surrounding material between the laser pulses results in less temperature at the zone sides than at the zone centre of the machined area, therefore, the central zone always ablated first due to the fast energy build-up at the central zone by incident pulses. In addition, the higher beam intensity at the centre of the Gaussian beam shape removes much material at the centre than at the side of the beam and leads to deeper cut at the central region and produces taper shape. Tilting the sample or offsetting the laser beam during a linear laser machining trial (Figure 6.22) shows it is possible to eliminate the taper walls (Figure 6.23) during laser hole drilling by tilting the laser beam using trepanning optics or 3D robotic laser head.

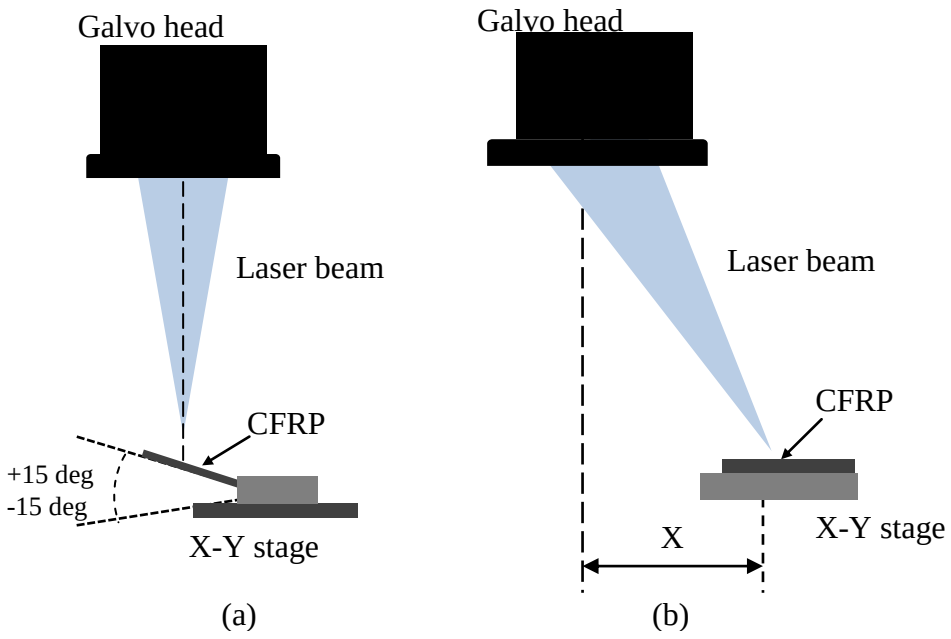

Figure 6.22 Taper elimination techniques; (a) sample tilting technique, (b) laser beam offset technique; X is laser beam offset distance.

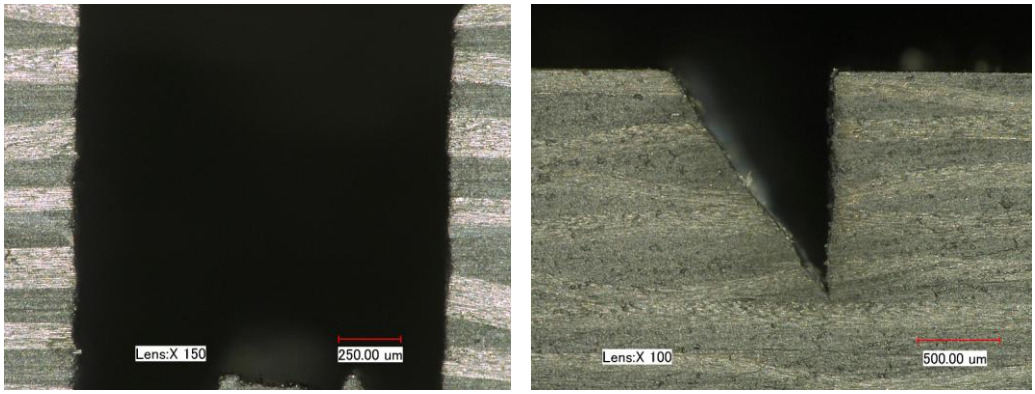

(a) (b)

Figure 6.23 Microscopic observations of samples cross-sections using; (a) tilting technique, no HAZ seen, (b) laser beam offset technique.

It can be noted in Figure 6.5 that as the scanning speed increases the HAZ was decreased. This could be attributed to the reduction in laser material interaction time. At high scanning speed the heat accumulation due to high pulses overlap at high repetition rates is reduced by which the laser energy delivered to the machining zone decreased. Increasing the repetition rate or reducing the scanning speed yields to large number of

pulses on the same position and thus the heat delivered to the sample increases and leads to heat accumulation. For laser beam spot size of 125 µm, scanning speed of 2000 mm/s and a repetition rate of 500 kHz the number of laser pulses generated on the same position are 31 pulses. Also the low heat conduction between the ply stacks and in transverse direction of the fibre axis enhances the heat accumulation and leads to high thermal damage. Moreover, the non-homogeneous nature of the CFRP composite and the effect of fibre orientation direction on heat conduction produce non-uniform HAZ. Machining perpendicular to the fibre direction produces wider HAZ than machining parallel to fibres direction due to the higher thermal conductivity of CFRP along the fibres than transversely to the fibres [146].

6.5 Summary

An investigation on drilling of CFRP using a state of the art 400 W picosecond laser system was presented in this chapter. The effect of laser parameters, such as laser power, scanning speed and repetition rate on HAZ and ablation depth was investigated From this work the following conclusions can be drawn:

1. The experimental study shows that the HAZ and ablation depths reduce as the laser power reduces and the scanning speed increases.
2. Holes with 6 mm diameter and 6 mm thickness of CFRP were drilled with high quality at a scanning speed of 2 m/s. HAZ is 25 µm at the entrance side, much smaller than previously reported results using nanosecond pulsed lasers. The holes produced in 6 mm thick CFRP showed a taper angle about 15º. Also the processing time was quite long. It took about half an hour to breakthrough this hole. Techniques to reduce taper were presented in this work.
3. High machining quality demands fast scanning speed for a given laser power.

CHAPTER 7 UNDERSTANDING THE SELF-LIMITING EFFECT IN HIGH POWER PICOSECOND LASER SINGLE AND MULTIPLE RING DRILLING/MACHINING OF CARBON FIBRE REINFORCED COMPOSITE AND MILD STEEL

7.1 Introduction

The availability of ultra-short laser pulse sources such as picosecond lasers makes it possible to improve the laser machining quality of carbon fibre reinforced polymer composite. The low processing rate of such lasers demands for better machining strategy for its acceptance as an industrial applications. Using multiple ring machining strategy showed it is possible to improve the processing rate during nanosecond pulsed laser machining of CFRP [36, 143]. This work compares the effect of single and multiple ring machining strategy on ablation depth, material removal rate and taper angle during picosecond laser machining of CFRP. The effect of laser peak power on taper angle was also investigated.

7.2 Experimental Material and Procedure

A woven CFRP sheet of 6 mm thickness with epoxy as the polymeric matrix and a mild steel (0.16 – 0.29 % carbon) of 2 mm thickness were used as the workpiece materials. Thermal properties of fibre and matrix are shown in Table 7.1. The laser used for the machining experiments was an Edgewave picosecond laser system. The machine specifications are listed in Table 7.2. The beam had a Gaussian intensity profile and was delivered to the workpiece by means of a 3-axis galvanometric scanner head with an f-theta focusing lens, which allowed the scanning of the laser beam with the same beam size and orientation across the scanning plane. The measured spot size was 70 µm. The focal plane position was placed on the upper surface of the workpiece during the experiments. An Aerotech computer-controlled x-y stage was used to mount the sample.

The experiments were performed using a single and multi-ring trepanning strategy for machining the 6 mm thick CFRP sheet to understand their effects on the machining characteristics such as ablation depth, kerf width, material removal rate and taper angles. The number of rings (parallel passes) examined was from 1 to 16. Furthermore, the effect of laser peak power (3 – 6.5 MW) on taper angles was also investigated in this work. The effect of track spacing (10 – 70 μm) on the material removal behaviour was also studied. The kerf width, ablation depth and taper angle were measured using optical microscopy.

Table 7.1 Thermal properties of fibres and matrix materials [167]

Material	Density (g/cm^3)	Conductivity (W/m/°K)	Specific heat (J/kg/°K)	Vaporization temperature (K)	Vaporization heat (J/g)
Epoxy	1.2	0.1	1800	700	1000
Carbon fibre	1.8	50	710	4000	43000

Table 7.2 Picosecond laser system specifications.

Parameters	**Specifications**
Operating mode	Pulsed
Wavelength	1064 nm
Maximum average power	100 W
Repetition rate	0.1-20 MHz
Pulse length	10 ps
Focal length	330 mm
Max. galvo scanning speed	10 m/s
Spot size at focus	70 μm (By ablation)

7.3 Results

In order to compare the effect of single and multiple rings (up to 16 rings) machining on the kerf width, ablation depth and material removal rate, several cuts were conducted at a constant power (8 W), repetition rate (103 kHz), scanning speed (1000 mm/s), hole diameter (6 mm) and processing time (4 min), i.e. the total energy delivered to the

material was the same in all the experiments. Figure 7.1 shows the effect of ring spacing (distance between the centre of adjacent rings) for multiple ring drilling/machining. The number of rings used was eight in all the cases. The ring spacing above 50 µm shows residual material between the rings and low machining depth. Despite the 50 µm ring spacing showing better machining depth, the residual material between the rings were still noticeable (top view photograph). Therefore, a comparative investigation of single and multiple ring strategies was carried out by fixing the ring spacing at 30 µm and the processing time for all investigations at 4 minutes so that the total energy delivered to the workpiece was identical in all the test cases. The processing time was adjusted to 4 minutes in all the experiments by controlling the number of repeat passes for each set of experiments. Figure 7.2 presents the microscopic observation of the top surfaces and the cross sections of CFRP sample machined using single and multiple ring strategies from 1 to 16 rings under the same total machining time of 4 minutes for each case. It clearly demonstrates a self-limiting effect (i.e. machining depth is limited even if additional laser energy is delivered to the site) and that the use of multiple rings produced deeper grooves and enhanced the machining rate than that with a single ring.

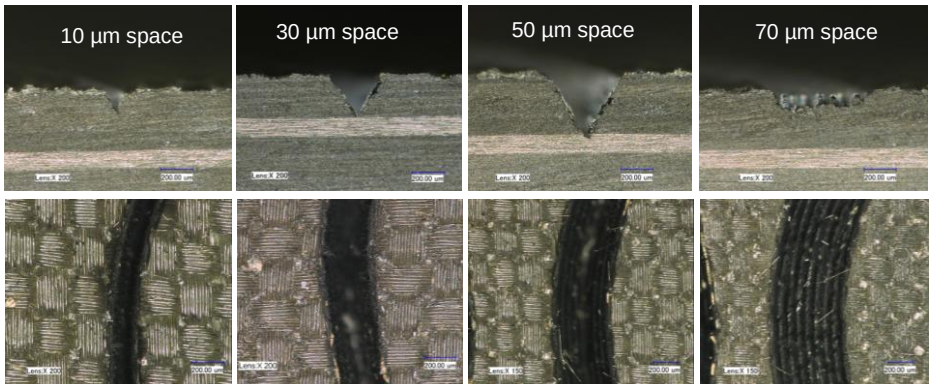

Figure 7.1 Microscopic photographs of cross sections (top row) and top surfaces (bottom row) of rings spacing effect with the machining time of 4 minutes in all the cases. Number of rings was eight in all the cases.

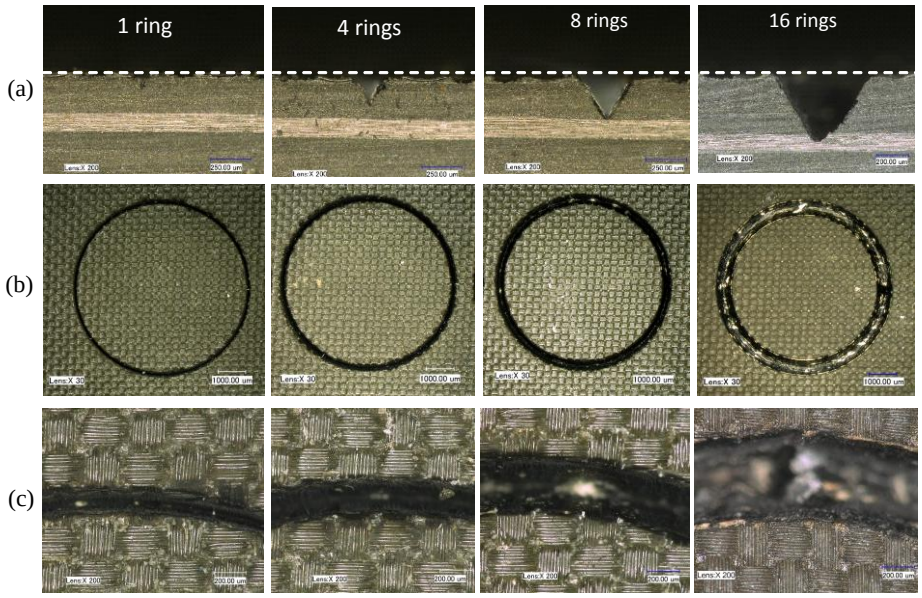

Figure 7.2 Microscopic photographs of number of rings effect, with the machining time of 4 minutes in all the cases; (a) cross section , (b) top surface, (c) close up views of top surface. Dotted line represents the top surface.

7.3.1 CFRP composite machining investigations

7.3.1.1 Effect of number of rings on kerf width, ablation depth and material removal rate

Figures 7.3–7.5 show the effect of ring (parallel pass) numbers on kerf width, ablation depth and material removal rate. The machining width in Figure 7.3 increases linearly by increasing the number of rings up to 16 rings. The ablation depth increases with the increase of number of rings as shown in Figure 7.4. The increase in the number of rings widens the machining groove and allows for better coupling of the laser energy with the processing zone. Figure 7.5 depicts the influence of number of rings upon material removal rate. The material removal rate increased significantly with the increase of rings number. Higher removal rates were obtained at larger number of rings (e.g. 16 rings). The wider and deeper grooves produced using multiple rings at the fixed processing time (4 min) increase the material ablated (Figure 7.2), which leads to higher material removal rates when compared to a single ring. Comparing the single ring and multiple ring strategies, multiple ring (or parallel pass) machining enhances the machining rate by increasing the kerf width and ablation depth even under the same machining time and total energy input to the workpiece compared to the single ring approach. For example with 16 rings, the material removal rate can be increased by

more than 10 times and machining depth can be increased by 4 times under the same total energy and machining time compared with the single ring approach. It is worth noting that the single ring (i.e. without parallel passes) approach is the common practice in laser based trepanning for drilling holes and common in laser cutting.

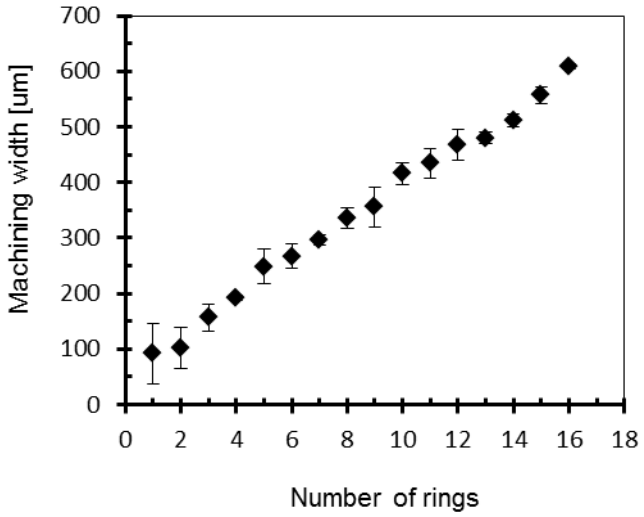

Figure 7.3 Machining width as a function of number of rings at a machining time of 4 minutes in all cases.

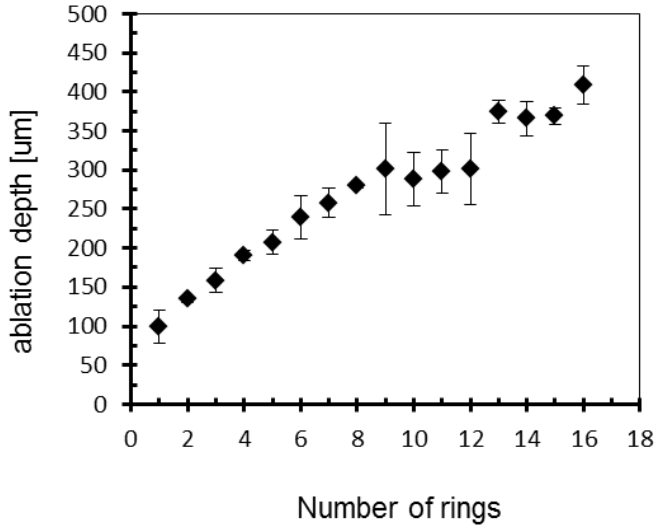

Figure 7.4 Ablation depth as a function of number of rings with a total machining time of 4 minutes in all cases.

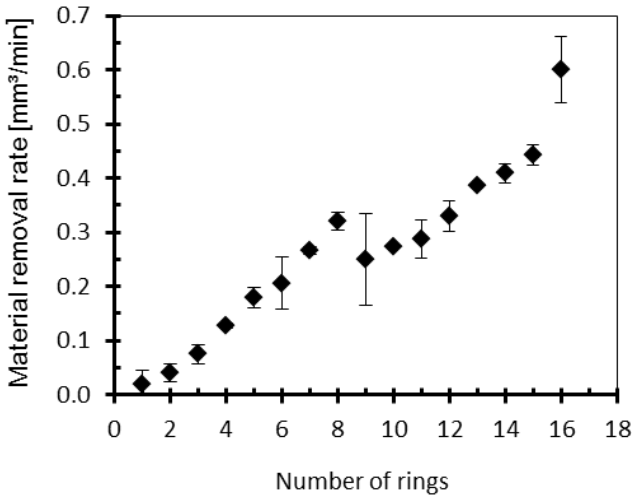

Figure 7.5 Material removal rate as a function of number of rings under the same machining time in all cases.

7.3.1.2 Effect of machining time on ablation depth limits

To further understand the self-limiting effect in the picosecond laser machining, long machining time (up to 10 minutes) was applied to see the ultimate depth that can be achieved by multiple ring (parallel passes) approach. Figure 7.6 shows the effect of machining time on the ablation depth for 8 rings and 16 rings. It is clearly seen that the ablation depth increases for both number of rings as the machining time increases up to certain value, then it reached a limit. Large number of rings shows deeper ablation for the same machining time after 2 minutes compared to a fewer number of rings. This can be attributed to the laser self-limitation when a cone like groove shape was generated as shown in Figure 7.7.

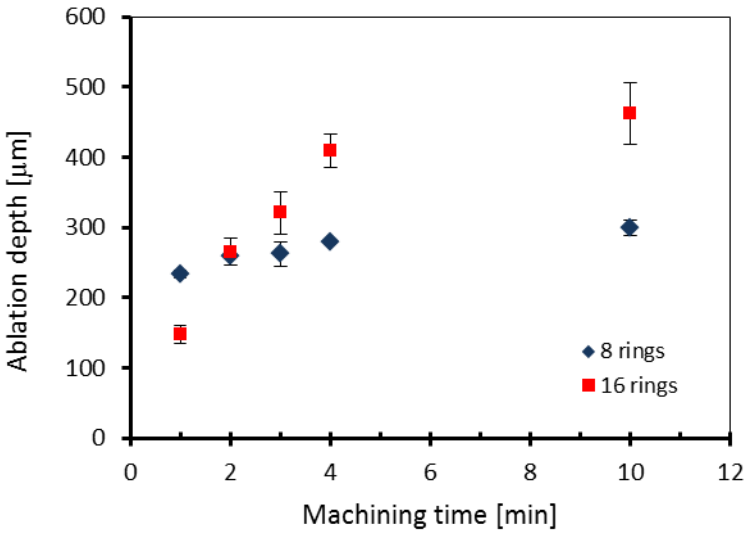

Figure 7.6 Ablation depth as a function of machining time and number of rings.

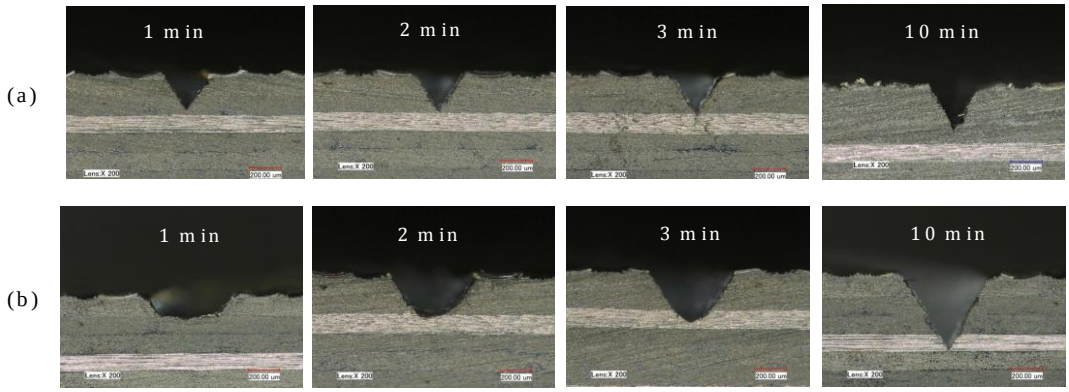

Figure 7.7 Cross section observations of machining time effect; (a) 4 rings, (b) 16 rings.

7.3.1.3 Effect of number of rings on taper angle

Tapered grooves were observed after single and multiple ring machining/drilling (Figure 7.2). The influence of number of rings on the taper angle is shown in Figure 7.8. The result shows no significant change in the taper angle by increasing number of rings. Figure 7.9 shows the effect of laser peak power on taper angle for a fixed number of rings (8 rings). The peak power was derived by dividing the pulse energy by the pulse length. Any increase in the peak power is directly reflected to the energy or heat transferred to the processing zone. It is seen that the taper angle is influenced by laser peak power and was decreased with the increase of peak power.

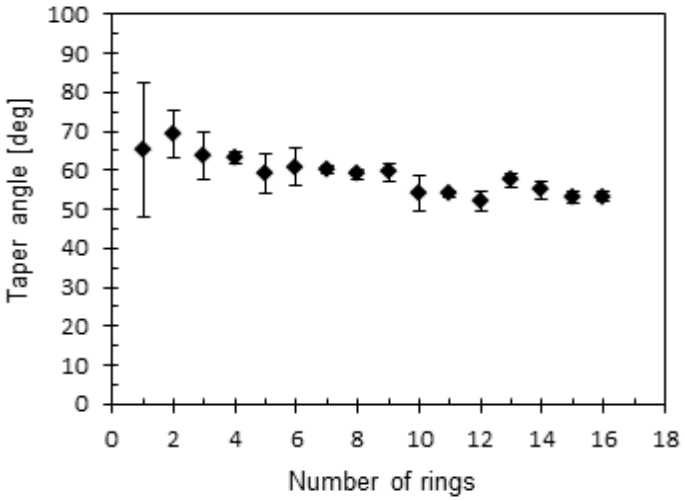

Figure 7.8 Taper angle as a function of number of rings.

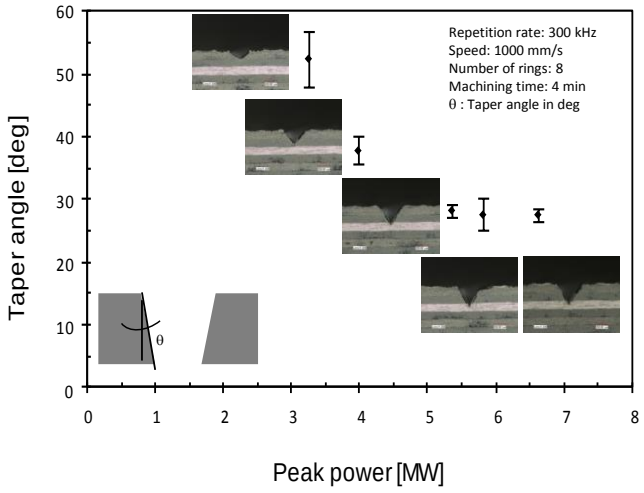

Figure 7.9 Taper angle as a function of peak power.

7.3.2 Mild steel machining investigations

7.3.2.1 Effect of number of rings and machining time on ablation depth

To understand whether the multiple ring effect also applies to other materials, similar experiments were performed for machining mild steel sheets. Figure 7.10 shows the influence of number of rings and machining time on the ablation depth of mild steel. The ablation depth increases as the number of rings increases to a certain number for a fixed machining time, then the ablation depth reduces as the number of rings increases. Increasing the machining time did not show much improvement in ablation depth for the same number of rings (4 rings) showing a self-limiting effect. In order to penetrate

deeper, more rings are required. Figure 7.11 shows the microscopic photographs of number of rings and machining time effects on ablation depth.

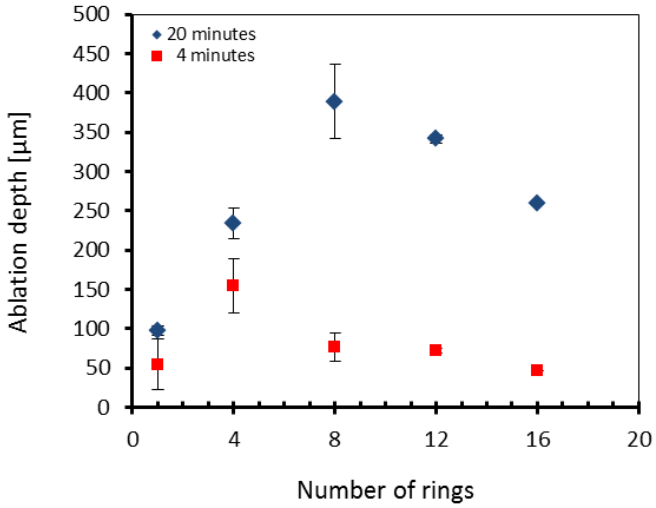

Figure 7.10 Ablation depth as a function of number of rings and machining time.

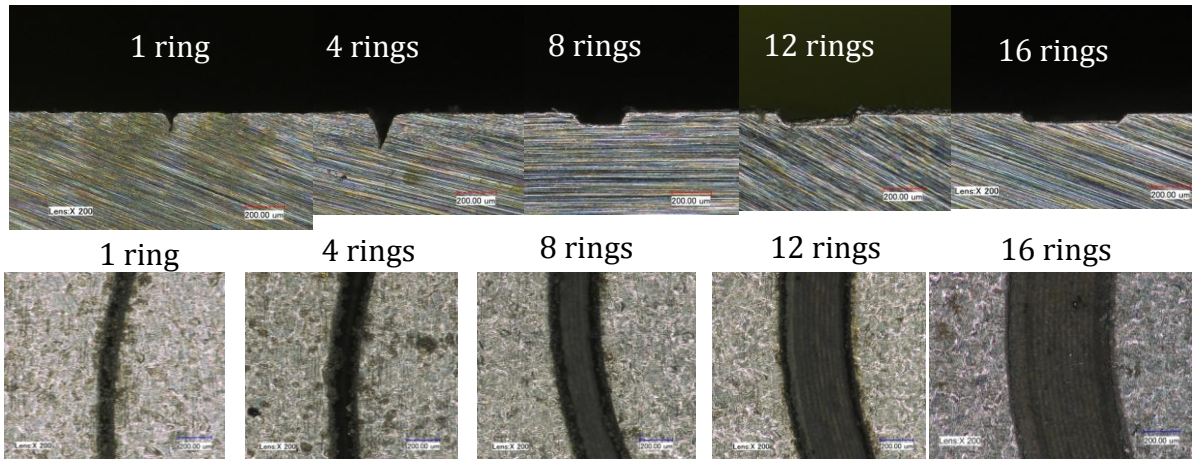

(a) 4 min machining time

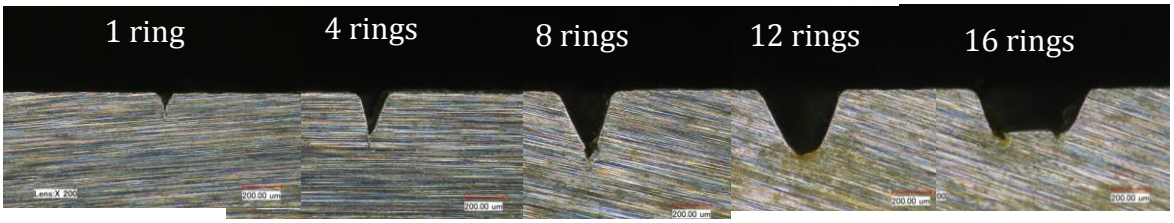

(b) 20 min machining time

Figure 7.11 Microscopic photographs of number of rings and machining time effects on ablation depth of a mild steel sheet. The second row is the top view.

7.3.2.2 Effect of number of rings on material removal rate

The effect of number of rings on material removal rate of machining mild steel is shown in Figure 7.12. Although, the ablation depth reduced after certain number of rings the material removal rate increases linearly with the number of rings.

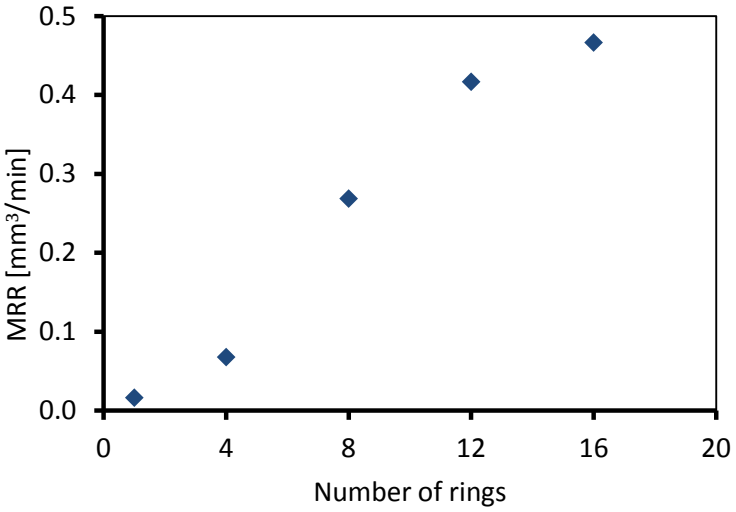

Figure 7.12 Material removal rate as a function of number of rings. Machining time 20 minutes in all the cases.

7.4 Discussion

A single ring trepanning with the picosecond laser reached a shallower limiting depth compared to the multiple ring strategy (Figure 7.2). This can be attributed to the narrower kerf produced by single ring, which prevents the ablated material to escape. The collapsed material blocked the incident laser beam to reach the material and hence a laser self-limitation phenomenon occurs. Also tapered walls are produced because of the Gaussian beam profile with a higher energy in the centre and the subsequent reflection from the side-walls reducing its contribution at the hole bottom. Referring to the multiple ring strategy presented by Li et al. [36] using a nanosecond a diode pumped solid state UV laser to machine CFRP, the method helps to widen the kerf and allows for the plume, plasma and fragmented fibres to escape from the machined area allowing for the laser beam to reach the internal m aterial and enhance the processing rate. In that strategy the spacing of laser beam tracks were greater than the laser beam size. Besides the direct ablation of CFRP, the high thermal conductivity of the carbon fibre and the higher temperature rises between the tracks also helped to evaporate the epoxy

surrounding the fibres or reduce its capability to hold the fibres. Therefore, the fibres ejected out of the cutting region were chopped fibres. This showed that laser beam overlapping was not essential to obtaining a flat ablation surface in composite material. In contrast, in our current study as shown in Figure 7.1, using the picosecond laser revealed that in order to achieve flat ablation surface, overlapping of laser beam is necessary. This can be attributed to the reason of the temperature rise between the tracks that is not high enough to evaporate the polymer surrounding the fibres, also less heat is conducted through the fibres at ultrashort pulsed lasers. The pulse overlap between the rings can be calculated considering the spacing between the rings and the laser spot diameter (70 µm); thus the pulse overlap (in %) = (1– rings spacing /spot diameter) x 100. Referring to Figure 7.1, the 30 µm and 50 µm spacing produce deeper kerf whereas the 70 µm spacing produces shallower depth and material left between the beam traces when 50 µm and 70 µm used. Calculating the pulse overlaps between the rings reveals that, 70 µm spacing produces 0 % overlap, whereas, 50 µm and 30 µm produces 29 % and 57 % overlaps respectively. However, 50 µm still shows some material left between the beam traces. Therefore, for a flat surface ablation, the ring spacing (i.e. the distance between the two adjacent rings or tracks) need to be less than 50 µm. The cone like shape produced in picosecond pulsed laser drilling using the multiple ring strategy (Figure 7.7) prevents deeper ablation of target materials. Widening the cutting area does not change the taper but delays the cone tip formation and hence allows for deeper cut. The taper walls absorb the laser beam and reflect the remaining laser radiation away from the kerf bottom causing the self-limiting effect for tapered blind holes or grooves.

The same strategy was applied for machining mild steel. It has been found that the multiple ring strategy performs the same role with metal. The processing rate was improved using the multiple ring approach compared with single trepanning ring. Also, laser self-limitation was noted with this metal as well.

. Figure 7.13 shows the reflectance (R) of CFRP with respect to wavelength for normal incidence. The typical absorptivity A=1-R≈0.95 at the laser wavelength of 1064 nm. When the laser pulses continually irradiated the sample surface, the material was ablated and then a blind hole was formed. Considering the drilling strategy used in this work, the progress can be described as in Figure 7.14(a). The absorbed fluence on the hole sidewall (F_{sw}) is expressed as:

$$F_{sw} = F \times \sin\theta \times A = F \times A_{sw} \tag{7-1}$$

Where A_{sw} is the equivalent absorptivity for the hole sidewall, F is the employed laser fluence, and θ is the hole taper angle. Figure 7.14(b) demonstrates the equivalent absorptivity varied with the hole taper decreasing. It can be clearly seen that the equivalent absorptivity is dramatically reduced as the hole taper is smaller than 65^{o}. When the hole taper is down to 32^{o}, F_{sw} is ~50% lower than normal incidence.

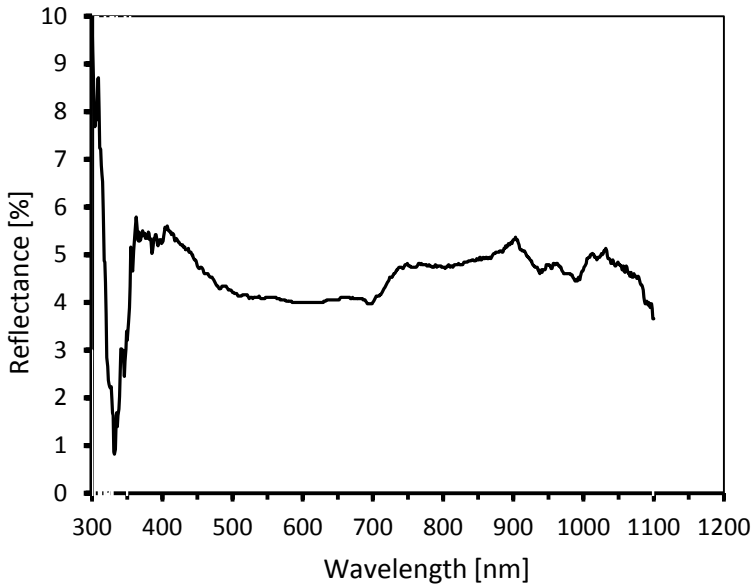

Figure 7.13 The reflectance of CFRP with respect to wavelength.

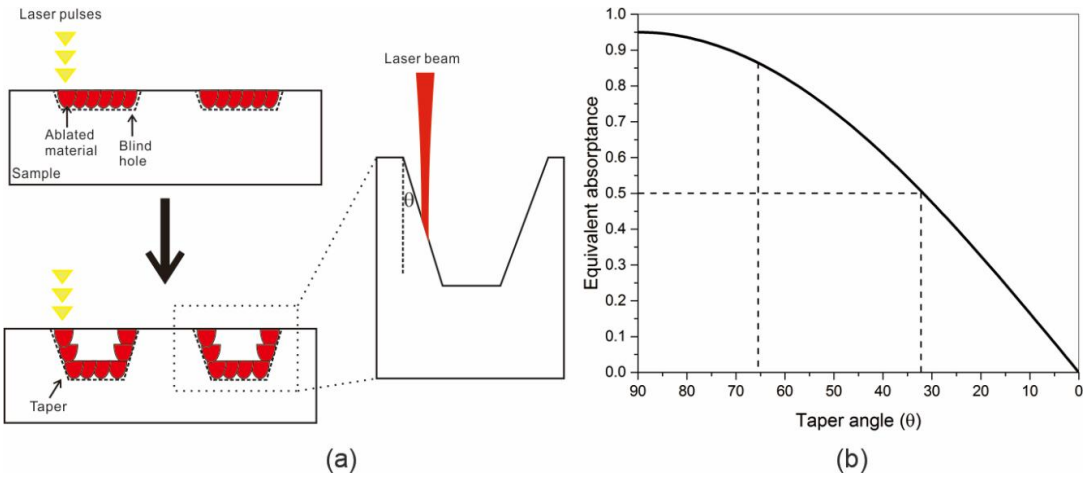

Figure 7.14 (a) The formation of the hole taper during laser drilling with multi-ring strategy and (b) the variation of equivalent absorptance with the hole taper.

The maximum hole taper in laser drilling with a specified fluence can be identified by Eq. (7-1) when F_{sw}=A*F_{th} [168]. A higher fluence is required to ablate materials from the sidewall for a higher tapered hole. The tapered hole sidewall would converge at a point to form a cone-like drilled hole, which stop the deepening of the hole. It is the self-limitation in ps-pulsed laser drilling. Two strategies can be employed to further increase the hole depth, (i) increasing the laser fluence or (ii) increasing the ring number for a large entrance width. According to Eq. (7-1), the hole taper is estimated by [168,169]:

$$\theta = \sin^{-1}\left(\frac{F_{th}}{F}\right) \tag{7-2}$$

As shown in Figure 7.15(a), the relationship between the laser fluence and the hole taper is in good agreement with the experimental results shown in Figure 7.9. In order to achieve the hole taper lower than 10^{o}, the laser fluence has to be higher than 7 times of F_{th}. Meanwhile, the maximum hole depth is increased with the taper angle reducing (as the inset in Figure 7.15(a)). Therefore, a better strategy of using ps laser machining is to use higher pulse energy at lower repetition rates rather than using lower pulse energy at higher repetition rates. This points a direction for the future high power ultra-fast laser development for materials processing, whilst most current higher average powered ultra-fast lasers are achieved with higher repetition rates at low pulse energies.

In addition to laser fluence, the wide entrance can also reduce the self-limitation in drilling. As mentioned above, the hole-tip formed by the convergence of inherent taper limits the pulse energy for material removal. The tip position, *d*, thereby is subjected to trigonometric rules as shown in Figure 7.15(b), which can be expressed by

$$d = \frac{1}{2}\times\frac{w}{\tan\theta} = \frac{1}{2}\times\frac{\left(w_0 + \left(N-1\right)\times w_d\right)}{\tan\theta} \tag{7-3}$$

where w is the entrance width, w_0 is the kerf width with a single ring, N is the number of rings, and w_d is the ring spacing. Taking Eq. (7-2) into Eq. (7-3), the tip position can therefore be determined by the entrance width and laser fluence as following

$$d = \frac{1}{2} \times \frac{w}{\tan\left(\sin^{-1}\left(\frac{F_{th}}{F}\right)\right)} = \frac{1}{2} \times \frac{\left(w_0 + (N-1) \times w_d\right)}{\tan\left(\sin^{-1}\left(\frac{F_{th}}{F}\right)\right)} \tag{7-4}$$

The tip position, d, is the maximum hole depth due to the self-limitation in ps-pulsed laser drilling. It depends on the employed laser fluence and entrance width, by which the maximum hole depth can be calculated via Eq. (7-4). Figure 7.16 shows the calculated and measured ablation depth as function of number of rings.

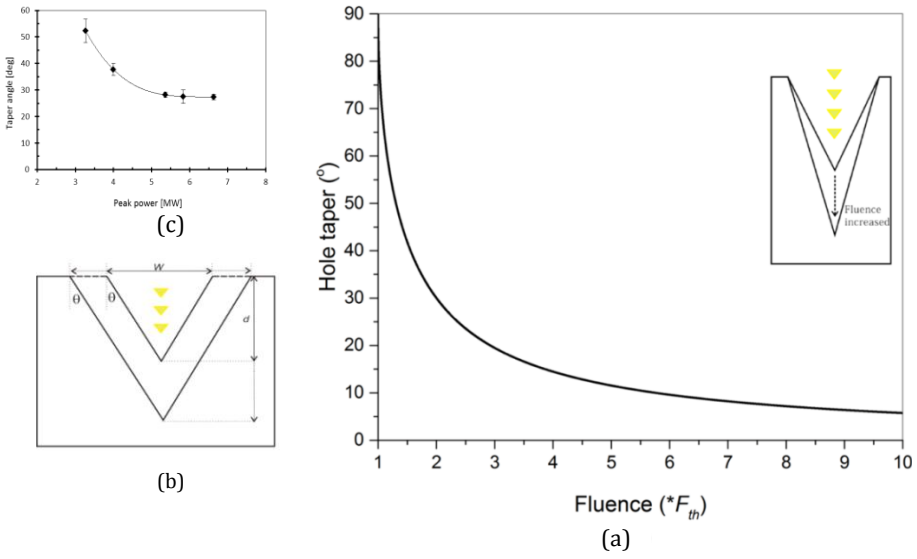

Figure 7.15 Strategies on hole deepening in ps-pulsed laser drilling. (a) The relationship of laser fluence with hole taper, (b) The hole tip position varied by the entrance width under the fixed laser fluence, and (c) the experimental results of taper angle as a function of peak power.

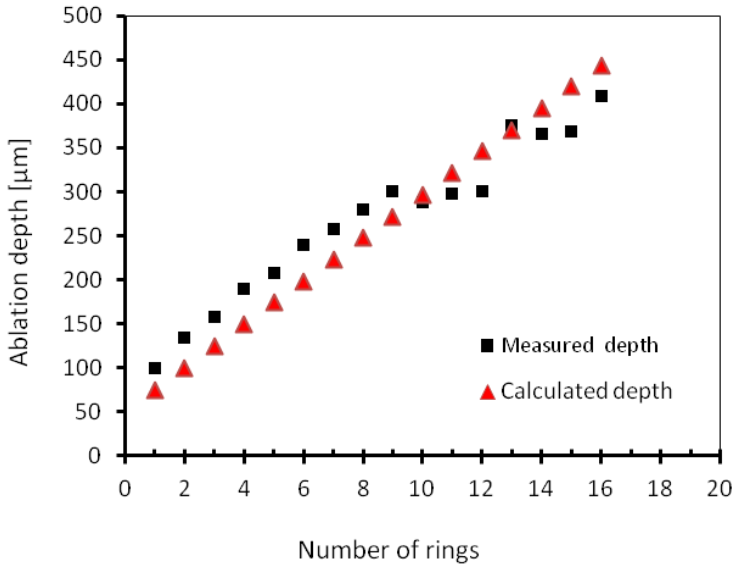

Figure 7.16 Calculated and measured maximum ablation depth as function of number of rings.

7.5 Conclusion

A self-limiting effect was identified in picosecond laser single ring and multiple ring (parallel passes) drilling/machining of CFRP composite and mild steel sheets. This was found to be due to hole taper and formation of a cone tip that deflects the laser beam away from the bottom of the hole. A theoretical model was proposed to determine the maximum machining depth for single and multiple rings (parallel tracks), validated by experiments. Using the multiple ring strategy increased the ablation depth and material removal rate than those using single ring trepanning. Laser beam overlaps between the rings is essential to insure flat surface ablation for both materials.

CHAPTER 8 STATISTICAL MODELLING OF PULSED FIBRE LASER DRILLING AND MACHINING OF CFRP COMPOSITE

8.1 Introduction

Although ultra-short pulsed lasers such as picosecond and femtosecond lasers have shown much reduced heat affected zones in machining CFRP, their material removal rates are very low and it is difficult to deliver ultra-short pulsed lasers through optical fibres. High power fibre laser machining could be a more practical tool for real industrial applications owing to its higher operating efficiency, higher beam quality (M^2 = 1.1-1.2), power stability, long depth of focus, flexible beam delivery and easy for automation, particularly with industrial robot [170]. A key challenge is to control the HAZ to within a certain accepted limit. In this chapter, design of experiments was used to investigate the effect of input process parameters such as laser power, scanning speed, laser off time and gas pressure on heat affected zone (HAZ), hole circularity, hole taper and drilling time during pulsed fibre laser drilling of CFRP. Also, empirical models for the out responses were developed and the output responses were numerically and graphically optimised and experimentally verified. The work in this chapter focuses on reducing HAZ through the use of a short-pulsed fibre laser for the machining CFRP with multiple passes.

8.2 Experiment Materials and Methods

8.2.1 Experimental Set-up and Materials

The experiments were conducted using a 1 kW IPG YLR-1000-SM ytterbium single-mode fibre laser system with a 1.07 µm wavelength, delivered through a 14 µm core diameter fibre as shown schematically in Figure 8.1. The laser beam was directed to a processing head containing a collimating lens and a focusing lens (190 mm focal length) and a gas nozzle. The minimum laser beam spot size at focus was 70 µm. This laser system can be operated in continuous wave (CW) and modulated pulsed mode. The modulated pulsed mode of this laser system was used in this work (a pulse width range

of 1-100 ms). The material used in the experiments was 1.5 mm thick carbon fibre reinforced polymer composite supplied by BAE Systems. The workpiece samples were mounted on an Aerotec CNC x-y stage. Argon gas was used as the assist gas in all the experiments [171]. The HAZ was characterised by the extent of fibre extruding out of the matrix and recession of the polymer matrix from the entry and exit edges of machined hole [132]. The average surface HAZ at different points around the hole entrance and exit sides was considered in this work. A Keyence VHX-500F digital microscope was used to measure the extension of HAZ, and the machined hole diameters at the entry and exit sides. The circularity was measured using the ratio of minimum to maximum diameters of machined hole at three different places around the hole [154]. The taper angle was calculated according to Eq. (8-1):

$$\text{Taper(deg)} = \frac{d_{en} - d_{ex}}{2t} \times \frac{180}{\pi} \tag{8-1}$$

Where d_{en} is the hole entrance diameter, d_{ex} is the hole exit diameter and t is the sample thickness.

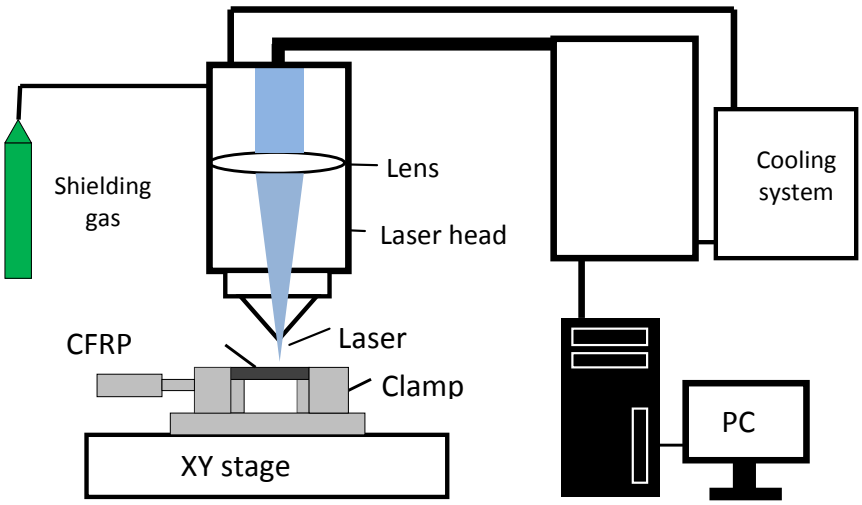

Figure 8.1 Schematic diagram of experimental setup.

8.2.2 Design of experiments

The Design Expert® software version 7.0.0 was used to design the experiment for four input variables (i.e. laser peak power, scanning speed, laser off time and gas pressure)

with five levels using the 1 kW pulsed fibre laser in drilling CFRP composites. These parametric variables and their levels are shown in Table 8.1. The screening tests revealed that longer pulse duration increases the HAZ dramatically; therefore it was kept fixed at 1 ms during the DOE runs. The other factors such as standoff distance, nozzle exit hole diameter, and beam focal position were kept on the top surface of the sample. Additionally, in order to enlarge the cut kerf and assure full through cut, two ring strategies with a 30 μm spacing between the rings was used for hole drilling experiments [36]. The responses were measured and presented in Table 8.2. The average HAZs at the entry and exit sides of the hole were measured and considered in this work. The drilling time was measured by counting the number of passes required to complete the hole drilling times the time required to complete each pass.

Table 8.1 Input variables with their levels used for DOE investigations

Symbol	Variables	Units	Level 1	Level 2	Level 3	Level 4	Level 5
A	Power	W	200	400	600	800	1000
B	Speed	mm/s	4	8	12	16	20
C	Laser off time	ms	4	8	12	16	20
D	Gas pressure	bar	4	5	6	7	8

8.2.3 Statistical Modelling

Statistical models with best fit relating the measured responses (entry HAZ, exit HAZ, circularity, taper angle and drilling time) with the laser cutting parameters were developed using Design Expert v7. To obtain the best fit models, the suitability of proposed models were tested according to *F*-value, lack of fit and ANOVA technique for a Prob>f of less than 0.05 (Tables 8.3 – 8.7). The Prob>f value of less than 0.05 for the model indicates that the model terms are statistically significant. The *F*-value for a model is a comparative test between the term variance and the residual variance. It is the ratio of mean square of the model to the mean square for the residual. Also the fitness of the developed models was checked by the regression coefficient $\acute{R}^2$ and adjusted $\acute{R}^2$ [140]. These values indicate the suitability of the RSM models. The closer the values

are to 1, the more accurate the models are. The $\acute{R}^2$ is the ratio of the sum of squares of the model to the sum of squares of the total. The adjusted $\acute{R}^2$ is calculated according to Eq. (8-2) [140]:

$$\acute{R}^2{}_{adj} = \left(\frac{\acute{n}-1}{\acute{n}-p}\right)\left(1-\acute{R}^2\right) \tag{8-2}$$

Where, $\acute{n}$ is the number of experiments and p is the number of model parameters. In order to optimise the response (η) and to analyse relationship between the response and the input variables (x_i and x_j) the general second-order polynomial Eq. (8-3) is usually used in RSM [155].

$$\eta = b_0 + \sum_{j=1}^{\acute{n}} b_j x_j + \sum_{j=1}^{\acute{n}} b_{jj} x_j^2 + \sum\sum_{i<j} b_{ij}\, x_i x_j \tag{8-3}$$

Where, b_0 is the responses at the centre point and b_i, b_{jj}, b_{ij} are the coefficients of linear, quadratic and interaction factors respectively.

8.3 Results and Discussion

8.3.1 Mathematical model development

8.3.1.1 Analysis of entry HAZ

The ANOVA Table 8.3 summarizes the analysis of variance of entry surface HAZ. The model F-value of 0.97 implies that the model is not significant. Also the signal to noise ratio (adequate precision) below 4 indicates inadequate model discrimination. Moreover, the negative predicted $\acute{R}^2$ implies that the overall mean is a better predictor to entry HAZ response than the developed model. Therefore the overall mean is considered for the entry HAZ prediction.

Table 8.2 Design matrix and measured responses.

Run	Variables				Responses				
	Peak Power [W]	Speed [mm/s]	Laser off time [ms]	Gas pressure [bar]	Entry HAZ [µm]	Exit HAZ [µm]	Circularity	Taper angle [deg]	Drilling time [ms]
1	200	12	12	6	379	137	0.996	0.93	44
2	600	12	12	6	469	321	0.997	0.95	26
3	600	4	12	6	491	607	0.998	1.11	23
4	400	8	16	5	421	273	0.992	0.55	48
5	1000	12	12	6	522	387	0.999	0.17	23
6	800	8	16	5	500	341	0.998	0.05	34
7	400	8	16	7	236	255	0.999	1.32	43
8	400	16	16	7	400	166	0.998	1.24	35
9	600	12	12	8	547	238	0.996	1.18	23
10	600	12	12	6	308	286	0.998	0.55	29
11	400	16	16	5	347	220	0.998	1.04	46
12	600	20	12	6	413	211	0.996	1.63	28
13	400	16	8	5	371	341	0.998	0.62	28
14	800	16	16	7	520	227	0.999	1.32	26
15	800	16	8	5	391	397	0.998	0.40	15
16	400	16	8	7	482	313	0.999	1.44	26
17	800	16	16	5	340	215	1.000	1.24	31
18	600	12	12	6	433	252	0.998	1.58	26
19	400	8	8	7	325	417	0.997	0.68	29
20	400	8	8	5	538	509	1.000	1.14	34
21	800	16	8	7	412	439	0.998	0.46	15
22	600	12	20	6	421	300	0.998	1.17	56
23	800	8	16	7	426	386	0.999	0.69	29
24	600	12	12	6	557	302	0.999	0.99	29
25	800	8	8	5	310	555	0.998	0.76	11
26	800	8	8	7	656	664	0.997	1.41	16
27	600	12	12	6	527	356	1.000	1.27	26
28	600	12	12	6	389	316	0.999	0.49	32
29	600	12	4	6	517	855	0.999	0.97	8
30	600	12	12	4	603	279	0.997	0.82	29

Table 8.3 ANOVA analysis of the entry HAZ

Source	Sum of squares	D_f	Mean squares	*f*-value	Prob>*f*	
Model	36048.44	4	9012.11	0.97	0.4419	Not significant
A	21659.13	1	21659.13	2.33	0.1395	
B	3837.18	1	3837.18	0.41	0.5265	
C	9867.43	1	9867.43	1.06	0.3129	
D	684.70	1	684.70	0.074	0.7884	
Residual	2.325E+005	25	9300.21			
Lack of Fit	1.906E+005	20	9530.28	1.14	0.4873	Not significant
Pure error	41899.72	5	8379.94			
Cor total	2.686E+005	29				
Standard deviation = 98.44				$\acute{R}^2$ = 0.1342		
Mean= 441.69				Adjusted $\acute{R}^2$ = -0.0043		
Coefficient of variation = 21.83				Predicted $\acute{R}^2$ = -0.2756		
Predicted residual error of sum of squares (PRESS) =3.426E+005				Adequate precision = 3.470		

D_f – Degrees of freedom

8.3.1.2 Analysis of exit HAZ

The summarized ANOVA analysis Table 8.4 shows the significant variables. The F-value of 41.75 implies that the model is significant. The Prob>f values less than 0.05 indicate model terms are significant. Values greater than 0.1 indicate the model terms are not significant. In this case *A, B, C, AD,* B^2 and C^2 are the significant model terms affecting exit surface HAZ. The *D* term added to the model for model hierarchy. The "Adeq Precision" value measures the signal to noise ratio. A ratio greater than 4 is desirable. The ratio of 27.3 indicates an adequate signal and model discrimination.The empirical model in terms of actual factors is:

$$\text{Exit HAZ} = 2008.74 - 0.49A - 58.96B - 130.41C - 77.76D + 0.13AD + 1.64B^2 + 4.28C^2 \quad (8\text{-}4)$$

Table 8.4 ANOVA analysis of exit side HAZ

Source	Sum of squares	D_f	Mean squares	*f*-value	Prob>*f*	
Model	6.580E+005	7	94002.64	41.75	< 0.0001	Significant
A	63091.19	1	63091.19	28.02	< 0.0001	
B	1.462E+005	1	1.462E+005	64.92	< 0.0001	
C	2.952E+005	1	2.952E+005	131.11	< 0.0001	
*D**	182.96	1	182.96	0.081	0.7783	
AD	9999.83	1	9999.83	4.44	0.0467	
B^2	19674.61	1	19674.61	8.74	0.0073	
C^2	1.333E+005	1	1.333E+005	59.20	< 0.0001	
Residual	49536.20	22	2251.65			
Lack of Fit	43376.99	17	2551.59	2.07	0.2157	Not significant
Pure error	6159.21	5	1231.84			
Cor total	7.076E+005	29				
Standard deviation = 47.45				$\acute{R}^2$ = 0.9300		
Mean= 352.16				Adjusted $\acute{R}^2$ = 0.9077		
Coefficient of variation = 13.47				Predicted $\acute{R}^2$ = 0.8203		
Predicted residual error of sum of squares (PRESS) = 1.3E+005				Adequate precision = 27.3		

**D* term added for model hierarchy

8.3.1.3 Analysis of circularity

It is seen in the ANOVA Table 8.5 of the hole circularity that the model is insignificant. Also the Prob>*f* values greater than 0.05 indicates the model terms is not significant. In this case there are no significant model terms. Consequently, a negative predicted $\acute{R}^2$ indicates that the overall mean is a better predictor of hole circularity than the current model.

Table 8.5 ANOVA analysis for circularity

Source	Sum of squares	D_f	Mean squares	*f*-value	Prob>*f*	
Model	1.910E-005	6	3.184E-006	1.51	0.2178	Not significant
A	4.919E-006	1	4.919E-006	2.34	0.1398	
B	1.028E-006	1	1.028E-006	0.49	0.4914	
C	1.593E-006	1	1.593E-006	0.76	0.3930	
D	3.216E-007	1	3.216E-007	0.15	0.6993	
AC	5.645E-006	1	5.645E-006	2.68	0.1149	
CD	5.598E-006	1	5.598E-006	2.66	0.1164	
Residual	4.836E-005	23	2.103E-006			
Lack of Fit	4.248E-005	18	2.360E-006	2.01	0.2261	Not significant
Pure error	5.874E-006	5	1.175E-006			
Cor total	6.746E-005	29				
Standard deviation = 1.450E-003				$\acute{R}^2$ = 0.2832		
Mean= 1.00				Adjusted $\acute{R}^2$ = 0.0962		
Coefficient of variation = 0.15				Predicted $\acute{R}^2$ = -0.3591		
Predicted residual error of sum of squares (PRESS) = 9.169E-005				Adequate precision = 5.599		

8.3.1.4 Analysis of taper angle

The ANOVA analysis of taper angle shown in Table 7.6 implies that the significant model terms are *D* and the interaction terms *BC*. Also the adequate precision ratio above 4 (7.242) indicates adequate model discrimination. The statistical, empirical model developed in terms of actual factors is:

$$\text{Taper angle} = 1.85 - 0.17B - 0.21C + 0.20D + 0.018BC \quad (8\text{-}5)$$

Table 8.6 ANOVA analysis of taper angle

Source	Sum of squares	D_f	Mean squares	*f*-value	Prob>*f*	
Model	2.66	4	0.66	3.81	0.0150	Significant
*B**	0.49	1	0.49	2.78	0.1080	
*C**	2.557E-003	1	2.557E-003	0.015	0.9046	
D	0.92	1	0.92	5.24	0.0307	
BC	1.26	1	1.26	7.19	0.0128	
Residual	4.36	25	0.17			
Lack of Fit	3.49	20	0.17	0.99	0.5601	Not significant
Pure error	0.88	5	0.18			
Cor total	7.02	29				
Standard deviation = 0.42				$\acute{R}^2$ = 0.3786		
Mean= 0.90				Adjusted $\acute{R}^2$ = 0.2792		
Coefficient of variation = 46.46				Predicted $\acute{R}^2$ = 0.1019		
Predicted residual error of sum of squares (PRESS) = 6.31				Adequate precision = 7.242		

**B* and *C* terms added for model hierarchy

8.3.1.5 Analysis of drilling time

Table 8.7 shows the significance of the model and model terms. In this case *A*, and *C* are the most significant model terms associated with drilling time. Also the adequate precision value that compares the signal-to noise ratio greater than 4 (24.2) is desirable. It indicates adequate model discrimination. The statistical/empirical model in terms of actual factors is:

$$\text{Drilling time} = 31.26 - 0.03A + 2.24C - 1.63D \quad (8\text{-}6)$$

Table 8.7 ANOVA analysis of drilling time

Source	Sum of squares	D_f	Mean squares	*f*-value	Prob>*f*	
Model	6.580E+005	7	94002.64	41.75	< 0.0001	Significant
A	63091.19	1	63091.19	28.02	< 0.0001	
C	2.952E+005	1	2.952E+005	131.11	< 0.0001	
D	64.08	1	64.08	3.92	0.0583	
Residual	424.76	26	16.34			
Lack of Fit	394.42	21	18.78	3.10	0.1065	Not significant
Pure Error	30.33	5	6.07			
Cor Total	3420.02	29				
Standard deviation = 4.04				$\acute{R}^2$ = 0.8758		
Mean= 28.8				Adjusted $\acute{R}^2$ = 0.862		
Coefficient of variation = 14.04				Predicted $\acute{R}^2$ = 0.825		
Predicted residual error of sum of squares (PRESS) = 598.85				Adequate precision = 24.2		

8.3.2 Effect of process parameters on the responses

The effect of laser drilled parameters and their interactions were summarised in this section by considering perturbation graphs and 3D response surfaces for all responses (Figures 8.2 – 8.11).

8.3.2.1 Entry side HAZ

Figure 8.2 shows the perturbation plot of the effect of process parameters on the entry side HAZ. It is apparent from this Figure that an increase of peak power increases the HAZ. This is because of the increase of laser power leading to a higher heat input to the beam/material interaction zone. It can also be observed from this plot that increasing the scanning speed and laser "off" time reduces HAZ due to a decrease in number of pulses delivered to each location. Moreover, a longer laser off time allows for enough cooling between the laser pulses. The plot shows very little effect of the gas pressure on the entry HAZ. Therefore, in order to reduce entry HAZ, a low peak power, a high scanning speed and a long laser off time is required in this case. This, however, will reduce the machining/drilling depth and increase the processing time. The relationships between all these process parameters are provided in Figure 8.3. The values of entry HAZ range from 235–665 μm. It is clearly seen in Figure 8.3d that reducing the laser peak power and increasing laser off time reduces the HAZ, also increasing the scanning speed

decreases the HAZ. Figure 8.3c shows that there is little effect to HAZ due to changes in gas pressure. The microscopic observations of the effect of lowest and highest values of process variables on entry side HAZ is shown in Figure 8.4.

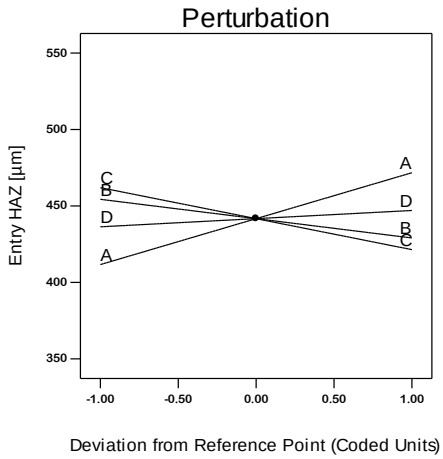

Figure 8.2 Perturbation plot of effect of parameters on the entry side HAZ. *A*: power, *B*: speed, *C*: laser off time and *D*: gas pressure.

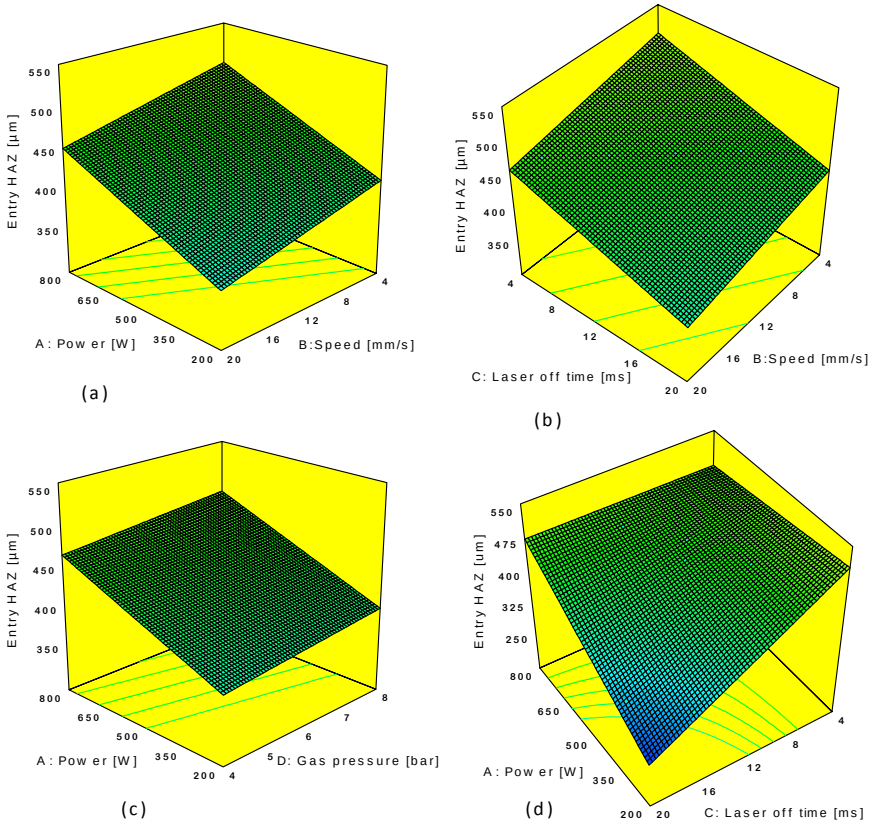

Figure 8.3 Surfaces response graphs of entry HAZ model; (a) power-cutting speed, (b) laser off time-cutting speed, (c) power-gas pressure, (d) power-laser off time.

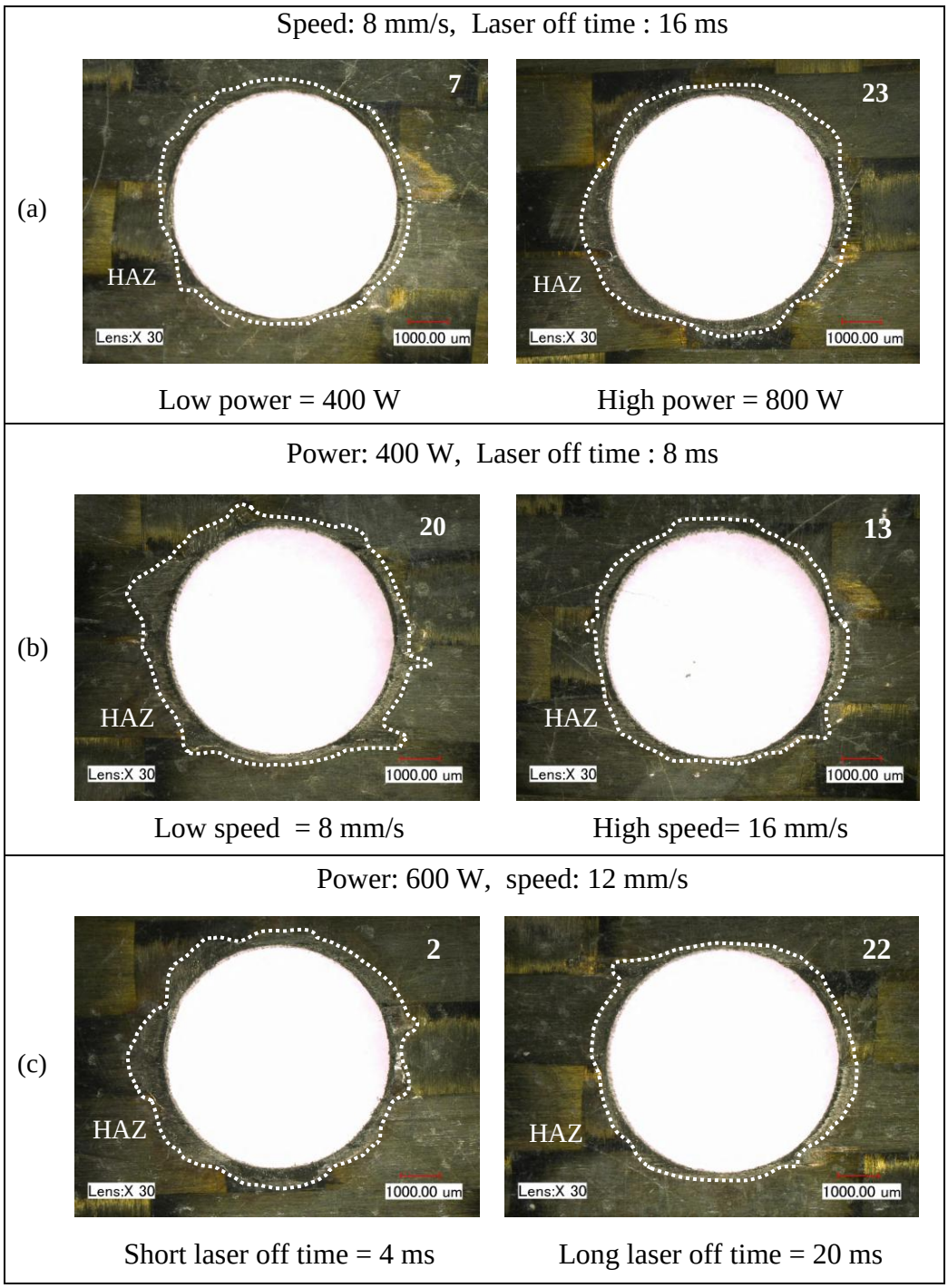

Figure 8.4 Microscopic observations of the effect of process parameters on entry side HAZ;(a) power effect, (b) speed effect, (c) laser off time effect. The number on each Figure indicates the run number. The dotted line represents the HAZ around the hole.

8.3.2.2 Exit side HAZ

The laser power, scanning speed and laser off time are the most significant parameters which control the HAZ, with laser off time having the most significant influence. The perturbation plot in Figure 8.5 shows that the exit surface HAZ is dramatically affected by laser off time that is reduced by giving long time between the pulses. Also the increase in laser power and decrease in scanning speed can increase HAZ due to the high energy deposited into the milling zone. The microscopic observations of the effect of lowest and highest values of process variables on entry side HAZ is shown in Figure 8.6. The effects of these parameters are illustrated in Figure 8.7 by a 3D surface response.

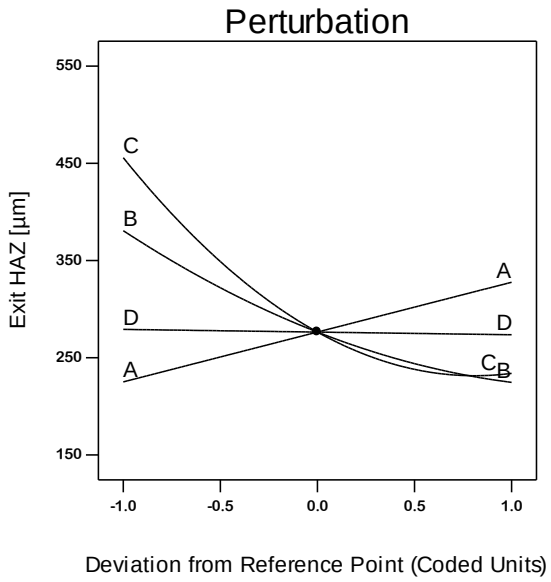

Figure 8.5 Perturbation plot of effect of parameters on the exit side HAZ. *A*: power, *B*: speed, *C*: laser off time and *D*: gas pressure.

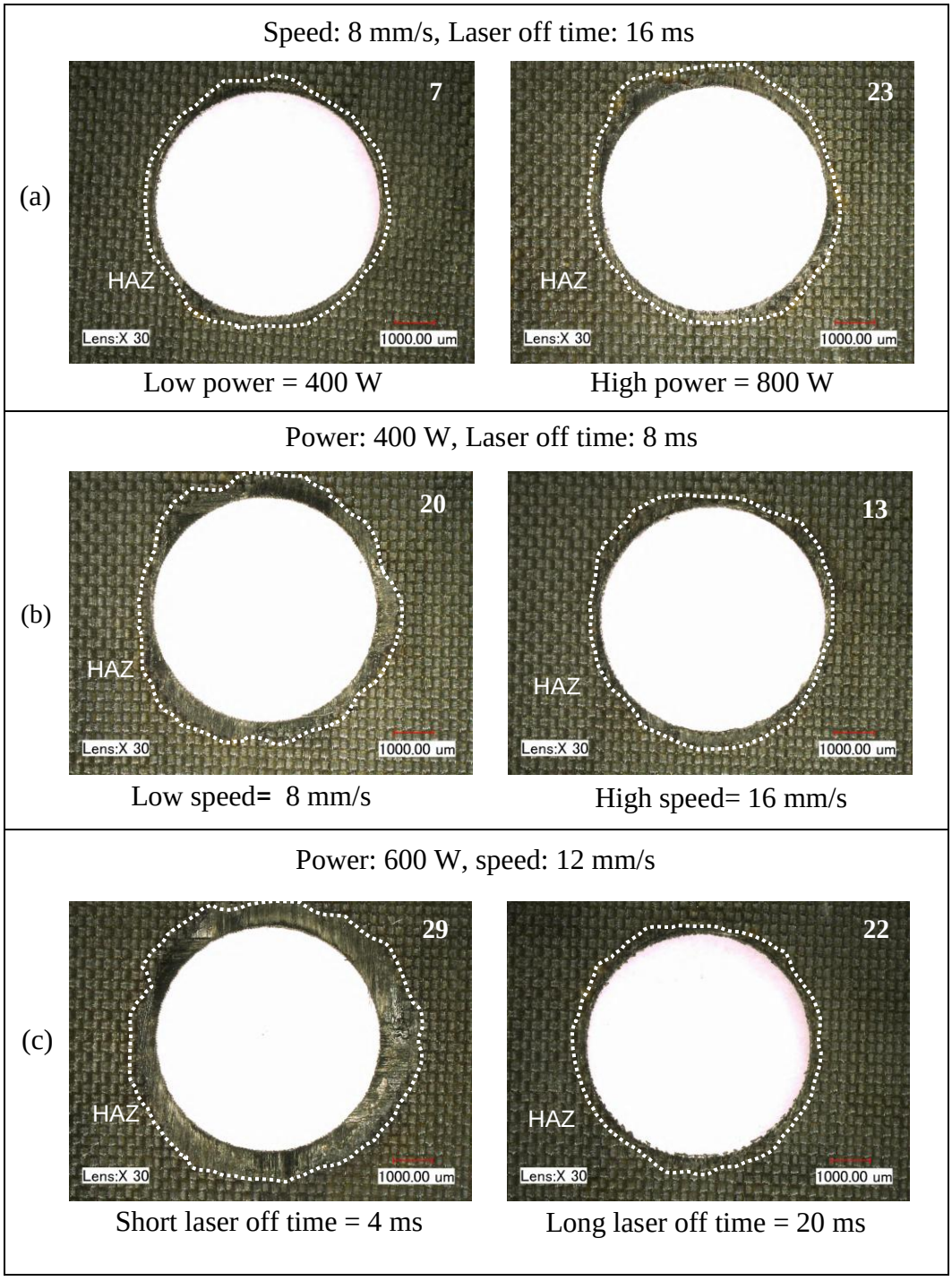

Figure 8.6 Microscopic observations of the effect of process parameters on exit side HAZ; (a) power effect, (b) speed effect, (c) laser off time effect. The number on each Figure indicates the run number. The dotted line represents the HAZ around the hole.

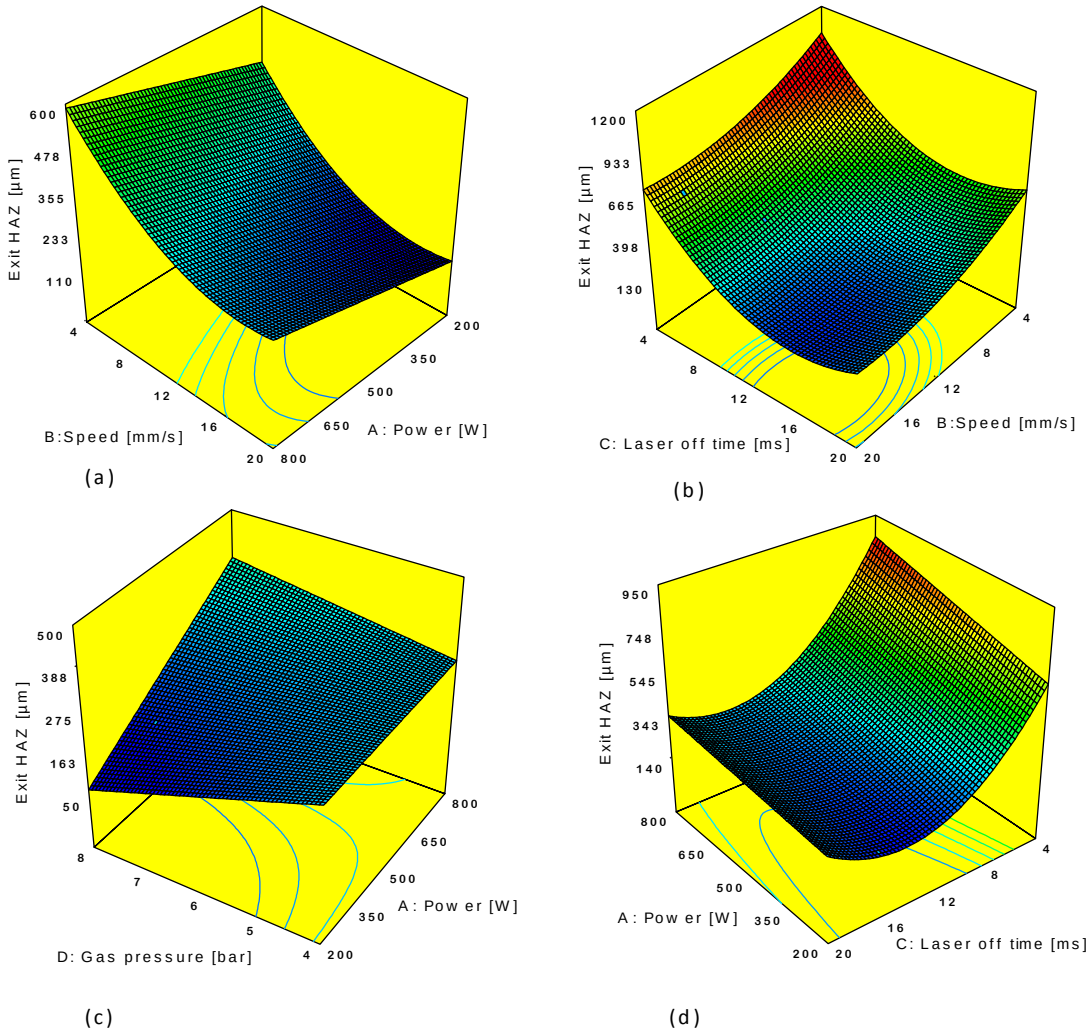

Figure 8.7 Surfaces response graphs of exit side HAZ model; (a) cutting speed-power, (b) laser off time-cutting speed, (c) gas pressure-power, (d) power-laser off time.

8.3.2.3 Hole circularity

The perturbation plot 8.8 shows the effect of laser parameters on hole drilled circularity with the laser power playing the most significant role. It is observed that the laser power and laser off time affect the response, whereas the scanning speed and the gas pressure have little effect. Figure 8.9 shows that the laser power - scanning speed interaction has a significant effect on the hole circularity.

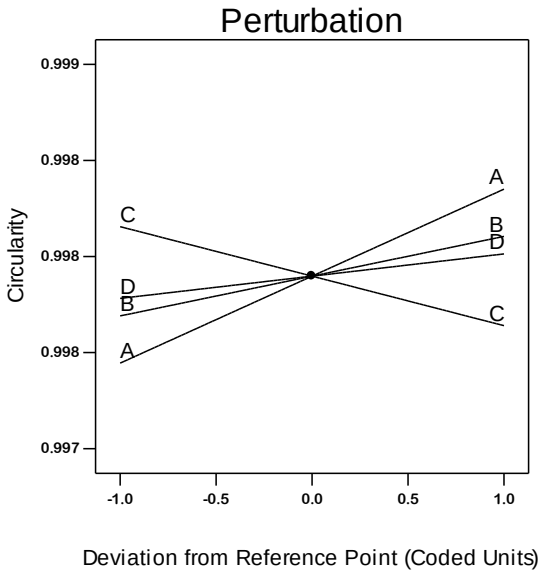

Figure 8.8 Perturbation plot of effect of parameters on hole circularity. *A*: power, *B*: speed, *C*: laser off time and *D*: gas pressure.

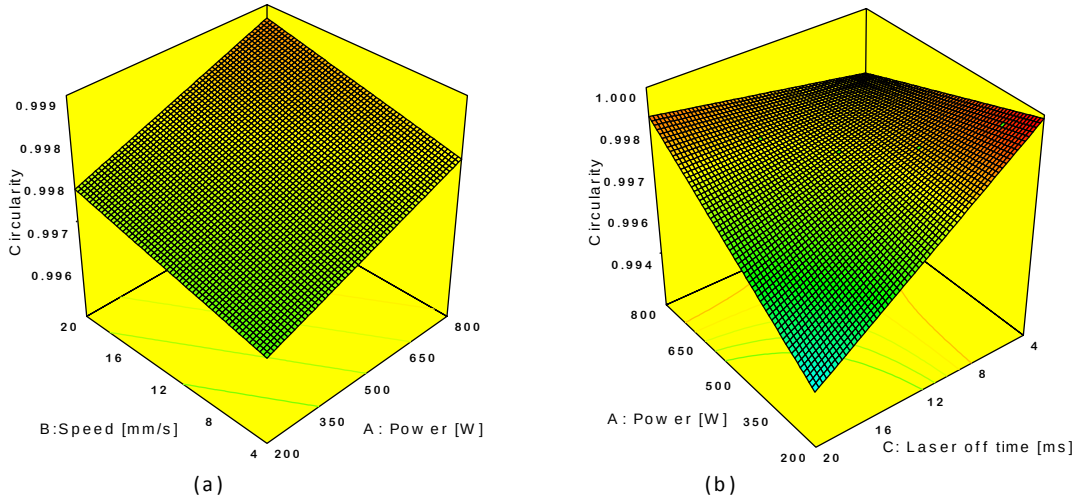

Figure 8.9 Surfaces response graph of hole circularity model; (a) cutting speed-power, (b) power-laser off time.

8.3.2.4 Taper angle

Figure 8.10 is a perturbation plot that shows the effect of laser power, scanning speed, laser "off" time and gas pressure on hole taper angle. It is observed that the scanning speed and gas pressure the most effective parameters on taper angle. The plot shows

that the laser “off” time has no effect on taper angle, whereas, the 3D sufrace response diagram Figure 8.11a shows that the cutting speed laser “off” time interaction has a signifigant effect on the taper angle. Also observed in Figure 8.11b is that the laser power has less effect on the taper angle where reducing gas pressure reduces the taper angle.

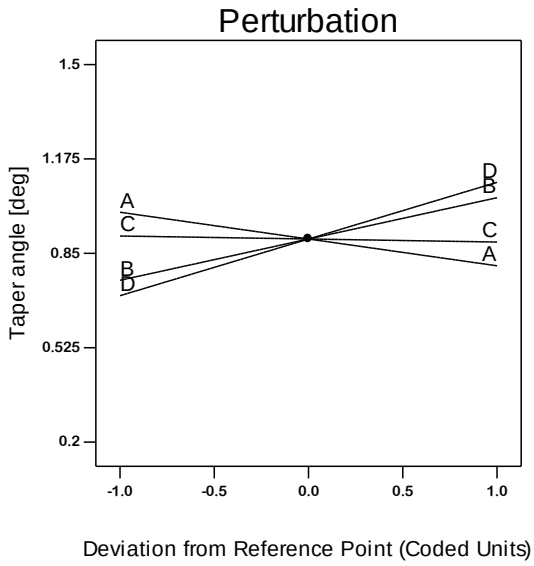

Figure 8.10 Perturbation plot of effect of parameters on taper angle. A: power, B: speed, C: laser off time and D: gas pressure.

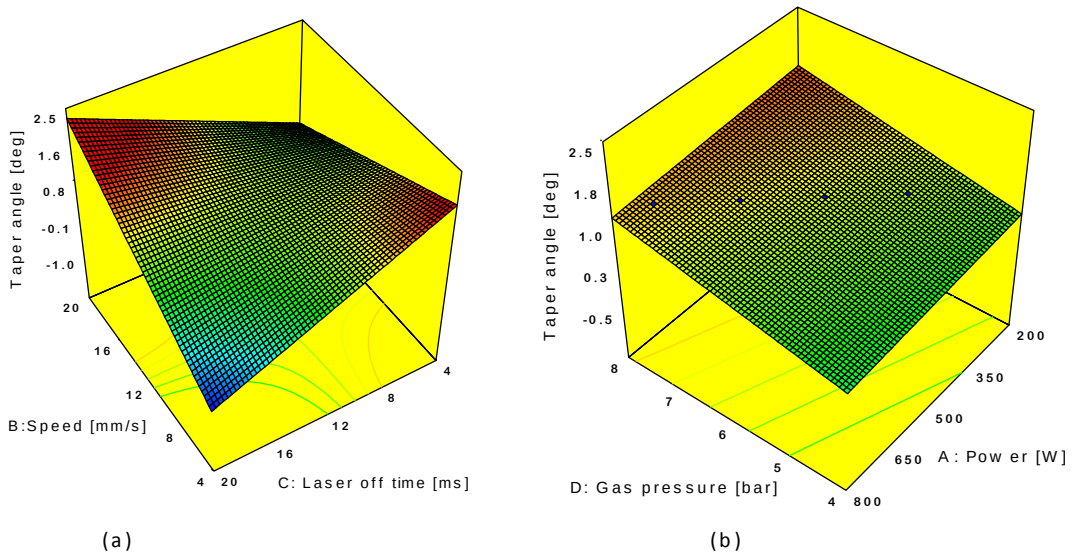

Figure 8.11 Surfaces response graphs of taper angle model; (a) cutting speed-laser off time, (b) gas pressure-power.

8.3.2.5 Drilling time

Figure 8.12 shows a perturbation plot to illustrate the effect of laser parameters on hole drilling time. It can be observed that the most affecting factors on drilling time are laser power and laser "off time", while scanning speed and gas pressure show little effect on drilling time.

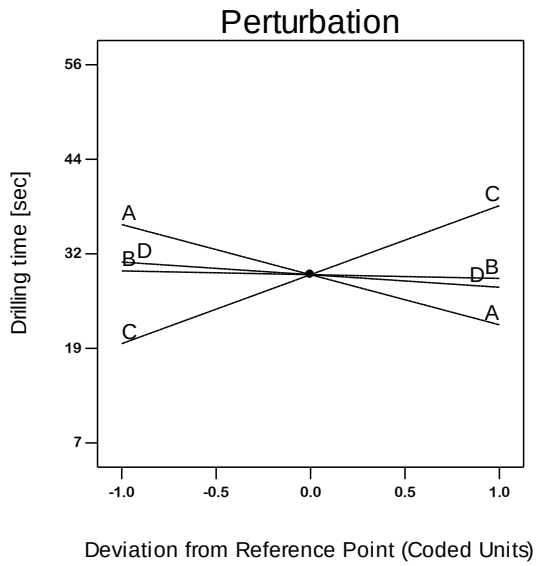

Figure 8.12 Perturbation plot of effect of parameters on drilling time. *A*: power, *B*: speed, *C*: laser off time and *D*: gas pressure.

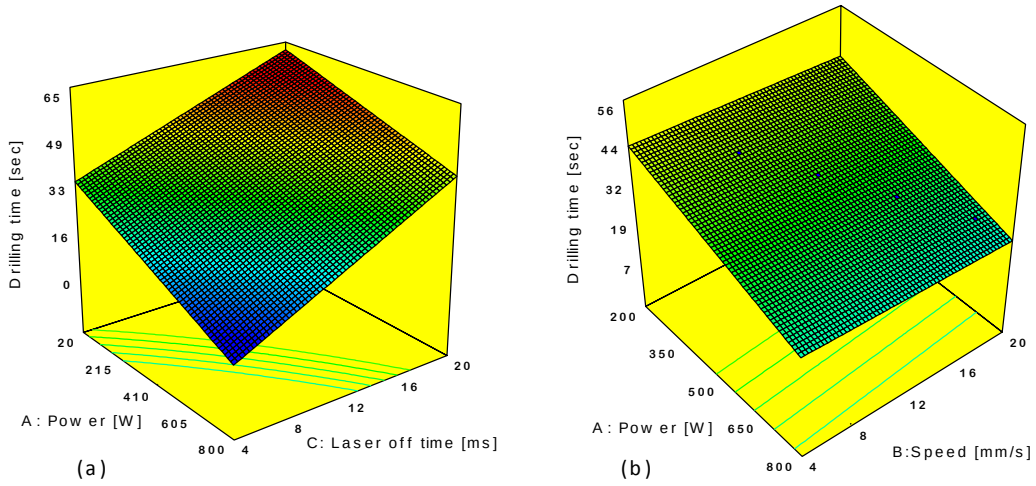

Figure 8.13 Surfaces response graphs of drilling time model; (a) power- laser off time, (b) power-cutting speed.

The plot shows high laser power and short laser off time can reduce the drilling time. This is because of high energy input to the processing region which can enhance the penetration rate and reduce the processing time. A high speed reduces the spot overlaps and the energy per unite length delivered to the machining region, therefore long time needed for full penetration. The effect of these factors on drilling time are well demonstrated on 3D surface response plots in Figure 8.13a, 8.13b.

8.3.3 Optimization

The optimization of the responses was performed using numerical and graphical methods by choosing the preferred goals for each variable and response. The statistical optimisation performed based on the desirability function which is the geometric mean of individual desirabilities ranging from zero for undesirable value to one for most desirable value. The desirability function is defined as [26]:

$$\xi = \left(\prod_{i=1}^{\acute{n}} d_i \right)^{\frac{1}{\acute{n}}} \tag{8-7}$$

Where ξ is the overall desirability, $\acute{n}$ is the number of responses and d_i is the i_{th} response desirability value. The proposed solutions will have the highest desirability depending on the responses obtained from the experiments. Depending on the process goal options (i.e. none, minimum, maximum, in range or target) set for individual responses the desirability value $`d_i`$ of individual responses is calculated as [154]:

$$d_i = \begin{cases} \left[\frac{\acute{y} - A}{B - A}\right]^s & , A \leq \acute{y} \leq B \\ \left[\frac{\acute{y} - C}{B - C}\right]^t & , B \leq \acute{y} \leq C \end{cases} \tag{8-8}$$

Where $\acute{y}$ is the predicted response value; *A*, *B*, and *C* are minimum, target, and maximum response values respectively; *s* and *t* are exponents that qualify the proximity of responses to the target value. The desirability varies from 0 to 1 according to the goal options and the response value $\acute{y}$, d_i=1 if response value equals the target *B*, di=0 if response value less than minimum value *A* and $0<d_i>1$ if the response value varies from minimum value *A* to maximum value *C*. The variables goal assigned an importance

ranging from 1 for low important to 5 for most important. The first part of Eq. (8-8) is used if maximised response is needed whereas second part is used for minimization. The numerical optimisation condition for all the variables and responses are shown in Table 8.8. The requirements in this work are to minimize entry and exit HAZs and drilling time. Therefore, they were given the most important at a setting of 5, whereas the other variables are kept as equally important at a default setting of 3. However, for good quality longer laser off time is required which will increase the drilling time.

Table 8.8 Numerical optimization condition

Variable	Goal	Lower limit	Upper limit	Importance
Power [W]	in range	250	600	3
Cutting speed [mm/s]	maximize	8	20	3
Laser off time [ms]	maximize	10	20	3
Gas pressure [bar]	in range	5	7	3
Entry HAZ [µm]	minimize	236	656	5
Exit HAZ [µm]	minimize	137	855	5
Circularity	in range	0.992	0.999	3
Taper [deg]	minimize	-0.551	1.629	3
Drilling time [sec]	in range	7.5	56	5

Table 8.9 Optimum numerical solutions

NO	Power [W]	Cutting speed [mm/s]	Laser off time [ms]	Gas pressure [bar]	Entry HAZ [µm]	Exit HAZ [µm]	Circularity	Taper angle [deg]	Drilling time [sec]	Desirability
1	250	14	18	5	346	199	0.994	0.96	56	0.65
2	250	14	18	5	346	199	0.994	0.96	56	0.65
3	250	14	18	5	345	197	0.994	0.98	56	0.65
4	250	14	18	5	346	200	0.994	0.95	56	0.65
5	252	14	18	5	346	200	0.994	0.96	56	0.65

Table 8.10 Experimental validation of optimum laser cutting parameters

NO	Power [W]	Cutting speed [mm/s]	Laser off time [ms]	Gas pressure [bar]	Entry HAZ [µm]	Exit HAZ [µm]	Circularity	Taper angle [deg]	Drilling time [sec]
1	250	14	18	5	315±154	201±33	1.001±002	0.764±0.149	56
2	250	14	18	5	332±176	200±38	1.002±001	0.955±0.135	56

The numerically optimised solutions are presented in Table 8.9. The optimum predicted solutions agree with the experimental validation data (Table 8.10), which shows that low power, long laser off time and medium scanning speed are required for low heat affected zones. These requirements increase the laser processing time. It can be clearly seen from Table 8.2 that low processing time (<15 sec) demands for high power, low scanning speed and short laser off time. This setting increases the thermal input to the machining region and consequently the HAZ increases. Figure 8.14 shows the region (overlay plot) for the optimal working condition. The shaded region shows the operating window where average minimum entry HAZ (< 350 µm) and average exit HAZ (< 200 µm) can be obtained. The microscopic images of entry side HAZ, exit side HAZ and cross sectional HAZ of the experimental validation trial are shown in Figures 8.15 and 8.16. The cross sectional HAZ obtained is in the range of 110- 321 µm, which is smaller than the entry/exit HAZ. The high peak power transferred to the material in short time during the pulsed laser mode can lead to direct vaporisation of the CFRP. Moreover, the higher cooling time of pulsed mode compared with CW laser beam can improve the machining quality in which the laser material interaction time is reduced and the period between the generated pulses allows the material to cool down and the heat to be conducted away from the machining region. Furthermore, the multi-pass technique used in this work helps to slice the carbon fibres into small pieces when machining perpendicular to the fibre direction. The heat accumulation between the laser traces raises the temperature within the island. This heat is high enough to decompose the polymer and result in fibres breaking up and they are blown out by assist gas [7]. Furthermore, the multi-pass widens the kerf and allows for the plume, plasma and fragmented fibres to escape from the machined area allowing for the laser beam to reach the inner material and enhance the processing rate.

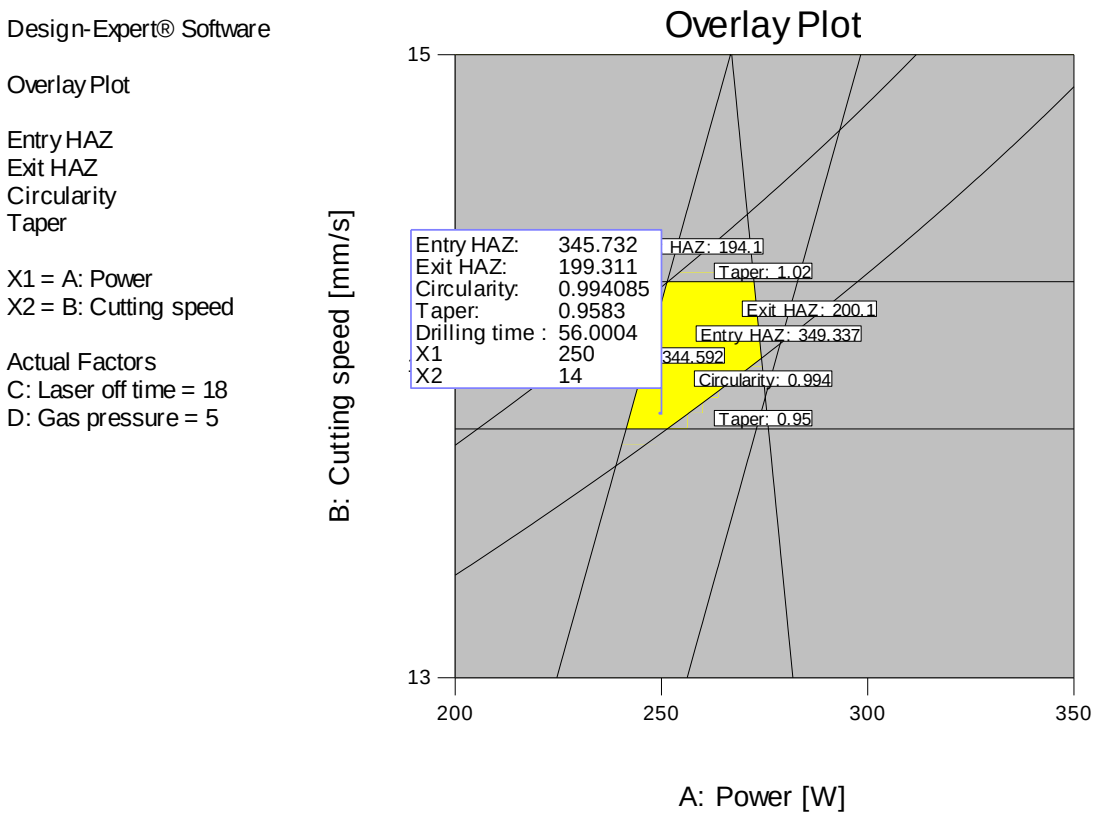

Figure 8.14 Overlay plot shows the reign of the optimal working condition.

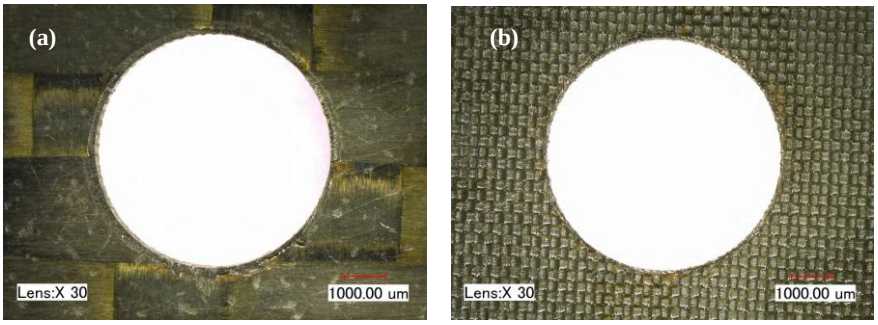

Figure 8.15 Microscopic observations of HAZ for optimum operating parameters at; (a) entry side, (b) exit side.

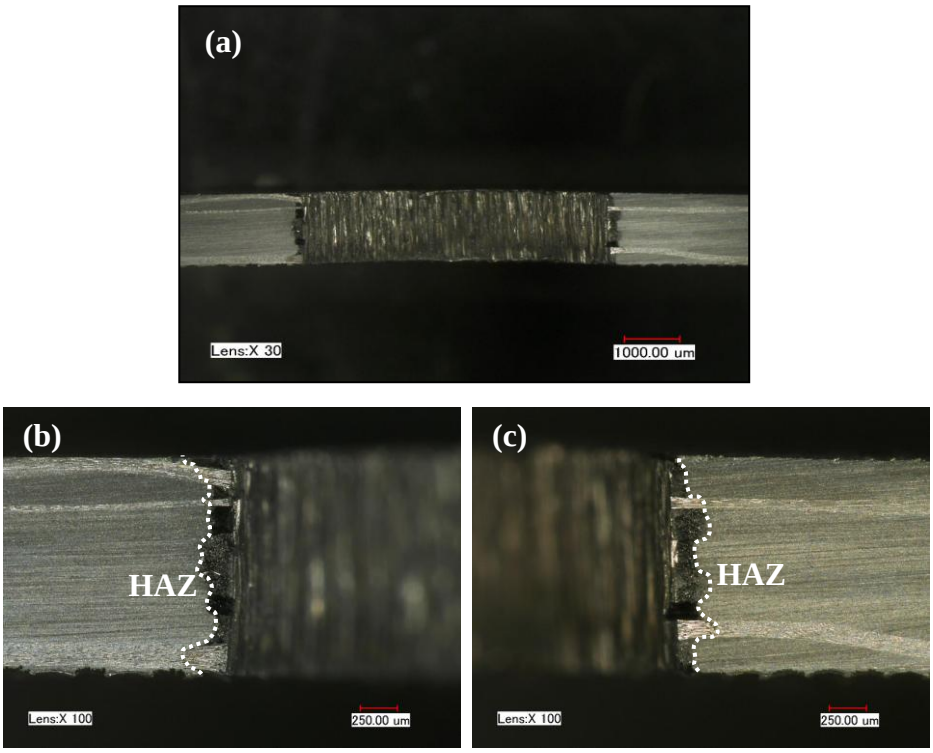

Figure 8.16 Micrographic observation of cross sectional HAZ for optimum operating parameters; (a) overall view, (b) left side close view, (b) right side close view. The dotted line represents the HAZ extensions.

8.4 Summary

Design of Experiment has been used in this chapter to examine the process parameter interactions in pulsed fibre laser (1 kW) for drilling/machining of 1.5 mm thickness CFRP composites with minimum HAZ and short processing time. From this work the following conclusions can be drawn:

1. Pulsed mode fibre laser milling and drilling with 1 ms pulse width can achieve 110 – 350 µm average HAZ at the entry/exit sides and cross-section.
2. For minimum HAZ, low laser power 250 W, short pulse duration (1ms), long laser off time (18 ms), a medium scanning speed (14 mm/s) and multi pass technique are essential.
3. Design of experiments reveals that laser power and laser off time are the most significant parameters affecting the HAZ and the processing time. The optimum solutions were confirmed by experimental validation.

CHAPTER 9 PULSED FIBRE LASER RE-MANUFACTURING AND BONDED REPAIR OF CFRP COMPOSITE PLATES

9.1 Introduction

The wide acceptance of CFRP in many applications and their brittle behaviour mean that the CFRP parts susceptible to damages during their service life. This damage comes from mechanical impact or hydraulic fluid and moisture absorption [172-173]. The need to repair such parts becomes essential especially when the damaged parts are very costly to be replaced and the repair can restore the mechanical properties (strength and stiffness) of the damaged component and permit safe operation. The acceptable repair methods of CFRP such as adhesively bonded repair demands proper and cost-effective material removal techniques. This process involves the removal of the damaged region and filling in the cut out area with a plug of the same material. The conventional mechanical cutting techniques used in composite repair require highly skilled operators and in certain occasions difficult access. Laser processing, as a contactless, tool wear free and dry process, is promising for repairs of large structures. Owing to its higher beam quality (M^2= 1.1-1.2), higher operating efficiency, power stability, long depth of focus, small beam spot diameter, flexible beam delivery and easy of automation [170], high power fibre laser machining could be a more practical tool for CFRP repair applications. A key challenge is to control the HAZ within certain accepted limit.

This chapter investigates the feasibility of using a pulsed fibre laser, delivered through an optical fibre cable, for the repair of CFRP composite plates. These plates can be curved with varied thickness, something that can be difficult to achieve using traditional cutting tools. The small beam spot size and the high laser beam quality enabled precise cutting of the damaged part to a specific taper angle. This allows for the CFRP plug of the same tapering to fit precisely to the created cut out. The effects of laser drilling parameters on geometry accuracy, taper angle, and heat affected zone are discussed in

addition to bonded repair of such plates is presented and underlying physical phenomena are discussed.

9.2 Experimental procedure

The experiments were conducted using a 1 kW IPG YLR-1000-SM ytterbium single-mode fibre laser (Figure 9.1) with a 1.07 µm wavelength, a TEM_{00} beam and a 14 µm fibre core diameter. The laser beam was directed to a laser head which contains a focusing lens (190 mm focal length) and a gas nozzle. The minimum laser beam spot size at focus was 70 µm. The workpiece samples were mounted using a CNC x-y stage. This laser system can be operated in continuous wave (CW) and modulated pulsed modes. Argon gas was used in all experiments. Various thickness (ranging from 1.5 to 6 mm) of carbon fibre reinforced plastic composite materials were used in the experiments. Optical microscopy and scanning electron microscopy were used to study the machining quality. The size of the HAZ (Figure 9.2) was obtained by averaging the measured results around the drilling hole and along the hole depth. The taper angle was calculated depending on the entry and exit diameter of the hole.

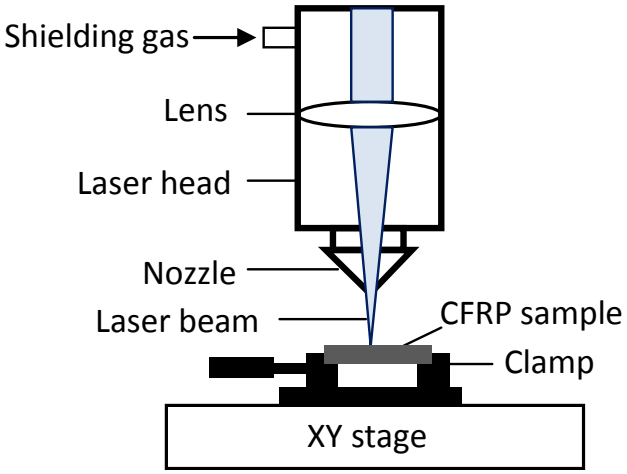

Figure 9.1 Schematic diagram of experimental setup.

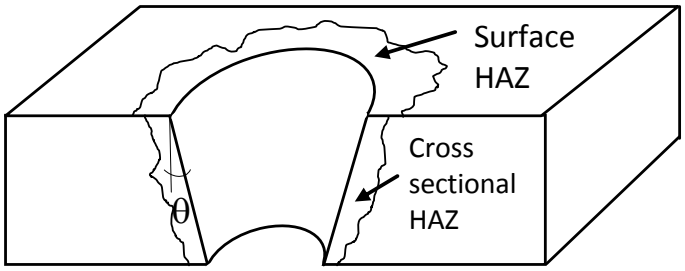

Figure 9.2 Schematic representation of the heat affected zone; θ is the taper angle.

9.3 Results and discussion

The feasibility of using the pulsed fibre laser for the remanufacture and repair of CFRP composite was investigated in this work. Holes were milled on different thickness of CFRP samples to investigate the laser parameters effect on machining quality and choose the optimum parameters value for good machining quality (less HAZ).

9.3.1 Pulsed fibre laser drilling investigations

The use of a pulsed mode laser reduces the laser beam material interaction and allows for the control of cooling period between the incident pulses. This minimise heat build-up in the workpiece and improves the machining quality. The effect of pulsed laser mode parameters such as laser power, laser off time and scanning speed on machining quality were investigated to evaluate the use of pulsed fibre laser for CFRP repair. The effect of laser power on top surface average HAZ is shown in Figure 9.3. It can be observed that the HAZ is increased by increasing the laser power. This is because of the increase in power intensity at high peak power. It is observed in Figure 9.4 that the HAZ at both sides of the hole is reduced by increasing laser off time. Longer laser off time produces less HAZ due to longer cooling interval between laser pulses. Moreover, in Figure 9.5 it is observed that increasing the scanning speed reduces

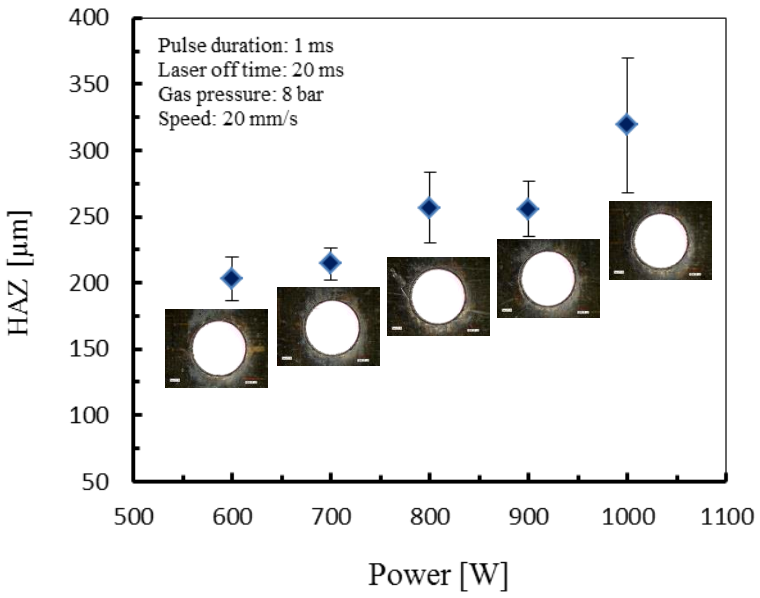

Figure 9.3 Heat affected zone as a function of laser power on top (entry) surface of a 3.3 mm thick CFRP plate.

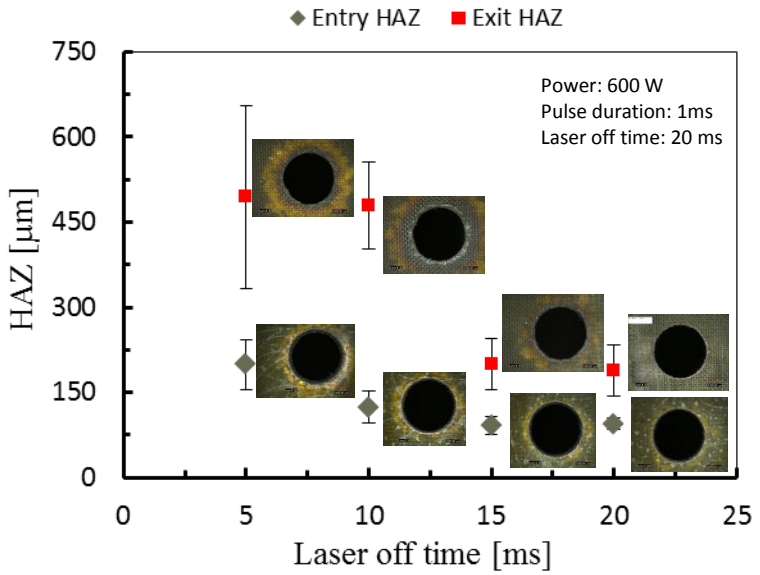

Figure 9.4 Heat affected zone as a function of laser off time on top (entry) and bottom (exit) surfaces of a 3.3 mm CFRP plate.

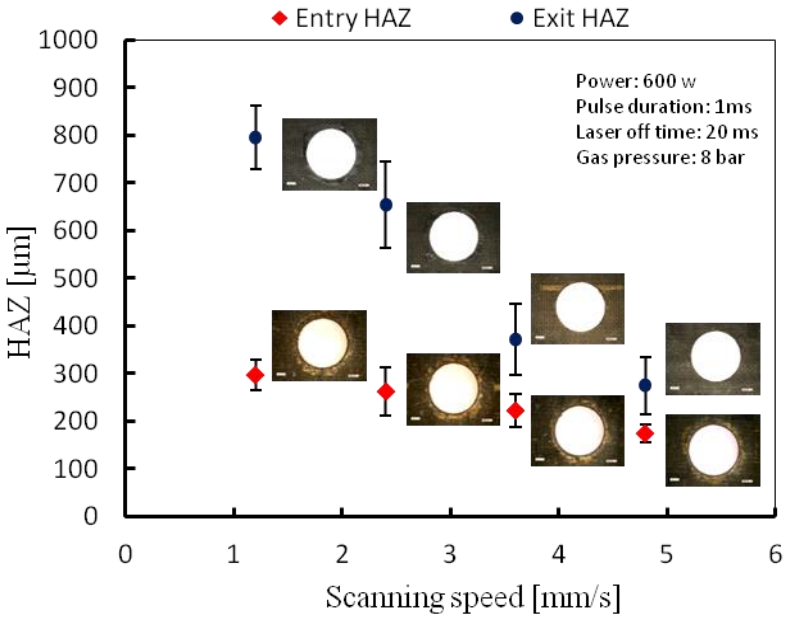

Figure 9.5 Heat affected zone as a function of scanning speed on top (entry) and bottom (exit) surfaces of a 2.3 mm thick CFRP plate.

the thermal damage due to the reduction in laser material interaction time. Also in Figure 9.6 the hole taper angle increases with the scanning speed. Consequently, it is essential to investigate multi pass drilling with high scanning speed and long pulse off time.

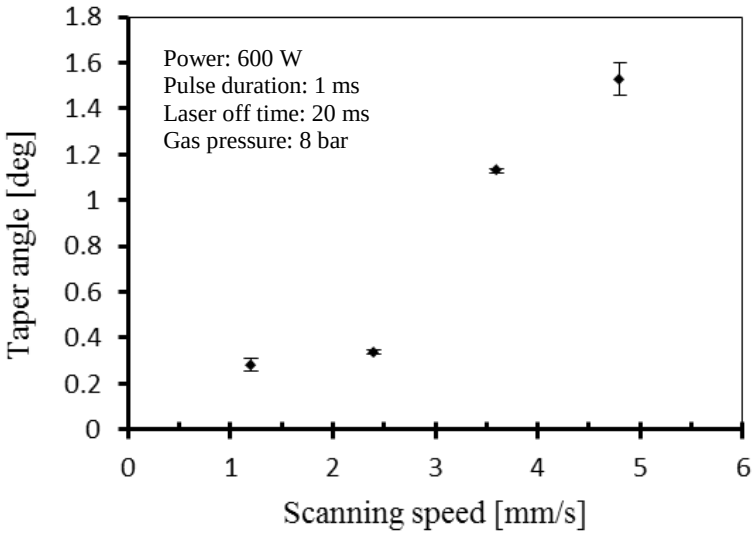

Figure 9.6 Taper angle as a function of scanning speed.

9.3.2 Multi-pass pulsed fibre laser drilling of CFRP plates

Table 9.1 shows the drilling investigations of multi pass drilling of 1.5 mm thick CFRP plate. It was found that, using a power of 350 W, laser off time 20 ms and scanning speed of 18 mm/s generates minimum HAZ in the range of 60 – 249 µm at the hole surfaces. Figure 9.7 shows SEM observations of the laser drilled hole.

Table 9.1 Pulsed laser mode parameters used for drilling of 1.5 mm thick CFRP

NO	Power [W]	Speed [mm/s]	Pulse duration [ms]	Laser off time [ms]	Gas pressure [bar]	HAZ range [µm]
1	1000	25	1	20	8	102-366
2	700	18	1	20	8	95-372
3	500	18	1	20	8	93-273
4	400	18	1	20	8	87-264
5	350	18	1	20	8	60-249
6	350	18	1	15	8	97-278
7	350	18	1	10	8	125-344
8	350	18	1	5	8	136-349

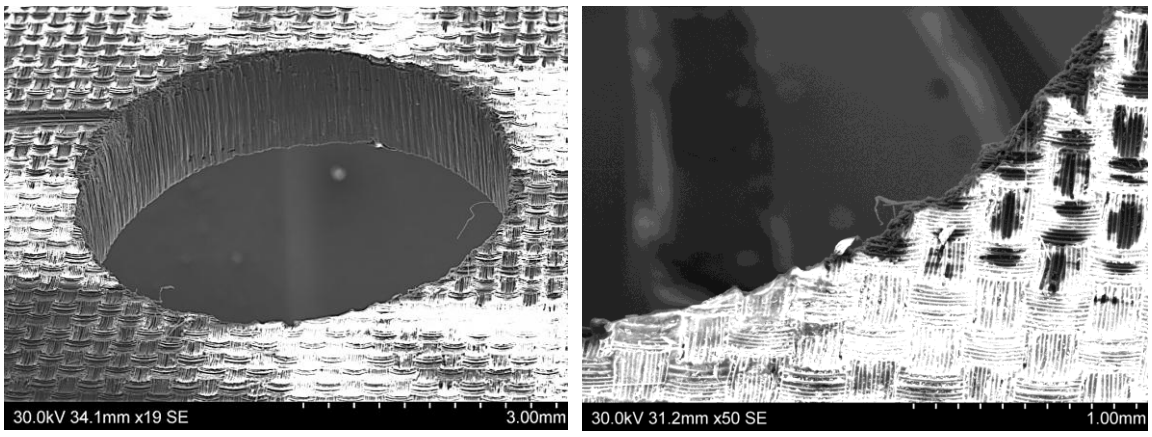

(a) (b)

Figure 9.7 SEM observations of HAZ on 1.5 mm thick CFRP plate; (a) top surface, (b) close-up view.

In Figure 9.8 drilling of 2.3 mm thick CFRP sample was investigated using two different speeds (20 and 22 mm/s) at the same hole path in order to distribute the laser pulses along the hole path when using a long laser off time. Therefore, the number of

passes required to drill the hole was reduced. The investigations show that the HAZ at both sides of the hole was in the range of 42 – 271 µm.

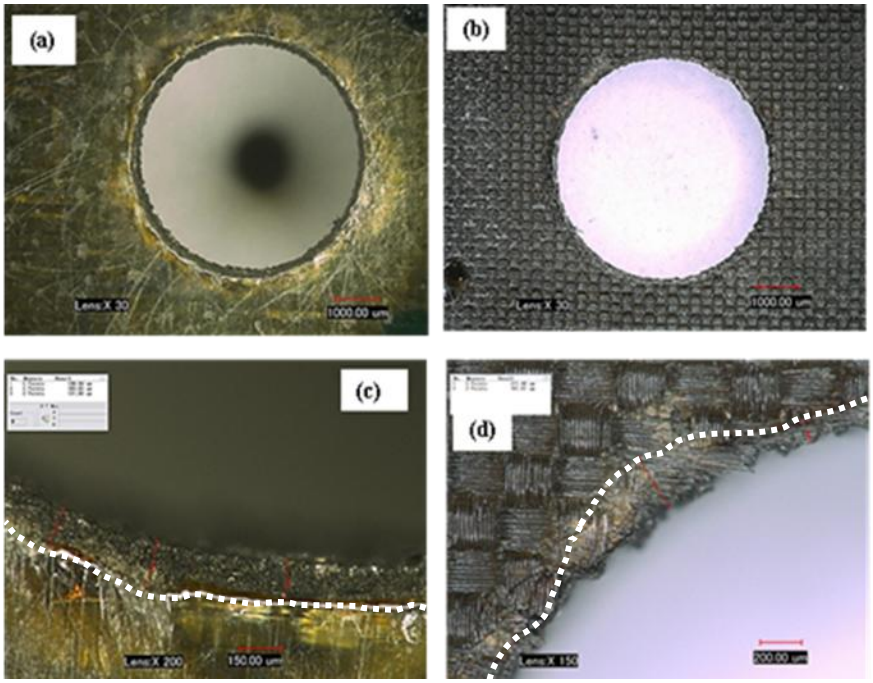

Figure 9.8 Multi pass laser drilling of 2.3 mm thick CFRP; (a) entry side, (b) exit side, (c) and (d) close-up view of both sides respectively. Power: 900 W, speed: 20&22 mm/s, gas pressure: 8 bar, pulse duration: 1 ms, laser off time: 20 ms, number of passes: 8. The dotted line represents the HAZ extensions and discoloration.

The drilling of 6 mm thick CFRP sample is shown in Figure 9.9. The measured HAZ at entry side was in the range of 26 – 185 µm whereas at the exit side was in the range of 44 – 422 µm. The thick sample required high number of passes to breakthrough. This leads to high heat accumulation at the hole exit side which increased the thermal damage compared to the entry side.

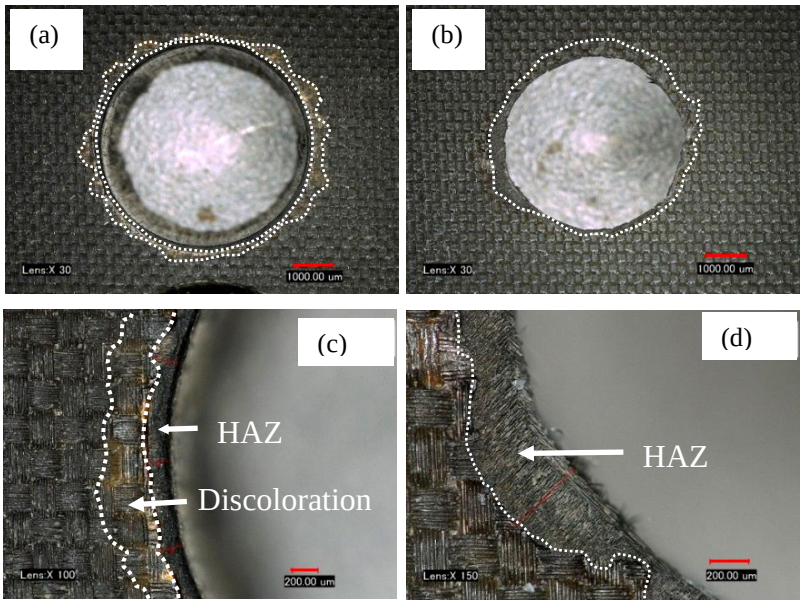

Figure 9.9 Multi pass laser drilling of a 6 mm thick CFRP; (a) entry side, (b) exit side, (c) and (d) close-up view of both sides respectively. Power: 1kW, speed: 12 mm/s, gas pressure: 8 bar, pulse duration: 1 ms, laser off time: 20 ms. The dotted line represents the HAZ extensions and discoloration.

9.3.3 Laser based re-manufacturing and repair of CFRP

Few researchers have investigated the laser-based repair of CFRP composite as an alternative technique to overcome the disadvantages of conventional techniques such as mechanical milling and grinding techniques [141-142]. The laser processing allows a full automation process, processing time reduction and high geometrical accuracy. Figure 9.10 shows the capability of lasers to mill different shapes in CFRP composites.

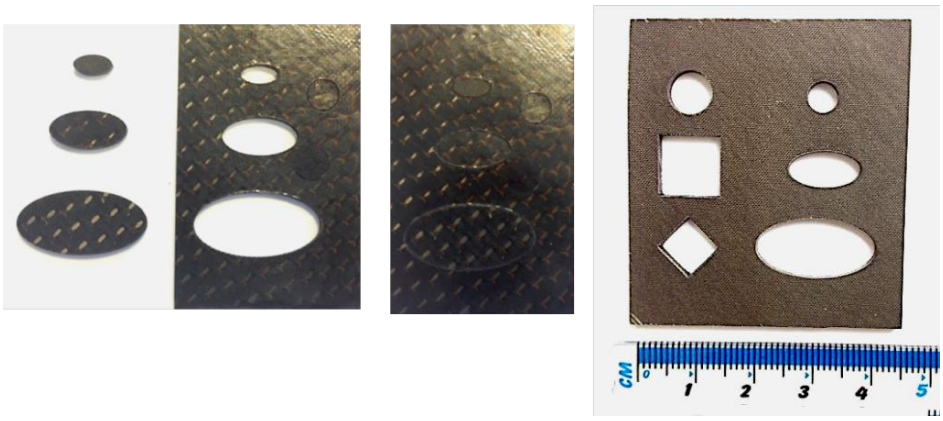

Figure 9.10 Different shapes milled in CFRP using pulsed fibre laser.

The experimental investigations in section 9.3.1 showed that the use of pulsed fibre laser mode offers better machining quality. The quality was improved using low laser power, medium scanning speed and long laser off time during machining of 1.5 mm thick CFRP plate. Therefore, from section 9.3.1 and from chapter 8 (Table 8.10), the parameters set of 250 W laser powers, 18 mm/s scanning speed and 20 ms laser-off time were used to demonstrate the re-manufacturing and repair of 1.95 mm thick CFRP plate using laser as the machining tool. The steps of the repair used are presented schematically in Figure 9.11. It involves the use of pulsed fibre laser to remove the damaged material and cut a new plug of the same size and configuration, which is adhesively bonded in the same place as shown in Figure 9.12.

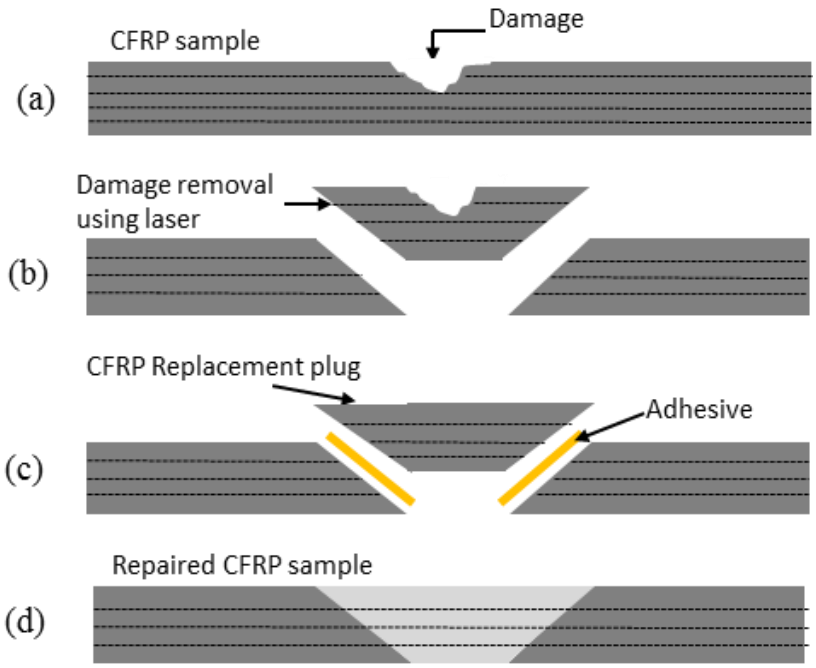

Figure 9.11 Schematic representation of CFRP re-manufacturing and repair procedures; (a) damaged sample (b) Laser damage removal, (c) new plug replace (d) repaired sample.

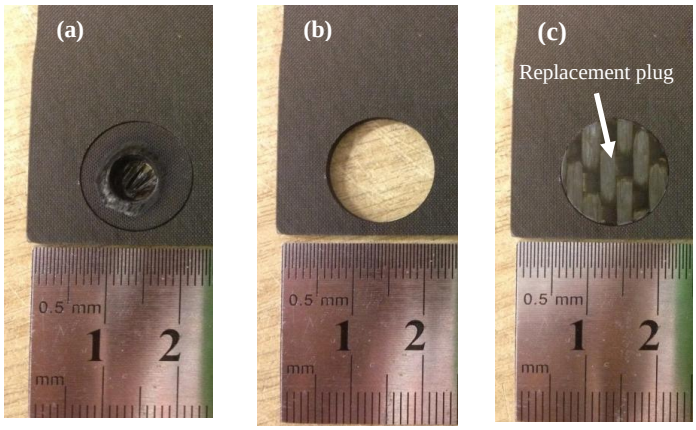

Figure 9.12 CFRP repair procedure; (a) damaged specimen (b) damage removed, (c) repaired specimen. No HAZ is observed.

Figure 9.13 illustrates that a woven fabric composite has been used for the plug depending on loading conditions. The full automation of the process allows for machining different shapes and material systems as shown in Figure 9.13. Furthermore, the investigations show the feasibility of using laser to machine a curved specimen with variable thicknesses as shown in Figure 9.14. The narrow kerf (100 µm) and taper walls (1˚) usually obtained during laser machining prevent the produced plug from falling through the other side (3D robotic laser head could be used for further control of the taper angle). This permits the remanufacture and repair of the closed parts such as airplane wings. The range of HAZ obtained at entry/exit sides and at the cross section of 1.95 CFRP plate (Figure 9.15) was 59 – 320 µm. The yellowish/brown ring created around the cut out is mainly due to discolouring of the composite material rather a heat affected zone.

(a (b

Figure 9.13 CFRP repair with different shapes; (a) after damage removal, (b) after repair.

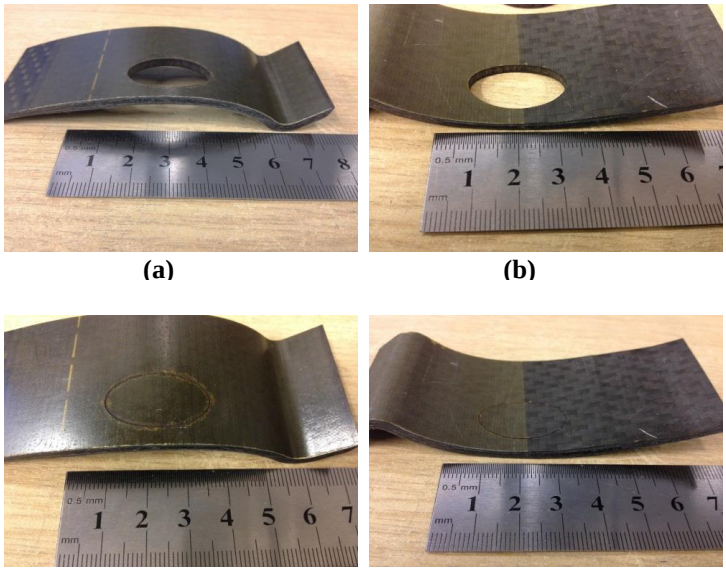

Figure 9.14 Re-manufacturing and repair of woven CFRP curved panels; (a) and (b) top/bottom sides after damage removal respectively, (c) and (d) top/bottom sides after repair, respectively.

-

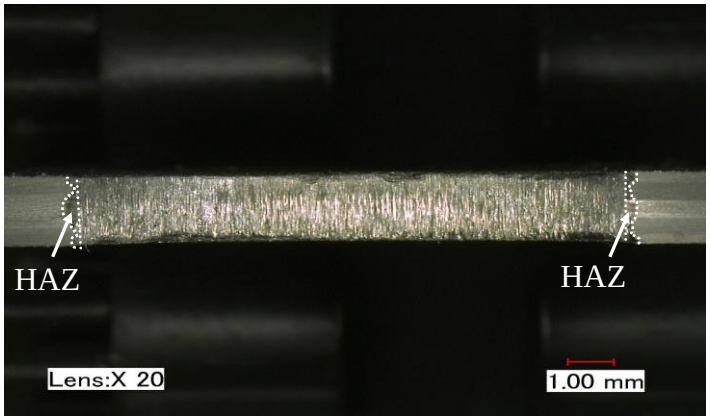

Figure 9.15 Cross-sectional image of elliptical shape of 1.95 mm thick CFRP plate. The dotted line represents the HAZ extensions.

9.4 Summary

This chapter presented the investigation of using a continuous and pulsed mode 1 kW fibre laser to machine a multi layered CFRP composite. Furthermore, the feasibility of using a pulsed fibre laser mode for CFRP remanufacture and repair is also presented. The objective was to mill holes in different CFRP thickness with controlled tapers and a small HAZ. Consequently, the following conclusions can be drawn from this work:

1. The cutting quality (HAZ) obtained by using pulsed fibre laser mode at the entry/exit sides and inside the bulk material was 26 – 422 µm.
2. Less thermal damage necessities the use of long laser off time and short interaction time during pulsed fibre laser processing.
3. The narrow laser kerf (~ 100 µm), the taper (1˚) generated during laser processing and the ease of automation of fibre laser make it possible to develop a new technique for laser-based repair of CFRP specially for closed parts such as airplane wings.
4. The technique performance strength of repaired parts needs to be evaluated in further investigations.

CHAPTER 10 SEQUENTIAL LASER AND MECHANICAL DRILLING OF CFRP COMPOSITE

10.1 Introduction

CFRP composite is anisotropic and very abrasive. Drilling of this material using a twist drill leads to many damage. These damage include excessive tool wear, fibre pull out and delamination [174]. Among these problems, delamination reduces the service life of the component, and nearly 60% of the components produced in the aircraft industry are rejected because of the delamination [44, 175]. Therefore, it is considered as the biggest challenge of using CFRP in wide industrial applications [176-177]. The delamination developed during drilling is related to the thrust force exerted by twist drill [178]. A worn drill may increase the thrust force that causes extra delamination [179]. Owing to the frequent use of the twist drill to create holes quickly and economically in industry [178, 180], reducing the associated thrust force and tool wear of the twist drill during CFRP drilling could reduce the risk of delamination. According to the twist drill configuration, the chisel edge of twist drill is considered as the main contributor to the thrust force[181]. The velocity at the chisel edge is zero, which makes the twist drill only push the target material at this point, more thrust force is exerted as the tool penetrates inside the sample generating delamination at the exit side [182]. It has been found that eliminating the thrust force created by the chisel edge can reduce the delamination hazard [174] With a pre-drilled hole the effect of chisel edge is eliminated and delamination can be reduced significantly [182]. Won et al.[181] studied the effect of the chisel edge on the thrust force, and the effect of pre-drilling the laminate with a pilot hole. They showed that the thrust force is largely reduced when a pilot hole is used, and the influence of the chisel edge was removed. Tsao [176, 183] studied the significance of using a pilot hole to reduce the delamination when using core drills and saw drills. He pre-drilled a pilot hole to eliminate the thrust force produced by the chisel edge of twist drill; hence significant reduction on delamination was observed. However, with CFRP composite drilling a pilot hole using mechanical tools subjected to drilling-induced delamination and excessive tool wear [183]. Lasers as contact less and wear

less tools and fast process, can be used to produce a pilot hole. Okasha et al.[184-186] used a laser to produce pre-drilled pilot holes. They presented a novel sequential laser and mechanical micro-drilling of Inconel 718 alloy. They first used a laser beam to drill a pilot hole, then the hole finished by mechanical drilling. They concluded that the process improves the imperfections associated with laser-drilled holes and releases the load on the drill point (chisel edge) and considerably increases drill life. Furthermore, they reported that 240–430% tool life increase obtained using the new drilling method. This chapter presents the use of a sequential laser-reaming and a sequential laser-mechanical drilling technique to overcome the damage generated during laser drilling of CFRP composite and improve the tool life in the case of mechanical drilling of CFRP. The aim of this research is to use the laser process to drill a hole first, then the hole is finished mechanically using reamer or twist drill in order to improve the hole quality and geometry (eliminate HAZ and hole taper) after laser processing. Moreover, the laser pilot hole will eliminate the drilling resistance by removing the material in front of the chisel edge of the twist drill. This will increase the tool life, reduce delamination and reduce the total machining cost. Furthermore, the effect of laser pre-drilled holes on tool wear is introduced in this work.

10.2 Experimental procedures

The material used in the experiments was 1.5, 3.36 and 4 mm thick CFRP samples. The workpiece samples were mounted using a CNC x-y stage. The experimental laser tests were conducted using a continuous wave and pulsed mode of 1 kW IPG YLR-1000-SM ytterbium single-mode fibre laser system presented in chapter 8 and 9. This laser can be modulated to produce a pulse train up to 5 kHz. The laser beam spot size at the sample surface was 70 µm. The assist gas used for all investigations was argon at 8 bar pressure. The stand-off distance between the nozzle and the sample was 1 mm. The investigations involved the use of the pulsed laser mode to produce 5.5 mm diameter holes with HAZ < 250 µm and then reamed to a final hole size of 6 mm diameter. Reaming lubricant was used with the reaming process. Additionally, a CW mode was used to produce 3 mm diameters holes with HAZ < 1.5 mm, then drilled to a final hole size of 6 mm diameter using mechanical twist drill. The lowest possible drilling time using laser was targeted. Trepanning drilling technique was used to create the laser pre-

drilled holes. Mechanical drilling tests were dry process and performed manually using a bench drilling machine. Back plate, different HSS drill sizes and refractive drilling approaches were used during sequential laser-mechanical process to reduce the delamination and finish the laser-drilled holes. The drilling quality of the samples at entry/exit and cross section sides was examined using optical microscope.

10.3 Results and discussion

Pulsed and CW fibre lasers were used to investigate the feasibility of using a sequential laser-reaming and sequential laser-mechanical drilling techniques to remove the heat damages generated during laser drilling and improve the mechanical tool life.

10.3.1 Pulsed fibre laser drilling of CFRP

10.3.1.1 Drilling of 1.5 mm thick

Based on the drilling investigations of pulsed fibre laser drilling of 1.5 mm CFRP sample in chapter 9 (section 9.3.2), it was found at a laser power of 350 W, laser off time 20 ms and scanning speed of 18 mm/s, a HAZ in the range of 60-249 µm was generated. This HAZ is within the required limit (<250 µm). Figure 10.1 shows the microscopic observations at the entry and exit sides of the drilled hole.

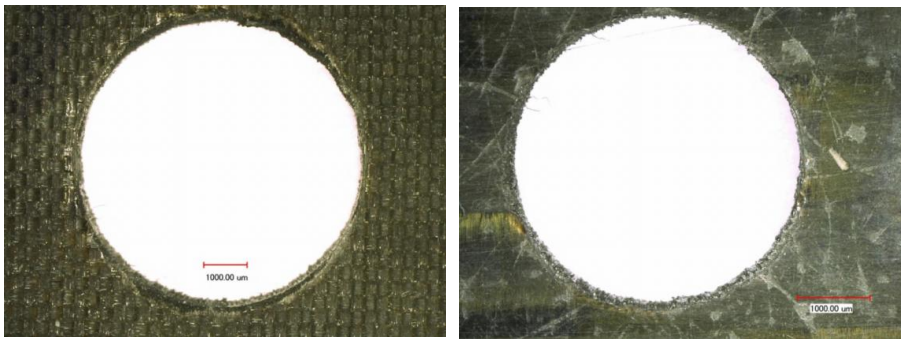

(a) (b)

Figure 10.1 Hole entry and exit surface observations of 1.5 mm thick sample: (a) entry side, (b) exit side.

10.3.1.2 Drilling of 3.36 mm thick CFRP

In Figure 10.2 drilling of 3.36 mm thick CFRP sample was investigated using two different speeds (18 and 20 mm/s) at the same hole path in order to distribute the laser pulses along the hole path when using a long laser off time. Therefore, the number of passes required to drill the hole was reduced. The investigations show that the HAZ at both sides of the hole was in the range of 27 – 147 µm; whereas the maximum cross sectional HAZ in Figure 10.3 was 309 µm.

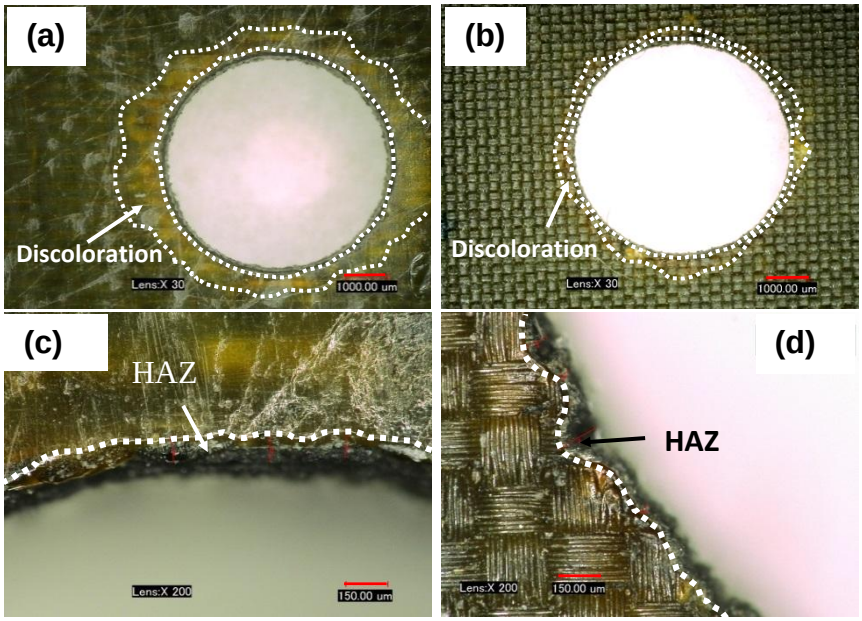

Figure 10.2 Multi passes laser milling of 3.36 mm thick CFRP plate; (a) entry side, (b) exit side, (c) and (d) close-up view of both sides respectively. Power: 600 W, speed: 18&20 mm/s, gas pressure: 8 bar, pulse duration: 1 ms, laser off time: 20 ms, number of passes: 20. The dotted line represents the HAZ extensions and discoloration.

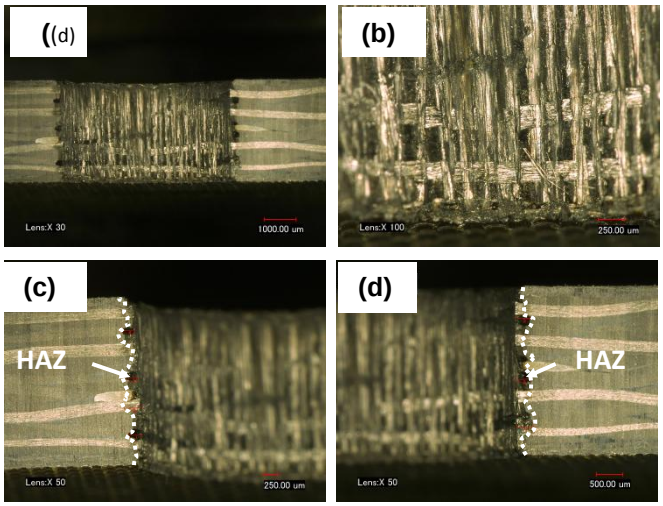

Figure 10.3 Cross-sectional images of multi passes laser milling of 3.36 mm thick CFRP; (a) Wide view, (b) inner wall, (c) and (d) close-up view of the cross cut, max HAZ 309 µm. The dotted line represents the HAZ extensions.

10.3.2 CW fibre laser drilling of CFRP

10.3.2.1 Drilling of 5.5 mm diameter hole

Figure 10.4 shows the effect of different scanning speed on the top surface HAZ of 1.5 mm thick CFRP samples at 1000 W laser power. It is seen that the HAZ is decreased by increasing the scanning speed. This is due to the reduction in energy per unit length and shorter interaction time. The average HAZ at scanning speed of 50 mm/s (maximum x-y stage speed) is about 650 µm. This thermal damage is beyond the required target. Therefore, the HAZ characteristic was investigated at different laser powers. Table 10.1 summarizes the parameters used and the HAZ values during these investigations. However, the HAZs shown in Table 10.1 are still beyond the required limit (< 250 µm) when drilling 5.5 mm diameter hole. The microscopic observations of effect of different laser power at different scanning speed are shown in Figure 10.5. The large thermal damage associated with CW mode necessitates the use of smaller laser pre-drilled holes.

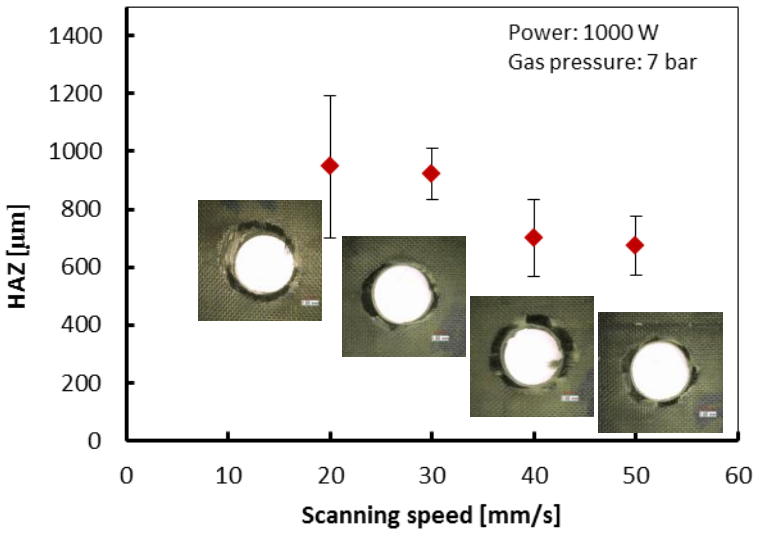

Figure 10.4 Effect of scanning speed on top surface HAZ using CW mode. Hole diameter 5.5 mm.

Table 10.1 CW laser parameters used for drilling of 1.5 mm CFRP plate.

NO	Power [W]	Scanning speed [mm/s]	passes	Standoff distance [mm]	Gas pressure [bar]	HAZ range [µm]
1	1000	50	3	1	7	490-930
2	1000	40	3	1	7	480- 1070
3	1000	30	2	1	7	710-1120
4	1000	20	1	1	7	490-1590
5	1000	16	1	1	7	530-1210
6	500	8	1	1	8	320-1590
7	250	16	4	1	5	270-850
8	200	16	5	1	5	259-720

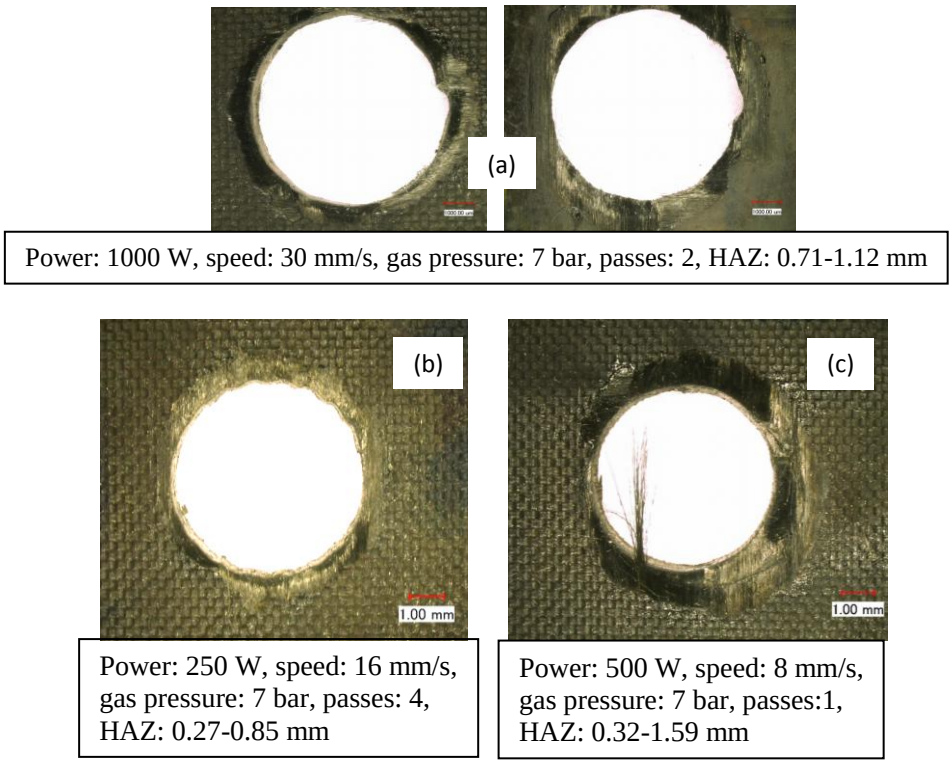

Figure 10.5 CW fibre laser drilling of 1.5 thick CFRP with different powers and scanning speed; (a) 1000 W, (b) 500 W, (c) 250 W

10.3.2.2 Drilling of 3 mm diameter hole

Based on the results obtained on section 10.3.2.1, experimental trails were conducted to define the suitable laser processing parameters to drill 3 mm diameter hole. The parameters were chosen to ensure full hole drilling in shortest possible time and lowest HAZ. With these trials, it was found that a 3 mm hole could be drilled in 1 sec with a HAZ less than 1.5 mm around the drilled hole using 300 W laser power, 20 mm/s scanning speed and 2 scanning passes. Figure 10.6 shows the microscopic photographs of the laser pre-drilled hole using a power of 300 W, a scanning speed of 20 mm/s and 2 scanning passes. The HAZ generated at the entry/exit sides and at the cross-section was less than 1.5 mm around the hole edges.

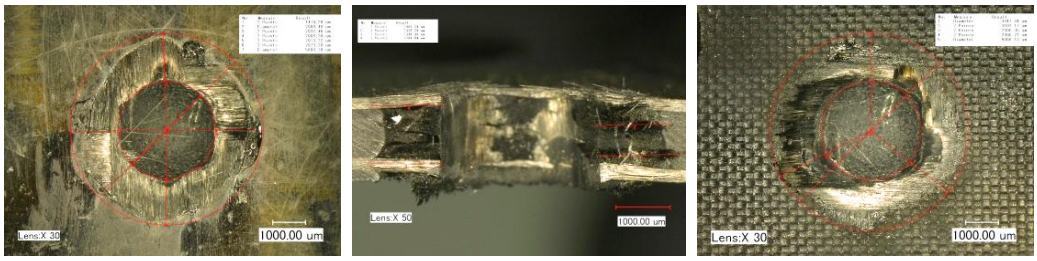

Figure 10.6 Microscopic photographs of laser pre-drilled hole; (a) entry side, (b) cross-section, (c) exit side.

10.3.3 Sequential laser-reaming investigation

CFRP samples of 1.5 mm and 3.36 mm thick following pulsed laser fibre laser drilling were reamed by reamer size of 5.7 mm. The reaming process was done within 1000-1500 rpm range. The mechanical reaming as sequential process was suggested in order to improve laser drilling quality by removing the imperfections and HAZ. Figure 10.7 and Figure 10.8 show the average residual HAZ after reaming of 1.5 mm and 3.36 mm thick CFRP samples by 5.7 mm reamer respectively. Figures 10.9 and 10.10 show the drilling quality at both sides and inside the bulk materials of 1.5 mm thick sample reamed by 5.7 mm reamer respectively. Figures 10.11 and 10.12 show the quality observations at both sides and inside the bulk materials of 3.36 mm thick sample reamed by 5.7 mm reamer respectively.

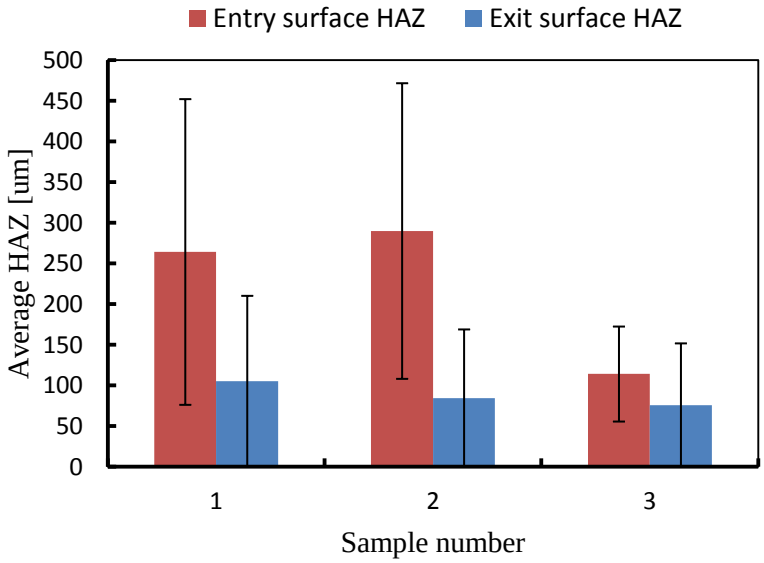

Figure 10.7 Average HAZ remaining after reaming of 1.5 mm thick CFRP by 5.7 mm reamer.

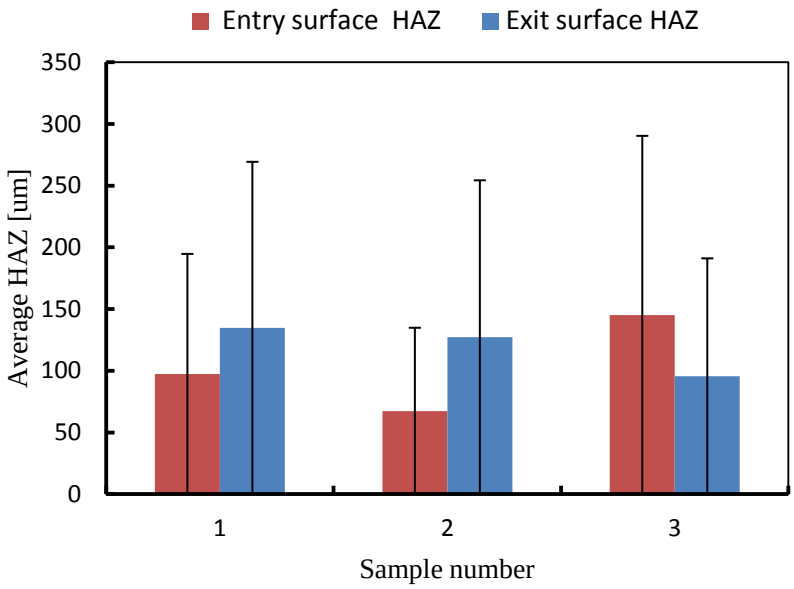

Figure 10.8 Average HAZ remaining after reaming of 3.36 mm thick CFRP by 5.7 mm reamer.

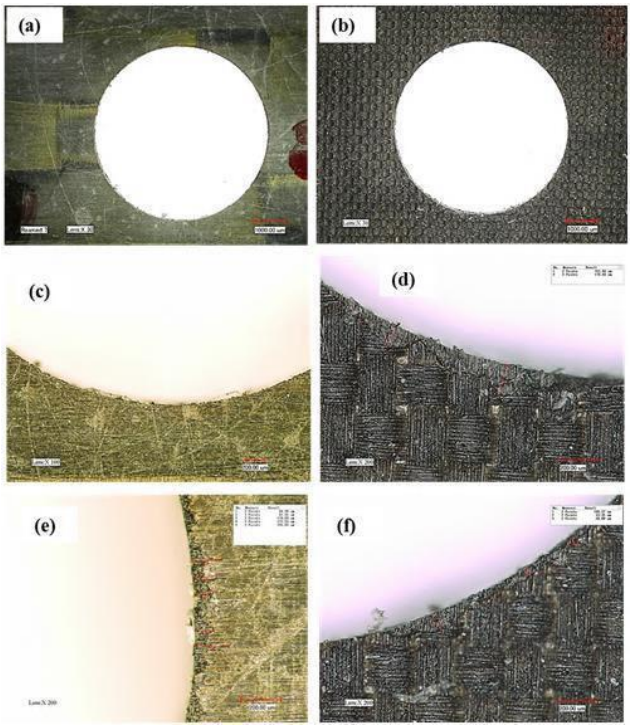

Figure 10.9 Hole entry and exit surface observations of 1.5 mm thick sample reamed by 5.7 mm reamer: (a) entry size, (b) exit size, (c), (d), (e), and (f) close-up views.

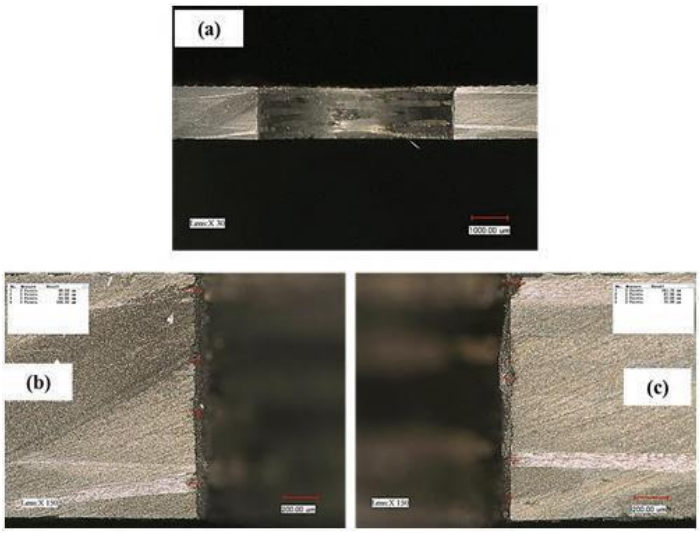

Figure 10.10 Hole cross sectional observations of 1.5 mm thick CFRP reamed by 5.7 mm reamer; (a) wide view, (b) and (c) close-up views.

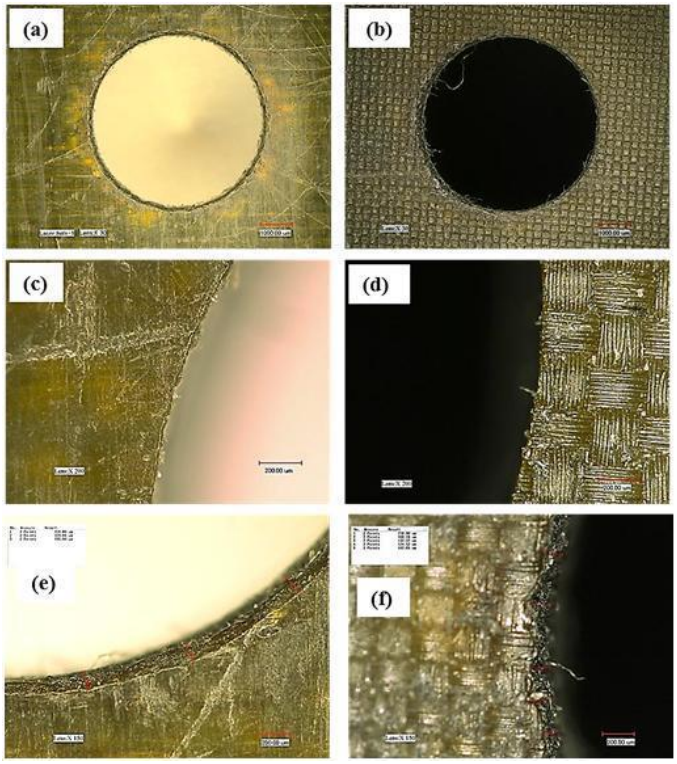

Figure 10.11 Hole entry and exit surface observations of 3.36 mm thick CFRP reamed by 5.7 mm reamer: (a) entry size, (b) exit size.

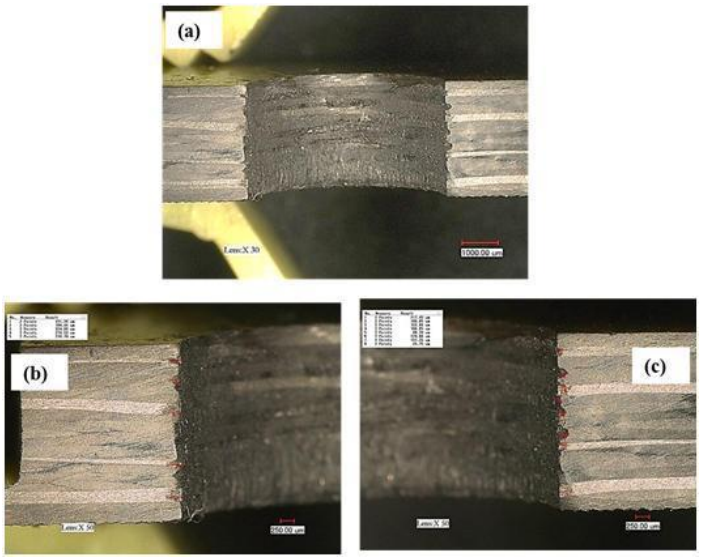

Figure 10.12 Hole cross sectional observations of 3.36 mm thick CFRP reamed by 5.7 mm reamer; (a) wide view, (b) and (c) close-up views.

It can be clearly seen from Figures 10.7–10.12 that the reaming process did not remove all the HAZ generated by laser drilling process. This is because the 5.7 mm reamer size used was small compared to the 5.5 mm size laser pre-drilled holes. Moreover, the reamer only designed to improve the holes quality by removing shallow materials from their walls surfaces. Therefore, mechanical drilling after laser pre-drilling is required to remove the thermal damage and improve the geometrical quality of the hole.

10.3.4 Sequential laser-mechanical investigation

Figure 10.13 shows the micrographs of a sequential laser and mechanical drilled hole. The final hole size was drilled mechanically by 6 mm twist drill. In order to reduce delamination different drills of 4 mm, 5 mm and 6 mm size were used. It can be seen that most of the thermal damage generated by laser processing was removed using mechanical drilling. However, the sequential laser and mechanical drilling process was performed in two different machines. Thus, the tool/workpiece alignment and the drill type used, play an important role on producing high hole quality using hybrid laser-mechanical technique.

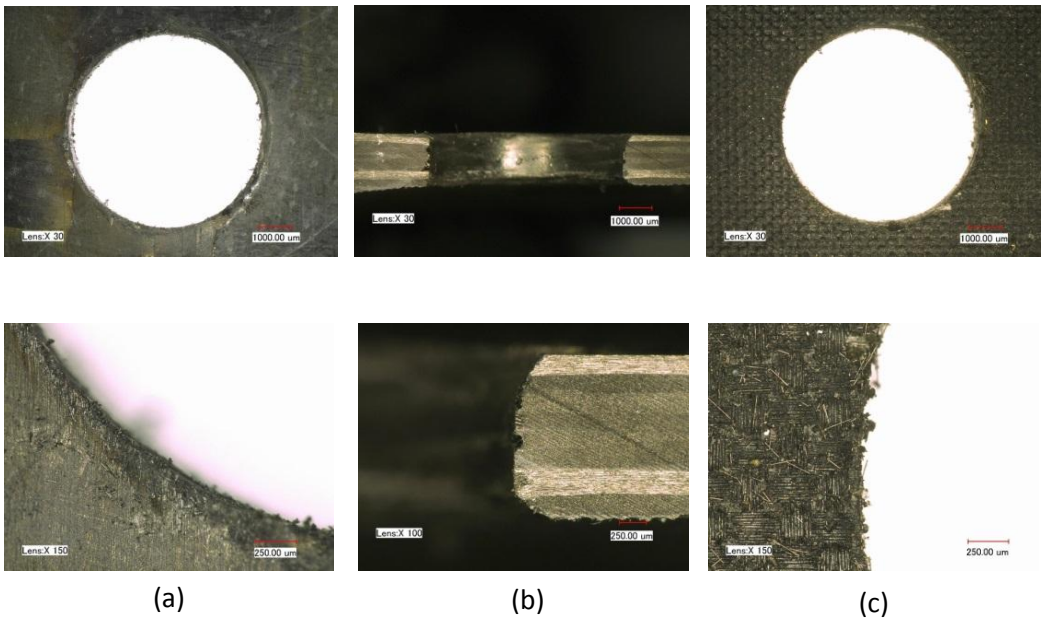

Figure 10.13 Microscopic photographs of a sequential laser and mechanical drilled hole; (a) entry side, (b) cross-section, (c) exit side. Second raw is close-up view.

10.3.5 Tool wear investigation

The effect of laser and mechanical drilling technique and mechanical only drilling of CFRP composite on tool wear of twist drill were investigated using 4 mm CFRP plates. 80 laser pre-drilled holes with 5 mm diameter were finished mechanically using 6 mm diameter twist drill. The microscopic observations in Figure 10.14a shows no tool damage occurs (i.e. the chisel and cutting edges not affected). In contrast, a massive damage to the chisel and cutting edges of the twist drill observed after mechanical only drilling. The edges rounded after only 22 holes as shown in Figure 10.14b. The laser pre-drilled holes help to eliminate the trust force created by the chisel edge and reduce the amount of material that need to be removed by mechanical drill. Thus, the tool life during mechanical drilling of CFRP composite could be improved.

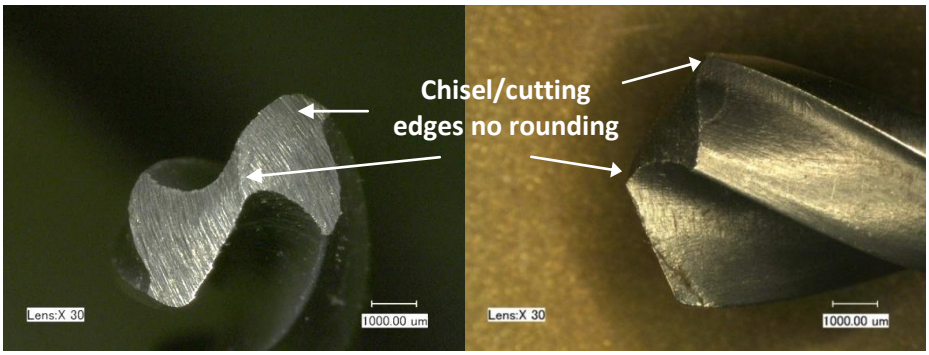

(a)

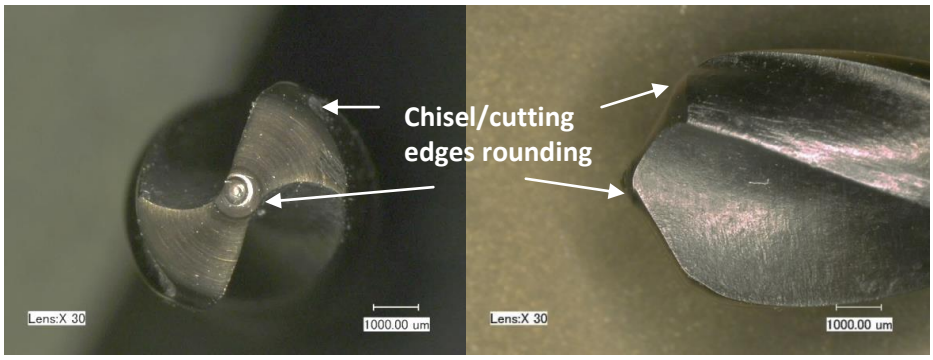

(b)

Figure 10.14 Microscopic photographs of tool status; (a) after laser and mechanical drilling (after 80 holes), (b) after mechanical only drilling (after 22 holes).

10.4 Summary

Sequential laser-reaming and sequential laser-mechanical drilling techniques were presented in order to drill CFRP composite with minimum HAZ and improve the mechanical tool life. The sequential-laser reaming did not remove all the HAZ.

The laser pre-drilled holes were drilled in short time (1 sec) using CW laser mode. The thermal damage associated with laser drilling was less than 1.5 mm and could be removed using 6 mm diameter twist drill. Sequential laser-mechanical drilling technique demands accurate tool/workpiece alignments and proper tool type for high drilling quality. The tool wear was reduced using laser and mechanical sequential drilling compared with mechanical only drilling.

CHAPTER 11 CONCLUSIONS AND FUTURE WORK

This thesis has presented an investigation of using three different types of laser system (pulsed TEA CO_2 laser, picosecond laser and fibre laser) to machine CFRP composite sheets. The TEA CO_2 laser machining of carbon fibre reinforced polymer composites was presented for the first time. The feasibility of using sequential laser and mechanical drilling technique to remove the HAZ generated by fibre laser milling and the capability of using pulsed fibre laser mode for CFRP remanufacture and repair has been investigated. Additionally, a comparison of single and multiple parallel ring/track machining strategy for CFRP composite drilling and its effect on processing rates and hole taper were investigated. Design of experiment was used to understand the influence of process parameters on the machining quality and the parameters were optimised to achieve good quality. The following conclusions and recommendations can be drawn from this work:

1. Using TEA CO_2 laser shows good machining quality (cross sectional HAZ) of CFRP composite. The optimum machining results achieved for average cross sectional HAZ, machining depth and material removal rate were 21±4 µm, 5.8±0.3 µm/pass and 11±0.4 mm^3/min respectively.
2. The surface protection technique introduced in this work by using a mask to reduce the thermal damage on the top surface during laser machining of CFRP is a promising method for the reduction of HAZ..
3. Using the high power picosecond laser, holes with 6 mm diameter at 6 mm thickness of CFRP was drilled with high quality at a scanning speed of 2 m/s. The HAZ is 25 µm at the entrance side and no HAZ was observed below the surface. Also, techniques to reduce taper were identified including the use of angled beam and higher pulse energy.
4. Better quality was obtained by pulsed fibre laser mode than continuous mode. A 490- 930 µm HAZ was generated at the CW mode, whereas 26 – 422 µm HAZ at the entry/exit sides and inside the bulk material was generated at the pulsed mode. Less thermal damage necessitie the use of low laser powers and short interaction time during pulsed fibre laser processing.

5. The narrow laser kerf (~ 100 μm), the taper (1˚) generated during laser processing and the ease of automation of fibre laser make it possible to demonstrate a new technique for laser-based repair of CFRP specially for closed parts such as airplane wings.
6. The multiple parallel track machining enabled significant improvement in machining rate compared with single ring machining. The ultra-short pulsed laser drilling of CFRP composite and metals is limited by cone like shape groove formation. More rings and higher energy are required to increase the ablation depth and material removal rate within the same time period and total energy delivery. The self-limiting effect was analysed both theoretically and experimentally. It has been found that higher pulse energy would reduce the taper and allow deeper ablation to take place.
7. The sequential laser- reaming and the sequential laser-mechanical drilling used did not remove all the HAZ. Tool/workpiece alignments and tool type play a significant role on producing high drilling quality. The investigations show that the technique could reduce the tool wear during mechanical drilling of CFRP composite.

For future work, modelling of TEA CO_2 laser machining of CFRP composite would help to further understand the process and simulate the induced thermal damage. Moreover, plume/plasma dynamics in picosecond laser interactions with CFRP composites using high speed holography imaging needs to be investigated to further understand and improve the machining quality and processing rate (Initial images using high speed holographic imaging presented in the Appendix). Further investigations are needed for laser-based repair of CFRP and sequential laser-mechanical techniques. The investigations can involve evaluating the performance strength of laser repaired samples and exploring a 3-stepped process based on laser pilot hole drilling, mechanical drilling and reaming technique for better laser hole drilling quality and long mechanical drilling tool life.

REFERENCES

1. Voisey, K.T., S. Fouquet, D. Roy, and T.W. Clyne, *Fibre swelling during laser drilling of carbon fibre composites.* Optics and Lasers in Engineering, 2006. **44**(11): p. 1185-1197.
2. Mathew, J., G.L. Goswami, N. Ramakrishnan, and N.K. Naik, *Parametric studies on pulsed Nd:YAG laser cutting of carbon fibre reinforced plastic composites.* Journal of Materials Processing Technology, 1999. **89–90**(0): p. 198-203.
3. Negarestani, R., L. Li, H.K. Sezer, D. Whitehead, and J. Methven, *Nano-second pulsed DPSS Nd:YAG laser cutting of CFRP composites with mixed reactive and inert gases.* The International Journal of Advanced Manufacturing Technology, 2010. **49**(5-8): p. 553-566.
4. Davim, J.P. and P. Reis, *Study of delamination in drilling carbon fiber reinforced plastics (CFRP) using design experiments.* Composite Structures, 2003. **59**(4): p. 481-487.
5. Kalla, D., J. Sheikh-Ahmad, and J. Twomey, *Prediction of cutting forces in helical end milling fiber reinforced polymers.* International Journal of Machine Tools and Manufacture, 2010. **50**(10): p. 882-891.
6. Shyha, I.S., D.K. Aspinwall, S.L. Soo, and S. Bradley, *Drill geometry and operating effects when cutting small diameter holes in CFRP.* International Journal of Machine Tools and Manufacture, 2009. **49**(12–13): p. 1008-1014.
7. Li, Z.L., P.L. Chu, H.Y. Zheng, G.C. Lim, L. Li, S. Marimuthu, R. Negarestani, M. Sheikh, and P. Mativenga, *Laser machining of carbon fibre-reinforced plastic composites*, in *Advances in Laser Materials Processing*, J. Lawrence, et al., Editors. 2010, Woodhead Publishing. p. 136-177.
8. Uhlmann, E., G. Spur, H. Hocheng, S. Liebelt, and C.T. Pan, *The extent of laser-induced thermal damage of UD and crossply composite laminates.* International Journal of Machine Tools and Manufacture, 1999. **39**(4): p. 639-650.
9. Pan, C.T. and H. Hocheng, *Evaluation of anisotropic thermal conductivity for unidirectional FRP in laser machining.* Composites Part A: Applied Science and Manufacturing, 2001. **32**(11): p. 1657-1667.
10. Muramatsu, M., Y. Harada, T. Suzuki, and H. Niino, *Infrared stress measurements of thermal damage to laser-processed carbon fiber reinforced plastics.* Composites Part A: Applied Science and Manufacturing, 2015. **68**: p. 242-250.
11. Negarestani, R., M. Sundar, M. Sheikh, P. Mativenga, L. Li, Z. Li, P. Chu, C. Khin, H. Zheng, and G. Lim, *Numerical simulation of laser machining of carbon-fibre-reinforced composites.* Proc. Inst. Mech. Eng. Pt. B: J. Eng. Manuf., 2010. **224**(7): p. 1017-1027.
12. Fenoughty, K.A., A. Jawaid, and I.R. Pashby, *Machining of advanced engineering materials using traditional and laser techniques.* Journal of Materials Processing Technology, 1994. **42**(4): p. 391-400.
13. Lau, W.S., T.M. Yue, T.C. Lee, and W.B. Lee, *Un-conventional machining of composite materials.* Journal of Materials Processing Technology, 1995. **48**(1–4): p. 199-205.

14. Shanmugam, D.K., F.L. Chen, E. Siores, and M. Brandt, *Comparative study of jetting machining technologies over laser machining technology for cutting composite materials.* Composite Structures, 2002. **57**(1–4): p. 289-296.
15. Abrate, S. and D.A. Walton, *Machining of composite materials. Part I: Traditional methods.* Composites Manufacturing, 1992. **3**(2): p. 75-83.
16. Vasiliev, V.V. and E.V. Morozov, *Advanced mechanics of composite materials*. 2007: Elsevier Science.
17. Teti, R., *Machining of Composite Materials.* CIRP Annals - Manufacturing Technology, 2002. **51**(2): p. 611-634.
18. Gaitonde, V.N., S.R. Karnik, J.C. Rubio, A.E. Correia, A.M. Abrão, and J.P. Davim, *Analysis of parametric influence on delamination in high-speed drilling of carbon fiber reinforced plastic composites.* Journal of Materials Processing Technology, 2008. **203**(1–3): p. 431-438.
19. Daniel, I.M. and O. Ishai, *Engineering Mechanics of Composite Materials*. 2006: Oxford University Press.
20. John, V., *Introduction to Engineering Materials*. 2003: Palgrave Macmillan.
21. Zweben, C.H., *Composites: Overview*, in *Encyclopedia of Condensed Matter Physics*, B. Franco, L.L. Gerald, and W. Peter, Editors. 2005, Elsevier: Oxford. p. 192-208.
22. Mazumdar, S.K., *Composites manufacturing: materials, product, and process engineering*. 2002: CRC.
23. Campbell, F.C., *Structural Composite Materials*. 2010: ASM International.
24. Lubin, G. and S.T. Peters, *Handbook of Composites*. 1998: Springer US.
25. Fisher, F.T. and L.C. Brinson, *Viscoelastic interphases in polymer–matrix composites: theoretical models and finite-element analysis.* Composites Sci. Technol., 2001. **61**(5): p. 731-748.
26. Naslain, R.R., *Ceramic Matrix Composites: Matrices and Processing*, in *Encyclopedia of Materials: Science and Technology*, K.H.J. Buschow, et al., Editors. 2001, Elsevier: Oxford. p. 1060-1066.
27. Kaw, A.K., *Mechanics of Composite Materials, Second Edition*. 2005: CRC Press.
28. Taylor, R., *Carbon Matrix Composites*, in *Comprehensive composite materials*, K. Anthony and Z. Carl, Editors. 2000, Pergamon: Oxford. p. 387-426.
29. Davim, J.P. and P. Reis, *Drilling carbon fiber reinforced plastics manufactured by autoclave—experimental and statistical study.* Materials & Design, 2003. **24**(5): p. 315-324.
30. Shyha, I., S.L. Soo, D. Aspinwall, and S. Bradley, *Effect of laminate configuration and feed rate on cutting performance when drilling holes in carbon fibre reinforced plastic composites.* Journal of Materials Processing Technology, 2010. **210**(8): p. 1023-1034.
31. Hull, D. and T. Clyne, *An introduction to composite materials*. 1996: Cambridge university press.
32. Campbell, F.C., *Manufacturing technology for aerospace structural materials*. 2006: Elsevier Science.
33. Sheikh-Ahmad, J.Y., *Machining of polymer composites*. 2009: Springer.
34. Edwards, K., *An overview of the technology of fibre-reinforced plastics for design purposes.* Materials & Design, 1998. **19**(1): p. 1-10.
35. Staab, G., *Laminar composites*. 1999: Butterworth-Heinemann.

36. Li, Z., H. Zheng, G. Lim, P. Chu, and L. Li, *Study on UV laser machining quality of carbon fibre reinforced composites.* Composites Part A: Applied Science and Manufacturing, 2010. **41**(10): p. 1403-1408.
37. Cenna, A.A. and P. Mathew, *Evaluation of cut quality of fibre-reinforced plastics—A review.* International Journal of Machine Tools and Manufacture, 1997. **37**(6): p. 723-736.
38. Mallick, P.K., *Fiber-reinforced composites: materials, manufacturing, and design*. 2007: CRC press.
39. Fuchs, A., M. Schoeberl, J. Tremmer, and M. Zaeh, *Laser cutting of carbon fiber fabrics.* Physics Procedia, 2013. **41**: p. 372-380.
40. Jacob, A., *BMW counts on carbon fibre for its Megacity Vehicle.* Reinforced Plastics, 2010. **54**(5): p. 38-41.
41. Arul, S., L. Vijayaraghavan, S.K. Malhotra, and R. Krishnamurthy, *The effect of vibratory drilling on hole quality in polymeric composites.* International Journal of Machine Tools and Manufacture, 2006. **46**(3–4): p. 252-259.
42. Rahman, M., S. Ramakrishna, and H.C. Thoo, *Machinability study of carbon/peek composites.* Machining Science and Technology, 1999. **3**(1): p. 49-59.
43. Santiuste, C., X. Soldani, and M.H. Miguélez, *Machining FEM model of long fiber composites for aeronautical components.* Composite Structures, 2010. **92**(3): p. 691-698.
44. Abrao, A., J.C. Rubio, P. Faria, and J. Davim, *The effect of cutting tool geometry on thrust force and delamination when drilling glass fibre reinforced plastic composite.* Materials & Design, 2008. **29**(2): p. 508-513.
45. Schulze, V., C. Becke, K. Weidenmann, and S. Dietrich, *Machining strategies for hole making in composites with minimal workpiece damage by directing the process forces inwards.* Journal of Materials Processing Technology, 2011. **211**(3): p. 329-338.
46. Hocheng, H. and C.C. Tsao, *The path towards delamination-free drilling of composite materials.* Journal of Materials Processing Technology, 2005. **167**(2-3): p. 251-264.
47. Capello, E., *Workpiece damping and its effect on delamination damage in drilling thin composite laminates.* Journal of Materials Processing Technology, 2004. **148**(2): p. 186-195.
48. Koenig, W., C. Wulf, P. Grass, and H. Willerscheid, *Machining of fibre reinforced plastics.* CIRP Annals-Manufacturing Technology, 1985. **34**(2): p. 537-548.
49. Campbell Jr, F.C., *Manufacturing processes for advanced composites*. 2003: Elsevier.
50. Tandon, S., V. Jain, P. Kumar, and K. Rajurkar, *Investigations into machining of composites.* Precision engineering, 1990. **12**(4): p. 227-238.
51. Lemma, E., L. Chen, E. Siores, and J. Wang, *Study of cutting fiber-reinforced composites by using abrasive water-jet with cutting head oscillation.* Composite Structures, 2002. **57**(1): p. 297-303.
52. Zheng, H., Z. Han, Z. Chen, W. Chen, and S. Yeo, *Quality and cost comparisons between laser and waterjet cutting.* Journal of Materials Processing Technology, 1996. **62**(4): p. 294-298.
53. Shanmugam, D. and S. Masood, *An investigation on kerf characteristics in abrasive waterjet cutting of layered composites.* Journal of Materials Processing Technology, 2009. **209**(8): p. 3887-3893.

54. Abrate, S. and D. Walton, *Machining of composite materials. Part II: Non-traditional methods.* Composites Manufacturing, 1992. **3**(2): p. 85-94.
55. Akkurt, A., M.K. Kulekci, U. Seker, and F. Ercan, *Effect of feed rate on surface roughness in abrasive waterjet cutting applications.* Journal of Materials Processing Technology, 2004. **147**(3): p. 389-396.
56. Kulekci, M.K., *Processes and apparatus developments in industrial waterjet applications.* International Journal of Machine Tools and Manufacture, 2002. **42**(12): p. 1297-1306.
57. Azmir, M. and A. Ahsan, *Investigation on glass/epoxy composite surfaces machined by abrasive water jet machining.* Journal of Materials Processing Technology, 2008. **198**(1): p. 122-128.
58. Wang, J. and D.M. Guo, *A predictive depth of penetration model for abrasive waterjet cutting of polymer matrix composites.* Journal of Materials Processing Technology, 2002. **121**(2–3): p. 390-394.
59. Shanmugam, D., T. Nguyen, and J. Wang, *A study of delamination on graphite/epoxy composites in abrasive waterjet machining.* Composites Part A: Applied Science and Manufacturing, 2008. **39**(6): p. 923-929.
60. Guu, Y., H. Hocheng, N. Tai, and S. Liu, *Effect of electrical discharge machining on the characteristics of carbon fiber reinforced carbon composites.* Journal of materials science, 2001. **36**(8): p. 2037-2043.
61. Kumar, H. and J.P. Davim, *Role of powder in the machining of Al-10% SiCp metal matrix composites by powder mixed electric discharge machining.* Journal of composite materials, 2011. **45**(2): p. 133-151.
62. Patil, N.G. and P. Brahmankar, *Determination of material removal rate in wire electro-discharge machining of metal matrix composites using dimensional analysis.* The International Journal of Advanced Manufacturing Technology, 2010. **51**(5-8): p. 599-610.
63. Ho, K. and S. Newman, *State of the art electrical discharge machining (EDM).* International Journal of Machine Tools and Manufacture, 2003. **43**(13): p. 1287-1300.
64. Lau, W., M. Wang, and W. Lee, *Electrical discharge machining of carbon fibre composite materials.* International Journal of Machine Tools and Manufacture, 1990. **30**(2): p. 297-308.
65. Cope, R. and J. Brown, *An investigation of electrical discharge machining of graphite/epoxy composites.* Composites Manufacturing, 1990. **1**(3): p. 167-171.
66. Thoe, T., D. Aspinwall, and M. Wise, *Review on ultrasonic machining.* International journal of machine tools and manufacture, 1998. **38**(4): p. 239-255.
67. Hocheng, H. and C. Hsu, *Preliminary study of ultrasonic drilling of fiber-reinforced plastics.* Journal of Materials Processing Technology, 1995. **48**(1): p. 255-266.
68. Komaraiah, M. and P.N. Reddy, *A study on the influence of workpiece properties in ultrasonic machining.* International journal of machine tools and manufacture, 1993. **33**(3): p. 495-505.
69. Hocheng, H., N. Tai, and C. Liu, *Assessment of ultrasonic drilling of C/SiC composite material.* Composites Part A: Applied Science and Manufacturing, 2000. **31**(2): p. 133-142.
70. Lin, Y.C., B.H. Yan, and Y.S. Chang, *Machining characteristics of titanium alloy (Ti–6Al–4V) using a combination process of EDM with USM.* Journal of Materials Processing Technology, 2000. **104**(3): p. 171-177.

71. Samant, A.N. and N.B. Dahotre, *Laser machining of structural ceramics—a review*. J. Eur. Ceram. Soc., 2009. **29**(6): p. 969-993.
72. Dubey, A.K. and V. Yadava, *Laser beam machining—a review.* International Journal of Machine Tools and Manufacture, 2008. **48**(6): p. 609-628.
73. Geng, H., *Manufacturing engineering handbook*. 2004: McGraw-Hill New York.
74. Yeo, C., S. Tam, S. Jana, and M.W. Lau, *A technical review of the laser drilling of aerospace materials.* Journal of Materials Processing Technology, 1994. **42**(1): p. 15-49.
75. Ready, J.F., D.F. Farson, and T. Feeley, *LIA handbook of laser materials processing*. 2001: Laser Institute of America Orlando.
76. Ion, J., *Laser processing of engineering materials: principles, procedure and industrial application*. 2005: Butterworth-Heinemann.
77. Dahotre, N.B. and S. Harimkar, *Laser Fabrication and Machining of Materials*. 2008: Springer US.
78. Powell, J., *CO_2 laser cutting*. Vol. 214. 1993: Cambridge Univ Press.
79. Hitz, C.B., J.J. Ewing, and J. Hecht, *Introduction to laser technology*. 2012: John Wiley & Sons.
80. Steen, W., *Laser Material Processing. 2003*, Springer, London. 408pp.
81. Arieli, R., *The Laser Adventure.* Versión en español por Requena A., Cruz C., Bastida A. y Zúñiga J. Universidad de Murcia. España, 2005.
82. Crafer, R.C. and P.J. Oakley, *Laser processing in manufacturing*. 1992: Springer Science & Business Media.
83. Ready, J.F., *Industrial applications of lasers*. 1997: Academic press.
84. Ghany, K.A. and M. Newishy, *Cutting of 1.2 mm thick austenitic stainless steel sheet using pulsed and CW Nd: YAG laser.* Journal of Materials Processing Technology, 2005. **168**(3): p. 438-447.
85. Li, L., *The advances and characteristics of high-power diode laser materials processing.* Optics and Lasers in Engineering, 2000. **34**(4): p. 231-253.
86. Luxon, J.T. and D.E. Parker, *Industrial Lasers & Their Applications*. 1985: Prentice-Hall.
87. Mende, J., E. Schmid, J. Speiser, G. Spindler, and A. Giesen. *Thin disk laser: power scaling to the kW regime in fundamental mode operation*. in *SPIE LASE: Lasers and Applications in Science and Engineering*. 2009: International Society for Optics and Photonics.
88. Renk, K.F., *Basics of Laser Physics: For Students of Science and Engineering*. 2012: Springer Science & Business Media.
89. Giesen, A. and J. Speiser, *Fifteen years of work on thin-disk lasers: results and scaling laws.* Selected Topics in Quantum Electronics, IEEE Journal of, 2007. **13**(3): p. 598-609.
90. Quintino, L., A. Costa, R. Miranda, D. Yapp, V. Kumar, and C. Kong, *Welding with high power fiber lasers–a preliminary study.* Materials & Design, 2007. **28**(4): p. 1231-1237.
91. Kawahito, Y., T. Terajima, H. Kimura, T. Kuroda, K. Nakata, S. Katayama, and A. Inoue, *High-power fiber laser welding and its application to metallic glass Zr 55 Al 10 Ni 5 Cu 30.* Materials Science and Engineering: B, 2008. **148**(1): p. 105-109.
92. Nilsson, J. and D.N. Payne, *High-power fiber lasers.* Science, 2011. **332**(6032): p. 921-922.

93. Das, D.K. and T.M. Pollock, *Femtosecond laser machining of cooling holes in thermal barrier coated CMSX4 superalloy.* Journal of Materials Processing Technology, 2009. **209**(15): p. 5661-5668.
94. Cheng, J., W. Perrie, B. Wu, S. Tao, S. Edwardson, G. Dearden, and K. Watkins, *Ablation mechanism study on metallic materials with a 10ps laser under high fluence.* Applied surface science, 2009. **255**(18): p. 8171-8175.
95. Huang, H., L.-M. Yang, and J. Liu, *Micro-hole drilling and cutting using femtosecond fiber laser.* Optical Engineering, 2014. **53**(5): p. 051513-051513.
96. Momma, C., U. Knop, and S. Nolte, *Laser cutting of slotted tube coronary stents—state-of-the-art and future developments.* Progress in Biomedical Research, 1999. **4**(1): p. 39-44.
97. Koechner, W., *Solid-State Laser Engineering*. 2006: Springer.
98. Cheng, J., W. Perrie, M. Sharp, S. Edwardson, N. Semaltianos, G. Dearden, and K. Watkins, *Single-pulse drilling study on Au, Al and Ti alloy by using a picosecond laser.* Applied Physics A, 2009. **95**(3): p. 739-746.
99. Fermann, M.E., A. Galvanauskas, and G. Sucha, *Ultrafast lasers: technology and applications*. Vol. 80. 2002: CRC Press.
100. Tam, S., R. Williams, L. Yang, S. Jana, L.E. Lim, and M.W. Lau, *A review of the laser processing of aircraft components.* Journal of Materials Processing Technology, 1990. **23**(2): p. 177-194.
101. Dahotre, N.B. and A. Samant, *Laser Machining of Advanced Materials*. 2011: CRC Press.
102. Meijer, J., K. Du, A. Gillner, D. Hoffmann, V. Kovalenko, T. Masuzawa, A. Ostendorf, R. Poprawe, and W. Schulz, *Laser machining by short and ultrashort pulses, state of the art and new opportunities in the age of the photons.* CIRP Annals-Manufacturing Technology, 2002. **51**(2): p. 531-550.
103. Pham, D., S. Dimov, P. Petkov, and S. Petkov, *Laser milling.* Proc. Inst. Mech. Eng. Pt. B: J. Eng. Manuf., 2002. **216**(5): p. 657-667.
104. Dell'Erba, M., L. Galantucci, and S. Miglietta, *An experimental study on laser drilling and cutting of composite materials for the aerospace industry using excimer and CO_2 sources.* Composites Manufacturing, 1992. **3**(1): p. 14-19.
105. Garrison, B.J. and R. Srinivasan, *Laser ablation of organic polymers: microscopic models for photochemical and thermal processes.* J. Appl. Phys., 1985. **57**(8): p. 2909-2914.
106. Dubey, A.K. and V. Yadava, *Multi-objective optimization of Nd: YAG laser cutting of nickel-based superalloy sheet using orthogonal array with principal component analysis.* Optics and Lasers in Engineering, 2008. **46**(2): p. 124-132.
107. Choi, W.C. and G. Chryssolouris, *Analysis of the laser grooving and cutting processes.* Journal of Physics D: Applied Physics, 1995. **28**(5): p. 873.
108. Lv, S., Y. Wang, and S.J. Ji, *Quality Analysis of Pulsed Laser Cutting of Superalloy Sheet.* Key Engineering Materials, 2006. **315**: p. 113-117.
109. Prasad, G., E. Siores, and W. Wong, *Laser cutting of metallic coated sheet steels.* Journal of Materials Processing Technology, 1998. **74**(1): p. 234-242.
110. Lei, H. and L. Lijun, *A study of laser cutting engineering ceramics.* Optics & Laser Technology, 1999. **31**(8): p. 531-538.
111. Wee, L.M. and L. Li, *An analytical model for striation formation in laser cutting.* Applied Surface Science, 2005. **247**(1): p. 277-284.
112. Horisawa, H., M. Tamura, and S. Kimura. *Plasma behaviors in laser cutting*. in *First International Symposium on Laser Precision Microfabrication (LPM2000)*. 2000: International Society for Optics and Photonics.

113. Kannatey-Asibu Jr, E., *Principles of laser materials processing*. Vol. 4. 2009: John Wiley & Sons.
114. Wolynski, A., T. Herrmann, P. Mucha, H. Haloui, and J. L'huillier, *Laser ablation of CFRP using picosecond laser pulses at different wavelengths from UV to IR.* Physics Procedia, 2011. **12**: p. 292-301.
115. Lawrence, J.R., J. Pou, D.K. Low, and E. Toyserkani, *Advances in laser materials processing: Technology, research and application*. 2010: Elsevier.
116. El-Taweel, T.A., A.M. Abdel-Maaboud, B.S. Azzam, and A.E. Mohammad, *Parametric studies on the CO2 laser cutting of Kevlar-49 composite.* The International Journal of Advanced Manufacturing Technology, 2009. **40**(9-10): p. 907-917.
117. Goeke, A. and C. Emmelmann, *Influence of laser cutting parameters on CFRP part quality.* Physics Procedia, 2010. **5**: p. 253-258.
118. Yilbas, B., *Investigation into Laser Cutting of Brush Bristles and Composite Plates.* Lasers in Engineering, 2003. **13**(3): p. 155-165.
119. Schuöcker, D., *Dynamic phenomena in laser cutting and cut quality.* Appl. Phys. B, 1986. **40**(1): p. 9-14.
120. Choudhury, I. and S. Shirley, *Laser cutting of polymeric materials: An experimental investigation.* Optics & Laser Technology, 2010. **42**(3): p. 503-508.
121. Riveiro, A., F. Quintero, F. Lusquiños, J. del Val, R. Comesaña, M. Boutinguiza, and J. Pou, *Experimental study on the CO_2 laser cutting of carbon fiber reinforced plastic composite.* Composites Part A: Applied Science and Manufacturing, 2012. **43**(8): p. 1400-1409.
122. Pan, C. and H. Hocheng, *Prediction of extent of heat affected zone in laser grooving of unidirectional fiber-reinforced plastics.* Transactions-american society of mechanical engineers journal of engineering materials and technology, 1998. **120**: p. 321-327.
123. Dyer, P., S. Lau, G. Oldershaw, and D. Schudel, *An investigation of XeCl laser ablation of polyetheretherketone (PEEK)-carbon fiber composite.* J. Mater. Res., 1992. **7**(05): p. 1152-1157.
124. Herzog, D., P. Jaeschke, O. Meier, and H. Haferkamp, *Investigations on the thermal effect caused by laser cutting with respect to static strength of CFRP.* International Journal of Machine Tools and Manufacture, 2008. **48**(12–13): p. 1464-1473.
125. Leone, C., S. Genna, and V. Tagliaferri, *Fibre laser cutting of CFRP thin sheets by multi-passes scan technique.* Optics and Lasers in Engineering, 2014. **53**(0): p. 43-50.
126. Finger, J., M. Weinand, and D. Wortmann, *Ablation and cutting of carbon-fiber reinforced plastics using picosecond pulsed laser radiation with high average power.* Journal of Laser Applications, 2013. **25**(4): p. 042007.
127. Freitag, C., M. Wiedenmann, J.-P. Negel, A. Loescher, V. Onuseit, R. Weber, M.A. Ahmed, and T. Graf, *High-quality processing of CFRP with a 1.1-kW picosecond laser.* Applied Physics A, 2015. **119**(4): p. 1237-1243.
128. Tagliaferri, V., A. Di Ilio, and C. Visconti, *Laser cutting of fibre-reinforced polyesters.* Composites, 1985. **16**(4): p. 317-325.
129. Hu, J. and H. Xu, *Pocket milling of carbon fiber-reinforced plastics using 532-nm nanosecond pulsed laser: An experimental investigation.* Journal of composite materials, 2015: p. 0021998315614990.

130. Leone, C., N. Pagano, V. Lopresto, and I. De Iorio. *Solid state Nd: YAG laser cutting of CFRP sheet: influence of process parameters on kerf geometry and HAZ*. in *Proc of 17th Int. Conf. on Composite Materials-ICCM-17*. 2009.
131. Niino, H., Y. Kawaguchi, T. Sato, A. Narazaki, R. Kurosaki, M. Muramatsu, Y. Harada, K. Wakabayashi, T. Nagashima, and Z. Kase. *Laser cutting of carbon fiber reinforced plastics (CFRP) by 1kW cw fiber laser irradiation*. in *SPIE LASE*. 2013: International Society for Optics and Photonics.
132. Negarestani, R. and L. Li, *Fibre laser cutting of carbon fibre–reinforced polymeric composites.* Proc. Inst. Mech. Eng. Pt. B: J. Eng. Manuf., 2013. **227**(12): p. 1755-1766.
133. Emmelmanna, C., M. Petersen, A. Goeke, and M. Canisius, *Analysis of Laser Ablation of CFRP by Ultra-Short Laser Pulses with Short Wavelength.* Physics Procedia, 2011. **12**(Part 1): p. 565-571.
134. Klotzbach, A., M. Hauser, and E. Beyer, *Laser cutting of carbon fiber reinforced polymers using highly brilliant laser beam sources.* Physics Procedia, 2011. **12**: p. 572-577.
135. Negarestani, R. and L. Li, *Laser machining of fibre-reinforced polymeric composite materials*, in *Machining Technology for Composite Materials*, H. Hocheng, Editor. 2012, Woodhead Publishing. p. 288-308.
136. Dell'Erba, M., L.M. Galantucci, and S. Miglietta, *An experimental study on laser drilling and cutting of composite materials for the aerospace industry using excimer and CO_2 sources.* Composites Manufacturing, 1992. **3**(1): p. 14-19.
137. Weber, R., T. Graf, P. Berger, V. Onuseit, M. Wiedenmann, C. Freitag, and A. Feuer, *Heat accumulation during pulsed laser materials processing.* 2014.
138. Carlos Hernández-Castañeda, J., H. Kursad Sezer, and L. Li, *The effect of moisture content in fibre laser cutting of pine wood.* Optics and Lasers in Engineering, 2011. **49**(9–10): p. 1139-1152.
139. Ghosal, A. and A. Manna, *Response surface method based optimization of ytterbium fiber laser parameter during machining of Al/Al2O3-MMC.* Optics & Laser Technology, 2013. **46**(0): p. 67-76.
140. Elmesalamy, A.S., L. Li, J.A. Francis, and H.K. Sezer, *Understanding the process parameter interactions in multiple-pass ultra-narrow-gap laser welding of thick-section stainless steels.* The International Journal of Advanced Manufacturing Technology, 2013. **68**(1-4): p. 1-17.
141. Fischer, F., L. Romoli, and R. Kling, *Laser-based repair of carbon fiber reinforced plastics.* CIRP Annals - Manufacturing Technology, 2010. **59**(1): p. 203-206.
142. Völkermeyer, F., F. Fischer, U. Stute, and D. Kracht, *LiM 2011 Laser-based approach for bonded repair of carbon fiber reinforced plastics.* Physics Procedia, 2011. **12**: p. 537-542.
143. Romoli, L., F. Fischer, and R. Kling, *A study on UV laser drilling of PEEK reinforced with carbon fibers.* Optics and Lasers in Engineering, 2012. **50**(3): p. 449-457.
144. Takahashi, K., M. Tsukamoto, S. Masuno, Y. Sato, H. Yoshida, K. Tsubakimoto, H. Fujita, N. Miyanaga, M. Fujita, and H. Ogata, *Influence of laser scanning conditions on CFRP processing with a pulsed fiber laser.* Journal of Materials Processing Technology, 2015. **222**: p. 110-121.
145. Herzog, D., M. Schmidt-Lehr, M. Oberlander, M. Canisius, M. Radek, and C. Emmelmann, *Laser cutting of carbon fibre reinforced plastics of high thickness.* Materials & Design, 2016. **92**: p. 742-749.

146. Li, Z., P. Chu, H. Zheng, G. Lim, L. Li, S. Marimuthu, R. Negarestani, M. Sheik, and P. Mativenga. *Process development of laser machining of carbon fibre reinforced plastic composites*. in *27th International Congress on Applications of Lasers and Electro-Optics, Laser Institute of America, Temecula, CA*. 2008.
147. Forrer, M., M. Frenz, V. Romano, H. Altermatt, H. Weber, A. Silenok, M. Istomyn, and V. Konov, *Bone-ablation mechanism using CO_2 lasers of different pulse duration and wavelength.* Appl. Phys. B, 1993. **56**(2): p. 104-112.
148. Dyer, P., I. Waldeck, and G. Roberts, *Fine-hole drilling in Upilex polyimide and glass by TEA laser ablation.* Journal of Physics D: Applied Physics, 1997. **30**(6): p. L19-L21.
149. Trtica, M.S., B.M. Gaković, T.M. Nenadović, and M.M. Mitrović, *Surface modification of stainless steels by TEA CO_2 laser.* Applied surface science, 2001. **177**(1): p. 48-57.
150. Tsunemi, A., K. Hagiwara, N. Saito, K. Nagasaka, Y. Miyamoto, O. Suto, and H. Tashiro, *Complete removal of paint from metal surface by ablation with a TEA CO2 laser.* Applied Physics A, 1996. **63**(5): p. 435-439.
151. Forbes, A., L.R. Botha, N. Du Preez, and T.E. Drake (2006) *Design and optimization of a pulsed CO_2laser for laser ultrasonic applications : the CSIR at 60*. **102**, p.329-334.
152. Beaulieu, A., *Transversely excited atmospheric pressure CO_2 lasers.* Applied Physics Letters, 1970. **16**(12): p. 504-505.
153. Schmidt, M.J.J., D.K.Y. Low, and L. Li, *Laser ablation of a B4C–polysiloxane composite.* Applied Surface Science, 2002. **186**(1–4): p. 271-275.
154. Leigh, S., K. Sezer, L. Li, C. Grafton-Reed, and M. Cuttell, *Statistical analysis of recast formation in laser drilled acute blind holes in CMSX-4 nickel superalloy.* The International Journal of Advanced Manufacturing Technology, 2009. **43**(11-12): p. 1094-1105.
155. Biswas, R., A.S. Kuar, S. Sarkar, and S. Mitra, *A parametric study of pulsed Nd:YAG laser micro-drilling of gamma-titanium aluminide.* Optics & Laser Technology, 2010. **42**(1): p. 23-31.
156. Hernandez-Castaneda, J.C., H.K. Sezer, and L. Li, *Statistical analysis of ytterbium-doped fibre laser cutting of dry pine wood.* Proceedings of The Institution of Mechanical Engineers Part B-journal of Engineering Manufacture, 2009. **223**(7): p. 775-789.
157. Yung, K.C., S.M. Mei, and T.M. Yue, *A study of the heat-affected zone in the UV YAG laser drilling of GFRP materials.* Journal of Materials Processing Technology, 2002. **122**(2-3): p. 278-285.
158. Li, C.-H., M.-J. Tsai, and C.-D. Yang, *Study of optimal laser parameters for cutting QFN packages by Taguchi's matrix method.* Optics & Laser Technology, 2007. **39**(4): p. 786-795.
159. Al-Sulaiman, F.A., B.S. Yilbas, and M. Ahsan, *CO_2 laser cutting of a carbon/carbon multi-lamelled plain-weave structure.* Journal of Materials Processing Technology, 2006. **173**(3): p. 345-351.
160. Stock, J., M.F. Zaeh, and M. Conrad, *Remote Laser Cutting of CFRP: Improvements in the Cut Surface.* Physics Procedia, 2012. **39**(0): p. 161-170.
161. Shyha, I., *An Investigation into CO_2 Laser Trimming of CFRP and GFRP Composites.* Procedia Engineering, 2013. **63**: p. 931-937.
162. Sumiyoshi, T., Y. Ninomiya, H. Ogasawara, M. Obara, and H. Tanaka, *Efficient ablation of organic polymers polyether sulphone and polyether ether ketone by a*

TEA CO_2 laser with high perforation ability. Applied Physics A, 1994. **58**(5): p. 475-479.
163. Morrison, J., T. Tessier, and B. Gu, *A Large Format Modified TEA CO2 Laser Based Process for Cost-effective Small Via Generation.* Circuit World, 1994. **21**(1): p. 24-27.
164. H. Hocheng et al., *in Machining Technology for Composite Materials*, H. Hocheng, Ed. (Woodhead Publishing, 2012), pp. xi-xv.
165. Muhammad, N., D. Whitehead, A. Boor, W. Oppenlander, Z. Liu, and L. Li, *Picosecond laser micromachining of nitinol and platinum–iridium alloy for coronary stent applications.* Applied Physics A, 2012. **106**(3): p. 607-617.
166. Meijer, J., K. Du, A. Gillner, D. Hoffmann, V.S. Kovalenko, T. Masuzawa, A. Ostendorf, R. Poprawe, and W. Schulz, *Laser Machining by short and ultrashort pulses, state of the art and new opportunities in the age of the photons.* CIRP Annals - Manufacturing Technology, 2002. **51**(2): p. 531-550.
167. Wu, C.-W., X.-Q. Wu, and C.-G. Huang, *Ablation behaviors of carbon reinforced polymer composites by laser of different operation modes.* Optics & Laser Technology, 2015. **73**: p. 23-28.
168. Dyer, P., S. Jenkins, and J. Sidhu, *Development and origin of conical structures on XeCl laser ablated polyimide.* Applied Physics Letters, 1986. **49**(8): p. 453-455.
169. Paterson, C., A. Holmes, and R. Smith, *Excimer laser ablation of microstructures: a numerical model.* J. Appl. Phys., 1999. **86**(11): p. 6538-6546.
170. Hernandez-Castaneda, J.C., H.K. Sezer, and L. Li, *The effect of moisture content in fibre laser cutting of pine wood.* Optics and Lasers in Engineering, 2011. **49**(9): p. 1139-1152.
171. Lau, W., W. Lee, and S. Pang, *Pulsed Nd: YAG laser cutting of carbon fibre composite materials.* CIRP Annals-Manufacturing Technology, 1990. **39**(1): p. 179-182.
172. Soutis, C., D.M. Duan, and P. Goutas, *Compressive behaviour of CFRP laminates repaired with adhesively bonded external patches.* Composite Structures, 1999. **45**(4): p. 289-301.
173. Hu, F.Z. and C. Soutis, *Strength prediction of patch-repaired CFRP laminates loaded in compression.* Composites Sci. Technol., 2000. **60**(7): p. 1103-1114.
174. Faraz, A., D. Biermann, and K. Weinert, *Cutting edge rounding: An innovative tool wear criterion in drilling CFRP composite laminates.* International journal of machine tools and manufacture, 2009. **49**(15): p. 1185-1196.
175. Tsao, C. and H. Hocheng, *Computerized tomography and C-Scan for measuring delamination in the drilling of composite materials using various drills.* International journal of machine tools and manufacture, 2005. **45**(11): p. 1282-1287.
176. Tsao, C., *Effect of pilot hole on thrust force by saw drill.* International journal of machine tools and manufacture, 2007. **47**(14): p. 2172-2176.
177. Velayudham, A. and R. Krishnamurthy, *Effect of point geometry and their influence on thrust and delamination in drilling of polymeric composites.* Journal of Materials Processing Technology, 2007. **185**(1): p. 204-209.
178. Iliescu, D., D. Gehin, M. Gutierrez, and F. Girot, *Modeling and tool wear in drilling of CFRP.* International journal of machine tools and manufacture, 2010. **50**(2): p. 204-213.
179. Lin, S. and I. Chen, *Drilling carbon fiber-reinforced composite material at high speed.* Wear, 1996. **194**(1): p. 156-162.

180. Tsao, C., *Investigation into the effects of drilling parameters on delamination by various step-core drills.* Journal of Materials Processing Technology, 2008. **206**(1): p. 405-411.
181. Won, M. and C. Dharan, *Chisel edge and pilot hole effects in drilling composite laminates.* Journal of manufacturing science and engineering, 2002. **124**(2): p. 242-247.
182. Tsao, C. and H. Hocheng, *The effect of chisel length and associated pilot hole on delamination when drilling composite materials.* International journal of machine tools and manufacture, 2003. **43**(11): p. 1087-1092.
183. Tsao, C., *The effect of pilot hole on delamination when core drill drilling composite materials.* International journal of machine tools and manufacture, 2006. **46**(12): p. 1653-1661.
184. Okasha, M., P. Mativenga, N. Driver, and L. Li, *Sequential laser and mechanical micro-drilling of Ni superalloy for aerospace application.* CIRP Annals-Manufacturing Technology, 2010. **59**(1): p. 199-202.
185. Okasha, M., P. Mativenga, and L. Li, *Sequential laser mechanical microdrilling of Inconel 718 alloy.* Journal of manufacturing science and engineering, 2011. **133**(1): p. 011008.
186. Okasha, M., N. Driver, P. Mativenga, and L. Li, *Mechanical microdrilling of negative-tapered laser-predrilled holes: a new approach for burr minimization.* The International Journal of Advanced Manufacturing Technology, 2012. **61**(1-4): p. 213-225.

APPENDIX A High speed holographic imaging

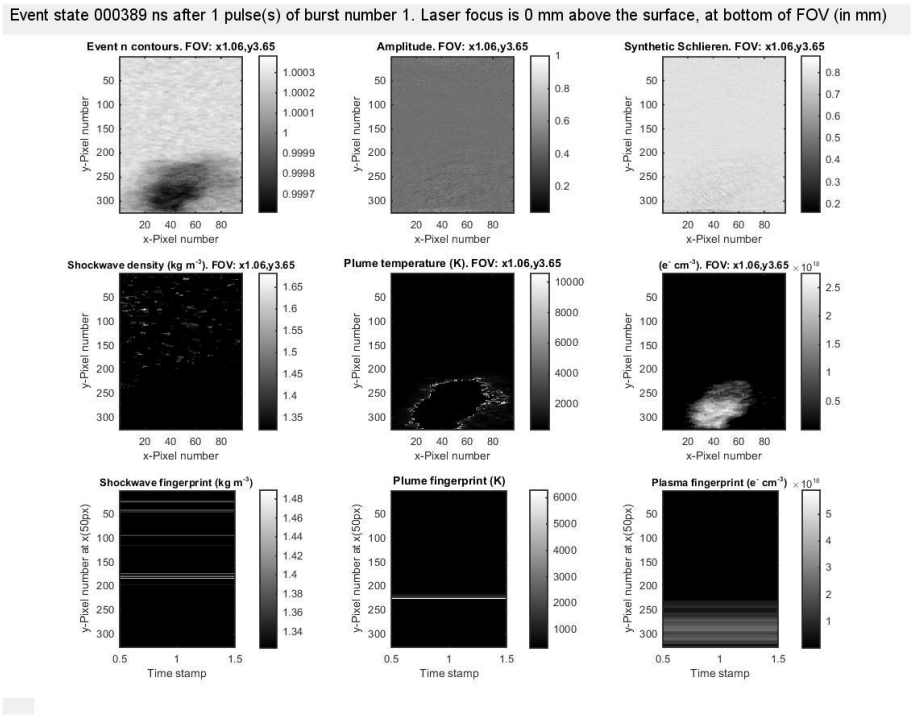

Figure A-1 High speed holographic imaging for 100 pulses, 1burst.

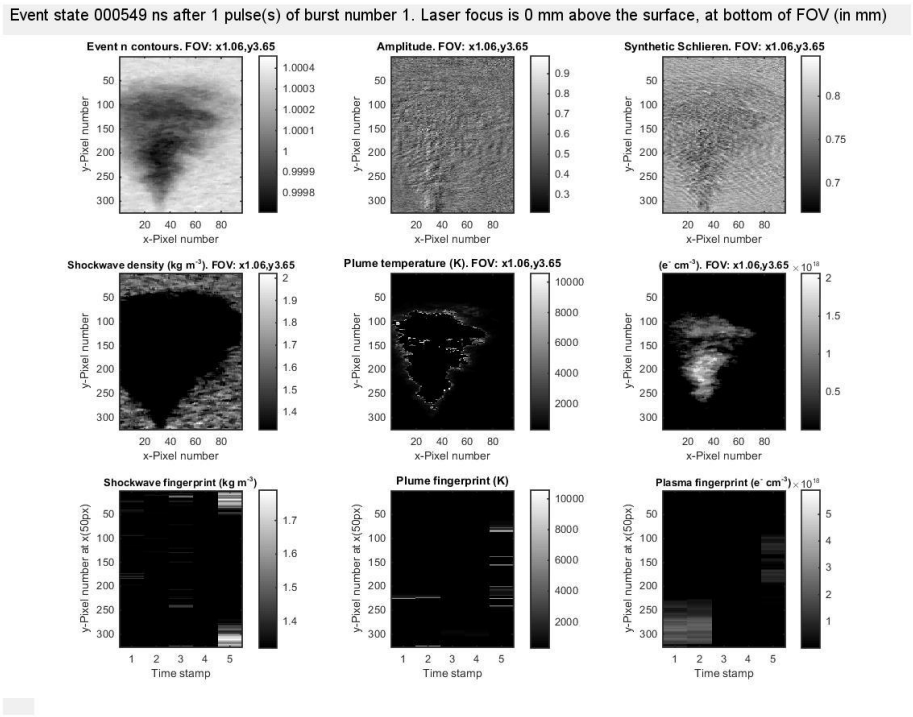

Figure A-2 High speed holographic imaging for 100 pulses, 2burst